

**A GENOTYPE – PHENOTYPE STUDY OF
CHILDHOOD ONSET RETINAL
DYSTROPHIES**

ARUNDHATI DEV BORMAN

FRCOphth

INSTITUTE OF OPHTHALMOLOGY

UCL

A THESIS SUBMITTED FOR THE DEGREE OF MD(Res)

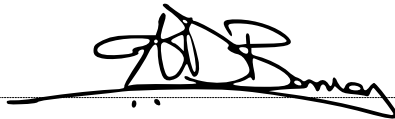
2015

Declaration

I, Arundhati Dev Borman, confirm that the work presented in this thesis is my own.

Where information has been derived from other sources, I confirm that this has been indicated in the thesis.

Signed:



Abstract

Introduction

The childhood onset retinal dystrophies comprise a clinically and molecularly heterogeneous group of disorders. To date, sixteen genes have been implicated in the pathogenesis of the spectrum of disorders comprising Leber Congenital Amaurosis (LCA) and Early Onset Retinal Dystrophy (EORD), accounting for approximately 70% of cases. Although a wide range of phenotypes have been observed within this spectrum, some genotype – phenotype associations are reported. Further detailed genotype – phenotype studies will be important for expanding our understanding of the effects of mutations in these genes on patients and their families. Our knowledge of the phenotypic effects of mutations in other genes implicated in childhood onset retinal dystrophies, such as the bestrophinopathies, continues to expand.

Purpose

To undertake detailed phenotypic studies into subjects with molecularly identified childhood onset retinal dystrophies, and to describe novel phenotypes.

Methods

Affected subjects and their families were recruited from Moorfields Eye Hospital to an ongoing Study into childhood onset retinal dystrophies. Subjects were examined clinically and those that were historically recruited to the Study were invited back for further phenotypic analyses, if their molecular cause was identified. Genetic analysis

was performed using a variety of methods including DNA microarray analysis, autozygosity mapping, direct sequencing and whole exome sequencing.

Results

Between August 2008 and August 2011, 201 subjects from 186 families were recruited into the Childhood Onset Retinal Dystrophy Study, and categorised into 2 cohorts: cohort 1 - the generalised retinal dystrophies, comprising 177 subjects (166 families); and cohort 2 – subjects with a macular phenotype, comprising 24 subjects (20 families). The molecular cause was identified in 34.5% of subjects in cohort 1 and 25% of subjects in cohort 2. *RDH12* accounted for 28% of mutations in cohort 1, 18% had mutations in *CEP290*, and 13% had mutations in *RPE65*. The subjects in cohort 2 with autosomal recessive bestrophinopathy all had bi-allelic mutations in *BEST1*. The phenotype associated with the different genes identified was expanded, and focused on those genes with limited reports of the phenotype, such as *SPATA7*, *LRAT*, *RGR* and *BEST1*. The phenotype associated with a gene not previously identified in human EORD, *TUB*, was studied, and the features associated with a novel macular phenotype named Benign Yellow Dot Dystrophy were characterised.

Conclusions

This study has expanded and refined our understanding of the phenotypes associated with mutations in genes that cause childhood onset retinal dystrophies, and has identified a novel phenotype. This work will allow accurate prognostic and genetic counselling to affected families, and provides phenotypic information that will be important in ascertaining disorders that may be suitable for clinical trials of novel therapies.

Table of Contents

DECLARATION	2
ABSTRACT	3
INTRODUCTION	3
PURPOSE	3
METHODS	3
RESULTS	4
CONCLUSIONS.....	4
TABLE OF CONTENTS	5
LIST OF FIGURES	10
LIST OF TABLES	12
ACKNOWLEDGEMENTS	13
1.0 INTRODUCTION	14
1.1 HISTORY AND EPIDEMIOLOGY OF LEBER CONGENITAL AMAUROSIS AND EARLY ONSET RETINAL DYSTROPHY	15
1.1.1 GENETICS OF INHERITED RETINAL DYSTROPHIES	16
1.1.2 HISTORY OF LEBER CONGENITAL AMAUROSIS.....	18
1.1.3 EPIDEMIOLOGY	21
1.1.4 SPECTRUM OF CLINICAL FEATURES.....	22
1.2 RETINAL STRUCTURE AND FUNCTION	24
1.2.1 ULTRASTRUCTURAL AND MICROSCOPIC STRUCTURE OF THE RETINA.....	25
1.2.1.1 <i>Photoreceptor cells</i>	27
1.2.1.2 <i>Neural cells</i>	31
1.2.1.3 <i>Supporting cells</i>	33
1.2.2 THE RETINAL PIGMENT EPITHELIUM	33
1.2.3 THE PHOTOTRANSDUCTION CASCADE.....	34
1.2.4 THE VISUAL CYCLE.....	36
1.3 TECHNIQUES FOR PHENOTYPING	39
1.3.1 VISUAL ACUITY	39
1.3.1.1 <i>Visual acuity testing in children</i>	42
1.3.2 COLOUR VISION	43
1.3.2.1 <i>Ishihara Pseudoisochromatic Plates</i>	43
1.3.2.2 <i>Hardy Rand Rittler Pseudoisochromatic Plates</i>	44
1.3.2.3 <i>Other tests of colour vision</i>	45
1.3.3 REFRACTIVE ERROR.....	46
1.3.4 PSYCHOPHYSICAL TESTING - PERIMETRY	47
1.3.4.1 <i>Kinetic Perimetry</i>	48
1.3.4.2 <i>Static Perimetry</i>	50
1.3.4.3 <i>Perimetry in children</i>	50
1.3.5 ADDITIONAL PSYCHOPHYSICAL TESTS.....	51
1.3.6 ELECTROPHYSIOLOGY	51
1.3.6.1 <i>The ISCEV standard Electro-Oculogram</i>	52
1.3.6.2 <i>The ISCEV standard Electro-Retinogram</i>	53

1.3.6.3	<i>Other electrodiagnostic tests</i>	55
1.3.6.4	<i>Electrodiagnostic testing in children</i>	56
1.3.7	OPTICAL COHERENCE TOMOGRAPHY	57
1.3.8	FUNDUS AUTOFLUORESCENCE IMAGING	59
1.3.9	FUNDUS IMAGING.....	62
1.4	TECHNIQUES FOR MOLECULAR ANALYSIS.....	63
1.4.1	LINKAGE	63
1.4.2	GENETIC MARKERS	65
1.4.2.1	<i>Restriction Fragment Length Polymorphisms</i>	66
1.4.2.2	<i>Microsatellites</i>	66
1.4.2.3	<i>Single nucleotide polymorphisms</i>	67
1.4.3	POLYMERASE CHAIN REACTION.....	68
1.4.4	AGAROSE GEL ELECTROPHORESIS	70
1.4.5	DNA SEQUENCING	71
1.4.6	DNA MICROARRAYS	73
1.4.7	AUTOZYGOSITY MAPPING	74
1.4.8	APEX MICROARRAY	76
1.4.9	NEXT GENERATION SEQUENCING.....	78
1.5	GENETICS OF LEBER CONGENITAL AMAUROSIS AND EARLY ONSET RETINAL DYSTROPHY	84
1.5.1	<i>GUCY2D</i> (LCA1).....	86
1.5.2	<i>RPE65</i> (LCA2)	88
1.5.3	<i>SPATA7</i> (LCA3).....	94
1.5.4	<i>AIPL1</i> (LCA4).....	96
1.5.5	<i>LEBERCILIN</i> (LCA5)	99
1.5.6	<i>RPGRIP1</i> (LCA6)	101
1.5.7	<i>CRX</i> (LCA7).....	103
1.5.8	<i>CRB1</i> (LCA8).....	107
1.5.9	LCA9 LOCUS.....	109
1.5.10	<i>CEP290</i> (LCA10).....	110
1.5.11	<i>IMPDH1</i> (LCA11).....	115
1.5.12	<i>RD3</i> (LCA12)	116
1.5.13	<i>RDH12</i> (LCA13)	118
1.5.14	<i>LRAT</i> (LCA14)	120
1.5.15	<i>TULP1</i> (RP14).....	122
1.5.16	<i>RGR</i> (RP44).....	124
1.5.17	<i>IQCB1 / NPHP5</i>	126
1.6	AIMS AND OBJECTIVES	128
1.6.1	AIMS	128
1.6.2	OBJECTIVES.....	128
2.0	MATERIALS AND METHODS	130
2.1	ETHICS / PATIENT SELECTION	131
2.1.1	ETHICAL APPROVAL.....	131
2.1.2	PATIENT SELECTION.....	131
2.1.3	CONSENT.....	133
2.2	PHENOTYPING.....	134
2.2.3	CLINICAL HISTORY	134

2.2.4	CLINICAL EXAMINATION.....	135
2.2.4.1	<i>Visual Acuity</i>	135
2.2.4.2	<i>Colour vision</i>	136
2.2.4.3	<i>General Ocular Examination</i>	137
2.2.5	FUNDUS AUTOFLUORESCENCE IMAGING	139
2.2.6	OPTICAL COHERENCE TOMOGRAPHY	139
2.2.7	PSYCHOPHYSICAL TESTING: GOLDMANN VISUAL FIELDS.....	140
2.2.8	COLOUR FUNDUS PHOTOGRAPHY.....	141
3.3	GENETIC METHODS	142
3.3.1	EXTRACTION OF DNA	142
3.3.2	GENOTYPE IDENTIFICATION STRATEGIES.....	143
3.3.2.1	<i>DNA microarray using the Asper LCA chip</i>	143
3.3.2.2	<i>Polymerase chain reaction and candidate gene sequencing</i>	144
3.3.2.3	<i>Autozygosity Mapping</i>	148
3.3.2.4	<i>Next Generation Sequencing</i>	149
3.3.3	BIOINFORMATICS	149
4.0	RESULTS	151
4.1	OVERVIEW OF STUDY.....	152
4.1.1	STUDY PERIOD AND PATIENT RECRUITMENT	152
4.1.2	DEMOGRAPHICS AND DIAGNOSES	153
4.1.2.1	<i>Cohort 1</i>	153
4.1.2.2	<i>Cohort 2</i>	154
4.2	OVERVIEW OF STUDY: OVERALL MOLECULAR FINDINGS	155
4.2.1	LCA CHIP RESULTS FOR COHORT 1	155
4.2.2	MOLECULAR DIAGNOSES IDENTIFIED IN THIS STUDY.....	159
4.2.2.1	<i>Molecular Diagnoses for Cohort 1</i>	159
4.2.2.2	<i>Cohort 2</i>	164
4.2.3	DIAGNOSIS BY GENE – COHORT 1	164
4.2.3.1	<i>AIPL1</i>	164
4.2.3.2	<i>CEP290</i>	164
4.2.3.3	<i>CRB1</i>	165
4.2.3.4	<i>GUCY2D</i>	166
4.2.3.5	<i>LCA5</i>	166
4.2.3.6	<i>MERTK</i>	167
4.2.3.7	<i>RDH12</i>	167
4.2.3.8	<i>RPE65</i>	168
4.2.3.9	<i>RPGRIP1</i>	169
4.2.3.10	<i>SPATA7, TULP1, LRAT, RGR</i>	169
4.2.4	DIAGNOSIS BY GENE – COHORT 2	169
4.2.5	SUMMARY OF OVERVIEW OF STUDY	169
4.3	GENOTYPE - PHENOTYPE ASSOCIATIONS	171
4.3.1	<i>AIPL1</i> GENOTYPE - PHENOTYPE ASSOCIATION.....	171
4.3.2	<i>CEP290</i> GENOTYPE - PHENOTYPE ASSOCIATION.....	173
4.3.3	<i>CRB1</i> GENOTYPE - PHENOTYPE ASSOCIATION	177
4.3.4	<i>GUCY2D</i> GENOTYPE - PHENOTYPE ASSOCIATION.....	182
4.3.5	<i>LCA5</i> GENOTYPE - PHENOTYPE ASSOCIATION.....	183
4.3.6	<i>MERTK</i> GENOTYPE - PHENOTYPE ASSOCIATION	185
4.3.7	<i>RDH12</i> GENOTYPE - PHENOTYPE ASSOCIATION.....	187

4.3.8	<i>RPE65</i> GENOTYPE - PHENOTYPE ASSOCIATION.....	193
4.3.9	<i>RPGRIP1</i> GENOTYPE - PHENOTYPE ASSOCIATION	200
4.4	<i>SPATA7</i> PHENOTYPE	202
4.4.1	CLINICAL HISTORY	202
4.4.2	CLINICAL EXAMINATION.....	203
4.4.3	FUNDUS AUTOFLUORESCENCE IMAGING	204
4.4.4	OCT IMAGING.....	204
4.4.5	PSYCHOPHYSICAL TESTING: GOLDMANN VISUAL FIELDS	207
4.4.6	ELECTROPHYSIOLOGICAL TESTING	208
4.4.7	MOLECULAR ANALYSIS	210
4.4.8	DISCUSSION.....	213
4.5	TUBBY AND TUBBY-LIKE PROTEIN GENOTYPE - PHENOTYPE ASSOCIATIONS	217
4.5.1	<i>TUB</i> GENOTYPE - PHENOTYPE ASSOCIATION.....	217
4.5.1.1	<i>Clinical History</i>	218
4.5.1.2	<i>Clinical Examination</i>	219
4.5.1.3	<i>Fundus Autofluorescence Imaging</i>	221
4.5.1.4	<i>OCT Imaging</i>	221
4.5.1.5	<i>Psychophysical testing: Goldmann Visual Fields</i>	223
4.5.1.6	<i>Electrophysiological Testing</i>	224
4.5.1.7	<i>Molecular analysis</i>	224
4.5.1.8	<i>Collaborative studies</i>	226
4.5.1.9	<i>Summary of TUB phenotype identified in this study</i>	226
4.5.2	<i>TULP1</i> GENOTYPE - PHENOTYPE ASSOCIATION.....	227
4.5.2.1	<i>Clinical History</i>	227
4.5.2.2	<i>Clinical Examination</i>	228
4.5.2.3	<i>Fundus Autofluorescence Imaging</i>	230
4.5.2.4	<i>OCT Imaging</i>	230
4.5.2.5	<i>Psychophysical Testing: Goldmann Visual Fields</i>	232
4.5.2.6	<i>Electrophysiological Testing</i>	233
4.5.2.7	<i>Molecular analysis</i>	233
4.5.2.8	<i>Summary of TULP1 phenotype identified in this study</i>	237
4.5.3	DISCUSSION.....	237
4.6	<i>LRAT</i> PHENOTYPE	243
4.6.1	CLINICAL HISTORY	243
4.6.2	CLINICAL EXAMINATION.....	244
4.6.3	FUNDUS AUTOFLUORESCENCE IMAGING	246
4.6.4	OCT IMAGING.....	246
4.6.5	ELECTROPHYSIOLOGICAL TESTING	252
4.6.6	PSYCHOPHYSICAL TESTING	253
4.6.6.1	<i>Goldmann Visual Fields</i>	253
4.6.6.2	<i>Dark Adapted Perimetry</i>	255
4.6.6.3	<i>Dark adapted spectral sensitivities</i>	256
4.6.6.4	<i>Critical Flicker Fusion</i>	258
4.6.7	MOLECULAR ANALYSIS	260
4.6.8	DISCUSSION.....	261
4.7	<i>RGR</i> PHENOTYPE	268
4.7.1	CLINICAL HISTORY	268

4.7.2	CLINICAL EXAMINATION.....	269
4.7.3	FUNDUS AUTOFLUORESCENCE IMAGING.....	270
4.7.4	OCT IMAGING.....	270
4.7.5	PSYCHOPHYSICAL TESTING – GOLDMANN VISUAL FIELDS.....	271
4.7.6	ELECTROPHYSIOLOGICAL TESTING.....	272
4.7.7	MOLECULAR ANALYSIS.....	273
4.7.8	DISCUSSION.....	274
4.8	CHILDHOOD ONSET AUTOSOMAL RECESSIVE BESTROPHINOPATHY	276
4.8.1	CLINICAL HISTORY.....	277
4.8.2	CLINICAL EXAMINATION.....	277
4.8.3	FUNDUS AUTOFLUORESCENCE IMAGING.....	279
4.8.4	OCT IMAGING.....	279
4.8.5	ELECTROPHYSIOLOGICAL STUDIES.....	284
4.8.6	MOLECULAR ANALYSIS.....	285
4.8.7	DISCUSSION.....	290
4.9	BENIGN YELLOW DOT DYSTROPHY	298
4.9.1	CLINICAL HISTORY.....	298
4.9.2	CLINICAL EXAMINATION.....	299
4.9.3	FUNDUS AUTOFLUORESCENCE IMAGING.....	307
4.9.4	OCT IMAGING.....	307
4.9.5	ELECTROPHYSIOLOGICAL STUDIES.....	310
4.9.6	DISCUSSION.....	310
5.0	DISCUSSION AND CONCLUSIONS.....	314
5.1	THE CHILDHOOD ONSET RETINAL DYSTROPHY STUDY.....	315
5.2	PHENOTYPIC HETEROGENEITY IN CHILDHOOD ONSET RETINAL DYSTROPHIES.....	318
5.3	THERAPEUTIC OPTIONS FOR CHILDHOOD ONSET RETINAL DYSTROPHIES.....	324
5.4	ADVANCES SINCE THIS STUDY WAS CONDUCTED.....	327
5.5	CONCLUSIONS AND FURTHER WORK.....	330
6.0	REFERENCES	332
7.0	APPENDICES.....	360
7.1	PATIENT DOCUMENTS.....	361
7.1.1	PATIENT INFORMATION LEAFLET.....	361
7.1.2	CONSENT FORM – ADULT.....	365
7.1.3	CONSENT FORM – CHILD.....	366
7.1.4	DATA PROTECTION CONSENT FORM.....	367
7.2	PRIMER SEQUENCES.....	368
7.2.1	<i>TULP1</i> PRIMERS.....	368
7.2.2	<i>RGR</i> PRIMERS.....	369
7.2.3	<i>BEST1</i> PRIMERS.....	369
7.3	PUBLICATIONS AND ABSTRACTS FROM THIS STUDY.....	370

List of Figures

FIGURE 1 – GROSS ANATOMY OF A NORMAL RETINA, RIGHT EYE	25
FIGURE 2 – SCHEMA OF THE LAYERS OF THE RETINA	27
FIGURE 3 – ROD PHOTORECEPTOR	29
FIGURE 4 – COMPARISON OF CONE AND ROD PHOTORECEPTOR ANATOMY	30
FIGURE 5 – PROCESSES IN HUMAN ROD AND RPE CELLS	37
FIGURE 6 – ETDRS VISUAL ACUITY CHART	41
FIGURE 7 – TESTS OF COLOUR VISION	44
FIGURE 8 – NORMAL SD-OCT IMAGE.....	58
FIGURE 9 – NORMAL FUNDUS AUTOFLUORESCENCE IMAGE, RIGHT EYE.....	61
FIGURE 10 – SPATIAL REPRESENTATION OF 14 DIFFERENT LCA / EORD GENES AND THEIR PUTATIVE ROLES	85
FIGURE 11 - RESULTS OF COHORT 1 SUBJECTS SENT FOR LCA CHIP ANALYSIS	158
FIGURE 12 - GENOTYPES OF ALL SUBJECTS IDENTIFIED WITH VARIANTS IN COHORT 1	160
FIGURE 13 - SUBJECT 2, <i>AIP1</i> , HYPOMORPHIC EORD	172
FIGURE 14 - GRAPHICAL REPRESENTATION OF AGE VERSUS VISUAL ACUITY IN <i>CEP290</i> RETINOPATHY	176
FIGURE 15 - SUBJECT 10, <i>CEP290</i> , EORD	176
FIGURE 16 - SUBJECT 19, <i>CRB1</i> . DIAGNOSIS EORD.....	179
FIGURE 17 - SUBJECT 15, <i>CRB1</i> , EORD	180
FIGURE 18 - SUBJECT 16, <i>CRB1</i>	181
FIGURE 19 - SUBJECT 20, <i>GUCY2D</i>	183
FIGURE 20 - SUBJECT 25, <i>LCA5</i>	185
FIGURE 21 - SUBJECT 29, <i>MERTK</i> , EORD.....	186
FIGURE 22 - GRAPHICAL REPRESENTATION OF AGE VERSUS VISUAL ACUITY IN <i>RDH12</i> RETINOPATHY	190
FIGURE 23 - <i>RDH12</i> SUBJECTS WITH EORD	191
FIGURE 24 - SUBJECT 35, <i>RDH12</i> , ROD-CONE DYSTROPHY	192
FIGURE 25 - SUBJECT 43, <i>RDH12</i> EORD.....	193
FIGURE 26 - GRAPHICAL REPRESENTATION OF AGE VERSUS VISUAL ACUITY IN <i>RPE65</i> RETINOPATHY	197
FIGURE 27 - SUBJECT 48, <i>RPE65</i> , LCA	197
FIGURE 28 - SUBJECT 54, <i>RPE65</i> , EORD	198
FIGURE 29 - SUBJECT 51, <i>RPE65</i> , LCA	199
FIGURE 30 - SUBJECT 52, <i>RPE65</i> , HYPOMORPHIC EORD.....	200
FIGURE 31 - SUBJECT 56, <i>RPGRIP1</i> EORD.....	201
FIGURE 32 - SUBJECT 1, FAMILY 1 <i>SPATA7</i>	205
FIGURE 33 - SUBJECT 2, FAMILY 1 <i>SPATA7</i>	206
FIGURE 34 - SUBJECT 5, FAMILY 3 <i>SPATA7</i>	206
FIGURE 35 - SUBJECT 10, FAMILY 5, <i>SPATA7</i>	207
FIGURE 36 – GOLDMANN VISUAL FIELD, SUBJECT 2, <i>SPATA7</i>	208
FIGURE 37 - PEDIGREE OF <i>TUB</i> FAMILY	219
FIGURE 38 - TUB FAMILY: PROBAND (VI.11).....	222
FIGURE 39 – TUB FAMILY: BROTHER (VI.10)	222
FIGURE 40 - TUB FAMILY: SISTER (VI.12)	223
FIGURE 41 – GOLDMANN VISUAL FIELD, SUBJECT VI.11, <i>TUB</i>	224
FIGURE 42 - PEDIGREES OF <i>TULP1</i> FAMILIES.....	228

FIGURE 43 - <i>TULPI</i> FAMILY 1: SUBJECT IV.4.....	231
FIGURE 44 - <i>TULPI</i> FAMILY 2: SUBJECT V.5.....	231
FIGURE 45 - <i>TULPI</i> FAMILY 3: SUBJECT III.3.....	232
FIGURE 46 - <i>TULPI</i> FAMILY 2: SUBJECT V.5, GOLDMANN VISUAL FIELDS.....	233
FIGURE 47 - <i>TULPI</i> FAMILY 1 ELECTROPHEROGRAMS.....	234
FIGURE 48 - <i>TULPI</i> FAMILY 2 ELECTROPHEROGRAMS.....	235
FIGURE 49 - <i>TULPI</i> FAMILY 3 ELECTROPHEROGRAMS.....	236
FIGURE 50 - SUBJECT 1, <i>LRAT</i>	249
FIGURE 51 - SUBJECT 2, <i>LRAT</i>	250
FIGURE 52 - SUBJECT 3, <i>LRAT</i>	251
FIGURE 53 - SUBJECT 4, <i>LRAT</i>	252
FIGURE 54 – GOLDMANN VISUAL FIELD PLOTS, <i>LRAT</i> SUBJECTS.....	254
FIGURE 55 - FULL STATIC THRESHOLD CENTRAL 30 ⁰ PHOTOPIC AND DARK ADAPTED PERIMETRY, <i>LRAT</i> SUBJECT 3.....	256
FIGURE 56 - DARK ADAPTED SPECTRAL SENSITIVITIES, <i>LRAT</i> SUBJECTS.....	257
FIGURE 57 - CRITICAL FLICKER FUSION FREQUENCIES IN <i>LRAT</i> SUBJECTS.....	259
FIGURE 58 - RETINAL IMAGING OF SUBJECT 47, <i>RGR</i> WITH EORD.....	271
FIGURE 59 - GOLDMANN VISUAL FIELDS, SUBJECT 47, <i>RGR</i>	272
FIGURE 60 - <i>RGR</i> SEQUENCING IN FAMILY 45.....	273
FIGURE 61 - SUBJECT 1 ARB.....	281
FIGURE 62 - SUBJECT 2 ARB.....	281
FIGURE 63 - SUBJECT 3 ARB.....	282
FIGURE 64 - SUBJECT 4 ARB.....	282
FIGURE 65 - SUBJECT 5 ARB.....	283
FIGURE 66 - SUBJECT 6 ARB.....	283
FIGURE 67 – ELECTROPHEROGRAMS ARB FAMILY 5.....	287
FIGURE 68 - ELECTROPHEROGRAMS ARB FAMILY 6.....	288
FIGURE 69 - SUBJECT 10, FAMILY BENIGN YELLOW DOT DYSTROPHY.....	303
FIGURE 70 - SUBJECT 15, SPORADIC BENIGN YELLOW DOT DYSTROPHY.....	304
FIGURE 71 - SUBJECT 17, SPORADIC BENIGN YELLOW DOT DYSTROPHY.....	305
FIGURE 72 - SUBJECT 19, SPORADIC BENIGN YELLOW DOT DYSTROPHY.....	306
FIGURE 73 - FUNDUS AUTOFLUORESCENCE IMAGES OF BENIGN YELLOW DOT DYSTROPHY SUBJECTS.....	308
FIGURE 74 - OCT OF SUBJECTS WITH BENIGN YELLOW DOT DYSTROPHY.....	309

List of Tables

TABLE 1 - PCR REAGENTS FOR EACH 30 ML PCR REACTION	144
TABLE 2 – REAGENTS AND VOLUMES FOR EACH 10 ML SEQUENCING REACTION USING BIG DYE TERMINATOR.....	146
TABLE 3 - DIAGNOSES OF SUBJECTS RECRUITED INTO COHORT 1 OF THE CHILDHOOD ONSET RETINAL DYSTROPHY STUDY, AUG 2009 – AUG 2011	154
TABLE 4 - DIAGNOSES OF SUBJECTS RECRUITED INTO COHORT 2 OF THE CHILDHOOD ONSET RETINAL DYSTROPHY STUDY, AUG 2009 – AUG 2011.....	154
TABLE 5 - BREAKDOWN OF LCA CHIP RESULTS FOR SAMPLES SENT FROM UCL BY GENE, DIAGNOSIS AND NUMBER OF VARIANTS IDENTIFIED.	157
TABLE 6 – SUBJECTS IDENTIFIED WITH VARIANTS USING THE LCA CHIP BY REFERRING HOSPITAL	159
TABLE 7 - GENOTYPE FOR COHORT 1 WITH BREAKDOWN ACCORDING TO DIAGNOSIS.	161
TABLE 8 - GENETIC VARIANTS IDENTIFIED IN COHORT 1	163
TABLE 9 - CLINICAL FEATURES OF <i>CEP290</i> SUBJECTS IN COHORT 1.....	175
TABLE 10 – CLINICAL FEATURES OF <i>RDH12</i> SUBJECTS IN COHORT 1	189
TABLE 11 - CLINICAL FEATURES OF <i>RPE65</i> SUBJECTS IN COHORT 1	196
TABLE 12 - CLINICAL FEATURES OF <i>SPATA7</i> SUBJECTS	209
TABLE 13 - AUGOZYGOSITY DATA, FAMILY 4	211
TABLE 14 - MUTATIONS IDENTIFIED IN <i>SPATA7</i> IN THIS STUDY.....	212
TABLE 15 - CLINICAL FEATURES OF <i>TULP1</i> SUBJECTS.....	229
TABLE 16 - AUGOZYGOSITY DATA, <i>TULP1</i> FAMILY 2	235
TABLE 17 - MUTATIONS IDENTIFIED IN <i>TULP1</i> IN THIS STUDY	236
TABLE 18 - DEMOGRAPHIC AND CLINICAL DATA OF <i>LRAT</i> SUBJECTS.....	248
TABLE 19 – MUTATIONS IDENTIFIED IN <i>LRAT</i> IN THIS STUDY	261
TABLE 20 - CLINICAL FEATURES OF PAEDIATRIC ARB SUBJECTS.....	280
TABLE 21 - <i>BEST1</i> MOLECULAR ANALYSIS	289
TABLE 22 - CLINICAL FEATURES OF SUBJECTS WITH BENIGN YELLOW DOT DYSTROPHY	301
TABLE 23 - FEATURES OF YELLOW DOTS AT THE FUNDUS IN BENIGN YELLOW DOT DYSTROPHY SUBJECTS.....	302
TABLE 24 - PRIMERS AND PCR CONDITIONS FOR <i>TULP1</i>	368
TABLE 25 - PRIMERS AND PCR CONDITIONS FOR <i>RGR</i>	369
TABLE 26 - PRIMERS AND PCR CONDITIONS FOR <i>BEST1</i>	369

Acknowledgements

I am grateful to the Moorfields Special Trustees, The National Institute for Health Research, The Foundation Fighting Blindness and Fight For Sight for providing the funding towards this Research.

I am most grateful to my supervisors Professor Tony Moore and Professor Andrew Webster. Thank you to you both for giving me the opportunity to work with you – I have enjoyed this project immensely. Tony, thank you for your wisdom and unwavering support. There were times that we really did not think I could finish, and without your help, I never could have! I am especially touched by the faith that you continue to put in me; ever since the day I strolled into your clinic at GOSH and pestered you to have this opportunity. Andrew, thank you for all your ideas and for helping me think laterally.

Thank you to Dr Donna Mackay who put up with ‘yet another medic’ in the lab, but without whose guidance and ongoing support from the other side of the Pond, I could not have completed this work. Thank you too, to Samantha Malka, Sarah Hull and Oliver Comyn, who have been absolutely brilliant in these last few months, and without whom I could not have completed this thesis.

My gratitude to my parents and loved ones is indescribable. Thank you to you all for being there for me every day, for supplying me with cups of tea (stirred properly!), for keeping me grounded when all around was up in the air, and for gently encouraging me when reserves were low.

1.0 Introduction

1.1 History and epidemiology of Leber Congenital Amaurosis and Early Onset Retinal Dystrophy

Following the invention of the ophthalmoscope by Helmholtz in 1851, van Trigt in 1853 reported the first authenticated case of pigmentary degeneration of the retina, but it was Donders in 1855 who devised the name Retinitis Pigmentosa [1, 2]. This term is rather a misnomer as this is not a predominantly inflammatory condition. Von Graefe, who identified the condition to be a pigmentary retinal degeneration with a hereditary component, subsequently made the first detailed description of the disease [3]. In fact, these inherited retinal dystrophies (historically known as ‘tapeto-retinal degenerations’) are a range of conditions characterised by progressive familial night blindness (nyctalopia) with severe visual field constriction, eventual diminution of the central vision, and attenuation of the electroretinal response [4]. The genetic aspects of this range of conditions have excited a great deal of interest and have generated an enormous amount of literature that has uncovered a wide underlying genetic heterogeneity.

Although the majority of these conditions are inherited in an autosomal recessive manner, other inheritance patterns are also present, including autosomal dominant, sex-linked and mitochondrial inheritance. Classification of these disorders is progressively moving towards one based upon their underlying genetic cause,

however the historical ‘umbrella’ terms under which they are known are continuing to be used. The research carried out towards this thesis is based upon these inherited retinal dystrophies, in particular those with a childhood onset, which are collectively known as the ‘Early Onset Retinal Dystrophies’, of which Leber Congenital Amaurosis represents the most severe form.

1.1.1 Genetics of inherited retinal dystrophies

Inherited retinal dystrophies affect millions of people worldwide; dozens of different types of diseases are included in this set of conditions and more than 190 genes have been identified as the cause for one or another form of inherited retinal disease. One group of these conditions is retinitis pigmentosa (RP). The heterogeneity associated with RP includes genetic heterogeneity (many different genes that may cause the same disease phenotype), allelic heterogeneity (many different disease-causing mutations in the same gene), phenotypic heterogeneity (different mutations in the same gene that may cause different diseases) and clinical heterogeneity (the same mutation in different individuals that may cause a different clinical picture) [5]. RP is a generic name that covers the retinal dystrophies that comprise of loss of photoreceptors and pigmentary retinal deposits, the most common type being primarily a rod photoreceptor degeneration that may progress to involve cone photoreceptors. These, therefore, present with nyctalopia and visual field constriction. The age of onset of RP can be variable. Most RP begins in adolescence or early adulthood, but there are later onset forms that may begin at or after mid-life. Childhood onset forms fall under the umbrella term ‘early onset retinal dystrophies’ (EORD).

RP may occur alone, as non-syndromic RP without any other clinical findings, or as syndromic or systemic RP with other neurosensory disorders, developmental abnormalities or other complex clinical phenotypes. Such syndromes include Usher syndrome (RP with congenital or early onset deafness) and Bardet Biedl syndrome (RP with renal disease, polydactyly, obesity and developmental delay).

There are autosomal dominant, autosomal recessive and X-linked forms of inheritance, as well as rare mitochondrial and digenic forms of RP [6, 7]. Traditionally, simplex RP is considered to be predominantly autosomal recessive in inheritance with unaffected carrier parents. However some of these cases will represent new (de novo) autosomal dominant mutations, or in males, may represent X-linked RP, where there is no known family history. It tends to typically begin in the first decade, but milder forms exist. There is a higher incidence in consanguineous families [8]. Autosomal dominant forms are usually the mildest of all, with some cases starting after the age of 50, however there are childhood onset forms that display autosomal dominant inheritance, such as those associated with mutations in the gene *CRX* [9]. X-linked forms start early and are often associated with myopia; they are usually recessive in inheritance, caused predominantly by mutations in *RPGR* or *RP2* [10]. The rare mitochondrial mutations have mostly been found in RP associated with other neurological and systemic dysfunction, such as with sensorineural deafness, or ataxia and dementia, or in Kearns Sayre syndrome [11-13].

However, the genetics of this group of conditions is much more complicated than this, as alluded to above. Many genes can cause more than one form of disease – such as

mutations in Rhodopsin, which usually cause autosomal dominant RP, but in which rare mutations have been identified to cause recessive RP [7]. In addition, mutations in a single gene very commonly cause different phenotypes, such as in those with *RPE65* mutations [14, 15]. Such complexity in these conditions has led to a huge international body of research into the underlying genetic causes and phenotypes of the inherited retinal dystrophies.

1.1.2 History of Leber Congenital Amaurosis

Theodore Karl Gustav von Leber (1840 – 1917), an eminent ophthalmologist and ocular pathologist, who studied under von Helmholtz, Ludwig and von Graefe, and who later became Professor of Ophthalmology in Berlin (1867 – 1870), and then in Heidelberg (1890 – 1910), was the first clinician to establish ophthalmological thought on the ‘tapeto-retinal degenerations’ [4]. He considered these conditions to be primary dystrophies of the retina, which included retinitis pigmentosa with and without pigment, retinitis punctata albescens, chorioretinal degenerations and scleroses such as gyrate atrophy and central papillary sclerosis, as well as congenital night blindness without ophthalmoscopic abnormalities. He thought that the underlying pathology in these conditions lay in the pigimentary epithelium, the ‘tapetum nigrum’, or black carpet. In 1869 and 1871, through his role as consultant oculist of the Ilvesheim Asylum for the Blind, Leber described a disease which he called ‘pigmentary retinopathy with congenital amaurosis’ (now known as Leber Congenital Amaurosis) in which, in the majority of cases, there was congenital blindness or development of blindness within the first year of life [2, 16, 17]. In his later writings, he distinguished two types: the first, a congenital form in which

blindness occurred in the first year of life; and the second, a juvenile form which manifested itself between the first year and puberty, that did not always entail blindness, but in which usually a severe degree of visual failure was observed [2, 4].

Leber's original description of the condition was of 'bilateral blindness, with coarse nystagmus, some retention of the pupillary reflexes and the eventual appearance of pigmentary and degenerative changes in the fundi' [4]. He recognised that the condition was familial (identified in 44.8% of the families he initially described) and observed a higher rate of consanguinity within these affected families (24.1% of his series), thus inadvertently describing an autosomal recessive inheritance pattern. Children usually presented at birth or within the first few months of life with very poor or absent vision, a coarse 'roving' nystagmus, photophobia, poor pupil responses, and a habit of pushing a fist or fingers into the orbit, a sign later described as the 'oculo-digital sign' of Franceschetti (cited in [2]). Initially the fundi appeared to be normal, which could remain the case in the first few months of life, but soon various polymorphic lesions were observed, the most typical being small white dots in the periphery of the fundus, followed later by pigmentation, which at first could look like 'salt and pepper' pigmentary change, but which later could become more typical of the bone-corporuscular pigmentation seen in the pigmentary retinopathy described by Mooren in 1867 (cited in [4]). The optic disc became pale and the retinal vessels attenuated, with atrophy of the retinal pigment epithelium. The milder cases were not necessarily associated with nyctalopia or severely constricted visual fields, but instead may have had severely irregular contraction of the visual fields with some reduced vision detectable within parts of the remaining fields [17]. In the infantile, or juvenile form, the vision was described by Leber to fail seriously by the 6th or 7th year of life,

and blindness to be complete before the age of 30 years; ophthalmoscopic examination at first was often normal, but from the age of 8 years, a more typical pigmentary degeneration was observed.

Although a few reports were published following Leber's initial paper, the spectrum of conditions were rarely recognised and remained neglected until the advent of electroretinography, when it was established that many cases of blindness in infants, often previously presumed to be of central origin, were due to a retinal dysplasia [2, 18]. A number of authors identified these individuals to have an absent electrical retinal response, reported in up to 92% of cases, suggesting that this is an imperative finding in congenital amaurosis [19, 20]. Subsequent studies further delineated characteristics associated with this condition such as keratoglobus, corneal opacification, cataract and photophobia [20, 21].

An extensive study by Alström and Olson, of 175 cases in Sweden, which they termed heredo-retinopathia congenitalis, monohybrida recessiva autosomalis, described in detail the longitudinal clinical and hereditary features of the disease and, in particular, hypothesised that this is a 'uniform condition with a monohybrid, autosomal recessive mode of inheritance and complete manifestation' [21]. They estimated the frequency of the condition to be 3 in 100 000, and also noted a higher rate of consanguinity among affected families. Waardenburg and Schappert-Kimmijser subsequently proposed that the condition may be genetically heterogeneous, following the study of a family in which the parents, who met in an asylum for the blind and who were both affected with LCA, had unaffected children [22]. Their conclusion was that Lebers amaurosis 'may be the result of homozygosity for different recessive genes'.

A variety of terms have been used to describe this condition, including: amaurosis congenita, dysgenesis neuro-epithelialis retinae, heredo-retinopathia congenitalis, retinal aplasia and tapeto-retinal dysplasia [19-21, 23]. However, the condition has subsequently, and more uniformly, become known as Leber Congenital Amaurosis (LCA) and is considered to be the most severe form of a spectrum of disorders known as the Early Onset Retinal Dystrophies (EORDs).

1.1.3 Epidemiology

LCA is rare, with a population frequency of between 1 in 30 000 and 1 in 81 000, accounting for at least 5% of all inherited retinopathies and approximately 20% of all children attending schools for the blind [24]. In the UK in 2000, retinal and macular dystrophies accounted for 14% of children registered with severe visual impairment or blindness (62/439 individuals), with LCA accounting for 15, and rod cone dystrophy (retinitis pigmentosa) or cone rod dystrophy accounting for 17 of these [25]. It is predominantly inherited in an autosomal recessive manner and consequently the condition is more prevalent in consanguineous families and in those families who are not known to be consanguineous, but who have a common ancestor [26]. To date, 16 genes have been implicated in the pathogenesis of LCA and EORD, demonstrating the genetic heterogeneity associated with this group of conditions. These will be explored further in this study.

1.1.4 Spectrum of clinical features

LCA and EORD are considered to be a ‘purely’ ocular spectrum of conditions, characterised by a constellation of four clinical features: early severe visual loss, nystagmus, sluggish pupils and an unrecordable ERG [24]. Traditionally, the classification of this spectrum of disorders has been based upon clinical characteristics. It is universally accepted that Leber Congenital Amaurosis represents the most severe end of this spectrum of conditions. However, early onset retinal dystrophy (EORD), early onset severe retinal dystrophy (EOSRD), severe early childhood onset retinal dystrophy (SECORD) and juvenile retinitis pigmentosa are all terms that are found in the literature to describe those progressive childhood retinal dystrophies that present at a slightly later age. Essentially these terms are describing the same clinical entities, but they have the potential of creating confusion about the exact diagnoses in these families. It is likely, in the future, that these terms will be superseded, and that the conditions will be named according to their causative gene, which should help avoid confusion from such descriptive terms.

Although LCA occurs from birth or the first few months of life, the term EORD (the most frequently used term for this spectrum of conditions) is reserved for those rod-cone dystrophies that have an infantile onset but which may have less nystagmus, better vision, normal pupil reactions but a severely attenuated ERG. Some of the genes associated with LCA have been identified to also cause the less severe phenotype of EORD [27]. In general, phenotypic variability exists for these conditions with respect to the retinal appearance, refractive error, symptomatology and age of symptom onset (such as photophobia and photophilia) and the oculodigital sign. The associated features of keratoconus (postulated to occur due to genetic,

traumatic or toxic factors), cataract, microphthalmia, ptosis and enophthalmos may also be variable.

The range of retinal appearances include a normal retina, mild retinal vessel attenuation, macular ‘coloboma’, macular pigmentation, retinal bone spicule pigmentation, nummular pigmentation, ‘salt and pepper’ appearance, white retinal spots, preservation of the para-arteriolar retinal pigment epithelium and a Coat’s like appearance [24]. There have been some genotype-phenotype associations, and these shall be explored in subsequent sections.

An ‘LCA-like ocular phenotype’ occurs in a number of syndromes that may initially present without the systemic features, but which may dominate the phenotype later in life. These include Alström syndrome, Batten disease, Joubert syndrome, Senior-Løken syndrome and peroxisomal disorders [28]. Subjects with these conditions were excluded from this study.

For the purposes of this study, LCA is defined as a severe early onset retinal dystrophy with absent or very poor vision from birth or the first few months of life, nystagmus, sluggish or ‘amaurotic’ pupillary responses, a variable retinal appearance and an un-recordable electroretinogram. EORD is defined as poor vision with infantile or early childhood onset below five years of age, with less nystagmus (if present at all), reduced vision, normal pupil reactions and a severely attenuated electroretinogram.

1.2 Retinal Structure and Function

It is thought that the first anatomical description of the eye was by Democritus (c.460-370 BC), who described it as two 'coats', filled with a homogenous fluid; there was no lens and the optic nerve was hollow [29]. Aristotle (384-322 BC) described it as a spherical organ with three layers, filled with a homogeneous fluid, connected to the brain by three tubes, one of which connected with a similar tube from the other eye. This was probably the first description of the optic chiasm. Galenus (130-200 AD), the most renowned physician in Roman times, considered the eye to have seven layers, and was the first to recognise the retina. He described it as an extension of the optic nerve, which nourished the vitreous humour and the lens. After this time there was a hiatus in scientific discovery and few new ideas regarding ocular anatomy were proposed. Although Vesalius (1514-1564), a Belgian academic considered to be the 'Father of Anatomy', vastly expanded the understanding of the human body, he made limited contributions to ocular anatomy. He described the retina as 'a tunic, which we compare to a net which is detached from the substance of the optic nerve'. It was not until the 17th century, when Van Leeuwenhoek, the inventor of the microscope, discovered the retinal photoreceptors. With newer microscopic techniques, the anatomy of the retina was further elucidated.

1.2.1 Ultrastructural and microscopic structure of the retina

The retina forms the innermost layer of the wall of the eye, with the choroid and sclera forming the middle and outer layers respectively. It lines the entire posterior portion of the eye, except at the optic nerve head, and extends anteriorly to end 360° circumferentially at the ora serrata. The outer pigmented layer (the retinal pigment epithelium) and inner neurosensory layer of the retina are embryologically derived from the neuroectoderm. The macula, demarcated by the supra-temporal and infra-temporal branches of the central retinal artery and vein, forms the anatomical centre of the retina and is responsible for central vision. The centre of the macula is the fovea centralis (Figure 1).

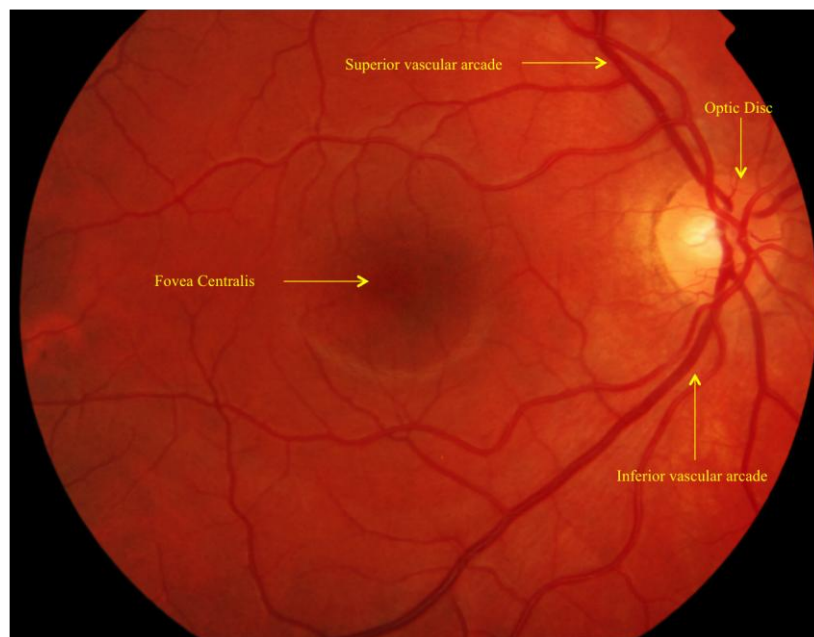


Figure 1 – Gross anatomy of a normal retina, right eye.

The neurosensory retina is transparent, which allows the underlying retinal pigment epithelium (RPE) to be visible. There is a potential space between these two layers, but they remain tightly attached to each other at the optic disc and the ora serrata. The retinal blood supply is derived from branches of the ophthalmic artery. In severe retinal dysfunction, the retinal arterioles may appear attenuated, the RPE may look abnormal and there may be retinal pigmentation of varying patterns.

Based upon light microscopic findings, the retina is comprised of 10 layers which, from the inner to the outer surface, are as follows: the internal limiting membrane (formed by the Müller cell end plates that separate the retina from the vitreous), the nerve fibre layer (predominantly comprised of ganglion cell axons), the ganglion cell layer, the inner plexiform layer (comprising the synapses between ganglion cells and amacrine cells), the inner nuclear layer (comprised of the nuclei of the amacrine cells, bipolar cells and horizontal cells), the outer plexiform layer (comprised of the synapses between the horizontal cells and the photoreceptor cells), the outer nuclear layer (nuclei of the photoreceptor cells), the external limiting membrane (formed at the bases of the photoreceptor inner segments), the photoreceptor layer (inner and outer segments of the photoreceptors) and the retinal pigment epithelium (Figure 2).

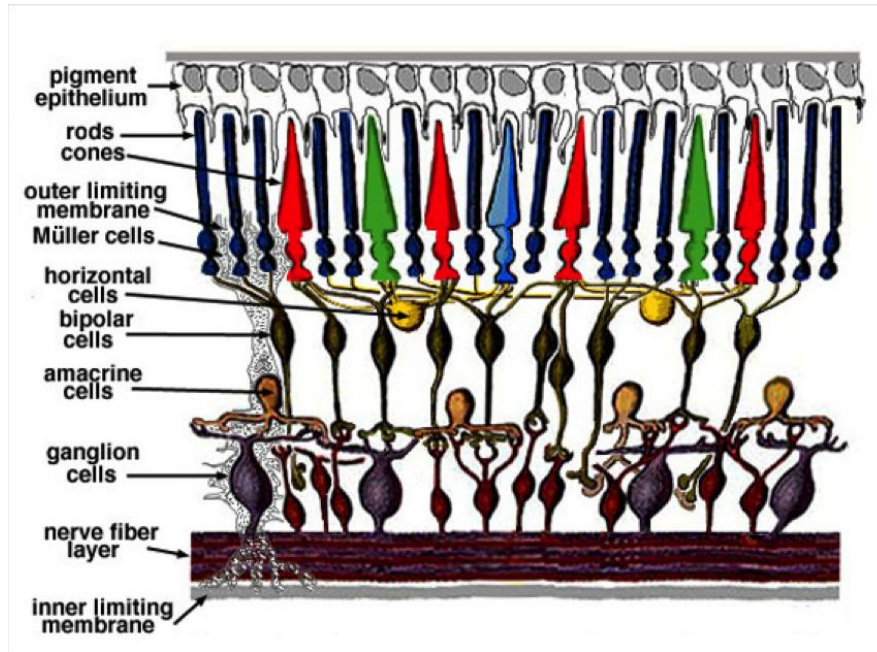


Figure 2 – Schema of the layers of the retina, adapted from [30].

1.2.1.1 *Photoreceptor cells*

The photoreceptor (PR) cells are predominantly made up of rods and cones; there are approximately 120 million rods and 60 million cones in each human retina. A third class of photoreceptor, the photosensitive ganglion cell, is involved in the regulation of circadian rhythms and the pupillary response. Rods function best in dim light and are responsible for producing images of varying shades of black and white; cones function better in bright light and are responsible for colour vision and resolution of fine detail. Rods are absent at the fovea, rising in number towards the retinal periphery, with their highest density at 20° eccentricity; cones are most dense at the fovea, and their numbers decrease at the retinal periphery [31]. Each PR cell is comprised of photoreceptor elements and a cell body containing the nucleus, which makes contact with the dendrites of the bipolar cells via a synaptic terminal, termed the spherule or the pedicle in rods and cones, respectively.

The photoreceptor portion of the rods and cones is anatomically divided into an inner segment (IS) and outer segment (OS). The IS contains cellular organelles and connects with the cell body. Its main function is to provide ATP for sodium-potassium pumps. The outer segments (OSs) interdigitate with the RPE cells and are considered to be modified sensory cilia, which are structures present in many aspects of sensation. In rods, the OS contains the photosensitive pigment rhodopsin, within membrane-bound lamellae, or discs, stacked tightly along the microtubule-based axoneme. These discs are unconnected to the plasma membrane. The axoneme is derived from and anchored to the cell via the basal body and enters the OS via the transition zone (or the ‘connecting cilium’) (Figure 3) [32]. A separate structure, also arising from the basal body, the ciliary rootlet, extends into the inner segments, through the cell body and into the synapse. The rootlet serves to anchor the cilium to the cell and functions as a channel for proteins destined for the outer segment. The outer segment and its cytoskeleton, including the rootlet, basal body and axoneme, are collectively called the ‘photoreceptor sensory cilium complex’, and have been implicated in the pathogenesis of a number of retinal dystrophies [33].

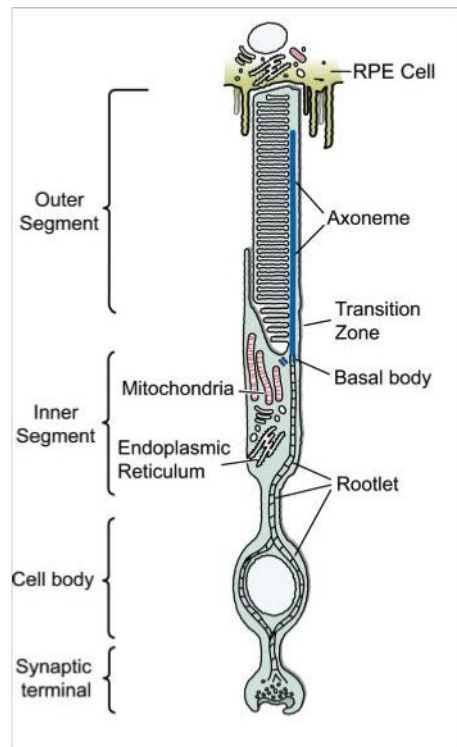


Figure 3 – Rod Photoreceptor. Adapted from [32].

The cone outer segment is conical, and considerably wider than a rod at its base, tapering down to a rounded tip. The membranes of the transversely arranged discs are continuous with the outer plasma membrane, which is arranged as a series of invaginations. Thus, unlike the rods, the laminae of the discs are continuous with the extracellular space, although the photosensitive pigments continue to be incorporated into the disc membranes. Cones also possess a connecting cilium, a photoreceptor sensory cilium complex and inner segment similar to the rods (Figure 4).

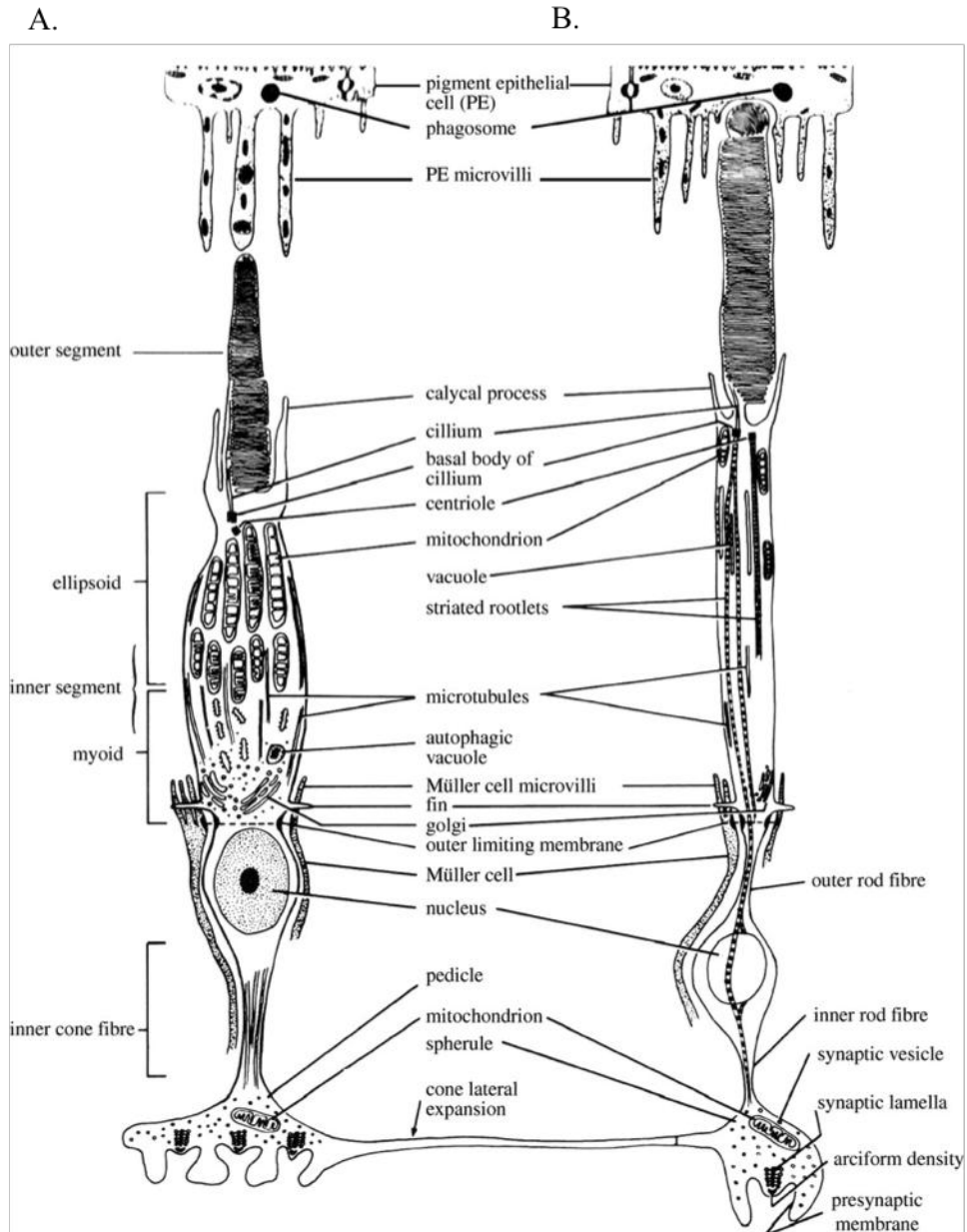


Figure 4 – Comparison of cone and rod photoreceptor anatomy. A – mammalian cone photoreceptor; B – mammalian rod photoreceptor. Adapted from [34].

Light absorption within the OSs of both rods and cones is achieved by pigments, known as opsins, which are G-protein coupled receptors that require a bound chromophore to absorb photons. There are 3 types of cones, each with sensitivity to a specific wavelength of light, depending on its iodopsin pigment: L cones (these absorb long wavelengths of light), M cones (which absorb medium wavelength light)

and S cones (which absorb short wavelength light). PR cells maintain a roughly constant length by continually generating new OSs from their base while simultaneously releasing mature OSs, that are engulfed and phagocytosed by the RPE [35].

1.2.1.2 Neural cells

The retinal nerve cells include the bipolar, ganglion, horizontal and amacrine cells. The bipolar cells are entirely contained within the retina and are orientated perpendicular to the retinal surface. They connect the PRs to the ganglion cells, and are post-synaptic to the PRs. There are many different types of bipolar cells, which are named according to their synaptic connections. These include rod bipolar cells, which connect several rod cells to 1-4 ganglion cells; diffuse bipolar cells, which connect many cone cells to many ganglion cells; and midget bipolar cells, which connect a single cone cell to a single midget ganglion cell, and thus provide a direct pathway from a cone to a single optic nerve fibre.

The ganglion cells are multi-polar and have dendrites that synapse with the bipolar cells and amacrine cells. The non-myelinated axons become the nerve fibre layer within the retina and converge at the optic disc to become the optic nerve fibres, which become myelinated after exiting the globe via the lamina cribrosa. The ganglion cells are the second order neurons in the visual pathway, and in most of the retina they form a single layer. However, from the periphery of the retina to the macula there may be as many as 10 layers; but these then decrease in number towards the fovea, where they are absent.

The horizontal cells are the laterally inter-connecting neurons within the outer plexiform layer. They are multipolar and have one long and several short processes that run parallel to the retinal surface. Those that are associated with cones have short processes that synapse with several cone pedicles; those associated with rods have short processes synapsing with 10-12 rod spherules. The long processes make contact with distant rods and cones, and with bipolar cells. They function in an inhibitory manner: following light excitation of the PRs, horizontal cells release an inhibitory neurotransmitter, gamma-aminobutyric acid (GABA), that inhibits bipolar cell activity some distance away, thus sharpening contrast and increasing spatial resolution.

The amacrine cells have long processes that radiate widely horizontally, and synapse with one another and with the dendrites of ganglion cells and axons of bipolar cells; they comprise the inner plexiform layer. There are many types of amacrine cells that each release a specific neurotransmitter – up to 30 different types are reported [36]. Their functions are variable but still incompletely resolved, and include: a role in generating contextual effects for the responses of the retinal ganglion cells, such as ‘centre surround’ antagonism and motion detection; vertical signal integration, such that they communicate across some, if not all of the inner plexiform layer, carrying ON information into OFF layers and vice versa; specific cell types that may be stimulated by bipolar cells, and in turn stimulate the ganglion cells; and modulation of PR signals. Amacrine cell function is the subject of much current investigation.

1.2.1.3 *Supporting cells*

The retinal supporting cells, comprised of Müller cells, are similar to other neuroglial cells. They fill up most of the neural retina that is not occupied by the neurons. Müller cell bodies lie in the inner nuclear layer and project processes in both directions to form the inner limiting membrane (at the vitreous surface of the neural retina) and the external limiting membrane (between the PRs and the Müller cells). Müller cells have been identified to possess a number of functions including: homeostatic and metabolic support of the retinal neurons; control of the composition of the extracellular matrix; trophic and anti-oxidative support; regulation of the blood retinal barrier; regulation of the synaptic activity within the inner retina; ‘guiding’ of light through the inner retina to minimise light scattering; and modulation of neuronal activity [37].

1.2.2 The retinal pigment epithelium

The retinal pigment epithelium (RPE) is a monolayer of cells lying beneath the neurosensory retina, whose apical membrane lies adjacent to the PR OSs, and basolateral membrane is in contact with Bruch’s membrane [38]. In tangential section, the cells are hexagonal. The apical ends of the cell show multiple microvilli that project between and surround the PR OSs. The adjacent cell membranes are bound together in the basal region by the zonula adherens and in the apical region by the zonula occludens. These are formed by tight junctions that maintain the blood retinal barrier. The cytoplasm of RPE cells contains numerous melanin granules that extend into the microvilli, a well-developed Golgi apparatus and endoplasmic reticulum, and multiple lysosomes and phagosomes. The apical microvilli continually erode the PR OSs, the RPE cells phagocytose the resultant debris and lysosomes break down the

contents of the phagosomes to produce lipofuscin granules. The RPE has a wide range of functions including phagocytosis of photoreceptor OSs; absorption of light to reduce the effects of photo-toxicity; repair of DNA, proteins and lipids; transport of nutrients and ions between the retina and the choriocapillaris, including retinoids essential to the visual cycle; regeneration of 11-*cis* retinal during the visual cycle; secretion of growth factors and factors necessary for maintenance of the structural integrity of the retina and choriocapillaris; and maintenance of the blood retinal barrier [35, 38]. Dysfunction of the RPE is implicated in a number of retinal dystrophies and in age related retinal degenerations.

1.2.3 The phototransduction cascade

Visual phototransduction is the process by which photons of light are converted to an electrical signal within the eye, via G-protein coupled receptors within the PRs called opsins that are bound to the chromophore 11-*cis* retinal. 11-*cis* retinal is a derivative of all-*trans* retinol (a vitamin A analogue), which is obtained through the diet. The chromophore is bound to the opsin by a Schiff base bond, and when exposed to a photon of light, undergoes photoisomerisation to all-*trans* retinal, which changes the conformation of the opsin G-protein coupled receptor. This initiates a signal cascade that eventually results in hyperpolarisation of the PR cell. 11-*cis* retinal is subsequently regenerated via a process known as the ‘visual cycle’ in rods and cones but there is evidence to suggest that an additional, alternative visual cycle for cones also exists.

PRs are maintained in a depolarised state in the absence of a stimulus. A high density of sodium-potassium pumps allows the cell to maintain a steady concentration of Na^+ and K^+ . In scotopic conditions, cyclic guanosine monophosphate (cGMP) gated Na^+ channels remain open, allowing a continuous influx of Na^+ into the cell, which keeps it depolarised at around -40 mV. This is known as the dark current. Depolarisation of the cell leads to the opening of voltage gated Ca^{2+} channels and the subsequent increase in intracellular Ca^{2+} levels causes release of the neurotransmitter glutamate, which hyperpolarises ON-bipolar cells and depolarises OFF-bipolar cells. In photopic conditions, PRs hyperpolarise to a potential of -60 mV; this 'switching off' of the depolarised state leads to a signal cascade that activates the neural pathway, as follows. When a photon of light reaches the PR, photoisomerisation of 11-*cis* retinal to all-*trans* retinal causes a change to the opsin binding site (Figure 5 – B, phototransduction cascade). Thus, rhodopsin (in rods) or cone opsin absorbs a photon of light and undergoes a conformational change to its active form, metarhodopsin II [39, 40]. Metarhodopsin II binds to transducin, a G protein within the membrane of the discs, and there is an exchange of guanosine triphosphate (GTP) for guanosine diphosphate (GDP). This leads to activation of phosphodiesterase (PDE), which hydrolyses cGMP to GMP. The reduction of cGMP leads to closure of Na^+ channels, which causes hyperpolarisation of the cell due to the on-going potassium current via non-gated K^+ channels. Hyperpolarisation of the cell leads to closure of voltage gated Ca^{2+} channels, causing a reduction in intracellular Ca^{2+} . Subsequent reduction in glutamate release results in depolarisation of ON-bipolar cells and hyperpolarisation of OFF-bipolar cells.

Deactivation of the phototransduction cascade occurs by activation of guanylate cyclase activating protein in response to falling Ca^{2+} levels. This activates guanylate cyclase, which converts GTP to cGMP and reopens Na^+ channels. Metarhodopsin II is deactivated: recoverin, a Ca^{2+} bound protein is normally bound to rhodopsin kinase when Ca^{2+} is present; when Ca^{2+} levels fall during phototransduction, it dissociates from recoverin, rhodopsin kinase is released and metarhodopsin II is phosphorylated to its inactive state metarhodopsin III, which reduces its affinity for transducin. Arrestin binds to metarhodopsin III, completely deactivating it, and the dark current is restored. Metarhodopsin III dissociates into opsin and all-*trans* retinol [41]. All-*trans* retinol subsequently enters the visual cycle (see section 1.2.4), and opsin binds with regenerated 11-*cis* retinal to reform the visual pigment [42]. Proteins involved in phototransduction are synthesised in the inner segments of the photoreceptors and are then translocated through the connecting cilium to the outer segments. However, there is evidence that cones may be able to regenerate cone pigment using the Müller cells in the alternative visual cycle (see Section 1.2.4).

1.2.4 The visual cycle

When photoactivated chromophore-bound opsin releases the toxic aldehyde all-*trans* retinal in the photoreceptor OS, it is converted to all-*trans* retinol by a number of retinol dehydrogenases, including RDH8, RDH12 and RETSDR1 (a cone specific dehydrogenase) [43, 44] (Figure 5 – A, retinoid, or visual, cycle). All-*trans* retinol is then removed from the OS and transferred to the RPE across the interphotoreceptor matrix (IPM), facilitated by interphotoreceptor binding protein (IRBP), where it then can be recycled to 11-*cis* retinal via a series of steps, as follows. All-*trans* retinol is

first esterified by lecithin retinol acyltransferase (LRAT) to form all-*trans* retinyl esters; the retinoid isomohydrolase activity of RPE65 then acts on the retinyl ester substrates to form 11-*cis* retinol; retinol dehydrogenases, predominantly RDH5, but also RDH11, facilitated by RLBP1 [43] [45], then oxidise 11-*cis* retinol to produce 11-*cis* retinal, which is transported out of the RPE cell by IRBP into the photoreceptor OSs where it combines with opsin to re-form visual pigment [41].

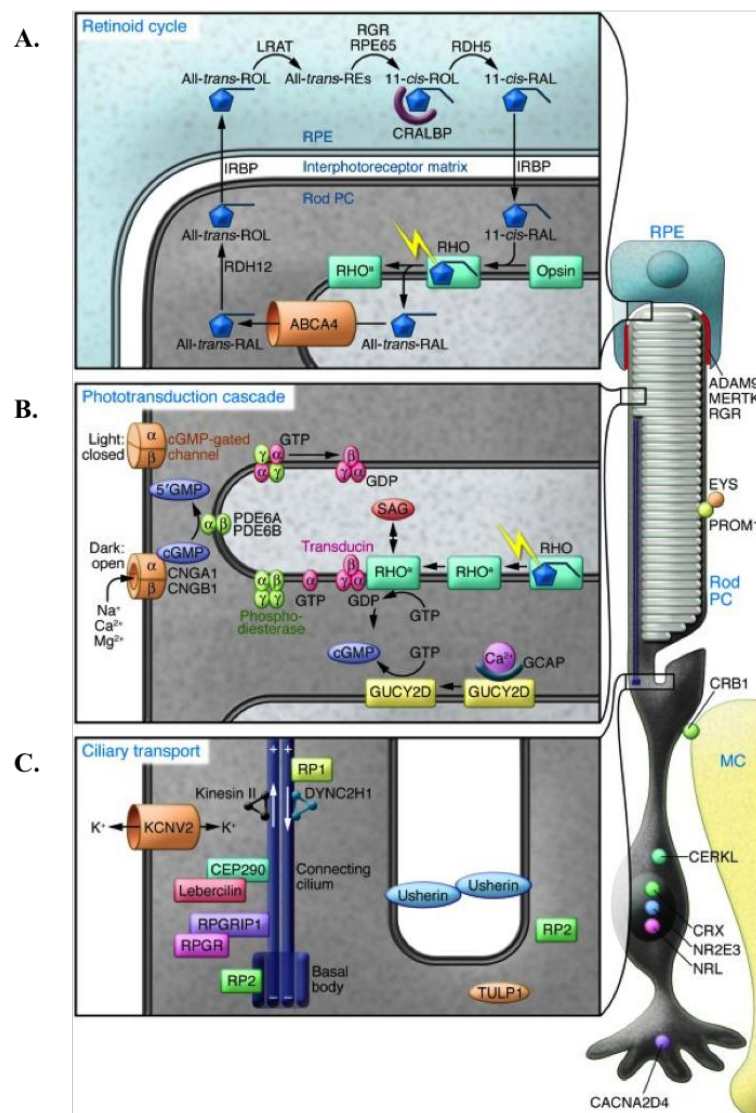


Figure 5 – Processes in human rod and RPE cells. Adapted from [46]. A – Retinoid or Visual cycle; B – phototransduction cascade; C – ciliary transport.

In addition to this ‘classical’ visual cycle, a cone-specific ‘alternative’ visual cycle exists to provide cones with an additional privileged source of 11-*cis* retinol, which they can utilise to regenerate cone pigment [40, 41, 47]. The existence of this additional pathway was proposed following observations that cones recover their sensitivity following bleach much more quickly than rods, and that cones cannot be completely saturated even in bright light [48]. This pathway is likely to occur in Müller cells as it has been observed that they are able to take up all-*trans* retinal and release 11-*cis* retinol, which cones are able to gain access to via 11-*cis* retinol dehydrogenase activity, which is not present in rods [49]. The proposed alternative pathway is likely to occur as follows. After photolysis, all-*trans* retinal is reduced to all-*trans* retinol in cone outer segments, which is released and transported across the interphotoreceptor matrix (IPM), possibly by IRBP, to the Müller cells [41]. Here, bound to cellular retinol binding protein, all-*trans* retinol is isomerised to 11-*cis* retinol, which is then released into the IPM. It is then transported to cone photoreceptor inner segments, possibly utilising IRBP, and moves freely to the OS. Here, it is oxidised to 11-*cis* retinal by an unknown 11-*cis* retinol dehydrogenase and/or utilising a retinal – retinol redox coupling reaction to regenerate pigment [43, 50].

1.3 Techniques for Phenotyping

The phenotyping techniques utilised to assess the effects of specific mutations on ocular structure and function in this study include many that are used in routine clinical practice such as visual acuity testing, assessment of colour vision deficiencies and of refractive error, visual field testing, electrodiagnostic testing and retinal imaging modalities such as optical coherence tomography and fundus autofluorescence imaging. These are reviewed in this chapter. More specialised tests utilised in the investigation of specific genetic subtypes will be described in the appropriate chapters.

1.3.1 Visual Acuity

There are references in antiquity suggesting that the ‘sharpness of vision’ could be measured by the ability to resolve double stars, and from the 17th century by Daça de Valdes, who described a method based on the ability to resolve mustard seeds, but the first convincing arguments for the standardisation of vision tests were not made until 1843 by Kuechler, who developed 3 vision charts to avoid memorisation. Unfortunately these did not gain popularity. In 1854 Jaeger published near vision reading plates and in 1861 Donders proposed a measurement of the ‘sharpness in vision’ while undertaking his studies on refraction and accommodation. A year later his co-worker Herman Snellen published his standardised acuity charts that soon became adopted worldwide.

Visual acuity is a measure of the ability to discriminate two stimuli separated in space. It is measured at high levels of illumination and at high contrast, and although it reflects only a small part of an individual's visual performance, it is traditionally the most widely used measure to describe the functional capacity of the eye.

Snellen notation is the most frequently used when measuring acuity. It consists of black letters ('optotypes') on a white, brightly lit background, each of which subtends an angle of 5 minutes of arc and the space between each optotype subtends 1 minute of arc. Conventional test charts contain about 10 lines of letters in a progression of sizes, each designated by the distance at which the overall height of the letters on that line continues to subtend 5 minutes of arc, with the width of each 'limb' of the letter subtending 1 minute of arc. The acuity is recorded as a 'fraction' in which the numerator is the recording distance (in meters or feet), and the denominator is the distance at which the letter subtends the standard visual angle of 5 minutes of arc. Thus, on the 6/6 line (20/20 in feet), the letters subtend an angle of 5 minutes of arc when viewed at 6 m, and on the 6/12 line (20/40), the letters subtend an angle of 10 minutes of arc when viewed at 6 m, or 5 minutes of arc when viewed at 12 m.

Snellen charts, however, posed a number of problems including the observation that the optotypes are not related to each other by geometric progressions in size, and that there are different numbers of letters per line. Thus, other charts have been developed, such as the Bailey-Lovie (or ETDRS) chart [51]. In this chart, LogMAR notation is used, which provides a measure of visual acuity known as the Logarithm of the Minimal angle of Resolution (LogMAR). The sizes of the letters progress systematically in geometric progression, each letter carries a value of 0.02 LogMAR

and there are 5 letters per line (Figure 6). Thus, each line represents a change in acuity by 0.1 LogMAR and acuity doubles every third line. 0.00 LogMAR is equivalent to 6/6 Snellen acuity and 1.0 LogMAR is equivalent to 6/60 Snellen acuity. The Snellen fraction can also be converted to the minimum angle of resolution, and the base-10 logarithm of this (LogMAR) determined [52]. This has allowed the standardisation of measurements such as counting fingers and hand movements to be denoted as 2.0 LogMAR and 3.0 LogMAR respectively. Perception of light (PL) and Nil Perception of Light (NPL) vision are arbitrarily denoted as 5.0 LogMAR and 6.0 LogMAR respectively [53]. Both the Snellen and Bailey-Lovie charts rely on the literacy of the subject being tested, and require the detection, resolution and recognition of the letters, and then the relaying of this information to the examiner.

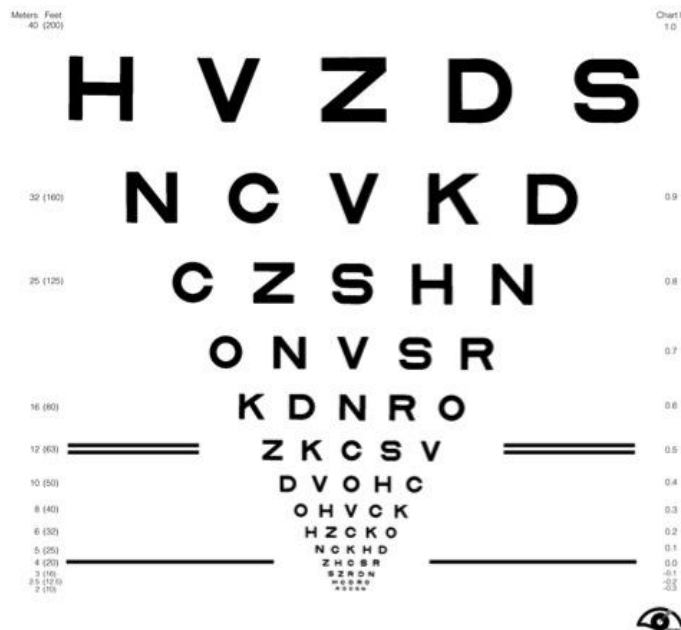


Figure 6 – ETDRS visual acuity chart. LogMAR acuity scale is on the right and equivalent Snellen acuity on the left.

1.3.1.1 Visual acuity testing in children

In young children and infants, the above methods are not possible. Letter matching tests in which the child can point to letters on a key card once they recognise the letter they are shown, most closely relate to the Bailey-Lovie test. Examples of these include the Sheridan Gardiner test, the Sonksen-Silver acuity system and Cambridge crowding tests, among others. Some tests are ‘pictorial’, where the child is asked to name or match the pictures shown to them, such as the Kay Picture Test, although this test tends to underestimate the visual acuity. ‘Preferential looking’ may be used to estimate the visual acuity in infants and non-verbal children who cannot complete letter/picture matching. It is based on the observation that infants would rather look at a pattern than a blank stimulus. Such tests include the Teller and the Keeler acuity cards, which consist of a series of large grey cards with a central peephole that have a black and white grating of specific frequencies on one side. The cards are shown to the child and their preference recorded. However, although these tests attempt to provide a measure of visual acuity, they do not equate to Snellen vision. The Cardiff Acuity test, another example of a preferential looking test, uses ‘vanishing optotypes’ which consist of pictures with increasingly fine outlines that are correspondingly difficult to see. In the youngest infants (from age 3 months), the objective is to determine whether they have the ability to steadily fixate and follow an object, and at the same time assess if they have any nystagmus or a manifest strabismus. Another crude method of assessing acuity is to measure the optokinetic response in an infant, which should be present before age 3 months. This can be performed using an OKN drum or tape.

1.3.2 Colour Vision

There are a number of tests available that test colour vision, most of which have been designed to assess inherited, rather than acquired, colour vision defects. Some are designed to detect more subtle colour deficiencies and may be more appropriate in the research setting. In the clinical setting, the Ishihara pseudoisochromatic test plates and Hardy Rand Rittler tests are the most widely available and the easiest to use to screen for colour vision deficits.

1.3.2.1 Ishihara Pseudoisochromatic Plates

The Ishihara Test (Handaya, Tokyo, Hongo Harukicho, 1917) was designed to detect protan (red) and deutan (green) colour vision deficiencies and has high sensitivity and specificity. There are a number of editions: the full 38-plate edition, an abridged 24-plate edition and a 14-plate edition for quick screening. In all editions the first plate is a 'test plate'; there are up to 20 numerical plates to screen for red-green colour deficiencies; and 4 plates to distinguish between protan and deutan deficiencies (Figure 7 – A). Errors on three or more of the numerical plates indicate a red-green colour vision deficit, with a small chance of misdiagnosing the deficit (2%); five or more errors signify certain red-green deficit [54]. However, specificity of the plates designed to distinguish between the colour deficits is reduced in 30%-40%. In addition, Ishihara test plates do not detect tritan defects. Nevertheless, it is a useful screening test in the clinical setting due to its speed and ease of use.

1.3.2.2 *Hardy Rand Rittler Pseudoisochromatic Plates*

The Hardy Rand Rittler test not only allows the identification of protan and deutan colour defects, but it is also able to test for tritan (blue) defects [54]. It is almost as sensitive and specific as the Ishihara test, and has the additional benefit of being able to test younger children who do not yet know numbers, but who can identify shapes. It can distinguish between the different colour axes, and grade the defects into mild, moderate and severe. Aside from the 4 introductory plates, there are 4 red-green screening plates that identify a definite red-green colour deficit if errors are made on 3 or 4 of these; and there are 2 tritan screening plates (Figure 7 – B). Depending on the number of subsequent plates that are read incorrectly (of which there are 14), the colour vision deficit can be described as mild, moderate or severe.

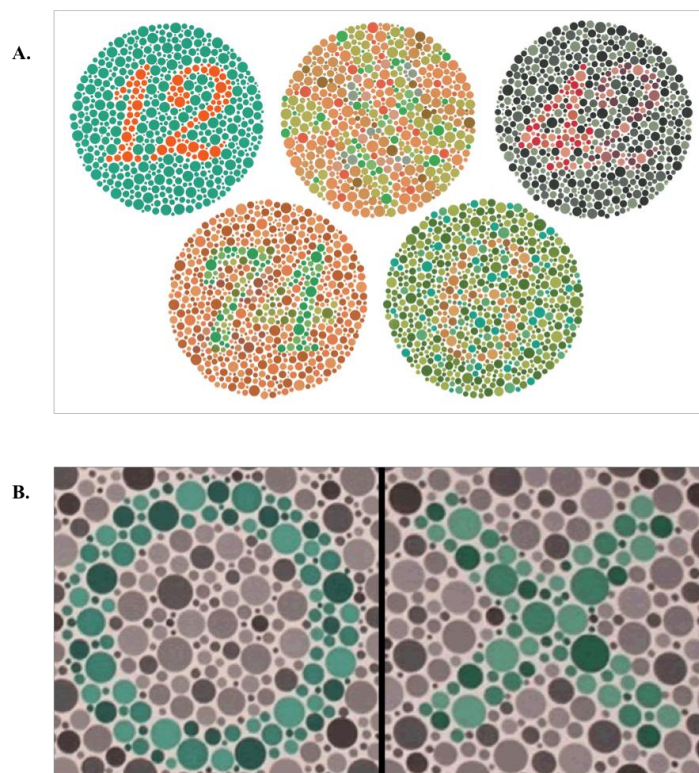


Figure 7 – Tests of Colour Vision. A – Ishihara pseudoisochromatic plates; B – Hardy Rand Rittler pseudoisochromatic plates.

1.3.2.3 *Other tests of colour vision*

The Nagel anomaloscope was introduced in 1907 and incorporates a Maxwellian view spectroscopy in which the field of view is split into two halves, one that is illuminated by monochromatic yellow (589 nm), and the other that is illuminated by a mixture of monochromatic red (670 nm) and green (546 nm) wavelengths. The subject first makes several exact colour matches by adjusting both the red-green mixture ratio and the luminance of the yellow test field. In a second step the examiner sets the red-green mixture ratio and the subject ascertains whether an exact match can be made, by altering the luminance of the yellow test field. Normal trichomats precisely match the colours within a small range of red-green mixture ratios. As protanopes and deuteranopes have only one photopigment in the spectral range that is provided by the instrument, they are able to match any red-green mixture ratio with yellow by adjusting the luminance of the yellow comparison field. Protanomalous trichromats obtain matching ranges with an excess of red and deuteranomalous trichromats obtain matches with an excess of green in the matching field. A scale is used to record readings with a red-green x-axis and yellow y-axis [55, 56].

The Farnsworth-Munsell 100 hue test is a hue discrimination test in which the subject is required to arrange small coloured caps according to hue, lightness and saturation. All the colours are presented at the same time and the subject asked to arrange them in what they perceive to be a natural order. The results are plotted on a polar diagram representing the 85 hues of the test, and a score for each colour cap is plotted on the radial line of the polar diagram representing the numbered cap [55]. This test is useful for moderate or severe colour vision deficiency.

1.3.3 Refractive Error

The refractive power of the eye is determined by four factors and their interactions: corneal steepness, depth of the anterior chamber, power of the lens (determined by its thickness and curvature) and axial length of the eye. In situations of refractive error, or ametropia, the error may be spherical or there may be astigmatism. In simple myopia, an image is formed in front of the retina (in essence the myopic eye has an optical system too powerful for its axial length) and in hypermetropia, the image forms behind the retina. Thus, spherical corrective lenses must be placed in front of the eye in order for the retinal image to fall on to the retina. In simple astigmatism, light rays do not fall on to one point on the retina due to variations in the curvature of the cornea or lens at 2 different meridians that are perpendicular to each other. Thus, correction is required for both meridians. Determination of the refractive error can be achieved by objective or subjective techniques; automated techniques are also possible, but these tend to be reserved for the screening of refractive errors. In children, objective measurement of the refractive error may be achieved under cycloplegic or non-cycloplegic conditions using retinoscopy.

Most retinoscopes use a 'streak' projection, which allows a straight beam of light to be shone through the pupil; the projected streak illuminates an area of the retina that reflects back towards the examiner. When this beam of light is moved in a sweeping motion, the reflected light will also move in a direction that reflects the refractive status of the eye: it can move in the same direction as the sweeping movement ('with' motion) or in the opposite direction to the sweeping movement ('against' motion). When the light fills the pupil and does not move, a point of 'neutrality' is reached. By using corrective lenses placed in front of the subjects' eye, the 'with' or 'against'

movement can be neutralised (plus lenses are placed if a 'with' movement is seen, minus lenses are placed if a 'plus' movement is seen). This gives a measure of the refractive error. The movement is measured in the 2 principle astigmatic meridians, which are at 90° to each other; thus when measuring refraction, the power in both axes needs to be measured, and the refraction recorded as a spherical optical power in one meridian, with a cylinder placed at the meridian 90° to it. The dioptric equivalent of the distance at which the examiner is working must be removed from the spherical power in order to determine the actual refractive error (usually +1.5 dioptres for a working distance of 67 cm).

Ideally, refraction should be measured with accommodation relaxed, which in a co-operative older subject may be possible by sustained fixation at a distance target during testing. However, in children such co-operation is often not possible, and accommodation can vastly affect the accuracy of measurement. In this situation, cycloplegia is necessary to fully relax accommodation, with the use of cycloplegic drops such as guttae cyclopentolate 0.5% (if below 1 year of age) or guttae cyclopentolate 1% (older than 1 year).

1.3.4 Psychophysical testing - Perimetry

Testing of the visual field can be achieved using either kinetic stimuli (kinetic perimetry), eg with the Goldmann Perimeter, or static stimuli (static perimetry). Both of these methods of perimetry rely upon sustained fixation on a central target, which can be challenging in children and in subjects with reduced central vision, such as those with retinal dystrophies.

1.3.4.1 Kinetic Perimetry

In kinetic perimetry a moving stimulus of known luminance and size is presented at various points in the visual field from an area outside the boundary of visual perception towards fixation. The patient indicates when the target is first seen, and the perimetrist plots this point. When successive points have been plotted they can be 'joined' together, producing a line of equal threshold sensitivity, known as the 'isopter'. Successive isopters may be plotted using stimuli that vary according to size and light intensity.

The most common type of manual kinetic perimeter is the Goldmann perimeter, which consists of a spherical bowl, whose luminescence at 31.5 asb is precisely controlled to allow constant retinal light adaptation, and a self-illuminated projection arm that allows the presentation of different stimuli. Assessment of maintained fixation is achieved by the perimetrist monitoring the subject's eye through a telescope while projecting moving spots of constant size and fixed contrast from the periphery into the centre. The size and intensity of the test stimulus is set using four levers – one that determines size and three for intensity. Roman numerals denote stimulus size (I-V): size I (with no interposed intensity filters) is the standard maximum stimulus, equivalent to 1,000 asb in intensity; increasing intensity is simulated by switching to larger stimulus sizes so that changing from size I to V is the equivalent of a 100-fold increase in intensity. Arabic numbers (1-4) denote the stimulus intensity: as the numbers increase, the stimulus intensity increases by 0.5 log units; position 4 is unfiltered. A letter is also used to indicate intensity (a-e); each stop increases the stimulus intensity by 1 dB from a to e, with e being unfiltered. The third stimulus lever has 3 positions; furthest to the right has no filter and it is in this

position that this lever is usually kept. The standard stimulus is size I with filters fully off, and is represented as I4e. The test requires considerable skill of the perimeter to map the visual field, and due to this, and the potential of prolonged testing time, there can be significant interobserver variability in the results obtained from Goldmann perimetry. Testing of the visual field using the Goldmann perimeter should be performed using both dynamic and static methods, and aside from mapping isopters as described above, it is important to map any scotomata that may be present within the field, for example in subjects with retinal dystrophies. The original Goldmann Field Analyser was manufactured by Haag-Streit (Bern), but this is no longer in production; automated kinetic perimeters have now superseded the original manual versions.

The progression of visual field abnormalities in RP has been investigated using the Goldmann perimeter, and visual field defects have been categorised into four different patterns: progressive concentric loss of the visual field; field loss beginning in the superior visual field and progressing to an arcuate scotoma; a complete or incomplete peripheral 'ring scotoma' that can break through into the periphery; and 'end stage' visual field defects in which only a small central visual field is retained, with possible additional peripherally preserved islands of vision [57]. The plotting of Goldmann visual fields may be quite challenging and requires a skilled and experienced perimetrist. In addition, in these subjects an appropriate period of light adaptation is required before testing commences, the test-retest variability is high and nystagmus can add to the variability of the results [58].

1.3.4.2 *Static Perimetry*

In static perimetry stationary stimuli are presented at defined points in the visual field. Although static perimetry can be measured using manual techniques including with the Goldmann perimeter, most static perimetry is carried out now using automated techniques using machines such as the Humphrey Visual Field Analyser (Carl Zeiss Meditech, Dublin, CA, USA). The benefit of automated perimetry is that both the stimulus presentation and the recording of patient's results can be standardised, with more detailed, reproducible, quantitative results that do not require a skilled perimetrist. The presented stimulus at a given point in the visual field changes in intensity until the sensitivity of the eye at that point is found. Testing involves the use of threshold or suprathreshold algorithms at a choice of degrees of eccentricity of the visual field, either monocularly or binocularly. In a full threshold strategy, a suprathreshold stimulus is presented at each location based on the threshold values determined from prior points. The intensity is decreased at fixed 4 dB increments until the stimulus is no longer seen, and then increased at fixed 2 dB increments until it is seen again. The threshold value is the intensity of the last stimulus seen at that location. This algorithm can take some time, and requires cooperation and concentration. The suprathreshold strategies are screening tests and are quick to perform, and calculate the threshold adjusted for age by measuring a few predetermined points using a 4-6 dB step.

1.3.4.3 *Perimetry in children*

Visual field testing in children can be challenging as it relies upon the child's cooperation, which can be hampered by fatigue, a lack of concentration and a lack of

comprehension of the test. In older children automated techniques may be successfully performed. However, in younger children testing often relies upon confrontation techniques using interesting colourful targets presented in the peripheral visual field that the child will make a saccadic movement to see.

1.3.5 Additional psychophysical tests

Detailed psychophysical tests may be used to investigate rod and cone function, such as dark adapted perimetry, dark adapted spectral sensitivities and cone critical flicker fusion tests. These tests are not used routinely and tend to be reserved for the research setting. They were used in the *LRAT* subjects in this study and will be explained further in chapter 4.6.

1.3.6 Electrophysiology

The objective measure of visual pathway function is achieved through visual electrophysiological testing, and such testing is fundamental to the diagnosis of all retinal dystrophies. It allows the assessment of the nature and severity of visual dysfunction, which may or may not be evident through clinical ocular examination. It is particularly useful in children, in whom subjective measures of visual dysfunction may not be accurate or possible. The main test armamentarium includes: the electro-oculogram (EOG), which measures retinal pigment epithelium (RPE) function, and its relationship with the rod photoreceptor; the full-field electro-retinogram (ERG), which measures the massed retinal response to light, and is a measure of

photoreceptor and inner nuclear layer function; the pattern electro-retinogram (PERG), which arises from retinal ganglion cell function and can give a measure of the macular function; and the visual evoked potential (VEP), which measures the function of the intracranial visual pathways. The International Society for Clinical Electrophysiology of Vision (ISCEV) regularly publishes minimum standards (and updates) to establish standardised worldwide protocols for electrophysiological examinations (<http://www.iscev.org/standards/>).

1.3.6.1 *The ISCEV standard Electro-Oculogram*

In this test, changes in the electrical potential across the RPE are measured during successive periods of dark and light adaptation [59]. The difference in electrical potential between the cornea and the posterior pole of the eye is known as the standing potential. This potential is generated by the RPE and it changes in response to the background retinal illumination. When switching to darkness, the potential continues to decrease for 8-10 minutes; there is then an initial fall in the standing potential over 60-75 seconds when the retina is subsequently illuminated (the fast oscillation), and then a slower but larger rise over 7-14 minutes (the light response). These changes are generated by changes in permeability of ion channels across the RPE basal membrane, which are (in part) encoded by the Bestrophin-1 (*BEST1*) gene.

When measuring the EOG, the amplitude of the standing potential is measured in the dark, and then again at its maximum amplitude in the light, with electrodes placed at the medial and lateral canthi. This is done by the patient making fixed 30° lateral eye movements during a period of 20 minutes dark adaptation, and then again during a 15

minute period of light adaptation. Eye movements are made every 1-2 seconds for 10 seconds every minute. The ratio of the maximum (peak) amplitude in the light to the minimum (trough) amplitude in the dark is expressed as the 'Arden' ratio (EOG light rise or light/dark ratio) and a normal EOG light rise is greater than 175%. This test is relatively difficult to perform and may not be possible in children below the age of 10 years. The principal use for the EOG in clinical practice is in the diagnosis of Bestrophin related conditions. It may also be used in inflammatory conditions of the choroid and retina.

1.3.6.2 The ISCEV standard Electro-Retinogram

The full field ERG (ffERG) represents the combined electrical activity of different cells of the retina to uniform illumination. This is measured using corneal electrodes and an integrating sphere, the Ganzfeld bowl, to deliver stimuli with whole field illumination. The ISCEV standard specifies 5 responses: (1) dark adapted 0.01 ERG (rod response); (2) dark adapted 3.0 ERG (combined rod-cone response); (3) dark adapted 3.0 oscillatory potentials; (4) light adapted 3.0 ERG (cone response); and (5) light adapted 3.0 flicker (30Hz flicker) [60]. An additional 'maximal' ERG is also undertaken in the dark adapted state. Measurements are taken with pupils pharmacologically dilated, and dark adapted ERGs are measured after 20 minutes dark adaptation, and light adapted ERGs after 10 minutes light adaptation. For the 'maximal' ERG, an 11 cd.s.m^{-2} flash is presented in the dark adapted state. The stimuli presented to attain the other responses range from a dim white flash of 0.01 cd.s.m^{-2} (dark adapted 0.01 ERG) to a bright white flash of 3.0 cd.s.m^{-2} on a dark adapted background (dark adapted 3.0 ERG) or 30 cd.s.m^{-2} background luminance

(light adapted 3.0ERG). In the 3.0 flicker ERG the same 3.0 cd.s.m⁻² stimulus is presented at a rate of 30 stimuli per second (30Hz), on an illuminated background.

The maximal ERG has an (negative) a-wave, the initial 8-10ms of which predominantly reflects rod photoreceptor hyperpolarisation. The subsequent (positive) b-wave is generated post-receptorally, secondary to depolarisation of the ON-bipolar cells. The oscillatory potentials are small oscillations on the ascending limb of the b-wave and are thought to arise from the amacrine cells. Rod system dysfunction will be seen as a reduction in the rod specific ERG b-wave, but this is generated in the inner nuclear layer so does not localise disease to the photoreceptors themselves. The maximal response a-wave does allow localisation as it is predominantly driven by rod photoreceptor function. If the rod response is poor, it could reflect either an ON-bipolar abnormality or poor rod photoreceptor function, so the bright flash maximal response in the dark adapted state needs to be measured. If it is a bipolar problem then the a-wave will be normal or near normal (an 'electronegative' ERG); if it is a rod photoreceptor problem then both the a and b waves will be reduced.

A cone-specific waveform, generated at the inner retinal level, is recorded when the 30Hz flicker is presented on a rod-suppressing background (in the light adapted state). The single flash cone response allows better localisation within the retina, with the photopic a-wave reflecting cone photoreceptor and OFF-bipolar cell hyperpolarisation, and photopic b-wave reflecting post-phototransduction activity. As the ERG is a massed retinal response, disease isolated to one part of the retina, eg the macula, will have a normal ERG.

1.3.6.3 *Other electrodiagnostic tests*

ISCEV have published standards on a number of other electrodiagnostic tests [61-63].

The Pattern ERG (PERG) assesses the retinal response to a contrast-reversing stimulus such as a black and white checkerboard, when the eyes are fixated centrally, and provides information regarding macular and retinal ganglion cell function [61].

The PERG waveform consists of a small initial negative waveform of 35 ms peak time (N35), followed at 45-60 ms by a large positive waveform (P50) and then a large negative component at 90-100 ms (N95). This is a 'transient' response that is complete before the next contrast reversal. The amplitudes of the PERG are measured from the peaks to the troughs of the waveform. The N95 component arises in relation to the retinal ganglion cells; the P50 component reflects macular function. In contrast to the ff-ERG, the PERG is a local response to the area that is covered by the stimulus image, and thus can sensitively indicate macular dysfunction. It can also be used in conjunction with the visual evoked potential in order to differentiate a central retinal abnormality from optic pathway dysfunction, when the VEP is abnormal.

The visual evoked potentials (VEP) provide diagnostic information regarding the functional integrity of the visual system. They are the visually evoked electrophysiological signals obtained from electroencephalographic activity of the visual cortex that are recorded from the scalp overlying this area [62]. They are used to assess the intracranial visual pathways, in particular the optic nerves and chiasm. ISCEV have published a range of stimuli and recording conditions including: pattern reversal VEPs and pattern onset/offset VEPs, both elicited by checkerboard stimuli with large 1° (60 minutes of arc) and small 0.25° (15 minute) check sizes; and flash

VEPs, elicited by a brief luminance increment, a flash, which subtends a visual field of at least 20°. Pattern reversal is used for most clinical situations, pattern onset/offset is useful to assess for malingering and in patients with nystagmus, and flash VEPs are used if there is poor cooperation, very poor vision levels or poor optics that make the use of pattern stimuli difficult.

1.3.6.4 Electrodiagnostic testing in children

Electrodiagnostic testing can be essential in the visual assessment and diagnosis of children with visual dysfunction, and can provide an indication of vision levels in non- or pre-verbal children. In very young or premature children it may not be possible to apply adult protocols, and as such they may require non-standard protocols. Most paediatric patients can be tested without anaesthesia or sedation, which is the preferred situation as anaesthesia carries a small risk and also may alter the VEP measurements. Although corneal electrodes may be applied, most young children (particularly between age 3 months to 5 years) will not tolerate them. In these situations, infra-orbital skin electrodes, close to the rim of the lower eyelid, may be used, but consideration must be taken into the variety of physical and physiological factors that can interfere with readings obtained in this manner [64]. Some laboratories advocate the recording of both the ERG and VEP concurrently, using skin electrodes [65]. In this situation, an estimate of gross retinal function (from the ERG) and macular pathway function (from the VEP) in a single recording session lasting 30-40 minutes can be achieved. In LCA, 56% show an un-recordable ERG or VEP; and in 44% no recordable ERG activity is detected but a small, degraded flash VEP is detectable, suggesting some residual retinal and visual pathway function. [66].

1.3.7 Optical Coherence Tomography

Optical coherence tomography (OCT) has become a standard tool in the field of ophthalmology and is a non-invasive method of imaging in which reflected light is used to produce detailed cross sectional and 3-dimensional images of the retina and anterior segment. Initial work relied upon low coherence interferometry to reflect light from biological tissues, which gives ‘time of flight’ information that in turn, yields spatial information about tissue microstructure [67]. The time of flight ‘delay’ from the reflective boundaries and backscattering sites in the tissue being imaged allows the longitudinal location of the reflective sites to be determined. Multiple longitudinal axial scans are performed to acquire a 2-dimensional map of the sample.

Multiple generations of OCT imaging techniques have since been developed. In the early time-domain OCT (TD-OCT), a series of longitudinal cross sections perpendicular or in the coronal plane to the retinal surface were acquired over time, giving depth information and an image resolution of 10-15 μm , but imaging speed was limited by the need for the reference mirrors to move mechanically. TD-OCT acquires approximately 400 axial scans (A scans) per second. More recently, advances have been made regarding image resolution – particularly by the development of high-resolution OCT – and in imaging speed, signal to noise ratio and sensitivity, in ultra-high resolution OCT or spectral domain OCT (SD-OCT), which can achieve a resolution of 2-3 μm [68, 69]. In SD-OCT, the reference mirror remains stationary and the OCT image is obtained either by using a spectrometer as a detector or by varying the narrowband wavelength of the light source over time (swept source). Different echo time delays of light, which produce different frequencies of fringes in the interference spectrum are measured and then a Fourier

transform (a mathematical procedure that extracts the frequency spectrum of a signal) is applied [70]. This method allows measurement of all echoes of light from different delays simultaneously, which dramatically increases speed and sensitivity. Motion artefact is diminished by the increased speed of image acquisition, and 3-dimensional images can be obtained that can give ‘volume scans’ of the retina.

The SPECTRALIS[®] OCT HRA + OCT imaging system (Heidelberg Engineering, Heidelberg, Germany), can obtain images 100 times faster than time-domain OCT (<http://www.heidelbergengineering.com/international/products/spectralis/technology/spectral-domain-oct/>) [71]. 40 000 A scans are acquired per second, and it can combine high resolution, high speed SD-OCT images with, among other modalities, fundus autofluorescence imaging. Image quality is improved by the use of confocal scanning laser ophthalmoscopy (cSLO), which uses laser light to illuminate the retina instead of a white light. Figure 8 illustrates a normal eye imaged using the Spectralis OCT.

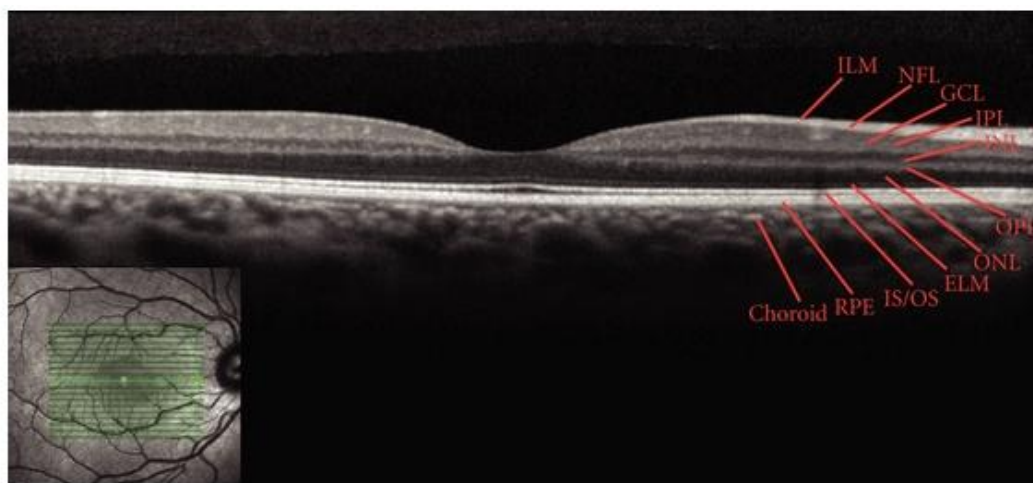


Figure 8 – Normal sd-OCT image. Adapted from [72]. Retinal layers are labelled as follows: ILM – Internal Limiting Membrane; NFL – Nerve Fibre Layer; GCL – Ganglion Cell Layer; IPL – Inner Plexiform Layer; INL – Inner Nuclear Layer; OPL – Outer Plexiform Layer; ONL – Outer Nuclear Layer; ELM – External Limiting Membrane; IS/OS – Inner segment / Outer segment junction; RPE – Retinal Pigment Epithelium; Choroid.

1.3.8 Fundus Autofluorescence Imaging

The retinal pigment epithelium (RPE), a polygonal monolayer of cells between the neurosensory retina and Bruch's membrane (which separates the RPE from the vascular choroid layer), has a number of vital functions, of which the phagocytic role is essential to the renewal of photoreceptors. Phagocytosed outer segment tips are digested in the extensive phagolysosomal system within the RPE cell, and solubilised waste material is transported across the basal in-foldings of the RPE cell into the choriocapillaris. With age, there is an accumulation of lipofuscin pigment, a storage material that accumulates as a result of cell senescence in post-mitotic cells such as neurons, retina and muscles [73]. In the RPE, lipofuscin 'granules' accumulate as a result of incomplete degradation of photoreceptor outer segment discs, with subsequent incomplete release of degraded material [74]. However, lipofuscin also accumulates as a result of a number of retinal disease processes such as age related macular degeneration and certain inherited retinal dystrophies such as Best disease and Stargardt disease [75, 76].

Lipofuscin possesses the phenomenon of 'autofluorescence' – the ability of a substance to emit light of a particular wavelength when illuminated by light of a different wavelength. There are at least 10 different fluorophores (fluorescent compounds) that accumulate within lipofuscin granules in the RPE [77]. One prominent fluorophore is the bisretinoid A2E (*N*-retinyl-*N*-retinylidene ethanolamine), which has toxic properties that may interfere with normal cell function by inhibition of lysosomal degradative capacity, loss of membrane integrity and phototoxicity [78].

In vivo recording of RPE autofluorescence as an index of lipofuscin accumulation can give important clues to the pathogenesis and progress of different retinal diseases. The first fundus spectrophotometer that could exhibit retinal autofluorescence *in vivo* demonstrated that fundus fluorescence has a broad emission spectrum between 500nm to 750nm, with a peak at 630nm and optimal excitation of 510nm [79]. This fluorescence is highest at 7° to 15° from the fovea and decreases towards the periphery, and it was confirmed that lipofuscin is the dominant source of autofluorescence within the retina. In order to address the issues of limitations due to the low intensity of the autofluorescence signal and interference from the crystalline lens, a fundus autofluorescence imaging system using a confocal scanning laser ophthalmoscope was developed [80]. In this system, a focused low power laser beam is swept across the fundus, and the confocal nature of the optics ensures that the reflectance and fluorescence are derived from the same optical plane. In order to reduce background noise and enhance image contrast, a series of several single fundus autofluorescence images are recorded, and a mean image (of 4-16 frames) is obtained after correction of eye movement during image acquisition. Consequently in situations where there is high eye movement, such as nystagmus, fundus autofluorescence image quality may be diminished or not possible. The Heidelberg Retinal Angiograph (HRA; Heidelberg Engineering, Germany) is the predominant commercially available device for measuring fundus autofluorescence, and at the time the work towards this thesis was carried out, the standard images obtained were of a 30° field, but a wider field was possible with a 55° lens. This technology has been combined with SD-OCT imaging, and other retinal imaging modalities [81] in the widely used SPECTRALIS® OCT HRA + OCT imaging system (Heidelberg Engineering, Heidelberg, Germany).

During fundus autofluorescence imaging in normal fundi the optic nerve head and retinal vessels appear dark due to the absence of the RPE and absorption by blood respectively (Figure 9). In the macula, autofluorescence in the fovea is reduced due to absorption by luteal pigments (lutein and zeaxanthin), and increases in the parafovea, but this is still of relative decreased intensity compared to the diffuse background signal in more peripheral retina [80]. This may be due to increased melanin and decreased lipofuscin granules in central RPE cells. Abnormal fundus autofluorescence signals may be due to either increased or decreased amounts or compositions of fluorophores in the RPE cytoplasm, or due to the presence of autofluorescent or absorbing material anterior to the RPE [82]. Autofluorescence is increased with RPE dysfunction and decreased when there is loss of photoreceptors. Media opacity within the cornea, lens or vitreous may also reduce the quality of the recorded image.

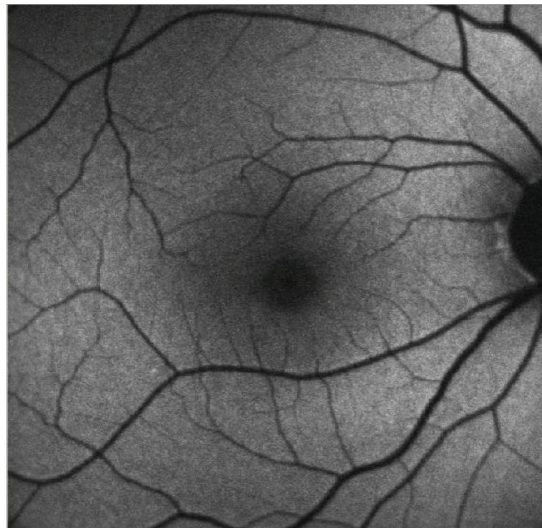


Figure 9 – Normal Fundus Autofluorescence image, right eye.

1.3.9 Fundus Imaging

The unique optical properties of the eye allow visualisation of the retina. The earliest ophthalmoscope was invented based upon principles put forward by Purkinje in 1823, and reinvented by Babbage in 1845 [83]. Von Helmholtz reinvented the direct ophthalmoscope again, in 1851, and Gerloff achieved the first useful photographic recording of the retinal blood vessels in 1891. Reports regarding the first fundus cameras vary: Dimmer in 1905, working with the Zeiss company developed a reflex free fundus camera; in 1910 a fundus camera was developed by Gullstrand; and in 1925 the Zeiss-Nordenson camera became a widely used fundus camera. Modifications to the imaging techniques led to the development of stereoscopic fundus imaging [84] and now, high-resolution digital fundus photography is the routine method by which the retina is photographed.

1.4 Techniques for Molecular Analysis

The genetic heterogeneity underlying LCA and EORD makes the process of identifying causative mutations in these families challenging. Various techniques have been utilised over time to refine genetic loci, determine gene sequences and identify mutations in causative genes. The history and principles of the available techniques will be described in this chapter.

1.4.1 Linkage

Present understanding of human genetics owes much to the Austrian monk Gregor Mendel who, in 1865, presented and published the results of his breeding experiments on garden peas [85]. Unfortunately these went largely unnoticed until 1900 when his work was rediscovered 16 years following his death, after scientists began to conduct experiments that upheld his principles of inheritance: the Law of Uniformity, the Law of Segregation and the Law of Independent Assortment. However, they also discovered situations that represented deviations from these principles. The Law of Independent Assortment refers to the observation that members of different pairs of genes segregate to offspring independently of one another. However, studies on pea plants by Bateson, Saunders and Punnett in 1905 revealed that not all crosses yielded results that reflected the law of independent assortment [86]. Looking at the inherited features of flower colour (purple and red) and pollen grain shape (long and round) they identified that there was a connection, or coupling, of these traits in successive generations when plants were inbred. Subsequent work by Thomas Morgan on ‘eye

colour, body colour, wing mutations and the sex factor for femaleness in *Drosophila*' unearthed the concept of genetic linkage, in which he concluded that when two genes are closely associated on the same chromosome, they do not assort independently [87, 88]. He observed that during meiosis 'homologous chromosomes twist around each other, but when the chromosomes separate (split) the split is in a single plane' and thus for short genetic distances 'original materials will...be more likely to fall on the same side of the split, while remoter regions will be as likely to fall on the same side as the last, as on the opposite side'. Thus, he concluded that during this crossing over, there is exchange of genetic material between homologous chromosomes. The linkage of the different traits was felt to be dependent upon the linear chromosomal distance between these traits.

Morgan's student, Alfred Sturtevant, was the first to use this hypothesis to create a genetic map, though not based on physical distance on chromosomes, but rather on the proportion of 'crossovers' (or recombination events) as an index of the distance between any two factors [89]. He proposed that the greater the distance between linked genes, the greater the chance that non-sister chromatids would cross over in the region between the genes. By calculating the number of recombinants, a measurement of the distance between genes could be made. This distance, defined as the distance between genes for which 1% of the products of meiosis is recombinant, is known as the Centimorgan. The relationship between linkage map units and physical length is not linear. Some chromosome regions appear to be prone to recombination, so called 'hot spots', and recombination tends to occur more frequently during meiosis in women than men.

Linkage analysis has proven to be an extremely valuable tool in the mapping of genes. The method involves the study of disease segregation with polymorphic 'markers' from each chromosome. Eventually a marker will be identified that co-segregates with the disease more often than would be expected by chance, such that the marker and disease loci are linked. The underlying principle involves the use of likelihood ratios, the logarithms of which are known as LOD scores (logarithm of the odds): the LOD score Z is equal to the logarithm of the odds that the loci are linked divided by the logarithm of the odds that they are not linked. This uses the recombination frequency (θ), which is the frequency with which a single cross over event will take place between two genes during meiosis. In reality, the LOD score is calculated for different recombination frequencies providing a maximum likelihood estimate for the recombination frequency (θ_{\max}) at which the greatest LOD score is observed (Z_{\max}) [90]. It is generally agreed that a LOD score of +3 or more is confirmation of linkage, as it indicates 1000 to 1 odds that the linkage being observed did not occur by chance, and a LOD score less than -2 excludes linkage. It is possible to calculate maximum likelihood estimates for multiple loci at a time and therefore to place disease loci on a map of ordered genetic marker loci.

1.4.2 Genetic Markers

Historically there have been a number of different types of DNA marker. These DNA polymorphisms can serve as a set of markers that are sufficiently numerous and adequately spaced across the entire genome to allow a whole-genome search for linkage. They have the advantage of being able to be typed by the same technique and their chromosomal location can be determined using radiation hybrid mapping or by

searching the genome for a match to the polymerase chain reaction (PCR) (see section 1.4.3) primer used to score the marker.

1.4.2.1 *Restriction Fragment Length Polymorphisms*

The first polymorphisms to be discovered were restriction fragment length polymorphisms (RFLPs). These usually form as a result of single base pair changes in DNA sequences and lead to the removal or, less commonly, the introduction of a recognition site for a restriction enzyme. This causes an increase or decrease in the length of restriction fragments, which can be detected by the altered mobility of different sized fragments on gel electrophoresis (see section 1.4.4). A difference in number or size of fragments between individuals tested indicates a polymorphism in the restriction site of the enzyme used. Initially RFLPs were typed by preparing Southern blots from restriction digests of the test DNA and hybridisation with radioactive probes – a procedure that was cumbersome and time consuming, requiring a large amount of sample DNA. Unfortunately RFLPs are limited by their low informativeness.

1.4.2.2 *Microsatellites*

With the advent of the PCR (see section 1.4.3), a novel class of short tandem repeat (STR) polymorphisms, or microsatellites, was discovered, which were highly informative for linkage analysis. These are dinucleotide, trinucleotide or tetranucleotide sequences, such as $(CA)_n$ or $(GATA)_n$, that can be repeated between 10 to 100 times, and that tend to occur in non-coding regions of DNA throughout the

genome. They are multi-allelic, which increases the probability that an individual is heterozygous for these markers, allowing paternal and maternal alleles to be distinguished [90]. On each side of the repeat unit are flanking regions that can be used to develop locus-specific primers to amplify the microsatellites by PCR. This allows amplification of alleles whose sizes differ by integral repeat units. A fluorescent nucleotide precursor can be incorporated into the PCR products, which are denatured and then size-fractionated by gel electrophoresis (see section 1.4.4). Microsatellites are useful genetic markers because they tend to be highly polymorphic. The reason for this is that they are prone to high rates of mutation due to ‘replication slippage’ during DNA replication – there is incorrect pairing of the nucleotide repeats of the two complementary strands during DNA replication. Microsatellites have formed an essential tool in genome mapping.

1.4.2.3 *Single nucleotide polymorphisms*

The newest generation of markers are single nucleotide polymorphisms (SNPs). A SNP is a DNA coding variation occurring commonly in a population in which two sequence alternatives (called ‘alleles’) exist, with the frequency of the least abundant allele in the population being at least 1%. There is a difference of a single nucleotide between members of a biological species or paired chromosomes. Approximately two-thirds of SNPs are cytosine (C) to thymine (T) variations. These are bi-allelic and occur in coding and non-coding regions. In coding regions, a SNP can be synonymous, where the amino acid sequence remains unchanged, or non-synonymous, where the amino acid sequence is altered. The combinations of SNPs in regulatory regions, as well as amino acid coding SNPs, have a substantial influence

on inter-individual differences. Within different populations in the human species there are different variations such that a SNP allele that is common in one geographical or ethnic group may be much more rare in another group. SNPs are the genetic marker with the highest abundance in the genome and occur with a frequency of around 1 in every 1000 base pairs. Although they are not as polymorphic (and therefore individually less powerful as a marker) as microsatellites because they are bi-allelic, their high frequency within the genome makes them extremely useful for genome wide studies. An international consortium of academic and industrial partners has generated a public database of millions of SNPs, known as 'dbSNP', available through the National Center for Biotechnology Information (<http://www.ncbi.nlm.nih.gov/SNP/index.html>). There are a number of other SNP databases available including the OMIM database and the International HapMap Project (<http://hapmap.ncbi.nlm.nih.gov/>), the SNP Consortium (TSC) [91], the 1000 genomes databases (<http://browser.1000genomes.org/index.html>) and the Exome Variant Server (<http://evs.gs.washington.edu/EVS/>).

1.4.3 Polymerase Chain Reaction

Since its advent in the mid-1980s, the polymerase chain reaction (PCR) has revolutionised molecular genetics by allowing the rapid cloning and analysis of DNA [92, 93]. It has become a robust and extremely sensitive technique, enabling amplification of minute amounts of target DNA even from tissues or cells that are badly degraded. The wide range of applications of PCR, including DNA cloning for sequencing, functional analysis of genes, diagnosis, genetic linkage analysis, detection and diagnosis of infectious diseases, and in forensic science, have prompted

the development of a variety of PCR approaches, many of which have arisen due to the need to optimise efficiency and specificity.

PCR may be used to permit selective amplification of a specific target of DNA, of known sequence, within a heterogeneous collection of DNA sequences – often the starting DNA is total genomic DNA from a particular tissue. Thus the target DNA is typically a tiny fraction of the starting DNA. PCR amplification involves the use of oligonucleotide primers that flank the DNA segment to be amplified, and subsequent repeated cycles of heat denaturation of the DNA, annealing of the primers to their complementary sequences, and extension of the annealed primers with a DNA polymerase enzyme. The custom designed primers (amplimers), optimally 18-25 nucleotides in length, are specific for sequences flanking the target sequence. They hybridise to opposite strands of the target sequence and are orientated so that polymerisation occurs between the amplimers, effectively doubling the amount of that DNA segment. Further exponential accumulation of the target DNA sequence occurs, as the extension products are capable of further amplification, thus each successive cycle theoretically doubles the amount of DNA synthesised in the previous cycle.

PCR is carried out in reaction volumes of 10-200 μ l, in small reaction tubes (0.2-0.5 ml volumes) using a thermal cycler. The components required for the successive reactions that take place during PCR amplification include: a DNA template that includes the target region to be amplified; two oligonucleotide primers that are complementary to the 3' ends of the sense and anti-sense strands of the DNA target; a DNA polymerase such as Taq polymerase which is heat stable and has an optimum temperature of approximately 70° C [94]; the four deoxynucleoside triphosphates

(dNTPs), nucleotides containing triphosphate groups, dATP, dCTP, dGTP and dTTP; a buffer solution; and cations such as magnesium and potassium. Each cycle consists of 3 steps: a denaturation step at 94-98°C for 20-30 seconds during which the DNA template is melted and single stranded DNA molecules are generated; an annealing step for 20-40 seconds at a temperature 3-5° below the T_m of the primers used; and an elongation step that is time and temperature specific to the DNA polymerase being used, during which dNTPs are added together to complement the DNA template, in a 5' to 3' direction. In total, 20-40 cycles are utilised. There may be an initialisation step for 1-9 minutes before the start of the cycles if the DNA polymerase requires heat activation; and there is usually a final elongation step at 70-74° for 5-15 minutes after the last PCR cycle to ensure that any remaining single stranded DNA is fully extended. To determine whether the correct PCR fragments were generated, agarose gel electrophoresis is used to separate the DNA fragments, and a molecular marker – a DNA ladder – is run alongside the products to determine the size of the fragments.

1.4.4 Agarose Gel electrophoresis

Agarose gel is a 3-dimensional matrix formed by helical agarose molecules in supercoiled bundles with channels and pores through which biomolecules can pass. Gel electrophoresis allows the separation of a population of DNA by the application of an electrical field - the negatively charged phosphate backbone of DNA molecules will migrate towards the positively charged anode. The rate of molecular migration depends on a number of factors including: the size of the DNA molecules (smaller molecules travel faster than larger molecules); the concentration of the gel (typically the higher the percentage of gel, the slower the DNA will migrate); the voltage of the

current applied (the higher the voltage, the faster the molecules migrate); the ionic strength of the buffer used; and the concentration of the intercalating dye such as ethidium bromide. A 0.8% gel allows good resolution of large 5-10 kB DNA fragments while a 2% gel gives good resolution of smaller 0.2-1 kB fragments. Buffer solutions are used during electrophoresis to reduce pH changes due to the electrical field, the most common being Tris/Acetate/EDTA (TAE).

The gel is cast in molten form in trays, with combs that, when removed form wells, once the gel has set. DNA samples are loaded into each well, with a dye such as bromphenol blue, and a DNA ladder is loaded into the first well that allows estimation of the molecular weight of the DNA samples. The dye co-migrates with the DNA during electrophoresis. When stained with ethidium bromide, and once the gel has been run, it is viewed under a UV light and an image of the gel can be taken with a camera, which can be printed.

Agarose gel electrophoresis may be used in a number of applications including analysis of PCR products, separation of DNA for extraction and purification, estimation of DNA molecular size after restriction digestion and separation of restricted DNA or RNA during Southern or Northern blotting respectively.

1.4.5 DNA sequencing

DNA sequencing, the process of determining the nucleotide order of a given DNA fragment, was pioneered by Frederick Sanger using the dideoxy sequencing, or chain termination, method [95]. At the time that the work towards this thesis was being

carried out, Sanger sequencing was the most abundantly used method of DNA sequencing. Since then, newer techniques involving large-scale automated genome analyses, such as Next Generation Sequencing (see section 1.4.9), have come to the fore. These will be discussed in subsequent sections.

In the dideoxy direct sequencing method, single-stranded DNA is used as a template to create a new complementary DNA strand *in vitro* using oligonucleotide primers (specific to the region of interest), a suitable DNA polymerase, the four dNTPs, and a small proportion of one of the four analogous dideoxynucleotides (ddNTPs: ddATP, ddCTP, ddGTP, ddTTP). The ddNTPs are closely related to the normal dNTPs utilised during PCR, but they differ in that they lack a hydroxyl group at the 3' and 2' carbon positions. Although a ddNTP can be incorporated into the growing DNA chain by forming a phosphodiester bond between its 5' carbon atom and the 3' carbon atom of the previously incorporated nucleotide, the lack of a hydroxyl group at its 3' carbon atom prevents a further phosphodiester bond to form in this position. This leads to termination of DNA chain synthesis at this point. As the incorporation of a 'chain terminating' nucleotide is a random process, there will be a mixture of DNA fragments of different lengths that terminate in their respective ddNTP.

Fragments that differ in size may be size fractionated on a denaturing polyacrylamide gel, which contains a denaturing agent that ensures that the DNA strands remain single stranded. Although Sanger sequencing originally utilised radioactive labelling with manual interpretation of data, this technique was superseded by the use of fluorescent labels incorporated into the ddNTPs [96]. As the DNA passes through a fixed point in the gel, a laser detects and records a fluorescence signal, which is

specific for the particular ddNTP that each DNA fragment terminates in. The sequence is read in the form of intensity profiles, known as chromatograms, for each of the differently coloured fluorophores. The interpreted sequence can be used to infer a polypeptide, and can be stored in a computer database. Automated DNA sequencers historically used slab acrylamide gels, but newer generation high throughput sequencers use capillary electrophoresis [97], where the DNA samples migrate through very thin long glass capillary tubes containing gel, allowing for a higher degree of throughput and accuracy. Examples include the ABI and Illumina platforms, which can sequence approximately 1 million bases per day.

1.4.6 DNA Microarrays

DNA microarrays can be used to rapidly measure the expression of a large number of genes simultaneously or to genotype multiple regions of a genome [98-102]. These ‘DNA chips’ consist of a number of DNA ‘spots’ attached to a solid surface. In a standard microarray, probes are synthesised and attached to a solid surface, such as glass or silicone, by a covalent bond to a chemical matrix (Affymetrix chip). Some platforms utilise microscopic beads instead of the large solid support (Illumina), and other microarrays can be constructed by the direct synthesis of oligonucleotide or peptide probes on solid surfaces. The original technology involved the utilisation of light directed combinatorial chemical synthesis – semiconductor based photolithography – to enable the synthesis of hundreds of thousands of compounds in precise locations on a chip, so that a target molecule labelled with a fluorescent dye that was incubated with the chip could hybridise to the probes. Using combined laser confocal fluorescence scanning the molecular binding events at individual sites on the

array were measured [98]. By generating an array consisting of oligonucleotides complementary to sub-sequences of a target sequence, the identity of the target sequence could be determined, its amount measured and differences detected between the target and a reference sequence [100]. The use of microarrays is now widespread and there are a diverse range of applications, including sequencing to compare hundreds of different genes assayed simultaneously, detection of gene expression of many genes in parallel, utilisation of genetic markers to identify pathogenic organisms and analysis of sequence specificity of RNA- or protein-DNA interaction.

1.4.7 Autozygosity Mapping

Autozygosity, a form of homozygosity, is the appearance of two copies of a DNA segment that are identical by descent, such that they have a common origin (contrary to being introduced into the genetic pool of a population independently, which is known as identity by state) [103]. In autosomal recessive disease, the probability that each parent is a carrier of a mutated recessive allele will depend on the carrier frequency in the general population. This tends to be very low due to selective pressure against these highly morbid alleles. However, in the consanguineous setting, the probability of one parent being a carrier is not independent of the other. For example, first cousin parents will share $1/8^{\text{th}}$ of their genome, substantially increasing the risk of autozygosity of a disease allele, and therefore the occurrence of a recessive disorder, in their offspring.

The concept of disease gene identification using mapping strategies that analyse autozygous regions in consanguineous families with recessive diseases was conceived

by Lander and Botstein [104]. They suggested that by searching regions that are consistently homozygous by descent, a recessive disease gene could be mapped in an affected child from a consanguineous marriage. They calculated that the fraction of a child's genome that is homozygous by descent is $1/4$, $1/16$ and $1/64$ for sibling, first cousin and second cousin marriages, respectively. Using RFLPs they mapped areas of homozygosity in affected offspring, searching for regions in which adjacent RFLPs were homozygous. They used the hypothesis that affected individuals of consanguineous families would be homozygous for markers residing within the region surrounding the disease locus, which are therefore linked to the causative gene, and thus that these regions of homozygosity may be searched for the causative gene.

Autozygosity mapping became more practical with the discovery of multiple highly polymorphic microsatellite repeat markers spread throughout the genome, allowing genome-wide association studies looking for linkage [105]. Subsequently, the International Hap Map Project provided a genome wide set of SNPs to tag variation throughout the genome (<http://hapmap.ncbi.nlm.nih.gov/>). While each SNP has far less power to detect a homozygous chromosomal segment than a microsatellite marker, it is both their high frequency and their ability to detect a heterozygous region, and hence exclude linkage, that suggested their potential use in autozygosity mapping [106]. Widespread genome-wide SNP studies have been made possible through the availability of microarrays incorporating a large set of SNPs.

These 'SNP-chips' are now commercially available from a number of companies. Our laboratory used the Affymetrix SNP Chip, and earlier generations incorporated up to 10,000 SNPs, with newer versions incorporating 1,000,000 SNPs. The farther

removed the common ancestor is from the parents of the proband, the more opportunity for cross over events to have occurred during meiosis to generate their gametes, and thus a greater chance that the ancestral haplotype is broken. Therefore, a higher density of SNPs is required to capture an autozygous block when the parents are more distantly related. The analysis is performed following a single hybridisation reaction with one individual's DNA. Results are produced as a spreadsheet of SNP allele calls. The largest detected regions of homozygosity may be sorted according to genetic size, chromosome, and genetic location on the chromosome, number of homozygous SNPs in a run, number of 'no calls' in the run and whether the results reach statistical significance. The autosomal recessive gene locus could reside in any of the statistically significant homozygous regions detected and a number of tools exist to facilitate the subsequent search for candidate genes [103].

1.4.8 APEX Microarray

Another microarray-based method designed to rapidly screen for known mutations in a DNA sample is the Arrayed Primer Extension (APEX) technique [107, 108]. In this technique, a detection primer anneals to the target nucleic acid immediately adjacent to a variable nucleotide position. A DNA polymerase is used to specifically extend the 3' end of the primer with a labelled nucleotide analogue complementary to the nucleotide at the variable site. In essence, the APEX reaction is a sequencing reaction on a solid support.

An 'LCA chip' has been designed that uses APEX technology to enable screening for a large number of known LCA variants and SNPs [109]. This DNA microarray

incorporates 5' modified sequence specific oligonucleotides arrayed on a glass slide, so that their 3' ends are immediately adjacent to the variable site. Target nucleic acids that have been prepared by PCR and then fragmented, are annealed to the oligonucleotides on the slide, followed by sequence specific extension of the 3' ends of the primers with dye labelled ddNTPs using a DNA polymerase. The process is rapid, taking 4 hours from sample preparation to analysis. As further LCA variants are discovered, the chip can be 'updated', making this technology a high volume, cost effective screening tool for known variants in this genetically heterogeneous condition. Asper Biotech Ltd (Tartu, Estonia) have commercialised this LCA chip (as well as many others) and utilise their Genorama® Genotyping Software™ to detect and analyse variants in both the sense and antisense strand, and thus provide one or two variants in the disease gene in informative samples (<http://www.asperbio.com/asper-ophthalmics/leber-congenital-amaurosis-lca-genetic-testing>). Currently, this chip analyses 780 variants in 15 genes.

The efficiency and efficacy of the LCA chip was analysed by Henderson *et al.* who identified one or two mutations in 46% of LCA and 24% of early onset retinal dystrophy patients [110]. The authors identified that overall, the chip is informative in around one third of patients, concluding that it is a sensitive technique with a low call failure rate, thus providing an excellent first pass screening tool for LCA. However, a number of anomalies between the chip and direct sequencing results were identified, including false-positive results in *AIPL1*, a false-negative result in *CRB1* and a relatively high call failure rate in certain SNPs, although these were on a par with the difficulties encountered with direct sequencing techniques.

1.4.9 Next generation sequencing

At the time that the work towards this thesis was being carried out, next-generation sequencing (NGS) technologies were in their infancy. They are now in the forefront of biological research, reaching unparalleled levels of sequencing capacity. As this technology was used by our laboratory and collaborators at the UCL Genetics Institute to identify the genetic cause in one patient in this study, the principles of NGS will be described here.

A number of different DNA sequencing platforms have now been generated and several commercial next-generation DNA sequencing systems are available, such as the Roche 454 Genome Analyzers (Roche Diagnostics Corp., West Sussex, UK) (<http://454.com/products/technology.asp>), the Illumina NGS platforms (Illumina Inc., California, USA) (<http://www.illumina.com/technology/next-generation-sequencing.html>), the Applied Biosystems SOLiD™ Genetic Analyzers (<http://www.lifetechnologies.com/uk/en/home/life-science/sequencing/next-generation-sequencing/solid-next-generation-sequencing.html>) by Life Technologies (Thermo Fisher Scientific Inc., Massachusetts, USA), and the Ion Torrent™ platform, also by Life Technologies (<http://www.lifetechnologies.com/uk/en/home/brands/ion-torrent.html>). The data obtained from NGS depends heavily on the high quality reference sequences produced by the Human Genome Project [111]. The major advantage of NGS technologies is the ability to process millions of sequence reads simultaneously, a technique known as massively parallel sequencing. This vastly reduces the required number of instruments and personnel compared to Sanger-type DNA capillary sequencers, and significantly accelerates the rate of data collection for DNA sequencing – current machines are capable of sequencing an entire genome

within a couple of weeks. This is likely to be accelerated further, with time, such that whole genome sequencing could be achieved within hours to days. Another important difference is that NGS technologies are derived from fragment libraries rather than depending on vector based cloning, which significantly speeds up the sequencing process. The read lengths are shorter: 35-250 base pairs (bp) for NGS compared to 650-800 bp for capillary sequencers. Finally, there is a significant reduction in the costs for NGS: in 2013 it cost approximately \$5,000 USD to sequence the entire genome of one person [112]. With time this will undoubtedly reduce further.

All NGS platforms first require the construction of a 'library' of the DNA to be sequenced before the sequencing process that follows. The processes involved in the construction of this library begin with random shearing of genomic DNA into 200-500 bp fragments of different sizes by sound waves, and subsequent ligation by DNA ligase of customised synthetic DNA linkers known as adapters, that are covalently linked to the end of the DNA fragments [112]. These adapters are universal sequences that are specific to each platform, which can be used in later steps to polymerase-amplify the fragments. The libraries are quantitated very precisely before they go on to the amplification process in order to obtain the correct amount of sequence data after amplification has occurred. Each of these synthetic library fragments is amplified by a few PCR cycles on a solid surface (either a bead or a flat silicone derived surface, depending on the platform used) that already has covalently bound adapters attached to the surface. These are complementary to the adapters that have been attached to the fragments. The amplification of the library fragments on the flow cell surface leads to the generation of clusters of fragments, all of which have originated from a single fragment.

In the Illumina® platform (Illumina Inc., California, USA), which was used in this study, the amplified fragments generate clusters by a method known as ‘bridge amplification’. In this process the denatured fragment on the flow cell surface anneals to an adapter bound to the fixed surface during the first annealing cycle, forming a ‘bridge’, following which the first extension cycle occurs from the bound and annealed adapter using the fragment as a template. This generates 2 strands in a bridge which are then denatured in the second cycle, followed by second cycle annealing and then second cycle extension. This process occurs around 35 times and generates clusters of amplified fragments, which are foci for subsequent sequencing.

Once the clusters have been generated, there is chemical ‘release’ of fragment ends that carry the same adapter, and denaturation of the fragments to single strands. There is subsequent ligation of a complementary synthetic DNA sequencing primer to the linear single stranded cluster DNAs, which provides a free 3’-OH group, which can be extended in subsequent stepwise sequencing reactions (see below). The sequencing occurs in a direction from the free end down to the surface of the chip. The clusters can be regenerated by another amplification process, with release of the other end of the bridged fragment, followed by ligation of a second primer and then sequencing. In this manner, ‘paired end reads’ are used to generate the sequence. These reads are paired with one another during the alignment step of the data analysis process, which provides an overall higher certainty of placement than would occur with a single end read of the same length.

The sequencing method utilised by Illumina® is known as massively parallel ‘sequencing by synthesis’, in that following the incorporation of each base during sequencing there is an imaging step to identify the incorporated nucleotide at each cluster. This is achieved by using a process known as reversible dye terminator sequencing: all four nucleotides, each with a specific fluorescent label, are provided by the fluidics of the instrument into the flow cell; the nucleotide is incorporated adjacent to the sequencing primer by a polymerase and is detected by the optics of the sequencer; the nucleotide has a ‘block’ incorporated into it at the 3’-OH position of the ribose sugar such that a second adjacent nucleotide can only be incorporated after steps in which the previous nucleotide is ‘unblocked’ and the fluorescent group is cleaved off and washed away. This prevents additional nucleotide incorporation reactions by the polymerase. Therefore, the overall series of steps occurs in the following sequence: a. the nucleotide becomes added by the polymerase; b. unincorporated nucleotides are washed away; c. the flow cell is imaged on both surfaces to identify each cluster that is reporting a fluorescent signal; d. the fluorescent groups are chemically cleaved, and e. the 3’-OH group is chemically cleaved [112]. This series of steps is repeated for up to 150 nucleotide additions, after which the second read preparations begin (for reading from the opposite end). To read from the opposite end of each fragment cluster (paired end read technology) the synthesised strands are removed by denaturation, the clusters are regenerated by limited bridge amplification, opposite ends of the fragments are released from the flow cell surface and the fragments are primed with the reverse primer. Sequencing can then proceed in the opposite direction, as above.

The technique of whole genome sequencing can be refined by using a method called ‘hybrid capture’ to specifically capture *exome* sequences (the ‘coding’ regions of DNA) from a whole genome library by generating synthetic probes specifically for all of the exons in which one is interested. These probes are ‘biotinylated’ and adhere to fragments of interest. The DNA is purified using magnetic beads that allow the specific capture of fragments of interest and the remaining fragments are washed away. These fragments can then be sequenced. The process is known as ‘whole exome sequencing’ (WES).

The interpretation of the vast amounts of data generated by NGS employs complex bioinformatics. The raw sequencing reads need to be aligned to the reference genome and the data require ‘cleaning up’ in order to remove duplicates, correct local misalignments and calculate quality scores. The number of SNP ‘calls’ is very important as this evaluates whether there is adequate and accurate coverage of the genome, which will subsequently allow investigators to reliably call true variants as variants. Not only is the coverage important (ie the percentage of the genome that has been sequenced), but so is the read depth (the number of times the genome base has been read) eg 10x, 30x.

The advent of NGS has revolutionised biological research, with significant increases in data-production capacity and significant lowering of costs. WES technologies are being superseded by whole genome sequencing as costs are falling, which have the added benefit of enabling identification of copy number variants and variants in non-coding regions. At present the technology is being utilised in a research setting but as

costs become further reduced, this technology will have a tremendously important impact in the clinical setting.

1.5 Genetics of Leber Congenital Amaurosis and Early Onset Retinal Dystrophy

Since Donders' and Leber's earliest descriptions of Leber Congenital Amaurosis (LCA) and the Early Onset Retinal Dystrophies (EORDs), it has become apparent that these are a highly heterogeneous group of disorders, both in terms of their molecular causes and in their phenotypes. In recent years, until the work towards this thesis was completed, the global effort at elucidating the genetic causes of these conditions had led to the discovery of 16 different genes, and an additional locus, that contribute to the pathogenesis of LCA and EORD. All of the genes, bar one (*CRX*) display an autosomal recessive inheritance pattern. The LCA9 locus had been known for some time, but the causative gene at this locus was only identified after this study was completed. The wide genetic heterogeneity reflects the different roles of these genes, which have a number of functions, including: photoreceptor structure and development; retinal function such as phototransduction and the visual cycle; transport across the photoreceptor cilium; chaperone functions; and some, as yet, unknown functions (Figure 10). There is considerable overlap of the genes that lead to LCA and EORD. The variability of the ocular phenotype can relate to the underlying molecular cause, but it can also vary between and within families affected by the same genetic variants. Typical phenotypes are associated with only a handful of

genes. Genotype-phenotype association studies are therefore particularly important for widening our understanding of these heterogeneous disorders.

This chapter examines each gene or genetic locus that, until the work towards this thesis was completed, have been implicated in the pathogenesis of LCA and EORD. A description of the published phenotypes associated with variants in these genes is also included. The genes are described in the historic order that they or their loci were identified.

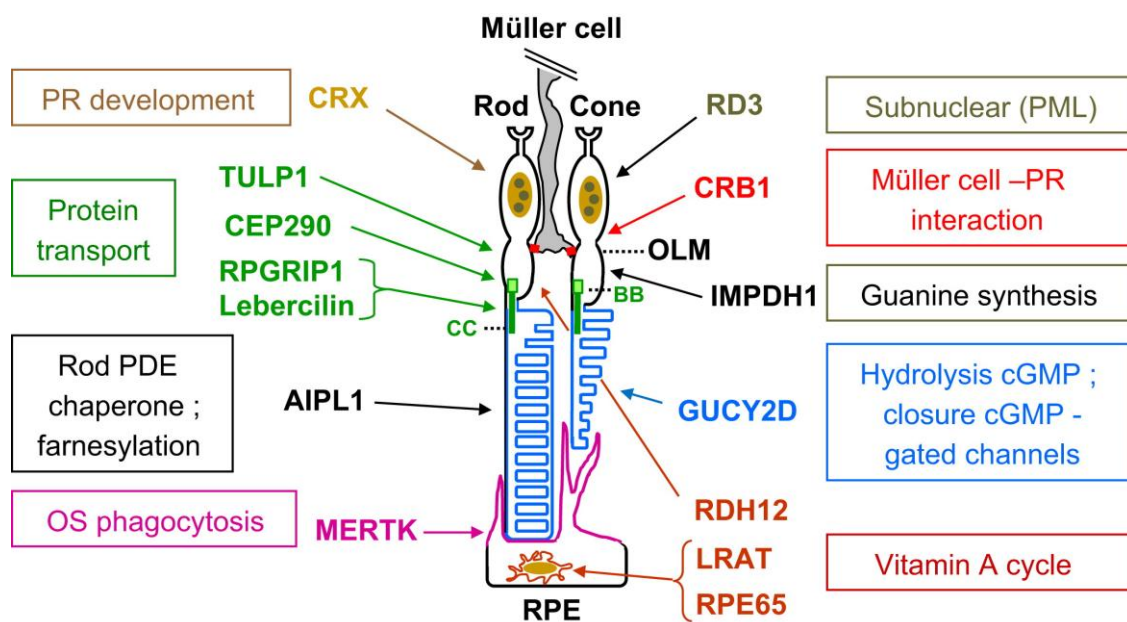


Figure 10 – Spatial representation of 14 different LCA / EORD genes and their putative roles. Adapted from [46]. AIPL1 predominantly locates to the rod outer segments; CRB1 is located in the Müller cell membrane; CEP290, TULP1, RPGRIP1 and Lebercilin are involved in protein transport through the cilia; RDH12 and IMPDH1 are located in the photoreceptor outer segments; LRAT and RPE65 are in the membranes of the endoplasmic reticulum of the RPE.

1.5.1 *GUCY2D* (LCA1)

Following both linkage analysis and homozygosity mapping in 5 unrelated families of North African origin, the locus for the putative *LCA1* gene was identified in 1995 on the short arm of chromosome 17 [113]. The causative gene was subsequently identified as the retinal guanylate cyclase 2D gene (*RetGC*, *GUCY2D*) (MIM 600179), located at chromosome 17p13.1 [114]. *GUCY2D* encodes a human photoreceptor specific guanylate cyclase located in the photoreceptor (PR) outer segments (OSs), which catalyses the conversion of guanosine triphosphate (GTP) to cyclic 3'5'-guanosine monophosphate (cGMP), a key process involved in the restoration of PRs to their dark adapted state following excitation by light [115]. Mutations in this gene may lead to a state of constant hyperpolarisation of rod and cone PR plasma membranes due to the constant closed state of cGMP gated cation channels [116]. This leads to a situation equivalent to constant light exposure, in which PR cGMP levels do not return to the levels present in the dark adapted state.

Mutations in *GUCY2D* account for about 11% of cases of LCA and EORD but the proportion can vary depending on the ethnic origin of the cohorts studied [109, 110, 115, 117-124]. There is a higher prevalence of *GUCY2D* mutations in Mediterranean populations. A Mediterranean ancestry was present in 70% of all *GUCY2D* mutations in one LCA cohort [115]. The phenotype associated with mutations in *GUCY2D* is one of severe visual loss from birth (light perception or counting fingers vision), roving eye movements, pendular nystagmus, severe photophobia, high hypermetropia of +7.00 dioptre sphere (DS) or greater, a normal fundus appearance at birth and an un-recordable ERG [115, 120, 124]. The normal fundus appearance may progress

with age with the development of pigment migration into the retina and macular atrophy. Some patients may show little progression until adult life [120, 122].

Heterozygous *GUCY2D* mutations have also been associated with an autosomal dominant cone-rod dystrophy (CORD6), with affected individuals displaying characteristic macular atrophy and marked loss of cone function, with minimal loss of rod function on electroretinography [125-127]. The *GUCY2D* mutations that lead to autosomal dominant cone-rod dystrophy target exon 13 and have been identified to target codons 837, 838 and 839 specifically [128].

Functional analysis of recessive missense mutations in *GUCY2D* in LCA subjects demonstrates location-specific effects of the mutations [129]. Missense mutations affecting the catalytic domain lead to severely impaired cGMP (basal activity), GCAP-1 and GCAP-2 (guanyl cyclase activating proteins) activity, and when these mutant cyclases are co-expressed with wild type alleles, the activity of the wild type allele is severely reduced, suggesting a dominant negative effect of mutations in the catalytic domain. However, in missense mutations affecting the extracellular domain there is no effect on basal cGMP activity, but GCAP-1 and GCAP-2 activity is reduced by 50%, suggesting that mutations in the extracellular domain moderately reduce cyclase activity. Therefore, with mutations in the catalytic domain, and not the extracellular domain, the dominant negative effect is expected to reduce *GUCY2D* function in heterozygotes with recessive mutations.

1.5.2 RPE65 (LCA2)

In 1993 an evolutionarily conserved RPE-specific retinol binding protein receptor, with a molecular weight of 65kD, was identified and its expression was demonstrated to occur prior to the appearance of the photoreceptor outer segments during retinal development in rats [130]. Cloning and characterization of the protein revealed the 533 amino acid structure [131]. The chromosomal locus of the relevant gene was subsequently mapped to 1p31 using fluorescence *in situ* hybridisation [132]. The human *RPE65* (MIM 180069) gene structure was characterised in 1995 and comprises 14 coding exons, spanning 20kB [133].

Subsequent studies identified RPE65 as the isomerohydrolase, within the RPE, involved in the conversion of all-*trans* retinyl esters to 11-*cis* retinol during the visual cycle [134-136]. The substrate for this hydrolysis-isomerisation process is provided by the preceding step of the visual cycle in which lecithin acyl transferase (LRAT) converts all-*trans* retinol to all-*trans* retinyl ester. Despite RPE65 expression being predominantly in the RPE, studies have identified that it is also expressed in mammalian cone, but not rod, photoreceptors [137]. The exact role of RPE65 in cones is unknown. It is evident from animal models and from investigation of the phenotype in humans with RPE65 deficiency that cones have an alternative source of chromophore. Cones utilise an additional pathway to recycle retinoids that involves Müller cells [41, 43, 138]. In this alternative cycle, all-*trans* retinol leaves the cone outer segments and, instead of being transported to the RPE, is transported to the Müller cells, where it is converted to 11-*cis*-retinol, and subsequently transported to the cone OSs, where it is converted to 11-*cis*-retinal [139]. Rods, on the other hand, are entirely dependent on *RPE65* in the RPE to recycle chromophore. This may

explain why patients with bi-allelic mutations in *RPE65* have evidence of residual cone function but absent rod function.

Recent studies using zebrafish, which have cone-dominant retinas, have characterized the isomerohydrolase likely to be involved in the cone visual cycle [138]. The identified protein, named RPE65c, shares 78% sequence homology with zebrafish RPE65a, the orthologue of human RPE65, and contains the key residues responsible for RPE65 enzyme activity. Immunohistochemistry has identified that RPE65c expression occurs in the Müller cells and inner retina, but not RPE, and that the chromosomal location of *RPE65c* is different to *RPE65a*. Further studies will be necessary to identify the human orthologue of RPE65c, its role in the visual cycle in humans and potential disease involvement.

Several *RPE65* animal models have been characterised, including the naturally occurring murine *Rpe65^{rd12}* [140] and canine Briard dog models [141, 142], and the genetically engineered *Rpe65^{-/-}* knockout mouse model [143]. These animal models have been useful in studies of the underlying biochemical, genetic, functional and pathological role of RPE65, and in the development of novel therapeutic strategies. The retinal degeneration 12 (*rd12*) mouse has a naturally occurring homozygous nonsense mutation in the mouse orthologue of human *RPE65*, *Rpe65*, and shows small lipid-like droplets in the RPE from 3 weeks of age [140]. Over time these droplets grow larger in size and are associated with rod OS shortening and degeneration. Electrophysiological evidence of rod degeneration is evident as early as 3 weeks of age, however histopathological examination suggests a slower retinal degeneration. The phenotype in these mice resembles, to some extent, that which is

seen in fundus albipunctatus, a condition caused predominantly by mutations in *RDH5*. The *Rpe65*^{-/-} knockout mouse was described prior to the discovery of the *rd12* mouse [143]. The visual changes observed in these mice are restricted to rod dysfunction, as observed by an abolished rod ERG, with relatively spared cone function, thus supporting the hypothesis of an alternative cone system visual cycle. A slow retinal degeneration is evident as the retinal anatomy is relatively normal from birth, but from 7 weeks of age some loss of density of the rod outer segment discs is seen. By 15 weeks the outer segments are short, with inclusions present in the RPE. The PR nuclear layers also degenerate slowly. Rhodopsin, 11-cis-retinal and 11-cis-retinyl esters are not present in *Rpe65*^{-/-} mice, and there is an over-accumulation of all-trans-retinyl esters in the RPE, supporting the hypothesis that RPE65 is essential in the isomerisation step within the visual cycle.

The naturally occurring Briard dog has a homozygous 4 nucleotide deletion in *RPE65* and has a phenotype similar to humans affected with mutations in this gene [141, 144-146], with severe nyctalopia, a normal retina to up to 4 years of age and a severe rod-cone dystrophy on electroretinography, with better preservation of cone function [141, 142, 144]. Ultrastructural studies in the RPE of these dogs identify large lipid-like inclusions in the central and tapetal retina [145]. Smaller lysosomal inclusions in the RPE cytoplasm were detected, as well as disorganisation of the rod outer segments. The cone OSs and inner retinal structures were better preserved.

The above animal models harbour mutations in *RPE65* that render the function of the protein 'null'. However, of the published *RPE65* mutations to date, approximately 50% are missense variants, and bi-allelic null mutations are extremely rare. Some

missense mutations may encode proteins that have residual enzymatic activity [147]. In ‘hypomorphic’ mutations, a milder phenotype may exist (see below), and studies using knock-in animal models for particular mutations, such as for the R91W *Rpe65* mutation, have been conducted to determine the effect of such missense mutations when compared to null mutations [147].

The overall mutation frequency of *RPE65* in early onset retinal dystrophy is around 6% [24]. The first families to be reported with *RPE65* mutations were identified using single stranded conformation analysis (SSCA) and harboured a variety of mutations including missense, splice site and rearrangements [148-150]. The phenotypes in these families also varied, with diagnoses including LCA and EORD to different degrees of severity. With further reports of *RPE65* retinopathy, the phenotypic variability associated with mutations in this gene has been highlighted, with affected individuals displaying a wide spectrum of severity, age of onset and progression [27, 151-157]. The diagnoses range from ‘classical’ LCA, with very severe early onset visual loss from birth, through to autosomal recessive RP, with a later age of onset and a milder clinical picture. A variety of mutational mechanisms have been described (missense, nonsense, insertion – deletion mutations and splicing abnormalities) in a variety of combinations.

The ‘classical’ phenotype of *RPE65* retinopathy is described as severe visual impairment of infantile onset, with nystagmus, nyctalopia, photophilia, visual field constriction and an absence of photophobia. The fundus is either normal or hypopigmented (a ‘blonde fundus’) with visible choroidal vessels and little to no intra-retinal pigmentation [152, 154, 155]. Atrophic macular changes may be present

and retinal ‘white dots’ have also been described [14, 154, 156]. The ERG is either undetectable or shows severe rod dysfunction with possible residual cone function in the young [151, 153-155]. Children may have poor but useful vision in early life such that they may be able to attend normal school, however there can be significant deterioration in VA by the second decade and some retention of peripheral islands of vision into the third decade [151]. In some, however, only rudimentary peripheral visual fields are maintained [157]. Colour vision is severely affected across all axes, but in those in whom colour vision can be tested, the disturbance appears to predominantly affect the tritan axis [27, 153, 155]. A range of refractive errors have been documented, however in a report of 10 *RPE65* patients, 50% had myopia or myopic astigmatism [158]. This group demonstrated absent or very low fundus autofluorescence in EORD due to *RPE65* mutations. OCT studies have demonstrated loss of the central PR layer in young patients, and foveal and extrafoveal outer nuclear layer (ONL) thinning corresponding to rod photoreceptor loss [159]. The ONL thinning is more prominent inferior to the fovea, however the extent of OCT changes is variable. In older subjects (as described in a patient age 43 years), severe retinal and RPE thinning may be present, corresponding to the areas of RPE atrophy seen on ophthalmoscopy [158].

Although there is no specific genotype – phenotype association, the presence of milder phenotypes suggests hypomorphic allelic function. Marlhens first reported a correlation between the severity of disease and the type of *RPE65* mutation in a compound heterozygote with two missense mutations and a mild clinical picture with slow progression [160]. In their series of 20 *RPE65* individuals identified from 453 retinal dystrophy patients, Thompson *et al.* described one individual with ‘nyctalopia

at age 3 years, a diagnosis of RP by age 20 and small islands of residual vision at age 58' who had a compound heterozygous mutation (Y79H/E95Q) [151]. Lorenz *et al.* described one subject with a homozygous p.P25L missense mutation who had best corrected visual acuities of 6/6 at age 5 and 6/9 at age 7 years [161]. He had reduced dark adaptation at age 3, an absence of nystagmus, hypopigmented fundi, and a small macular reflex. Goldmann kinetic perimetry at age 6 was normal to the V4e and III4e targets, but to the I4e target demonstrated slight constriction. Two-colour threshold perimetry detected predominantly cone mediated scotopic responses, and in the photopic state, cone responses were 1.5 log units below normal. Fundus autofluorescence was low but detectable, and OCT by age 7 showed outer retinal thinning. The ERG rod responses were severely impaired but cone mediated responses were detectable, albeit with 30% reduced amplitudes. These reports provide a convincing case for *RPE65* hypomorphic variants causing a milder phenotype. Recently a knock-in mouse model with the R91W missense mutation was characterised which has comprehensively demonstrated the functional differences in the production of 11-cis-retinal and rhodopsin compared to *Rpe65* null mutations [147].

The phenotypic heterogeneity associated with *RPE65* mutations is further complicated by a report of a patient with 'fundus albipunctatus' harbouring a compound heterozygous *RPE65* mutation [15]. In addition, there have been reports of heterozygote carriers displaying multiple hard drusen at the posterior pole and mid-peripheral retina, in some patients associated with rod ERG and dark-adapted threshold perimetry dysfunction [154, 157].

1.5.3 *SPATA7* (LCA3)

The *LCA3* locus was identified through the analysis of a large consanguineous Saudi Arabian family with LCA [162]. Using homozygosity mapping the *LCA3* locus was mapped to chromosome 14q24, but no obvious positional candidate genes were apparent in the identified region. In 2009, after further fine mapping of this region in this and other linked families, *SPATA7* (MIM 609868) was identified as the causative gene [163].

First cloned in 2003 from the rat testis, *SPATA7* (spermatogenesis associated protein 7) cDNA was also found to be expressed in the human testis [164]. In humans, *SPATA7* consists of 12 exons and maps to chromosome 14q31.3. It encodes a 599 amino acid protein with one transmembrane domain but no known functional domains [163]. In the mouse, *Spata7* is expressed in multiple retinal layers including the inner segments of photoreceptors, inner nuclear layer and ganglion cell layer. The protein appears to be important in retinal function rather than development. Of the two known isoforms of *SPATA7*, isoform 1 is predominantly expressed in neuronal tissues including the retina, cerebellum and whole brain [165] and isoform 2 in the testis [166]. The exact function of *SPATA7* remains to be identified.

The incidence of *SPATA7* mutations in LCA and EORD is around 2-3% [165, 166]. At the time that this study was conducted the limited phenotypic data available suggested that mutations in *SPATA7* are associated with a severe LCA-like phenotype, but that less severe phenotypes also occur. The affected individuals in the original Saudi Arabian family, homozygous for a p.R108X mutation, had poor vision from birth, nystagmus, hypermetropic astigmatism and a non-recordable ERG [163].

The same mutation was identified in a Dutch male with poor vision and nystagmus from birth who, at the age of 6 years, had retinal pigmentation and peripheral chorioretinal atrophy. A less severe phenotype was described in a 7 year old Portuguese female harbouring a homozygous nonsense mutation, p.R395X, who had juvenile onset RP with early onset nyctalopia, 6/6 visual acuity, an absence of nystagmus, severely constricted visual fields to the central 5° and undetectable ERGs. A diffuse hypopigmented parafoveal annulus was present. Another patient in this series, a male of French Canadian ancestry with a homozygous frameshift *SPATA7* mutation, p.Q465fsX505, carried a diagnosis of juvenile onset RP. He had normal vision in childhood, but developed nyctalopia and nystagmus. By age 55 years he had advanced retinal pigmentation and maculopathy, with a flat ERG. From their panel of 134 LCA patients, Perrault *et al.* identified 4 families harbouring *SPATA7* mutations, three of which were functionally ‘null’ [166]. All were of European ancestry and had a typical LCA phenotype. Photophobia was an initial feature, but by age 3 years all had nyctalopia. The retinae were normal initially but gradually developed a ‘salt and pepper’ appearance with vascular attenuation, retinal atrophy and typical fundus features of RP. There was complete absence of autofluorescence by adulthood. This group postulated that due to the expression profile of *SPATA7*, there may be an effect on male infertility, however their only male patient was not of child-bearing age. Mutations in *SPATA7* thus may be associated with LCA or childhood onset rod cone dystrophy.

1.5.4 AIPL1 (LCA4)

In 2000, linkage analysis in a Pakistani LCA family, in whom mutations in the nearby *GUCY2D* gene had been excluded, led to the identification of a separate LCA locus, termed *LCA4*, located on chromosome 17p13 [167]. The *AIPL1* (aryl hydrocarbon receptor-interacting protein-like 1) gene (MIM 604392) was subsequently identified as the causative gene at this locus in the original *LCA4* family [168].

The AIPL1 protein was named due to its similarity (49% identity) to the human aryl hydrocarbon receptor (AhR) interacting protein, AIP [168]. It is comprised of 384 amino acids, and contains a 34-amino acid motif, that contains 3 tetratricopeptide repeats, that are present in proteins with nuclear transport or protein chaperone activity [169]. *In situ* hybridisation studies in rats and mice have shown *Aipl1* expression in the pineal gland and mouse photoreceptors [168]. In humans, AIPL1 is expressed in the pineal gland, and in the inner segments and outer plexiform layers of the rod photoreceptors in the central and peripheral retina [170]. It is not detected in cone photoreceptors in the mature retina. It is, however, expressed in both rod and cone photoreceptors of the developing retina, which may explain why there is severe and early rod and cone dysfunction in LCA patients with *AIPL1* mutations [171].

Early functional studies of AIPL1 have sought clues from the AIPL1 homologue AIP (aryl hydrocarbon receptor activated protein 9), which shares 49% identity and 69% similarity with AIPL1, and which in turn shares identity with the immunophilin co-chaperones FKBP (FK506-binding protein) 51 and FKBP52 [172]. The results of such studies indicate that these molecules are components of cytosolic heterocomplexes [170], which play various functional roles. The ligand-induced transcriptional activity

of the AhR (aryl hydrocarbon receptor) is enhanced by AIP, which both stabilizes the cytosolic levels and modulates the intracellular localisation of the AhR. Thus the role of AIP is to regulate the nuclear translocation and transactivation of the AhR.

AIPL1 interacts and aids with the farnesylation of proteins [173, 174]. Farnesylation is a 3-step prenylation process in which post-translational modification occurs at the c-terminus of a number of proteins. In the first step, a farnesyl group is covalently attached to the protein, in the cytosol. These farnesylated proteins are then targeted to the endoplasmic reticulum (ER) in step two, where proteases remove the last 3 amino acid residues. In step three, carboxymethylation of the proteins occurs in the ER. The farnesylated proteins are subsequently transported to their target membranes. AIPL1 plays a role in at least one of these steps. The farnesylation process enhances protein-membrane interactions and protein-protein interactions, and is important for the maintenance of the retinal and photoreceptor cytoarchitecture.

Knock down mouse models of *Aipl1*, in which there is hypomorphic Aipl1 function, have identified AIPL1 as a chaperone for the biosynthesis of phosphodiesterases in rod photoreceptors [175]. AIPL1 is probably also required for the normal development of cone photoreceptors. This study has refuted the findings of previous studies that AIPL1 is involved in protein farnesylation. In these hypomorphic *Aipl1* mutant retinas, the retinal degeneration occurred more slowly, and by 8 months of age half of the photoreceptors were lost and the inner and outer segments were shortened. In *Aipl1*^{-/-} knockout mice photoreceptors initially develop normally, but once outer segments begin to develop, the rod and cone photoreceptors degenerate rapidly, in a light independent state, and in a process that is mediated by the destabilization of the

rod phosphodiesterase holoenzyme [176]. The mechanism by which AIPL1 affects the stability of the phosphodiesterase heterotrimer is unknown. AIPL1 and the molecular chaperones Hsp70 and Hsp90, may interact in regulating the production of phosphodiesterase [177].

The role of AIPL1 in cone photoreceptor viability has been recently investigated using a transgenic mouse in which human AIPL1, under the control of a rod specific promoter, was expressed in an *Aipl1*^{-/-} knockout mouse model [178]. This group hypothesized that the cone degeneration observed in *Aipl1*^{-/-} mice may be due to an indirect ‘bystander effect’ due to rod photoreceptor death, or due to a direct role of AIPL1 in cones. Their findings demonstrated that cone photoreceptors degenerate more slowly in mice rescued by the transgenic expression of human AIPL1 in rods compared to the *Aipl1*^{-/-} knockout, and that there is rescue of rod function. In addition to this, structural defects were seen in the surviving cones including thinner and shorter outer segments with disorganisation of the disc membranes. In the absence of AIPL1, the lack of cone function is due to the drastic destabilization of the cone PDE6 subunits, as observed by the highly reduced levels of cone PDE6 in the transgenic mice. This study demonstrates that AIPL1 is required for cone function and survival but that in the presence of viable rods there is a reduced rate of cone degeneration.

The incidence of *AIPL1* mutations in LCA and EORD is 5.3% [24]. The original *LCA4* family was subsequently identified to harbour the homozygous variant p.Trp278X [167, 168]. This has subsequently been identified to be the most common mutation associated with *AIPL1* disease reported in both the homozygous and compound heterozygous states [179, 180]. One compound heterozygous subject

harbouring the variants p.Trp278X and p.Gly122Arg has been described with a milder phenotype, suggesting that the p.Gly122Arg variant acts as a hypomorphic allele [179].

The phenotype associated with *AIP1I* mutations is typical of LCA, with severe visual loss from birth or within the first few months of life, nystagmus and nyctalopia [167, 168, 179-183]. Visual acuity ranges from between 6/120 to no light perception [181, 183]. There is predominantly a hypermetropic refractive error. Keratoconus and cataract are common [167, 179-181]. Characteristic fundus features include a maculopathy and pigmentary retinopathy. However, the severity of these features may be variable, and in some cases, age related. In the youngest patients, below 3 years of age, the retina may appear normal [180, 181]. The mildest maculopathy is described as an indistinct foveal reflex while the most severe appear as macular ‘colobomatous’ lesions. A pigmentary retinopathy over the age of 3 years is universal. Fundus autofluorescence imaging may show a hyperautofluorescent fovea with a hypoautofluorescent surrounding annulus or show complete lack of autofluorescence, corresponding with severe macular atrophy [179, 180].

1.5.5 *Lebercilin (LCA5)*

The LCA5 locus was mapped to chromosome 16q11-16 in 2000, through linkage analysis of a consanguineous family belonging to the Old Order River Brethren, a religious isolate originating from Switzerland which emigrated to America in the 1750s [184]. Three retina specific genes were excluded as the disease-causing gene in three affected members of this kindred. A second consanguineous family from

Pakistan was subsequently described in 2003 that also mapped to this region [185]. However, it was not until 2007 that the causative gene, *LCA5* or lebercilin (MIM 611408), was identified through homozygosity mapping of these two, and 4 other, families linking to the same region [186].

LCA5 encodes a 697 amino acid ciliary protein containing 4 regions that are predicted to form coiled coils, a feature that is shared with some other ciliary proteins [186]. Lebercilin is expressed widely in human tissues. Murine *in situ* hybridisation studies have demonstrated that lebercilin expression occurs during embryogenesis and it is present in the eye, inner ear, kidney, central and peripheral nervous systems, gut and the ciliated epithelium of the nasopharynx, trachea and lungs. In adult mice, expression is confined to the retinal photoreceptors. Immunohistochemical studies of ciliated cells have localised lebercilin to the ciliary axoneme at the base of primary cilia. In the eye it is localized to the connecting cilium and basal bodies of photoreceptor cells, in particular to the axonemal microtubules of the connecting cilium. Proteins that interact with lebercilin exist as an ‘interactome’ that consists of 24 proteins, many of which are associated with microtubules and/or have centrosomal or ciliary functions. This interactome specifically interacts with the intraflagellar transport (IFT) machinery that is involved in protein transport through the photoreceptor cilia [187]. A defect in IFT results in the failure of outer segment formation, causing photoreceptor degradation.

The phenotype associated with *LCA5* mutations is one with severe visual loss from birth, nystagmus, nyctalopia and an unrecordable ERG [184-186, 188-191]. Subjects are highly hypermetropic, have poor colour vision and pupillary responses. Visual

acuity ranges from 0.20 to light perception, and kinetic perimetry may detect only a small central area of retained vision. Anterior segments are normal, except in one recent report, which identified affected individuals with keratoconus and spoke-like cataracts [191]. Macular atrophy is a striking and frequent finding; in its mildest form, this may appear as mild perifoveal atrophy, but with age the atrophic macula becomes pigmented and takes on the appearance of a macular staphyloma [185]. Funduscopy in the youngest subjects shows widespread RPE atrophy and white dots, or a ‘salt and pepper’ pigment distribution [185]. With age, RPE atrophy becomes more widespread, bone spicule pigmentation or a ‘salt and pepper’ fundus may be seen and there is arteriolar attenuation [184, 185, 188, 189, 191]. There is a low autofluorescence signal corresponding to the macular atrophy [190]. OCT shows disorganized and abnormal retinal lamination eccentric to the fovea, that takes on a ‘bilaminar’ appearance, with loss of the photoreceptor and outer nuclear layers, suggestive of retinal remodeling [190]. At the fovea the photoreceptor layer may be retained, although the IS/OS junction may be ill defined, and the foveal ONL thickness reduced, suggestive of loss of cones. Although lebercilin is expressed in a number of tissues, there have been no reports of extraocular abnormalities in *LCA5* mutations. One subject with *LCA5* retinopathy died from asphyxia and the authors propose that there may be a connection between the cause of death and the presence of lebercilin in the ciliated epithelial cells of the bronchi [189].

1.5.6 *RPGRIP1* (LCA6)

LCA6 was identified through studies investigating the molecular pathogenesis of the retinitis pigmentosa GTPase regulator (*RPGR*) gene, mutations in which account for

up to 60% of X-linked RP, and which are also implicated in X-linked cone, and X-linked cone-rod dystrophy [192-196]. Yeast two-hybrid experiments, which allow the identification of the interacting partners of a particular gene by investigating the modular nature of transcription factors, were performed for RPGR by 3 independent groups in 2000 [197-199].

At that time, as the only identified mutations within *RPGR* were located within its RCC1-homologous domain (RHD), Roepman *et al* utilized RPGR and RHD in two-yeast hybrid studies to identify several novel and retina-specific gene products that were alternatively spliced from the same gene that was localized to chromosome 14q11 [199]. They named them RP GTPase regulator-interacting protein 1 (RPGIP1) isoforms and identified that they each contain an RPGR interacting domain at the C terminal and have stretches of coiled coil domains that share homology with proteins involved in vesicular transport. In human and bovine rod photoreceptor outer segments these proteins co-localise with RPGR. Mutations in *RPGR* lead to impaired interaction between these two proteins, suggesting that they could be candidate genes for RP. They suggested that RPGRIP1 might belong to a family of proteins that play a role in vesicular-transport and have neurone-specific function.

Concurrently, Boylan *et al* identified the RPGR interacting protein RPGRIP1 [197]. They identified two human RPGRIP1 orthologues, which are expressed in the retina and testis. They also mapped the *RPGRIP1* gene to 14q11. Studies of murine retinal cDNA also identified an RPGR interacting protein that, in contrast to the views of Roepman *et al.*, was exclusively localised to the photoreceptor connecting cilium

[198]. The authors concluded that *RPGRIP1* is involved in regulating protein transport to or from the OS, through the connecting cilium.

RPGRIP1 (MIM 605446) was first identified as a cause of LCA in 2001 [200]. Subsequent studies have determined the prevalence of *RPGRIP1* mutations in LCA to be 4.2% [24]. The phenotype associated with null mutations in *RPGRIP1* is typical of LCA and consists of severe visual loss and nystagmus from early childhood [200]. Nyctalopia and photoaversion are uncommon [182, 201]. Visual acuity is poor and ranges between 20/100 to no light perception [183, 200, 201], and hypermetropic refractive errors predominate [182, 183]. The retinal appearance is variable; being described as normal, unassociated with pigment, having circumferential bone spicule pigment or having drusen-like deposits [182, 200]. Vascular attenuation is widespread and macular atrophy, if present, may be seen by the third decade [200, 201]. There has been one report of 4 families diagnosed with cone rod dystrophy and mutations in *RPGRIP1*, in which the affected individuals had poor vision, colour blindness and severe photophobia from childhood, with variable fundus changes consisting of ‘granularity’ in the retina, macular degeneration and a bull’s eye maculopathy [202].

1.5.7 CRX (LCA7)

The cone-rod homeobox (*CRX*) gene (MIM 602225) was the third gene to be identified in the pathogenesis of LCA [9]. It is a member of the highly conserved orthodenticle-related (*otx*) family of homeobox genes, encoding a 299 amino acid protein with a molecular mass of 32kDa [203]. This gene was first identified in the mouse retina and was found to be expressed in developing and mature photoreceptor

cells. It is required for the differentiation of photoreceptor outer segments and is essential for photoreceptor cell survival [204].

CRX acts synergistically with neural retinal leucine zipper (NRL) in transactivating *Rhodopsin* [205]. It also regulates the expression of several other photoreceptor specific proteins including rhodopsin, the cone opsins, interphotoreceptor retinoid-binding protein, β -phosphodiesterase, and arrestin. Both NRL and CRX can independently induce rhodopsin promoter activity but the leucine zipper of NRL interacts with CRX and this leads to the establishment and maintenance of photoreceptor function [206].

In 2002 the human and murine gene structure of *CRX* was characterised [207]. Human *CRX* has a molecular mass of 25Kb and is comprised of 6 exons, while murine *crx* is 15Kb and comprises 4 exons. Both share an evolutionarily conserved promoter containing OTX/CRX and SP1/AP1 binding sites that lead to two different transcripts that are conserved in both species. The human gene has an additional human specific promoter that leads to 5 further transcripts.

The *otx* family of homeobox genes includes *PAX6*, *OTX1* and *OTX2*, which are also essential to ocular development [208]. The homeodomain of human *CRX* has 88%, 86% and 88% identity to mouse *OTX1*, *OTX2* and drosophila *otd* homeodomains respectively, and 60% identity to the homeodomain of other OTX-related proteins such as Ptx1/Potx [203]. The conserved sequences lie in the OTX tail at the carboxyl terminus and in other regions of these proteins. Animal studies have demonstrated that *crx*^{-/-} mice fail to develop photoreceptor outer segments and have a thin outer

nuclear layer, while *crx*^{+/-} mice develop short outer segments early in development, which eventually grow to the same length as those in wild type mice [209].

Pathogenic mutations in *CRX* were first identified in autosomal dominant cone rod dystrophy [204, 210]. Subsequently, a patient with LCA was identified with a heterozygous *CRX* mutation in whom the second mutation was not found [9]. Until that time, it had been considered that LCA was exclusively inherited in an autosomal recessive manner. However, in the report by Freund *et al.* the identification of only one heterozygous variant left open the possibility that these changes represented de novo mutations in autosomal recessive disease, in which a second mutation was not found, or that this was a de novo mutation in autosomal dominant disease. The parents of the affected patient did not carry the mutations and had normal phenotypes, suggesting the latter scenario. Subsequent studies have expanded the phenotype of LCA associated with mutations in *CRX*, and suggest that the condition is predominantly inherited in an autosomal dominant manner [211-219].

Phenotypic variability has been described within the cohorts of patients screened and identified with *CRX* mutations, who have diagnoses of autosomal dominant cone rod dystrophy and LCA [211, 212]. *CRX* mutation frequency in LCA is reported to be 1% [24]. The phenotype is typical of LCA, with poor vision from birth or early infancy, roving nystagmus, nyctalopia, constricted visual fields and undetectable ERGs. Visual acuity loss is usually very severe, ranging from between counting fingers to no light perception vision, although there have been some reports of better vision [217, 218]. At a younger age the retina may be normal or have a granular appearance, with RPE atrophy and white spots [211, 212, 215]. At this age the macula can appear irregular,

granular or atrophic, with RPE atrophy [211, 213-216, 219]. At an older age there may be varying degrees of pigment clumping that may be confined to the retinal periphery, with widespread RPE atrophy [211, 212, 217, 218]. In addition, there is severe macular atrophy, which can appear colobomatous [212, 213, 216].

In keeping with the autosomal dominant nature of inheritance, almost all of the LCA-associated *CRX* mutations identified to date have been in the heterozygous state. Unaffected parents have been reported to not carry the mutation, indicating that de novo mutations occur relatively frequently in *CRX* associated LCA [9, 212, 214-216, 220]. It has been proposed, however, that the heterozygous mutations identified in these subjects may be explained by the presence of an unidentified mutation on the other *CRX* allele, in autosomal recessive disease, or that there may be a mutation on another gene that would suggest digenic inheritance [221]. To date, all but one mutation has been identified in the final exon of *CRX*. Missense mutations predominantly affect the homeodomain (a region of the protein comprising 20% of all amino acid residues) and frame shift mutations generate premature stop codons and predominantly affect the OTX domain (encoded by the final exon). Only one family has been described with a null mutation affecting the first exon of *CRX* [220]. In this family the p.Pro9(1-bpins) mutation was heterozygous in both the proband, who had LCA and other systemic abnormalities, and in the unaffected father. In this family, a number of possibilities arise: if the condition is inherited in an autosomal dominant manner, it is likely to be incompletely penetrant; the father may display mosaicism and hence not display the retinal phenotype; the condition could be inherited in an autosomal recessive manner in which the second *CRX* allele was not identified; or that *CRX* is not the causative gene in this family [221].

There is only one report of a homozygous *CRX* mutation in a family with LCA that could suggest autosomal recessive inheritance [222]. Although the proband, who was from a non consanguineous family, had features consistent with LCA and carried the homozygous mutation p.W90R, the parents carried the mutation in the heterozygous state and they subsequently developed visual symptoms later in life and had signs of photoreceptor degeneration. It has therefore been proposed that in this family, a ‘semi dominant’ mode of inheritance exists in which the phenotype is severe in the homozygous state and milder in the heterozygous state [221].

1.5.8 *CRB1* (LCA8)

The 1q31-q32.1 locus was identified by linkage analysis in a large Dutch family with autosomal recessive retinitis pigmentosa (ARRP) and preserved para-arteriolar retinal pigment epithelium (PPRPE) in 1994 (RP12) [223]. The causative gene was subsequently identified as the crumbs homologue 1 gene (*CRB1*) (MIM 604210), so called due to homology to the *Drosophila* Crumbs (CRB) protein [224]. The CRB proteins are highly conserved throughout evolution and were first characterised in *Drosophila melanogaster* [225]. CRB is required to maintain epithelial cell polarity, and is located in the zonula adherens, a cell-cell adherens junction located at the apical surface of cells of epithelial origin, including photoreceptor cells in *Drosophila* and vertebrates, and vertebrate Müller glial cells [226, 227]. CRB is also required for the morphogenesis and maintenance of the vertebrate and invertebrate retina [228]. In the adult mouse retina, *Crb1* is present in the apical region of all retinal epithelial cells, the rod and cone photoreceptors and Müller glial cells.

The *CRB1* gene consists of 4,361 base pairs, comprising 11 exons, and encodes a 1,376 amino acid protein [224]. RT-PCR analysis identified *CRB1* expression in human neural retina and brain, but not in the RPE or any other extra-ocular structures. The predicted protein sequence consists of a signal peptide, 19 EGF-like domains, 3 laminin A G-like domains and a C-type lectin domain.

The phenotype associated with mutations in *CRB1* is variable. First described in 1982, autosomal recessive RP with relative preservation of the RPE adjacent to and under retinal arterioles (RP12) has now been reported in a number of families [229]. This condition is characterised by early onset progressive visual field constriction, hypermetropia, nystagmus, optic nerve head drusen, vascular sheathing and RP with preserved para-arteriolar RPE (PPRPE) (MIM 600105). *CRB1* mutations are also associated with LCA and EORD, with a prevalence of 7-13% in this group of disorders [53, 124, 230, 231]. In addition, *CRB1* mutations have been detected in subjects with RP without PPRPE [232], in asymptomatic subjects with pigmented paravenous chorioretinopathy [233] and in RP subjects who developed a Coats-like exudative vasculopathy, characterised by peripheral retinal telangiectasia and extravascular yellow sub-retinal lipid exudation, that may progress to an exudative retinal detachment [53, 230].

The phenotype in subjects with LCA or EORD that harbour mutations in *CRB1* is particularly distinctive. In a large series, *CRB1* mutations were identified in 12% of subjects with LCA, EORD and ARRP [53]. The condition is clinically progressive, with visual acuity at counting fingers or worse by the fourth decade. Hypermetropia is

common. Widespread sub-retinal white dots and macular atrophy occur from infancy, with characteristic deep nummular pigmentation at the level of the RPE developing by later childhood. This may become more extensive with age, and PPRPE, particularly associated with peripheral retinal telangeiectasia, is highly suggestive of *CRB1*-related disease. OCT imaging characteristically identifies retinal thickening around the foveal pit and disorganised retinal lamination with coarse outer and inner zones, resembling the normal immature retina [234]. Preservation of the retinal layers has been identified in younger patients, but at an older age there may be coarse retinal lamination and loss of the outer limiting membrane or atrophy of the macula with loss of the central macular volume, suggesting that the retinal changes may not represent a developmental abnormality but that there is loss of the normal architecture over time [53]. Intra-retinal cysts have additionally been described as a common feature in LCA and EORD associated with mutations in *CRB1*.

1.5.9 LCA9 locus

The LCA9 locus was identified in a study of a large consanguineous Pakistani family with LCA in 2003 [235]. The affected family members displayed typical features of LCA, with widespread pigmentation in the retina, retinal white spots, optic disc pallor and macular staphyloma. Linkage analysis in this family identified a 10 cM region of autozygosity between the markers D1S1612 and D1S228 on chromosome 1p36. This region contains at least 5.7 Mb of DNA and, at the time of identification of this locus, contained around 50 genes. For many years the causative gene at this locus remained unidentified, and a number of techniques were utilised, including candidate gene screening in an attempt to identify the gene. At the time that the work presented in

this thesis was being carried out, the causative gene at the LCA9 locus had not been identified.

However, in 2012, the gene nicotinamide nucleotide adenylyltransferase (*NMNAT1*) was identified simultaneously by 4 different groups, using exome sequencing, as the causative gene at the LCA9 locus [236-239]. *NMNAT1* (MIM 608700) encodes a 279 residue protein that plays an important role in NAD⁺ biosynthesis, in that it catalyses the formation of NAD⁺ from nicotinamide mononucleotide (NMN) and ATP [239]. It is a well-conserved protein with embryonic lethality in knockout mice and death in null mutations in *Drosophila melanogaster*. *NMNAT1* is also necessary for cell signaling and DNA metabolism [236]. Subjects with *NMNAT1* mutations have a severe LCA phenotype but have normal general health [237]. The retinal appearance is characterised by severe macular atrophy and pigmentation, with scattered peripheral retinal pigmentation [236, 237]. Vision is severely reduced to between counting fingers and nil light perception.

1.5.10 *CEP290* (LCA10)

In 2006, linkage analysis in a consanguineous French Canadian LCA family with four affected siblings identified a region on chromosome 12q21-q22 containing fifteen genes including *CEP290* (MIM 610142) [240]. This gene had recently been identified to cause Joubert syndrome-related disorders [241]. Sequencing of all 53 exons and splice junctions in this family identified only one synonymous sequence variant in exon 21 that was predicted to have an effect on exon splicing [240]. However, RT-PCR analysis in one of the affected siblings did not identify aberrant splicing of exon

21. Subsequent RT-PCR analysis of the entire CEP290 mRNA identified an aberrant splice product, and sequencing identified that a 128bp cryptic exon had been inserted between exons 26 and 27, that had introduced a stop codon immediately downstream of exon 26. Further sequencing of the genomic DNA identified a mutation in the intronic sequence (c.2991+1655A>G) that created a strong splice donor site and which had inserted the cryptic exon into the CEP290 mRNA. In a subsequent screen of 76 unrelated LCA families, this intronic mutation was identified in 4 patients in the homozygous state and in 12 patients in the heterozygous state. In the 12 heterozygous patients, the second mutation was identified in *CEP290*, confirming the autosomal recessive inheritance pattern with this gene.

Further *CEP290* mutations in families with Joubert syndrome-related disorders and Senior Loken syndrome were identified and the protein was characterised [242]. *CEP290* encodes centrosomal protein 290 (also known as nephrocystin 6, NPHP6), spans 55 exons, and 93.2kb on human chromosome 12q21.32. This is a multi-domain protein found in the centrosomes and nuclei of renal epithelial cells and in the cilia of retinal photoreceptors. The *rd16* mouse, which has early onset retinal dystrophy and absent olfactograms, suggesting anosmia, was found to harbour an 897bp in-frame deletion in *Cep290* which led to the formation of truncated CEP290 [243, 244]. Murine CEP290 is similar to human CEP290 and localises to the centrosomes of dividing cells and the connecting cilium of photoreceptors. It is present in complex with other centrosomal and microtubule based transport proteins including RPGR, RPGRIP, dynectin subunits, kinesin subunit KIF3A, γ -tubulin, centrin and ATF [242, 243], and has a role in the regulation of intracellular protein trafficking. In this mouse model, the misrouting and redistribution of phototransduction proteins leads to

photoreceptor degeneration; the connecting cilia themselves do not show any obvious structural abnormalities.

A detailed study of the single cell green alga with 2 flagella, *chlamydomonas reinhardtii*, in which most of *CEP290* is deleted, identified that *CEP290* forms part of a complex linking the flagellar membrane to microtubules in the transition zone, and regulates the entry of proteins into the cilium [245]. The transition zone is a short region of the cilium between the basal body and the axonemal microtubules where the triplet microtubules of the basal body transition into the axonemal doublets [246].

The phenotype associated with mutations in *CEP290* varies from isolated blindness (LCA) to the lethal Meckel-Gruber syndrome (MKS) [247, 248]. Other partially overlapping, yet distinct, disorders caused by *CEP290* mutations include Joubert syndrome-related disorders and Senior Løken syndrome [241, 249, 250]. The phenotype in the original French Canadian family was typical of LCA, with blindness or severe visual impairment from birth, roving nystagmus from 6 weeks, high hyperopia, the oculodigital sign, keratoconus and cataract [240]. The retinal appearance ranges from looking normal in infancy, to one with vascular attenuation, a mottled RPE, intra-retinal white dots, a salt and pepper appearance, and subsequent specular pigmentary retinal degeneration with or without nummular pigmentation in adulthood [240, 251, 252]. The macular appearance is also variable and may be normal, show a blunt foveal reflex, have a bull's eye appearance or late geographic atrophy [251, 253]. A milder phenotype, in which the vision was 20/40 at best, was reported in a family with a *CEP290* mutation that induces exon skipping [254]. OCT imaging studies have described preservation of the outer nuclear layer at the central

macula in the first few decades of life, with an age related centrifugal thinning of this layer when extending into the perifoveal area [253, 255]. The PR inner segment / outer segment junction is poorly defined in the central macula and is invisible in the periphery. The demonstration that in cone rich areas (ie the fovea) there is normal photoreceptor lamination without thinning and a detectable RPE, leads this group to suggest that *CEP290* patients may be amenable to cone photoreceptor targeted therapeutic strategies. AF imaging has revealed a hyperautofluorescent ring around the macula [252].

Cilia are essential for many different cell types and are highly conserved organelles. The extensive presence of cilia throughout the body may account for the wide range of phenotypes associated with mutations in genes that encode ciliary proteins. The olfactory system contains sensory neurons that terminate in dendritic knobs containing basal bodies, from which numerous sensory cilia that compartmentalise the signaling molecules required for odour detection, project towards the nasal mucosa [244]. Olfactory investigation in *CEP290* mutation has identified severe dysfunction in one family with LCA, and reduced electro-olfactogram responses in *rd16* mice, demonstrating anosmia. The mechanism of this olfactory dysfunction is due to the altered ciliary localisation of olfactory G proteins in the olfactory sensory neurons. In addition to this, abnormal respiratory cilia in the nasal epithelial cells of *CEP290* LCA patients, which are short, rarefied and possess abnormalities of several axonemal components, has been described [256]. These findings suggest an additional role of *CEP290* in the development of respiratory cilia in addition to photoreceptor cilia.

Mutations in *CEP290* are reported to represent the most common cause of LCA in European cohorts, comprising up to 30% of cases [24, 119, 240, 251, 252, 257]. However, the incidence of *CEP290* mutations in other cohorts worldwide is almost zero [258-260]. The majority of mutations described in *CEP290* are protein truncating, caused by nonsense or frame-shift mutations [247]. The most frequent variant, a probable founder mutation, is the intronic variant c.2991+1655A>G described in the original French Canadian family, which accounts for up to 89% of *CEP290* mutations in Northern European cohorts [24, 251, 252]. It was hypothesised that in *CEP290* related LCA, there is a small amount of functioning residual wild type protein, resulting in a dosage-dependent mechanism with sufficient residual *CEP290* activity for normal cerebellar and renal function but not for photoreceptor function; and that loss of function from both alleles leads to Joubert syndrome [240]. However, this hypothesis has since been debated as families with truncating mutations on both alleles have been identified with LCA [251]. The c.2991+1655A>G mutation had been considered to lead solely to LCA, but there have now been reports of LCA families who carry this mutation who have additional renal dysfunction [252].

CEP290 disease remains a highly heterogenous condition and there is no clear-cut correlation between genotype and clinical expression. In general, mutations leading to Joubert syndrome-related disorders tend to cluster in the second half of the gene, while there is a more homogeneous distribution to the mutations segregating with LCA, Senior Løken syndrome and MKS [247]. This clinical variability may be due to second-site modifier alleles that encode proteins that also comprise the ciliary proteome. Variants in genes such as *AH11* (associated with Joubert syndrome-related disorders), *TMEM67* (associated with a number of clinical phenotypes) and *NPHP4*

(associated with nephronophthisis and Senior Løken Syndrome) may affect the interaction and function of *CEP290*. Conversely, variants in *CEP290* may affect the phenotype caused by mutations in other ciliary genes.

1.5.11 *IMPDH1* (LCA11)

Mutations in the *IMPDH1* gene (MIM 146690) were initially identified in autosomal dominant retinitis pigmentosa [261, 262]. In a subsequent screen of different retinal phenotypes, 2 subjects with pathogenic heterozygous variants in *IMPDH1*, one with LCA and the other with EORD, were identified [263]. One child was diagnosed with LCA at 8 months of age as he did not fix or follow and had roving nystagmus. He had hypotonia and developmental delay. His retina showed diffuse RPE mottling, no pigment and an identifiable macular reflex. The second child had nyctalopia and reduced peripheral visual fields, and was diagnosed with an early onset retinal dystrophy phenotype at age 33 months. Her vision was 20/40 and she had moderate hypermetropia. Her fundus was de-pigmented, with vascular attenuation and optic nerve pallor. Both mutations were considered *de novo*, and may lead to an inheritance pattern consistent with autosomal dominant inheritance. *IMPDH1* associated LCA is extremely rare, and has not been identified in other studies worldwide of LCA screening [118, 119, 124, 201, 252, 258-260].

IMPDH1, found on chromosome 7q32.1, encodes inosine monophosphate dehydrogenase type 1 (IMPDH1), a highly conserved, widely expressed, housekeeping gene [263, 264]. It catalyses the rate limiting step of de novo guanine synthesis by oxidizing inosine monophosphate to xanthosine-5'-monophosphate with

reduction of nicotinamide adenine dinucleotide (NAD). Humans have 2 *IMPDH* genes: 1 and 2. Although *IMPDH1* is found in many tissues, its expression is highest in the retina, particularly the inner segments [264]. These retina specific isoforms may explain why mutations in *IMPDH1* restrict the phenotype to the retina.

1.5.12 *RD3* (LCA12)

Following the identification of *Rd3* gene in the RD3 mouse, which has early onset retinal degeneration, the first family with *RD3* associated LCA was discovered [265]. Mutations in *RD3* (MIM 180040) are an extremely rare cause of LCA and by the time that work towards this thesis had been completed, this was the only family to be reported with an *RD3* mutation.

Human RD3 is located on chromosome 1q32.1, and encodes a 22 KDa protein with 2 putative coiled coil domains that are presumed to be protein interaction sites. In the mouse, *Rd3* is preferentially expressed in the retina, with increased expression in early post-natal development. The exact function of RD3 is not completely understood. It is known to co-localise and interact with guanylate cyclases 1 and 2 (GC1 and GC2) in the rod and cone photoreceptors of normal mice, and one study proposed that it mediates the export of GC1 (encoded by *GUCY2D*) from the endoplasmic reticulum to endosomal vesicles, playing a crucial role in the stable expression and in the photoreceptor membrane trafficking of GC1 and GC2 [266]. Subsequent studies have proposed that RD3 inhibits *GUCY2D* activity and may play a role in retinal maturation [267].

The phenotype described in the original RD3 family, a consanguineous family of Indian origin, is typical of LCA, with poor vision from birth, nystagmus, macular atrophy, RPE mottling and both macular and peripheral pigmentation [265].

Since the work towards this thesis was carried out, further families with *RD3* mutations have been identified [268, 269]. A multiply consanguineous Kurdish family with 6 affected individuals was studied in detail, and found to have a typical LCA phenotype with poor vision from birth (never better than 1.12 logMAR) that deteriorated with age to light perception, severe nystagmus, photosensitivity, sluggish pupils, and a low hypermetropic refractive error that progressed to myopia [268]. The fundus appearance below 2 years was normal, but progressed to one with attenuated vessels, a reduced macular reflex that eventually became atrophic and a mottled peripheral retina by the third decade with bone spicule pigmentation. The OCT showed severely disorganised photoreceptor and RPE layers and a very poor autofluorescence signal was attained. The GVF was severely reduced to less than 20 degrees and the ERG was un-recordable.

A subsequent worldwide collaborative study has identified 7 further families, from 574 LCA families, giving a prevalence of 1.21% [269]. Photoaversion and low, if any, hypermetropia were common findings, with visual acuity reaching counting fingers, at best. In addition to the most frequent features of LCA, these patients had macular abnormalities ranging from ‘rearrangement’ to atrophy, little to no retinal pigmentation, and RPE atrophy with a salt and pepper fundus.

All human *RD3* mutations to date cluster in exon 2, and six of 9 families described are of Mediterranean origin, suggesting mutations ‘hotspots’ or an ancient founder mutation in this region. The phenotype bears strong resemblance to that associated with mutations in *GUCY2D*, also more common in Mediterranean populations, and it has been recommended that LCA patients with a cone rod phenotype who have moderate to no hypermetropia, and are of Mediterranean origin, should have *RD3* screening prior to the screening of other cone related LCA genes such as *GUCY2D*, *CEP290* or *RPGRIP1* when searching for the causative gene [269].

1.5.13 *RDH12* (LCA13)

The first human *RDH12* (MIM 608830) mutation was identified in 3 consanguineous Austrian families with early onset retinal dystrophy, following microarray analysis that identified a region that overlapped with the region containing the putative *LCA3* gene [270]. This region contained 29 genes and *RDH12* was selected as a candidate gene due to its location in the retina and role as a retinol dehydrogenase that was proposed to function in the visual cycle. All three families harboured the same c.677A>G variation, suggesting a founder mutation for retinal dystrophy in Western Austria. Concurrently, screening of a panel of unrelated LCA subjects in France identified a significant subset (4.1%) of patients with a range of mutations in *RDH12* [271]. The mutation spectrum in this gene was further expanded through a screening of 1011 autosomal recessive retinal dystrophy patients, at a prevalence of 2.2%, and haplotype analysis in the original *LCA3* family excluded *RDH12* as the causative gene in this locus [272].

RDH12, located on chromosome 14q23.3, encodes a 35KDa protein, retinol dehydrogenase 12, which is a member of the short chain alcohol dehydrogenase / reductase superfamily that catalyse the transformation of retinol to retinal [273]. This family of enzymes has been the subject of much study and the specific role of *RDH12* in the visual cycle remains to be elucidated. *RDH12* is localised to the inner segments of both rod and cone photoreceptors and has dual substrate specificity in that it can utilise both *cis*- and *trans*- retinoids as substrates [273], and it is also active against medium chain aldehydes [274]. The *RDH12*^{-/-} knock out mouse has a milder phenotype than in human *RDH12* mutations, suggesting that the role of murine *RDH12* is different to humans [275]. In this knock out mouse however, dark adaptation is slower and all-*trans*-retinal accumulation occurs after excessive bleaching, albeit less than in the *RDH8*^{-/-} mouse, suggesting that *RDH12* contributes less to all-*trans*-retinal reduction than *RDH8*. However, *RDH12*^{-/-} mice are more susceptible to light induced apoptosis, suggesting that *RDH12* has an important role in photoreceptor protection from all-*trans*-retinal accumulation during excessive illumination.

There are separate visual cycles in rods and cones. In the rod visual cycle, *RDH12* appears to function with, but contributes less than, *RDH8* in the reduction of all-*trans*-retinal in the photoreceptor [276]. In cones, some all-*trans*-retinal is transported out to Müller cells, isomerised to 11-*cis*-retinol, and then transported to cones for oxidation to 11-*cis*-retinal [48, 277]. Whether *RDH12* plays a role in this process remains to be elucidated. Since the work towards this thesis was carried out, an additional role for *RDH12* in rods has been hypothesised to be in the protection of

inner segment organelles against aldehyde toxicity caused by intracellular leakage of all-*trans*-retinal and other aldehydes, originating from the outer segments [44].

The phenotype associated with human *RDH12* mutations is of an early onset retinal dystrophy with symptoms beginning in the first few years of life, progressing to legal blindness by the second to third decade [270-272]. This is a severe progressive rod cone dystrophy, with widespread RPE atrophy, pronounced intra-retinal pigmentary deposition, attenuation of blood vessels and severe macular atrophy, with extinction of the ERG as early as 5 years old. The phenotype has been further described in a number of studies, and *RDH12* mutations represent a significant cause of LCA and EORD worldwide [278-284].

1.5.14 *LRAT* (LCA14)

Mutations in the Lecithin Retinol Acyl Transferase (*LRAT*) gene (MIM 604863) were first identified in individuals with early onset retinal dystrophy [285]. Located on chromosome 4q31.2, and comprising of 3 exons, *LRAT* encodes a 230 amino acid, 25KDa protein, which is expressed in a number of foetal and adult tissues including the RPE and liver [286, 287]. Its function in the RPE, and other tissues, is to transfer an acyl group from lecithin to all-*trans*-retinol (vitamin A), derived from the photoreceptors or the circulation, to generate all-*trans*-retinyl esters, a crucial step of the visual cycle.

The *Lrat*^{-/-} mouse develops normally but shows slow degeneration of the retina [288]. At 6-8 weeks of age its rod outer segments are 35% shorter than wild type mice but

the other neuronal layers are normal. The RPE is devoid of all-*trans*-retinol and all-*trans*-retinyl esters, the photoreceptors have no functional rhodopsin and the photopic and scotopic ERGs demonstrate severely attenuated rod and cone function at an early age. Similar to the *Rpe65*^{-/-} mouse, the *Lrat*^{-/-} mouse does not produce 11-*cis*-retinal [289]. Both of these models show slow degeneration of rods and failure of cone opsins to traffic appropriately to the outer segments, leading to rapid cone degeneration.

The human phenotype of *LRAT* mutations is that of a severe early onset retinal dystrophy, with onset of nyctalopia and reduced vision in the first few years of life [26, 285, 290, 291]. Only 8 patients have been reported to date. Of the limited phenotypic information available, the retina can vary from looking normal to one with vascular attenuation, peripheral retinal mottling and bone spicule pigmentation. Moderate to marked hypermetropia and visual field constriction to between 10-30 degrees is reported, and the ERG demonstrates a severe rod cone dystrophy.

Since the work toward this thesis was completed, a further family with EORD and a homozygous mutation in *LRAT* has been described [292], as well as two families of Dutch descent with a homozygous frame shift mutation in *LRAT* who have a phenotype consistent with retinitis punctata albescens, usually caused by mutations in *RLBP1* [45]. These subjects had relatively good vision (6/9.5 or better), nyctalopia and normal visual fields. The fundus showed few to numerous white dots in the mid-periphery. The ERG demonstrated reduced or non-recordable scotopic responses after standard and prolonged dark adaptation, and normal or slightly reduced photopic

responses, in keeping with retinitis punctata albescens. This finding, therefore, further expands the phenotype associated with mutations in *LRAT*.

1.5.15 *TULP1* (RP14)

Following identification of a recessive mutation in *tub* in the tubby mouse, which causes progressive retinal and cochlear degeneration and maturity onset obesity with insulin resistance and impaired glucose tolerance [293-295], mutations in genes encoding other members of the Tubby-like protein (TULP) family were sought. TULP1 (Tubby-like protein 1) is a member of this family, in which to date, 5 members have been identified: TUB, TULP1, TULP2, TULP3 and TUSP (TULP4) [296-298]. *TULP1* (MIM 602280) mutations in humans were first identified following mapping to the RP14 locus on chromosome 6q21 in two large Dominican kindreds with a severe retinal phenotype consistent with early onset retinal degeneration [299]. Concurrently, screening of *TULP1* in large panels of autosomal recessive RP families identified further pathogenic variants [300, 301].

TUB maps to chromosome 11p15.4 and *TULP1* to 6p21.3, which maps to the RP14 locus identified in autosomal recessive RP [296]. Both TUB and TULP1 have a 90% shared amino acid identity, and the members of the TULP family of proteins share a highly conserved c-terminal ‘tubby’ domain that is capable of highly selective binding to specific phosphoinositides [302, 303]. The tubby-like proteins are present in a wide range of species and show distinct expression in a number of tissues. Murine studies using *in situ* hybridisation and immunohistochemistry have identified the cell specific expression of these proteins within the retina: TUB is expressed throughout the retina,

with its highest expression in the ganglion cell layer and photoreceptors; TULP1 is expressed exclusively in the photoreceptors, localising predominantly to the inner segments, connecting cilium perikarya and terminals; TULP2 shows no retinal expression; and there is moderate expression of TULP3 in the inner nuclear and ganglion cell layers [304, 305].

It is suggested that the primary site of action of the tubby family of genes is in neuronal cells, including hypothalamic, sensory and differentiating neurones [306], and that TULP1 plays a role in intracellular trafficking in the inner segments and at the photoreceptor synapse [307]. In *Tulp1*^{-/-} mice, the photoreceptor cells degenerate, rod and cone opsins mislocalise and vesicles containing rhodopsin accumulate, suggesting that Tulp1 plays a role in protein transport through the connecting cilium between the inner and outer segments. Further studies have identified that absence of Tulp1 leads to photoreceptor synapse malformation that precedes photoreceptor degeneration, and therefore that Tulp1 is essential for photoreceptor synapse development and in photoreceptor function and survival [308].

The phenotype associated with human mutations in *TULP1* has been well documented and appears to be solely ocular. One of the original multiply consanguineous Dominican kindreds, with 16 affected members, was closely phenotyped, and the pedigree traced back to 2 founders born in the 1800s [309]. Disease onset was in early childhood with nyctalopia (as young as 10 months), poor vision (no better than 1.00 LogMAR), reduced colour vision, nystagmus and myopia. Kinetic visual field testing in the young demonstrated preservation of the peripheral field, but older subjects had only preserved 'islands' of vision. Psychophysical testing with dark-adapted

perimetry demonstrated no rod function and markedly reduced cone function, which subsequently deteriorated. The ERG was undetectable. In the first decade, the retina displayed vascular attenuation and minimal pigmentation. By the 2nd and 3rd decades, yellow deposits were seen in the macula with bone spicule pigmentation from the arcades to the periphery. By the 5th decade, subjects developed a ‘bull’s eye’ maculopathy and peripheral retinal pigmentation. The optic discs showed a ‘waxy pallor’. These individuals were otherwise in good health, were not obese and had normal hearing and balance. A similar phenotype has been described by a number of other authors [258, 310-314]. Fundus autofluorescence imaging has identified an annulus of increased perifoveal autofluorescence, and OCT imaging has shown abnormal lamination, with complete loss of the outer nuclear layer and inner segment outer segment junction [311]. Only in one study did patients predominantly have a hypermetropic refractive error [258]. Mutations in *TULP1* appear to be more common in families from the Middle East and in South East Asia. At the time the research towards this study began, no reports of human *TUB* mutations were published. We have since identified the first mutations in the human *TUB* gene causing retinal dystrophy (see chapter 4.4).

1.5.16 RGR (RP44)

The retinal pigment epithelium G protein-coupled receptor (RGR) is an intracellular membrane bound protein located in RPE cells and Müller cells, and plays a role in the visual cycle [315]. It had been proposed that RGR functions in an ‘alternative’ visual cycle that is dependent upon light, in which it regenerates 11-*cis*-retinal from all-*trans*-retinal during periods of light exposure [316]. However, experiments have

shown that RGR accelerates rhodopsin regeneration by inducing isomerohydrolase activity and accelerating the conversion of retinyl esters to 11-*cis*-retinal in a process that is independent of light levels [317]. The exact role of RGR in the regulation of the visual cycle continues to be investigated. Radu *et al.* recently identified that RPE cells respond to light by mobilising all-trans retinyl esters, and that RGR mediates this mobilisation [318]. In addition, in the dark, *in vitro* studies show that RGR inhibits LRAT and all-*trans*-retinyl ester hydrolase, and that this inhibition is reversed in the light.

RGR (MIM 600342), located on chromosome 10q23, comprises 7 exons [315]. Although extremely rare, mutations in *RGR* have been identified as a cause of retinitis pigmentosa [319]. A missense mutation, c. 196A>C, p.Ser66Arg, was identified in the homozygous state in 5 affected siblings of one RP family, suggesting a recessive inheritance pattern. The age of onset of symptoms was not reported, however vision in the 4th and 5th decades was severely reduced (to less than 1.00 LogMAR), with severe visual field constriction and severe rod cone dysfunction demonstrated by the ERG. The retina displayed diffuse depigmentation of the RPE, including the macula, with vascular attenuation and peripheral pigmentation. A second family with a heterozygous *RGR* mutation comprising a 1 base pair insertion, p.Gly275, in 2 affected siblings, suggested a dominant inheritance pattern. Vision in the 7th decade was reduced but better than in the recessive family, and the ERG was severely attenuated. One further family with the p.Ser66Arg mutation was recently reported with a severe childhood onset phenotype progressing to perception of light vision, macular RPE changes, peripheral retinal degeneration, RPE atrophy and bone spicule pigmentation by the 4th decade [292]. Further screening of *RGR* in a range of inherited

retinal dystrophies has failed to find any other pathogenic variants, confirming that *RGR* mutations are a rare cause of early onset retinal dystrophy [320, 321].

1.5.17 *IQCB1* / *NPHP5*

In 2011, mutations in *NPHP5* (*IQCB1*) (MIM 609237) were first reported in a number of non-syndromic LCA families [250, 322]. This gene was previously identified to be the predominant causative gene in individuals with Senior Løken syndrome, an oculo-renal syndrome characterised by nephronophthisis and LCA [323]. Located on chromosome 3q13.33, and comprising 15 exons, it encodes the ciliary protein nephrocystin-5, which localises to the connecting cilium of photoreceptors and the primary cilia of renal epithelial cells. *NPHP5* has been shown to interact with *NPHP6* (also known as *CEP290*), and mutations in the genes encoding these proteins are associated with LCA [324]. Knockdown of both of these genes in zebrafish leads to similar phenotypes with both ocular and systemic manifestations.

Screening of *IQCB1* in a panel of 225 LCA patients identified 11 with pathogenic mutations, 7 of whom were subsequently diagnosed with Senior Løken syndrome, and 4 of whom had ‘isolated’ LCA, giving a prevalence of 2% of isolated LCA in this cohort [322]. Concurrently, the screening of *NPHP5* in an enriched panel of 276 LCA probands identified 9 pathogenic mutations, 2 of which developed nephronophthisis in the second decade, giving a prevalence of 2.5% of ‘isolated’ LCA in this cohort [250]. The authors report that there is a highly variable age of onset of renal failure in *IQCB1* mutations, so all these patients will require lifelong screening for renal dysfunction.

The ocular phenotype in these subjects is typical of LCA, and there is little disparity between those with ‘isolated’ LCA and Senior Løken syndrome. There is significant and progressive loss of vision from birth, with pendular nystagmus, high hyperopia and an undetectable ERG [250, 322, 325]. The retina shows prominent diffuse RPE atrophy and vascular attenuation. OCT imaging demonstrates preservation of the outer nuclear layer only at the fovea and a disorganised inner segment outer segment line. Overall the phenotype is suggested to be similar to other ciliopathies such as that caused by mutations in *CEP290*. The preservation of cone photoreceptor nuclei in both *NHPH5* and *NHPH6* mutations, albeit with abnormal inner and outer segments, has led to the proposal that these subjects may be good candidates for cone-directed gene augmentation therapy [326].

1.6 Aims and Objectives

1.6.1 Aims

1. To recruit probands with childhood onset retinal dystrophies, and family members, into 2 cohorts of the Childhood Onset Retinal Dystrophy Study:
 - a. Subjects with Leber Congenital Amaurosis (LCA), Early Onset Retinal Dystrophy (EORD) and early onset rod-cone or cone-rod dystrophies
 - b. Subjects with Childhood Onset macular phenotypes;
2. To use information gathered from phenotypic studies to understand the natural history and heterogeneity of the condition(s) in order to help provide prognostic and genetic counselling to affected families;
3. To identify novel phenotypes of childhood onset retinal dystrophies.

1.6.2 Objectives

1. To undertake detailed phenotypic studies of affected subjects with mutations in specific genes in order to explore, expand and refine our understanding of the phenotypes associated with variants in these genes;
2. To obtain blood samples for DNA extraction for molecular analysis of probands and family members in order to identify causative mutation(s);

3. To work with colleagues to identify mutations in known and newly identified genes in the two cohorts, using a variety of molecular techniques.

2.0 Materials and Methods

2.1 Ethics / Patient selection

2.1.1 Ethical Approval

Ethical approval for this study, entitled ‘A Clinical Trial and Genetic Investigation of Childhood Retinal Dystrophies’ was previously granted by the Moorfields Local Research Ethics Committee (REC) in December 2004, REC reference number MOOA1005. This study is also known as the ‘Childhood Onset Retinal Dystrophy Study’, and will be referred to as such from this point on. A number of amendments had been made and approved by the REC prior to this author’s involvement in the study, and the ethical approval was extended to 2012. Following this date, new ethical approval was sought and this study was incorporated into a larger study held at Moorfields Eye Hospital (MEH) and University College London (UCL) entitled ‘A Genetic Study of Inherited Retinal Eye Disease’. Ethical approval for this study was granted by the National Research Ethics Committee Camden and Islington REC Office, REC reference number 12/LO/0141, on 30th January 2012.

2.1.2 Patient Selection

There were two separate cohorts of patients that were recruited to this study. A few different approaches to patient ascertainment were utilised, as described below.

The first, and largest cohort, were those patients and families where the proband had a generalised retinal dystrophy, which predominantly included subjects who carried a diagnosis of Leber congenital amaurosis (LCA), early onset retinal dystrophy

(EORD), childhood onset rod-cone dystrophy, childhood onset cone-rod dystrophy and childhood onset cone dystrophy. Any patients with symptoms or signs suggesting syndromic involvement were excluded.

The second cohort of patients had childhood onset signs that predominantly involved the macular region of the retina, and in particular included patients with a phenotype similar to Best disease and a newly recognised phenotype with drusen – like yellow deposits at the macula.

Patients and their families were predominantly recruited into the Childhood Onset Retinal Dystrophy Study from the paediatric and adult retina clinics at Moorfields Eye Hospital NHS Foundation Trust, London, UK and Great Ormond Street Hospital for Children NHS Foundation Trust, London, UK. Some patients were referred by Ophthalmologists or Geneticists from other hospitals, both nationally and internationally, who were aware of the study. Some of these families were then invited to take part in the study by a postal invitation if they were not able to attend MEH.

There is a large database of families with inherited retinal diseases at MEH that spans over a 40-year period. The Inherited Eye Disease (IED) Database, keeps a log of these patients and their families, along with their genetic mutations, where known. This database includes all families with inherited retinal diseases, regardless of diagnosis, age of disease onset or inheritance pattern. DNA of patients held in this database is stored at the Institute of Ophthalmology, UCL. Mr Robert Henderson and Mr Phillip Moradi, who were the research fellows involved in the Childhood Onset Retinal

Dystrophy study between 2004-2006 and 2006-2008 respectively, had previously recruited some of these families and had logged them into the IED database. A record of these 'historic' subjects was kept in a Microsoft Access (Microsoft, Washington, USA) database, to which this author had access while conducting the study.

Other researchers within the Genetics Unit were investigating patients who carried a diagnosis of autosomal recessive retinitis pigmentosa (ARRP). Several panels of DNA were screened for mutations in EORD genes by them, which included patients with ARRP but whose symptom onset, when later probed, was identified to have begun in childhood, before the age of 5 years. These subjects and their families were subsequently recruited into the Childhood Onset Retinal Dystrophy study and invited to attend for further phenotyping. These subjects will be clearly identified in this thesis.

2.1.3 Consent

Patients and their families were consented to enter this study using approved consent forms for adults and children (Appendix 7.1.2, 7.1.3, 7.1.4). Patient information sheets had been previously prepared, and included information about the study (Appendix 7.1.1). For those patients or families that were not seen and consented at MEH, a letter was sent out by post, inviting them into the study. Along with the letter, Patient Information sheets, consent forms, letters to their GP / local hospital and blood collecting tubes were also provided, so that they could have their blood samples taken locally and subsequently returned by post.

2.2 Phenotyping

All phenotyping in this study was performed at Moorfields Eye Hospital (MEH), London, UK or at the Institute of Ophthalmology, University College London (UCL), London, UK.

2.2.3 Clinical History

All subjects recruited into the study underwent detailed questioning from them or their parents regarding age of onset and course of symptoms, functional level of vision, presence and age of onset of nystagmus, nyctalopia, photophobia, photoattraction, visual field deficits, colour vision deficits and history of eye poking or rubbing. Information regarding the past ocular history including any glasses wear, presence of strabismus and previous ocular surgery or amblyopia therapy was sought. An enquiry regarding the past medical history was made, in particular any systemic illnesses or previous or on going investigations such as those looking into renal, neurological or endocrine dysfunction. These may have included radiological imaging and haematological or biochemical investigations, and was undertaken to ensure that no patients with syndromic associations were included. Birth and developmental histories were taken, including any maternal problems encountered during pregnancy, and ages that developmental milestones were met. Any current or historical use of medications was recorded. A full pedigree, including ethnicity and family history of consanguinity, was also taken.

2.2.4 Clinical Examination

2.2.4.1 Visual Acuity

Where possible, best corrected LogMAR visual acuity (VA) was obtained using the ETDRS vision chart at 4 metres. If this was not possible, the best corrected Snellen VA was measured and converted to a LogMAR scale. The Snellen VA was initially measured at 6 metres, but if subjects were unable to view the chart at this distance, it was brought closer to 2 metre or 1 metre viewing distances. If at this distance the chart was not detectable, VA was recorded in the following step-wise denominations: detection of counting fingers (CF), the LogMAR equivalent of which was recorded as 2.0; detection of hand movements (HM), the LogMAR equivalent of which was recorded as 3.0; perception of light (PL), the LogMAR equivalent of which was recorded as 5.0; or no perception of light (NPL), the LogMAR equivalent of which was recorded as 6.0 [52, 53]. Best-corrected VA (BCVA) was measured monocularly in the right eye (RE) and left eye (LE) respectively, and with both eyes open (BEO).

In infants and younger children VA was measured by orthoptic colleagues using age appropriate methods and recorded or converted into LogMAR equivalent as above. If the baby or infant was not able to undergo this assessment, its ability to fixate and / or follow a light target was recorded, and documentation made as to whether this fixation was central, steady and maintained.

2.2.4.2 Colour vision

Colour vision testing was performed on subjects with VA of CF or better. Where possible, this was done using the Hardy Rand Rittler (HRR) pseudoisochromatic plates (Richmond Products Inc., New Mexico, USA) or the Ishihara pseudoisochromatic plates (Kanehara and Co. Ltd., Tokyo, Japan) in standard room lighting. Subjects were tested with both eyes open for each of these tests. The plates were held 60 cm away from the patient at a perpendicular angle to the line of sight. The plates are intended to be presented for 4 seconds at a time, but in this study they were presented for longer if necessary, to account for poor vision and nystagmus, which could influence the speed at which the subjects could respond. The subject was required to identify the shape and position of the symbol (for the HRR test), or the number (Ishihara test), on the plate presented to them; an immediate response was required. A point was given for each correctly identified plate.

The HRR test began with the presentation of the first four demonstration plates: if these were identified correctly, testing was continued; if not, testing was abandoned. The 6 screening plates (plate numbers 5-10) were then presented; if all were identified correctly the subject was recorded as having normal colour vision and the test was complete. If the first two screening plates (plate numbers 5 and 6) were incorrect, the subject was identified to have a defect in the tritan axis (a blue-yellow defect), and was subsequently shown the tritan axis grading plates (plate numbers 21-24). If plates 21 and 22 were failed, a moderate tritan defect was recorded; if plates 23 and 24 were failed a severe tritan defect was recorded. If the last four screening plates (plate numbers 7-10) were incorrect, the subject was identified to have a defect in the protan-deutan axis (red-green defect), and was subsequently shown the plates to grade

deficiencies on these axes (plate numbers 11-20). Failure to identify only plates 11-15 indicated a mild protan and deutan deficiency; failure to identify plates 16-18 indicated a moderate protan and deutan deficiency; failure to identify plates 19-20 indicated a severe protan and deutan deficiency. Subjects' responses were recorded on the HRR scoring sheet that was supplied with the test.

Ishihara colour plate testing began with presentation of the first plate (the 'test plate'). If this was correctly identified, the subsequent plates with numbers were presented and the number of correct plates that were identified was recorded. If none of these subsequent plates were correctly identified, the subject was shown the 'hidden digits' plates. This test is designed to assess protan and deutan defects; it is not designed to identify tritan defects, and it is not able to quantify the red-green defect.

In a subset of subjects, more detailed colour vision assessment was performed using additional tests; these will be described in the appropriate chapters.

2.2.4.3 General Ocular Examination

The ocular examination involved assessment of nystagmus, in which the character, direction, velocity and amplitude were recorded. Any ocular motility abnormalities and manifest strabismus measured by the cover – uncover test were recorded. Pupillary examination was performed in scotopic conditions using a bright white light source and reactions recorded as being normal or abnormal; abnormal pupils were recorded as being sluggish, non-reactive and with or without the presence of a relative afferent pupil defect.

Slit lamp biomicroscopy (Haag-Streit, Switzerland) was used to examine the anterior segments for corneal changes and lenticular opacities in those old enough to tolerate the examination. Funduscopy was performed after the instillation of guttae tropicamide 1% and guttae phenylephrine 2.5% or of guttae cyclopentolate 0.5% (if less than 1 year old) or 1% (older than 1 year) and guttae phenylephrine 2.5% into each eye. Indirect (non contact) methods using slit lamp biomicroscopy and a Volk[®] Super Field NC[®] lens (Volk Optical Inc., Ohio, USA) were used if the subject could cooperate. Otherwise, indirect ophthalmoscopy using a Keeler Vantage Indirect Ophthalmoscope (Keeler Ltd., Windsor, UK), and a 20 dioptre Nikon lens (Nikon, Japan) or a 28 dioptre Volk[®] Double Aspheric lens (Volk Optical Inc., Ohio, USA) was performed. Recordings were made regarding retinal appearance including the vasculature, macular appearance and optic disc appearance.

An assessment of the patients' refractive status was made if the refraction was not previously available. In infants and small children this was performed by cycloplegic refraction using neutralising lenses, by Professor Anthony Moore (ATM), Miss Dev Borman (ADB) or optometric colleagues

Data from the clinical examination were recorded using a phenotyping form that had been prepared by Mr Robert Henderson, a previous research fellow who lead the Childhood Onset Retinal Dystrophy Study between 2004-2006, and entered into an Excel spreadsheet.

2.2.5 Fundus Autofluorescence Imaging

Fundus autofluorescence imaging (FAF) was performed using the Heidelberg Spectralis® HRA + OCT (Heidelberg Engineering GmbH, Heidelberg, Germany) machine, with viewing module version 5.1.2.0, in those patients old enough to cooperate with the test. This was performed at a viewing angle of 30°, centred on the fovea, using blue laser autofluorescence imaging, in each eye. An excitation wavelength of 488 nm was used and emitted light was detected above 500 nm. Several frames were taken and the signal averaged using in-built software. Due to nystagmus and photophobia, the quality of the FAF images obtained was frequently poor.

2.2.6 Optical Coherence Tomography

Optical Coherence Tomography (OCT) was performed using the Heidelberg Spectralis® HRA + OCT machine (Heidelberg Engineering GmbH, Heidelberg, Germany), with viewing module version 5.1.2.0, in those subjects old enough to cooperate with the test. The scanning protocol included a horizontal linear scan centred on the fovea and a ‘volume’ scan (19 B-scans, 20° x 15°) also centred on the fovea, for each eye. Sd-OCT data were analysed qualitatively. HEYEX software interface (version 1.6.2.0, Heidelberg Engineering GmbH, Heidelberg, Germany) was used for any measurements taken. Due to nystagmus and fixation difficulties, the images obtained were frequently not ideal.

2.2.7 Psychophysical testing: Goldmann visual fields

Goldmann visual field (GVF) testing was performed on subjects who were old enough to understand the test and if their VA was CF or better. This was a difficult test to perform for many subjects, as it required sustained central fixation that was often quite difficult to achieve due to poor central vision and nystagmus. It was performed more frequently in subjects without nystagmus and in those who had better levels of concentration and central fixation.

The perimeter was calibrated according to the manufacturer's instructions. The testing conditions were prepared prior to the subject being positioned for testing: the appropriate lens for central 30° field assessment was selected by calculating the spherical equivalent if the cylinder was 1.00 dioptre or less, with an age appropriate addition incorporated; the perimeter paper was locked into place within the machine; the patients' ability to press the buzzer was assessed, and if not possible, an alternative method of response was used such as tapping on the table or a verbal response; the subjects' chin rest was moved into place and their ability to maintain central fixation with the testing eye and with the fellow eye covered was ascertained; testing was performed with the room lights turned off.

Perimetry was performed beginning with the V4e isopter; if this was easily visible testing was repeated with the III4e and I4e targets. Subjects were asked to fixate on the central dark fixation target; eyes were tested monocularly. Testing of the peripheral field was performed without correction; for the central 30° a lens was used. Peripheral visual field testing was performed before central visual field testing. Static targets were first presented for 1 second in a variety of positions in the visual field in

order to assess areas of visual field loss and to familiarise the subject with the test. Kinetic targets were then presented by using the pantograph handle to move the stimulus from a non-seeing area into a seeing area at 3-5° per second, in all meridians. The subject was instructed to indicate when they first saw the target and a mark was made on the perimeter paper; once all the meridians had been tested, the points were 'joined up' to map the isopter. The central 30° was plotted by repeating the test with the appropriate lens. If any scotomata were found, they were mapped by moving the target from the centre of the scotoma out and the subject was instructed to indicate when they could see it. An attempt was made to map the physiological blind spot by this method as well, using the appropriate lens. Throughout testing the subjects' fixation was monitored using the telescope. Both eyes were examined in this manner.

2.2.8 Colour fundus photography

Fundus photography was performed using a Topcon TRC 501A retinal camera (Topcon Corporation, Tokyo, Japan). Composite images were created using i2k Retina™ technology (DualAlign™ LLC, New York, USA).

3.3 Genetic Methods

3.3.1 Extraction of DNA

Blood samples were collected from the proband and other affected family members, unaffected siblings and parents, where available. For those family members that were not available for sampling on the day of visit, blood sampling tubes, a letter and consent form were sent by post for the samples to be taken locally and then returned back to the Genetics Unit at Moorfields Eye Hospital, London.

Two 9 ml EDTA (Vacutainer) tubes of peripheral venous blood were obtained per person. In young children a topical anaesthetic cream, EMLA 5% (AstraZeneca, Macclesfield, UK), which contains lidocaine 2.5% and prilocaine 2.5%, was applied to the skin for 1 hour prior to venepuncture. Once the samples were obtained they were labelled, stored at 4°C, and logged on to the Moorfields Inherited Eye Diseases (IED) database.

DNA was extracted by the department core facility at the Department of Genetics, Institute of Ophthalmology, UCL, using the Nucleon BACC-2 genomic DNA kit (GE Healthcare Life Sciences, Buckinghamshire, UK), or the Puregene DNA extraction kit (Invitrogen, Paisley, UK), as per manufacturers' instructions. Extracted DNA was stored at 4°C if intended for immediate use, or at -20°C for longer-term storage.

3.3.2 Genotype identification strategies

The identification of the genetic variants in individuals affected with LCA or EORD was achieved using different techniques. As a first pass screen, APEX analysis was used; based on the phenotype, some probands underwent candidate gene screening using the polymerase chain reaction (PCR) and direct Sanger sequencing; this technique was also used to screen genes in enriched ‘panels’ of patients in whom the causative gene had not been found to date; autozygosity mapping was utilised for some families in which there was a history of consanguinity; and next generation sequencing was utilised in a family in whom all the above techniques had failed to identify the causative mutation. In our laboratory a number of researchers were investigating different inherited retinal diseases, with different phenotypic characteristics. The Inherited Eye Disease (IED) database provided subjects that were included in a variety of ‘panels’, which were investigated by a number of different researchers. As such, in a collaborative manner, different members of the group performed some of the genotyping for the subjects described in this study. This will be indicated in the relevant chapters.

3.3.2.1 DNA microarray using the Asper LCA chip

APEX analysis using the Asper LCA chip (Asper Biotech Ltd., Tartu, Estonia) was used to analyse DNA of subjects with LCA or EORD as a first pass screen for mutations known to cause LCA. In total, 104 subjects from this cohort were analysed using this method. 3.5 µg of concentrated DNA was sent to Asper Ophthalmics for analysis using this DNA chip. The technology and methods have previously been described [109].

3.3.2.2 *Polymerase chain reaction and candidate gene sequencing*

Oligonucleotide primers were designed for amplification and subsequent Sanger sequencing of the following genes: *CEP290*, *TULP1*, *RGR*, and *BEST1*. The Ensembl genome database (<http://www.ensembl.org/index.html>) was used to obtain the reference sequence, and primers were designed by hand or by utilising the Primer 3 Software (http://biotools.umassmed.edu/bioapps/primer3_www.cgi). Primer sequences are provided within the Appendix (Chapter 7.2). Oligonucleotide primers were ordered and manufactured by Sigma Life Science (Sigma – Aldrich Co. Ltd., Dorset, UK) or by Eurofins Genomics (Ebersberg, Germany). The primers were re-suspended, and concentrated stock solutions were prepared as per the manufacturer’s instructions (<http://www.sigmaaldrich.com/technical-documents/articles/biology/handling-guidelines-for-dna-and-rna-oligonucleotides.html>). All polymerase chain reactions (PCRs) were performed in a total volume of 30 µl and performed on a PTC200DNA engine thermal cycler (Bio-Rad Laboratories Inc., Hemel Hempstead, UK) equipped with a heated lid, which negated the need for the overlay of mineral oil in the PCR tube to prevent evaporation.

Table 1 outlines the components that a typical 30 µl PCR reaction consisted of.

PCR Reagents	Volume (µl)	Final Concentration
Buffer *	3.00	1X
Enhancer (100%)	0.30	10%
dNTPs (25mM)	0.24	200 µM
Forward Primer (100pmol)	0.20	20 pmol
Reverse Primer (100pmol)	0.20	20 pmol
Moltag: Taq polymerase (5U/µl)	0.20	0.5-2.5 unit
Template DNA (100ng/µl)	1.00	100 ng
Sterile H₂O	24.86	
Total PCR Volume	30	

Table 1 - PCR reagents for each 30 µl PCR reaction.

Buffer, dNTPs and Moltaq were all supplied by VH Bio (VH Bio Ltd., Gateshead, UK). The buffer contained a final concentration of 1.5mM of MgCl₂, however in order to optimise the specificity of primer annealing, extra MgCl₂ was occasionally used. A negative control with no DNA was always included in each experiment. The standard PCR cycling programme was carried out under the following general conditions:

1.	Initial denaturation:	94°C	2 minutes	
2. a.	Denaturation	94°C	30 seconds	} 35 cycles
2. b.	Annealing	50-70°C	30 seconds	
2. c.	Extension	72°C	45 seconds	
3.	Final extension	72°C	7 minutes	
4.	Hold	10°C		

PCR conditions were varied slightly according to: (i) the primer annealing temperature, which was generally taken to be approximately 2°C lower than the lowest T_m of the two primers, and (ii) the expected length of the amplified product. A gradient PCR was used when the primer annealing temperatures had not yet been optimised. This was performed at a range of temperatures based upon the T_m of the two primers.

Visualisation of the PCR products was generally performed on a 1% agarose gel, although this concentration was dependent upon the size of the expected PCR product. A 2% agarose gel was prepared by adding 2 grams of agarose (Bioline,

London, UK) to 100 ml of 1x Tris Acetate EDTA (Eppendorf, Germany) and heated in a microwave oven for 2 minutes. Before the gel was set, and once it had cooled to less than 60°C, 5 µl of Ethidium Bromide (at 10 mg/ml) was added. The gels were poured into pre-prepared gel trays that contained combs to create wells and allowed to cool. Once set, they were placed into a gel buffer tank containing TAE buffer. A size marker was loaded into the first well of each row – usually 5 µl of HyperLadder IV (Bioline, London, UK), and then 5 µl of the PCR product plus 2 µl of loading dye (containing bromphenol blue and glycerol) was loaded into each successive well. Gels were run for 30 minutes at 100 mV and then checked under a UV light.

The correct sized PCR products were purified in order to remove excess buffer, dNTPs and primers, using Montage PCR cleanup (purple) plates, as per standard protocols (Millipore, Watford, UK). PCR products were sequenced directly by using the ABI Big Dye terminator kit version 3.1 (Life Technologies, California, USA) in a total volume of 10 µl. Table 2 outlines the components that a typical 10 µl Big Dye sequencing PCR consisted of.

Sequencing PCR Reagents	Volume (µl)
Sequencing buffer (5x)	2.50
Forward or Reverse Primer (10pmol)	1.00
PCR product	1.00
BigDye Terminator	0.50
Sterile H2O	5.00
Total PCR volume	10

Table 2 – Reagents and volumes for each 10 µl sequencing reaction using Big Dye Terminator.

The sequencing reaction performed was as follows:

- | | | | |
|-------|------|------------|-------------|
| 1. | 96°C | 2 minutes | |
| 2. a. | 96°C | 10 seconds | } 24 cycles |
| 2. b. | 50°C | 5 seconds | |
| 3. | 60°C | 4 minutes | |
| 4. | Hold | 4°C | |

Following the sequencing reaction the mixture was purified using Montage sequencing cleanup (blue) plates, as per standard protocols (Millipore, Watford, UK), and run on the Applied Biosystems 3730 DNA sequencer. Analysis of the electropherograms was performed by hand using the Lasergene software package (Version 8.1) (DNASTAR, Wisconsin USA). Any mutations that were identified were confirmed bi-directionally and family members were checked for segregation of the mutation. Any novel missense mutations were checked in at least 100 control DNA chromosomes via ethnically matched DNA samples and the European Collection of Cell Cultures (ECACC) (<https://www.phenoculturecollections.org.uk/collections/ecacc.aspx>). Missense mutations were analysed using a number of mutation prediction software programmes, namely: ‘Sorting Intolerance from Tolerance’ (SIFT) (<http://sift.jcvi.org/>) and the PolyPhen-2 algorithm (<http://genetics.bwh.harvard.edu/pph2/index.shtml>). SIFT results are reported to be tolerant if the tolerant index is at least 0.05, or intolerant if the tolerant index is less than 0.05. PolyPhen-2 appraises mutations as benign, possibly damaging, or probably damaging based on the false positive rate of the model. Novel splice site

mutations were analysed using an *in silico* analysis programme available at www.fruitfly.org.

3.3.2.3 *Autozygosity Mapping*

Autozygosity mapping was performed in a number of consanguineous families in order to identify regions of autozygosity that would be predicted to contain the putative causative gene defect in that family. Families were selected to undergo autozygosity mapping if previous molecular analysis did not identify the causative mutation, if they had a high level of consanguinity (second cousin parent families were considered to be more informative), and if there was sufficient high quality DNA available for this technique. Samples were sent from our laboratory by Dr Mackay (DSM), Dr Sergouniotis (PIS) or Dr Davidson (AED) to the University of Manchester where they were analysed using the Affymetrix GeneChip® SNP array 6.0 (Affymetrix, California, USA). The Affymetrix SNP array 6.0 contains 1.8 million markers of genetic variation, with more than 906 000 SNPs and more than 946 000 probes for copy number variant detection [327]. Detailed methodology for genotyping using the GeneChip® array has been described previously [328].

The GeneChip® DNA Analysis Software (GDAS version 3; Affymetrix, California, USA), AutoSNPa software [329] and an alternative method of analysis [327] was used by Dr Mackay, Dr Davidson or Dr Sergouniotis to call SNPs for genome-wide autozygosity scans. The Microsoft Excel (Microsoft, Washington, USA) programme was used to detect regions with a shared haplotype. These regions were assorted according to size (up to the 10 largest homozygous regions were determined) and

candidate genes known to be associated with retinal diseases were selected within these regions. Subsequent positional gene sequencing and mutation analysis was performed for probands in candidate genes based upon the above methods.

3.3.2.4 *Next Generation Sequencing*

Exome capture and high-throughput sequencing was undertaken in one patient from a consanguineous family, by Dr Mackay and Dr Davidson, in collaboration with colleagues at the UCL Genetics Institute. The method has been previously described [327]. Whole exome sequencing was undertaken using the Agilent SureSelect38 Mb Human All Exon Kit and the HiSeq2000 Sequencer (Illumina Inc., California, USA). Average sequencing depth on target was 43, with 78.4% of the targeted region being covered by a read depth of 10x [330]. Calls with minor allele frequencies greater than 0.5% in the 1000 genomes dataset (<http://www.1000genomes.org/>) were filtered, based upon the prior belief that RP-related mutations are rare. Homozygous, presumed loss-of-function mutations were prioritised in this family.

3.3.3 **Bioinformatics**

A Microsoft Access (Microsoft, Washington, USA) database had been set up prior to the onset of this study in which recruited patients were stored, with some clinical data recorded within it. In addition, Microsoft Excel (Microsoft, Washington, USA) was used to record the patients recruited into the study. Pedigrees were drawn using Cyrillic 2.1 (FamilyGenetix Ltd., Oxford, UK). Composite images of fundus photographs were generated using i2k Retina™ technology (DualAlign™ LLC, New

York, USA). DNA sequencing analysis was performed using the Lasergene software package (version 8.1) (DNA Star Inc., Wisconsin USA).

4.0 Results

4.1 Overview of study

4.1.1 Study period and Patient recruitment

Subjects and their families were recruited to the Childhood Onset Retinal Dystrophy Study between August 2008 and August 2011. An electronic database in Microsoft Excel (Microsoft, Washington, USA) was kept of all families recruited during this period and categorised into the two separate cohorts of patients. Subjects were predominantly recruited from the paediatric and adult retina clinics at Moorfields Eye Hospital, London, UK and Great Ormond Street Hospital for Children, London, UK. A cohort of subjects were referred to the study by other Ophthalmologists or Geneticists who were aware of the study; in a sub-group of these subjects the genotype had been identified prior to their recruitment into the study. Access was available to the database that had been created and maintained by previous researchers involved in the Childhood Onset Retinal Dystrophy Study, so that subjects who had been recruited prior to August 2008 could be invited to attend for further phenotyping, when necessary. The data presented in this chapter represent the results obtained from these two cohorts of subjects recruited between August 2008 and August 2011. Any results identified in these subjects after this study period was complete are not included. Some of the subjects investigated according to genotype that are presented in subsequent chapters may have been recruited prior to this study period but were recalled for phenotyping. These subjects will be indicated in the relevant chapters.

4.1.2 Demographics and Diagnoses

Between August 2008 and August 2011, 201 subjects from 186 families were recruited into the Childhood Onset Retinal Dystrophy Study. The cohort comprising the generalised retinal dystrophies consisted of 177 subjects from 166 families (Cohort 1). The cohort comprising subjects with a macular phenotype consisted of 24 subjects from 20 families (Cohort 2). The results from these two cohorts will be presented separately.

4.1.2.1 Cohort 1

Of the 177 subjects in Cohort 1, 102 were male and 75 were female. The diagnoses in these subjects were made based upon their clinical histories, clinical examination and electrophysiological data, where available. Subjects diagnosed with LCA had absent or very poor vision from birth or within the first few months of life, nystagmus, sluggish pupillary responses and an undetectable ERG. Those diagnosed with EORD had a later onset of visual symptoms, in infancy or early childhood (less than 5 years of age), less nystagmus (if present at all), variably reduced vision, normal pupil reactions and a severely attenuated ERG. A diagnosis of rod-cone dystrophy (synonymous with retinitis pigmentosa) or cone-rod dystrophy was made in children with age of onset of 5 years or older, if there was ERG evidence of the class of photoreceptor that was predominantly involved, or if there was clinical evidence to suggest first rod (rod-cone) or cone (cone-rod) involvement. Those with only cone involvement, on ERG or clinical examination, were diagnosed with a cone dystrophy. EORD comprised the largest number of subjects at 96 (90 families), followed by LCA at 67 subjects (63 families), rod-cone dystrophy at 8 subjects (8 families), cone-rod

dystrophy at 3 subjects (3 families) and cone dystrophy at 3 subjects (3 families) (Table 3). In one family with two affected individuals harbouring the same mutation, symptom onset differed between these individuals, resulting in one carrying a diagnosis of EORD and one of rod-cone dystrophy (Family 40). All subjects with cone dystrophy had symptom onset below 5 years of age, and ERG confirmation of cone dysfunction but relatively normal rod function.

Diagnosis	Number of Subjects	Number of families
Early Onset Retinal Dystrophy	96	90
Leber Congenital Amaurosis	67	63
Rod-Cone Dystrophy	8	8
Cone-Rod Dystrophy	3	3
Cone Dystrophy	3	3
Total	177	167

Table 3 - Diagnoses of subjects recruited into Cohort 1 of the Childhood Onset Retinal Dystrophy Study, Aug 2009 – Aug 2011. One family is counted twice as there were two diagnoses within this family.

4.1.2.2 Cohort 2

Of the 24 subjects in cohort 2, 9 were male and 15 were female. Their diagnoses were made based upon their clinical examination and electrophysiological tests, where available. Two diagnoses comprised this cohort of subjects: 6 subjects (6 families) with autosomal recessive bestrophinopathy (ARB) and 18 subjects (14 families) with a newly recognised phenotype termed ‘yellow dot dystrophy’ (Table 4).

Diagnosis	Number of Subjects	Number of Families
Autosomal Recessive Bestrophinopathy (ARB)	6	6
Yellow Dot Dystrophy	18	14
Total	24	20

Table 4 - Diagnoses of Subjects recruited into Cohort 2 of the Childhood Onset Retinal Dystrophy Study, Aug 2009 – Aug 2011.

4.2 Overview of Study: overall

molecular findings

In this chapter the results from the molecular analyses undertaken in this Study, using a variety of techniques, will be presented. These techniques included APEX Array using the Asper Chip, direct sequencing of candidate genes, autozygosity mapping with subsequent positional candidate gene screening and exome sequencing for subjects in Cohorts 1 and 2.

4.2.1 LCA Chip results for Cohort 1

Of the 177 subjects in Cohort 1, the DNA of 104 subjects (from 102 families) was sent from UCL to be analysed across the LCA Chip (Asper Ophthalmics, Tartu, Estonia). The diagnoses in these subjects were as follows: LCA 47 subjects (45 families); EORD 51 subjects (51 families); rod-cone dystrophy 3 subjects (3 families); cone dystrophy 2 subjects (2 families); cone-rod dystrophy 1 subject (1 family). Not all subjects with LCA or EORD were sent for LCA chip analysis as they may have belonged to a sibling group, their phenotype may have suggested a particular gene and so they were pre-selected for candidate gene screening, the proband may not have provided a blood sample, or there was an insufficient amount of good quality DNA available for chip analysis. The reasons that subjects with rod-cone, cone-rod and cone dystrophies were screened using this technique were that later on in the study additional funding became available to screen more families

across the chip, so 2 subjects suggestive of a very early onset condition were screened; in addition, in 4 subjects their original diagnosis of EORD was revised to rod-cone dystrophy after further interrogation of symptoms and signs; and in 2 subjects the fundus appearance was similar to that seen in subjects with known LCA / EORD genes.

Screening for known disease associated variants in families from UCL, using the LCA chip, identified 29 subjects (from 29 families) with either 2 variants (homozygous or compound heterozygous) or with 1 variant only. This resulted in an overall variant identification rate by the LCA chip for the subjects sent from UCL of 27.9%. The results of 3 subjects are outstanding.

Of these 29 subjects identified by the LCA chip to harbour variants, 11 (37.9%) had two variants identified, of which 5 (17.2% of those identified with variants) were homozygous and 6 (20.7% of those identified with variants) were compound heterozygous variants. The LCA chip identified 18 subjects (62.1% of those identified with variants) to harbour one only variant. LCA was the most frequent diagnosis for those subjects who were identified by the chip to harbour any variants. Of the 47 LCA subjects sent for chip analysis, 12 (25.5%) were identified to harbour one variant and 5 (10.6%) to harbour two variants using this method only. Of the 51 EORD subjects screened with the chip, 6 (11.8%) were identified to harbour one variant and 6 (11.8%) were identified to harbour two variants (Table 5).

Gene	No identified by LCA chip	LCA patients sent for chip analysis (n=47)		EORD patients sent for chip analysis (n=51)	
		1 variant	2 variants	1 variant	2 variants
<i>AIPL1</i>	1	0	0	1	0
<i>CEP290</i>	9	5	2	0	2
<i>CRB1</i>	4	1	0	1	2
<i>GUCY2D</i>	5	4	1	0	0
<i>LCA5</i>	1	1	0	0	0
<i>MERTK</i>	1	0	0	0	1
<i>RDH12</i>	2	0	0	2	0
<i>RPE65</i>	2	0	1	1	0
<i>RPGRIPI</i>	2	1	0	1	0
<i>SPATA7</i>	1	0	1	0	0
<i>TULP1</i>	1	0	0	0	1
Total	29	12 (25.5%)	5 (10.6%)	6 (11.8%)	6 (11.8%)

Table 5 - Breakdown of LCA chip results for samples sent from UCL by gene, diagnosis and number of variants identified.

The most frequent gene identified by the LCA chip for subjects sent from UCL was *CEP290*, which accounted for 31.0% of the genes identified by this method, but this was only in 8.7% of all subjects sent for analysis with the chip (Figure 11). The most frequent mutation identified was the common *CEP290* intronic variant c.2991+1655A>G, p.Cys998X, occurring in 6 of 40 (15.0%) alleles identified by the LCA chip for the UCL cohort of subjects.

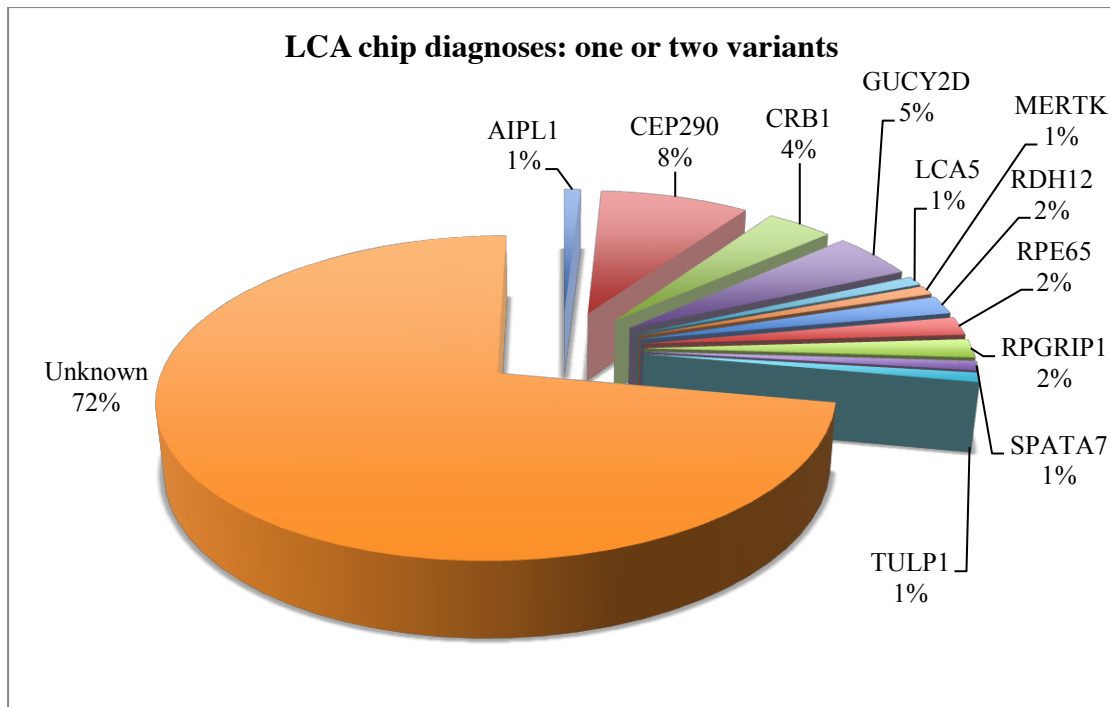


Figure 11 - Results of Cohort 1 subjects sent for LCA Chip analysis. Outstanding results are included in 'unknown' group.

For those subjects in whom only one variant was found using the chip (12 LCA and 6 EORD subjects), the second variant was investigated using direct sequencing where funding was available. Of these, in 6 LCA and 4 EORD subjects who underwent a screen in search of the second allele (in *AIPL1*, *CEP290*, *GUCY2D*, *LCA5*, *RDH12* and *RPE65*), direct sequencing identified the second variant in 3 LCA subjects (in *CEP290* and *LCA5*) and in 4 EORD subjects (in *AIPL1*, *RDH12* and *RPE65*). This search failed to identify the second allele in one subject with a *CEP290* mutation found by the chip, and 2 with a *GUCY2D* mutation found by the chip. No subjects with rod-cone dystrophy, cone-rod dystrophy or cone dystrophy who were screened across the LCA chip were identified to harbour pathogenic variants by chip analysis.

In 5 additional subjects, the LCA chip was used by the referring hospital to identify the disease causing mutations; these subjects were recruited into the study and stored on the IED database. Two of these five subjects were invited to attend Moorfields Eye Hospital for phenotypic investigations and they will be described further in subsequent chapters (Table 6).

Subject	Gene	Variant 1 (identified by Asper Chip)	Variant 2 (identified by Asper Chip)	Location of referring hospital	Invited for further phenotyping?
4	<i>CEP290</i>	c.2991+1655A>G, p.Cys998X [240]	Not found	Poland	No
12	<i>CEP290</i>	c.4723A>T, p.Lys1575X [251]	c.4966G>T, p.Glu1656X [240]	Cape Town, South Africa	No
19	<i>CRBI</i>	c.2555T>C p.Ile852Thr [124]	c.3427delT p.Cys1143AlafsX67 [331]	Firenze, Italy	No
28	<i>LRAT</i>	c.525T>A, p.Ser175Arg [285]	c.525T>A, p.Ser175Arg [285]	Manchester, UK	Yes
47	<i>RGR</i>	c.196A>C, p.Ser66Arg [319]	c.196A>C, p.Ser66Arg [319]	Rovereto, Italy	Yes

Table 6 – Subjects identified with variants using the LCA chip by referring hospital.

4.2.2 Molecular diagnoses identified in this Study

Of the subjects recruited into this study between August 2008 and August 2011, the causative gene was identified in 67 subjects (63 families) using a number of strategies. The proportions by gene and diagnoses are described below.

4.2.2.1 Molecular Diagnoses for Cohort 1

For the subjects in Cohort 1, a molecular diagnosis was obtained in 61 subjects (57 families) (34.5%) in total, using the following strategies: LCA APEX analysis (29

subjects from UCL, 5 subjects from elsewhere); direct sequencing of candidate genes to identify one or two variants by different researchers (*AIPL1* – 2 subjects, *CEP290* – 2 subjects, *LCA5* – 2 subjects, *LRAT* – 1 subject, *RDH12* – 17 subjects, *RPE65* – 7 subjects, *SPATA7* – 1 subject, *TULP1* – 1 subject); autozygosity mapping using the SNP6 chip followed by positional candidate gene screening (2 subjects: 1 *LCA5*, 1 *RDH12*) and exome sequencing (1 subject, *CRB1*). No molecular diagnosis was obtained for 116 subjects (65.5%) (109 families), which includes those families in whom the chip results are outstanding (Figure 12).

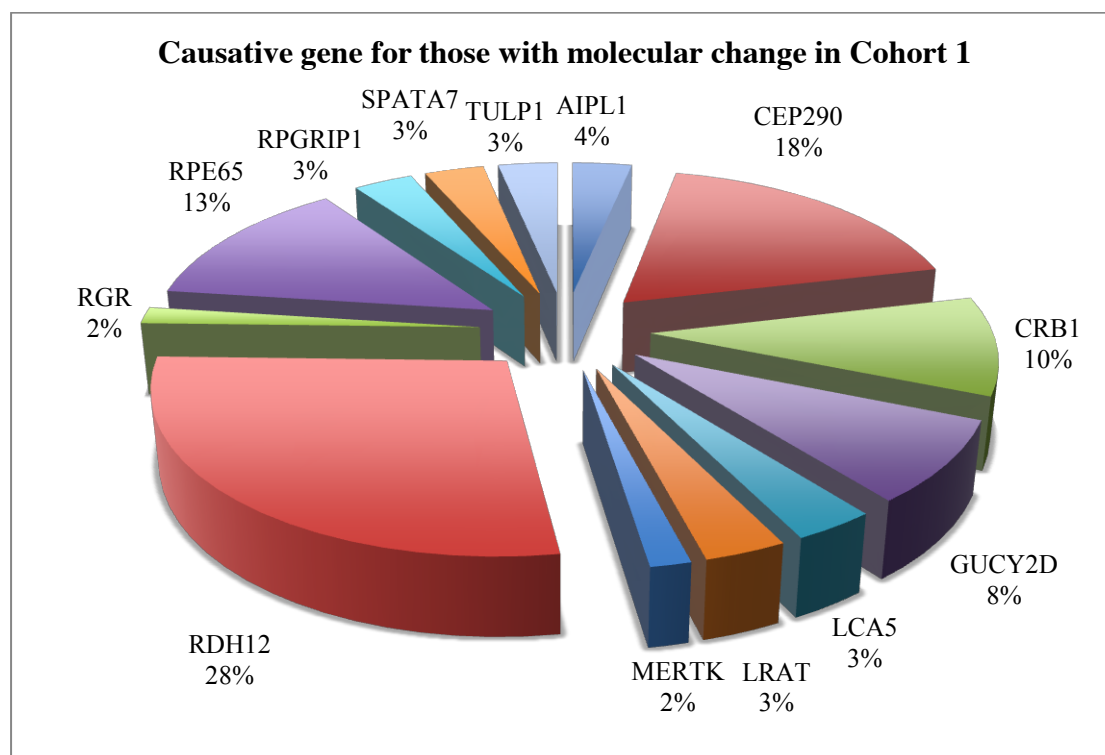


Figure 12 - Genotypes of all subjects identified with variants in Cohort 1.

Of the 61 subjects in cohort 1 in whom the causative gene was identified, 12 subjects (19.7%) (12 families) had only one variant identified and 49 subjects (80.3%) (45 families) had both variants identified. The most frequent gene identified in cohort 1

was *RDH12*, comprising 28% of all genes identified. In the subjects who only underwent direct sequencing or exome sequencing, and not Asper chip analysis (27 of 61 subjects identified with a molecular cause), molecular analysis identified both variants in all (*AIPL1* – 1 subject, *CRB1* – 1 subject [exome sequencing], *LCA5* – 1 subject, *LRAT* – 1 subject, *RDH12* – 15 subjects, *RPE65* – 6 subjects, *SPATA7* – 1 subject, *TULP1* – 1 subject). Of these, 19 (70.4%) were homozygous and 8 (29.6%) were compound heterozygous mutations. These compound heterozygous mutations were only identified in *CRB1*, *RDH12* and *RPE65*; the attributed diagnoses are indicated in Table 7. The most frequent gene to affect subjects with LCA was *CEP290* and for subjects with EORD was *RDH12*. No mutations were identified for any of the subjects who carried a diagnosis of cone-rod dystrophy or cone dystrophy (Table 7).

Gene	Total No Patients	EORD (n=96)	LCA (n=67)	Rod-Cone Dystrophy (n=8)	Cone-Rod Dystrophy (n=3)	Cone Dystrophy (n=3)
<i>AIPL1</i>	2	1	1	0	0	0
<i>CEP290</i>	11	2	9	0	0	0
<i>CRB1</i>	6	4	1	1	0	0
<i>GUCY2D</i>	5	0	5	0	0	0
<i>LCA5</i>	2	0	2	0	0	0
<i>LRAT</i>	2	2	0	0	0	0
<i>MERTK</i>	1	1	0	0	0	0
<i>RDH12</i>	17	14	0	3	0	0
<i>RGR</i>	1	1	0	0	0	0
<i>RPE65</i>	8	5	3	0	0	0
<i>RPGRIPI</i>	2	1	1	0	0	0
<i>SPATA7</i>	2	0	2	0	0	0
<i>TULP1</i>	2	2	0	0	0	0
Total	61	33	24	4	0	0

Table 7 - Genotype for Cohort 1 with breakdown according to diagnosis.

The complete list of variants identified, with method of identification and researcher who identified them, are listed in Table 8.

Subject No.	Family No.	Diagnosis	Gene	Mutation Type	Allele 1	Allele 1	Method ^{Person identifying}	Allele 2	Allele 2	Method ^{Person identifying}
					Nucleotide change	Protein change		Nucleotide change	Protein change	
1	1	LCA	<i>AIP1</i>	Hom	c.487C>T	p.Gln163X	Direct seq – novel ^a	c.487C>T	p.Gln163X	Direct seq – novel ^a
2	2	EORD	<i>AIP1</i>	Comp het	c.834G>A	p.Trp278X	Asper	c.190G>A	p.Gly64Arg	Direct seq - novel ^d
3	3	LCA	<i>CEP290</i>	Comp het	c.3175_3176insA	p.Ile1059fs	Asper	not found	not found	
4	4	LCA	<i>CEP290</i>	Comp het	c.2991+1655A>G	p.Cys998X	Asper (Poland)	not found	not found	
5	5	LCA	<i>CEP290</i>	Comp het	c.2991+1655A>G	p.Cys998X	Asper	not found	not found	
6	6	EORD	<i>CEP290</i>	Comp het	c.2991+1655A>G	p.Cys998X	Asper	c.4723A>T	p.Lys1575X	Asper
7	7	LCA	<i>CEP290</i>	Comp het	c.4723A>T	p.Lys1575X	Asper	c.712G>T	p.Glu238X	Direct seq - novel ^e
8	8	LCA	<i>CEP290</i>	Hom	c.5668G>T	p.Gly1890X	Asper	c.5668G>T	p.Gly1890X	Asper
9	9	LCA	<i>CEP290</i>	Comp het	c.4723A>T	p.Lys1575X	Asper	c.6079delG	p.Glu2027LysfsX5	Direct seq ^f
10	10	EORD	<i>CEP290</i>	Comp het	c.2991+1655A>G	p.Cys998X	Asper	c.5668G>T	p.Gly1890X	Asper
11	11	LCA	<i>CEP290</i>	Comp het	c.2991+1655A>G	p.Cys998X	Asper	c.1066-1G>A	splice site	Asper
12	12	LCA	<i>CEP290</i>	Comp het	c.4723A>T	p.Lys1575X	Asper (SA)	c.4966G>T	p.Glu1656X	Asper (SA)
13	13	LCA	<i>CEP290</i>	Comp het	c.2991+1655A>G	p.Cys998X	Asper	not found	not found	
14	14	LCA	<i>CRB1</i>	Comp het	c.2401A>T	p.Lys801X	Asper	not found	not found	
15	15	EORD	<i>CRB1</i>	Comp het	c.2843G>A	p.Cys948Tyr	Asper	not found	not found	
16	16	Rod-cone	<i>CRB1</i>	Comp het	c.3655C>T	p.Gln1219X	Exome	c.1312T>C	p.Cys438Arg	Exome
17	17	EORD	<i>CRB1</i>	Comp het	c.2555T>C	p.Ile852Thr	Asper	c.3307G>A	p.Gly1103Arg	Asper
18	18	EORD	<i>CRB1</i>	Comp het	c.2555T>C	p.Ile852Thr	Asper	c.2843G>A	p.Cys948Tyr	Asper
19	19	EORD	<i>CRB1</i>	Comp het	c.2555T>C	p.Ile852Thr	Asper (Italy)	c.3427delT	p.Cys1143AlafsX67	Asper (Italy)
20	20	LCA	<i>GUCY2D</i>	Het	c.2302C>T	p.Arg768Trp	Asper	not found	not found	
21	21	LCA	<i>GUCY2D</i>	Comp het	c.2302C>T	p.Arg768Trp	Asper	c.307G>A	p.Glu103Lys	Asper
22	22	LCA	<i>GUCY2D</i>	Het	c.121C>T	p.Leu41Phe	Asper	not found	not found	
23	23	LCA	<i>GUCY2D</i>	Het	c.2943delG	p.Ser981SerfsX39	Asper	not found	not found	
24	24	LCA	<i>GUCY2D</i>	Het	c.2849C>T	p.Ala950Val	Asper	not found	not found	
25	25	LCA	<i>LCA5</i>	Hom	c.439_449dup	p.Glu151X	Direct seq - novel ^b ; SNP6	c.439_449dup	p.Glu151X	Direct seq - novel ^b ; SNP6
26	26	LCA	<i>LCA5</i>	Comp het	c.835C>T	p.Gln279X	Asper	c.3G>A	p.Met1Ile	Direct seq - novel ^d
27	27	EORD	<i>LRAT</i>	Hom	c.316G>A	p.Ala106Thr	Direct seq - novel ^c	c.316G>A	p.Ala106Thr	Direct seq - novel ^c
28	28	EORD	<i>LRAT</i>	Hom	c.525T>A	p.Ser175Arg	Asper (Manchester)	c.525T>A	p.Ser175Arg	Asper (Manchester)
29	29	EORD	<i>MERTK</i>	Hom	c.2214delT	p.Cys738TrpfsX31	Asper	c.2214delT	p.Cys738TrpfsX31	Asper
30	30	EORD	<i>RDH12</i>	Hom	c.609C>A	p.Ser203Arg	Direct seq - novel ^d	c.609C>A	p.Ser203Arg	Direct seq - novel ^d
31	31	EORD	<i>RDH12</i>	Hom	c.609C>A	p.Ser203Arg	Direct seq - novel ^d	c.609C>A	p.Ser203Arg	Direct seq - novel ^d
32	31	EORD	<i>RDH12</i>	Hom	c.609C>A	p.Ser203Arg	Direct seq - novel ^d	c.609C>A	p.Ser203Arg	Direct seq - novel ^d
33	32	EORD	<i>RDH12</i>	Hom	c.146C>A	p.Thr49Lys	Direct seq ^d	c.146C>A	p.Thr49Lys	Direct seq - novel ^d
34	33	EORD	<i>RDH12</i>	Hom	c.601T>C	p.Cys201Arg	Direct seq ^d	c.601T>C	p.Cys201Arg	Direct seq ^d
35	34	Rod-cone	<i>RDH12</i>	Comp het	c.481C>T	p.Arg161Trp	Direct seq - novel ^d	c.714insC	p.Val238fsX34	Direct seq - novel ^d
36	35	EORD	<i>RDH12</i>	Comp het	c.57_60del	p.Pro20delfs	Asper	c.506G>A	p.Arg169Gln	Direct seq - novel ^d

37	36	EORD	<i>RDH12</i>	Hom	c.379G>T	p.Gly127X	Direct seq ^d	c.379G>T	p.Gly127X	Direct seq ^d
38	37	EORD	<i>RDH12</i>	Comp het	c.481C>T	p.Arg161Trp	Direct seq - novel ^d	c.806_810del5bp	p.Ala269fsX5	Direct seq ^d
39	38	EORD	<i>RDH12</i>	Comp het	c.806_810del5bp	p.Ala269fsX5	Asper	c.209G>A	p.Cys70Tyr	Direct seq - novel ^d
40	39	EORD	<i>RDH12</i>	Hom	c.146C>T	p.Thr49Met	Direct seq ^d	c.146C>T	p.Thr49Met	Direct seq ^d
41	40	EORD	<i>RDH12</i>	Hom	c.619A>G	p.Asn207Asp	Direct seq - novel ^d	c.619A>G	p.Asn207Asp	Direct seq - novel ^d
42	40	Rod-cone	<i>RDH12</i>	Hom	c.619A>G	p.Asn207Asp	Direct seq - novel ^d	c.619A>G	p.Asn207Asp	Direct seq - novel ^d
43	41	EORD	<i>RDH12</i>	Hom	c.601T>C	p.Cys201Arg	Direct seq ^d	c.601T>C	p.Cys201Arg	Direct seq ^d
44	42	EORD	<i>RDH12</i>	Hom	c.454T>A	p.Phe152Ile	Direct seq - novel ^d , SNP6	c.454T>A	p.Phe152Ile	Direct seq - novel ^d , SNP6
45	43	Rod-cone	<i>RDH12</i>	Hom	c.601T>C	p.Cys201Arg	Direct seq ^d	c.601T>C	p.Cys201Arg	Direct seq ^d
46	44	EORD	<i>RDH12</i>	Comp het	c.448+1G>A	splice site	Direct seq - novel ^d	c.698insGT	p.Val233ValfsX45	Direct seq - novel ^d
47	45	EORD	<i>RGR</i>	Hom	c.196A>C	p.Ser66Arg	Asper (Italy)	c.196A>C	p.Ser66Arg	Asper (Italy)
48	46	LCA	<i>RPE65</i>	Hom	c.1451G>A	p.Gly484Asp	Asper	c.1451G>A	p.G484D	Asper
49	46	LCA	<i>RPE65</i>	Hom	c.1451G>A	p.Gly484Asp	Direct seq ^e	c.1451G>A	p.Gly484Asp	Direct seq ^e
50	47	EORD	<i>RPE65</i>	Comp het	c.131G>A	p.Arg44Gln	Asper	c.1024T>C	p.Tyr342His	Direct seq - novel ^e
51	48	LCA	<i>RPE65</i>	Comp het	c.257C>A	p.Thr86Asn	Direct seq - novel ^e	c.760G>A	p.Glu254Lys	Direct seq - novel ^e
52	49	EORD	<i>RPE65</i>	Comp het	c.1543C>T	p.Arg515Trp	Direct seq ^e	c.1067dupA	p.Asn356Lysfs*8	Direct seq - novel ^e
53	50	EORD	<i>RPE65</i>	Hom	c.353G>A	p.Arg118Lys	Direct seq - novel ^e	c.353G>A	p.Arg118Lys	Direct seq - novel ^e
54	51	EORD	<i>RPE65</i>	Comp het	c.11+5G>A	cryptic splice site	Direct seq ^e	c.245G>A	p.Arg82Lys	Direct seq - novel ^e
55	52	EORD	<i>RPE65</i>	Comp het	c.1087C>A	p.Pro363Thr	Direct seq ^e	c.1418T>A	p.Val473Asp	Direct seq ^e
56	53	EORD	<i>RPGRIP1</i>	Comp het	c.1447C>T	p.Gln483X	Asper	not found	not found	
57	54	LCA	<i>RPGRIP1</i>	Comp het	c.1447C>T	p.Gln483X	Asper	not found	not found	
58	55	LCA	<i>SPATA7</i>	Hom	c.253C>T	p.Arg85X	Direct seq ^d	c.253C>T	p.Arg85X	Direct seq ^d
59	56	LCA	<i>SPATA7</i>	Hom	c.961dupA	p.Pro321ThrfsX5	Asper	c.961dupA	p.Pro321ThrfsX5	Asper
60	57	EORD	<i>TULP1</i>	Hom	c.1511_1521del	p.Leu504fsX140	Asper	c.1511_1521del	p.Leu504fsX140	Asper
61	57	EORD	<i>TULP1</i>	Hom	c.1511_1521del	p.Leu504fsX140	Direct seq ^f	c.1511_1521del	p.Leu504fsX140	Direct seq ^f

Table 8 - Genetic variants identified in cohort 1 including method and researcher identifying the variant.

a. Dr Tan, b. Dr Davidson, c. Dr Ocaka, d. Dr Mackay, e. NGRL, f. Miss Dev Borman, g. Centre for Nephrology and metabolic disorders; Abbreviations: No. – Number, LCA – Leber Congenital Amaurosis, EORD – Early Onset Retinal Dystrophy, Hom – Homozygous, Comp het – Compound Heterozygous, Seq – sequencing, SA – South Africa, SNP6 – autozygosity mapping.

4.2.2.2 Cohort 2

Molecular analysis was performed for the ARB subjects of cohort 2 in the Bestrophin-1 (*BEST1*) gene and genotype identified for all six subjects. Dr Davidson, University of Manchester, identified the variants in subjects 1-4 of this cohort and Miss Dev Borman (ADB) identified the variants in subjects 5 and 6 of this cohort. The phenotype and genetic variants will be discussed in the ARB chapter (Chapter 4.7). No molecular investigations have been carried out in the Yellow Dot Dystrophy group of subjects to date.

4.2.3 Diagnosis by Gene – Cohort 1

4.2.3.1 *AIPL1*

Mutations in *AIPL1* were identified in 2 subjects in this cohort (Subjects 1 and 2); 1 by the LCA chip (only one variant was identified), and 1 by direct sequencing by Dr Tan, UCL. In the subject in whom the Asper chip identified one variant, Dr Mackay, UCL, identified the second variant by direct sequencing. One subject carried a diagnosis of LCA and one of EORD. The phenotype associated with *AIPL1* mutations in this cohort will be discussed in chapter 4.3.

4.2.3.2 *CEP290*

CEP290 was the most frequent gene identified in subjects with LCA (affecting 13.4% of subjects with LCA) and in the subjects who were screened across the LCA chip

(identified in 31.0% of subjects sent for LCA chip analysis from UCL). The most frequent mutation identified was the common intronic variant, c.2991+1655A>G, p.Cys998X, occurring in 6 of 40 (15.0%) alleles identified by the LCA chip. This variant is reported to be the most common LCA variant, identified in up to 26% of LCA cases in North Western European populations, but it has a much lower incidence in other populations [247]. All but one of the subjects identified with variants in *CEP290* in this cohort (Subjects 3 – 13) were of European origin; the one subject who was not was from South Africa although he is presumed to be of British and Dutch descent. The genotype-phenotype associations for *CEP290* will be discussed briefly in chapter 4.3.

4.2.3.3 *CRBI*

Mutations in *CRBI* comprised 9.8% of those identified with mutations in this cohort (Subjects 14 - 19) and the strategies used to identify them included screening using the LCA chip (5 subjects) and exome sequencing (1 subject). This patient (Subject 16) had been screened across the LCA chip prior to exome sequencing, but no variants were identified. The compound heterozygous mutations in *CRBI* identified in this subject (c.3655C>T, p.Q1219X and c.1312T>C, p.C438R) were excluded from the 1000 genomes project and exome variant server, and were considered to be novel. The phenotype associated with *CRBI* mutations in this cohort will be discussed briefly in chapter 4.3.

4.2.3.4 *GUCY2D*

GUCY2D mutations were identified in 5 subjects in cohort 1, all via the LCA chip (Subjects 20 – 24). All 5 subjects carried a diagnosis of LCA. The chip identified two variants in only one subject, but one variant in 4 subjects. Direct sequencing of *GUCY2D* was performed by Dr Ocaka, UCL, in 2 of these four subjects, which did not identify a second variant. These two subjects had no other affected family members and no family history of consanguinity. *GUCY2D* has been identified to segregate both in an autosomal dominant and a recessive manner [114, 126-128]; it may be postulated that in this cohort the identification of only one variant in *GUCY2D* could suggest an autosomal dominant inheritance pattern with a possible de novo mutation in these individuals. However, this is unlikely to be the case as all dominant mutations in *GUCY2D* have been identified, to date, to cluster in 3 particular codons, 837, 838 and 839 [128]. These were not implicated in any of the *GUCY2D* subjects identified in this study. The genotype-phenotype associations of *GUCY2D* will be discussed in chapter 4.3.

4.2.3.5 *LCA5*

2 subjects were identified with *LCA5* mutations. One subject (Subject 25) had undergone autozygosity mapping due to her consanguineous ancestry, which identified a region of homozygosity in which *LCA5* resided. Positional gene screening was carried out, which identified the c.439_449dup, p.Glu151X variant in the homozygous state. The molecular analysis in this family was performed by Dr Davidson, UCL. The other subject (Subject 26), identified with compound heterozygous mutations in *LCA5*, had one variant identified by the Asper chip and the

other variant by direct sequencing by Dr Mackay, UCL. The phenotypes in these individuals will be briefly discussed in chapter 4.3.

4.2.3.6 *MERTK*

A homozygous mutation in *MERTK* was identified in one subject by the Asper chip (Subject 29). This subject carried a diagnosis of EORD. The phenotype associated with this *MERTK* variant will be discussed in chapter 4.3.

4.2.3.7 *RDH12*

RDH12 was the most frequently identified gene, comprising 27.8% of the genes identified in cohort 1 (Subjects 30 – 46). All 17 subjects identified with *RDH12* mutations underwent direct sequencing by Dr Mackay, which identified both alleles in 15 of 17 (88.2%) subjects, and one allele in 2 subjects, both of whom had one allele identified by the LCA chip. The reason for the high proportion of subjects with *RDH12* mutations in this series is that the distinctive phenotype associated with *RDH12* mutations had recently been described [278], and the majority of these subjects were selected for *RDH12* screening based upon their phenotype. A number of novel mutations were identified. These subjects were combined with those with *RDH12* mutations that were identified and phenotyped by the previous research registrar, Mr Phillip Moradi, and published [284]. The genotype-phenotype associations for *RDH12* identified in this study will be discussed in chapter 4.3.

4.2.3.8 *RPE65*

Mutations in *RPE65* were identified in 13.1% of the subjects in whom a molecular diagnosis was identified (Subjects 48 – 55). The Asper chip identified variants in 2 subjects, but the majority of the *RPE65* variants were identified by direct screening at the National Genetics Reference Laboratory (NGRL) in Manchester, part of the Central Manchester University Hospitals NHS Foundation Trust, UK, who at the time of conducting this study, provided a clinical service in which molecular analysis of *RPE65* was performed using direct screening. The subjects were selected for *RPE65* screening based upon their history and clinical features, and referred directly to the NGRL, who identified variants in 7 of the 8 subjects with mutations in *RPE65* ascertained in this study. 6 of these variants were novel. The phenotype associated with mutations in *RPE65* will be discussed in chapter 4.3.

There was one *RPE65* subject who displayed hypomorphic features (Subject 52), and he was a compound heterozygote, as were 5 of the 7 families identified with *RPE65* mutations. However, he was the only subject to harbour a duplication on one allele, c.1067dupA, p.Asn356Lysfs*8, which occurs beyond halfway in the transcript. His other variant, c.1543C>T, p.Arg525Trp occurs late in the transcript, and *in silico* analysis suggests that it is damaging (SIFT) or probably damaging (PolyPhen2). It is presumed that his mutation leads to some functional protein product. However, comparison of the location of these variants to the other milder cases reported in the literature, which have occurred much earlier in the transcript, do not identify any true correlation between mutation location and phenotypic severity [151, 161].

4.2.3.9 *RPGRIP1*

2 subjects (Subjects 56 and 57) were identified by the Asper chip to harbour only one variant each in *RPGRIP1*. This was the same variant in both subjects, c.1447C>T, p.Gln483X. No further molecular screening was carried out in these subjects, and so the second variants were not identified. The phenotypes in these individuals will be briefly discussed in chapter 4.3.

4.2.3.10 *SPATA7, TULP1, LRAT, RGR*

The variants identified in these genes and the associated phenotypes observed will be discussed in the appropriate chapters (4.4 – 4.7).

4.2.4 Diagnosis by Gene – Cohort 2

The subjects in cohort 2 who underwent molecular screening all carried a diagnosis of autosomal recessive bestrophinopathy. In collaboration with Dr Davidson, University of Manchester, the disease-causing variants were identified in *BEST1*. These subjects underwent phenotypic studies at Moorfields Eye Hospital by Miss Dev Borman. The findings and associated phenotypes in these subjects will be presented in chapter 4.8.

4.2.5 Summary of overview of study

In total, 201 subjects were recruited into this study, with 177 carrying a diagnosis of a generalised retinal dystrophy (cohort 1) and 24 with a macular phenotype (cohort 2).

In cohort 1, the LCA chip was used as a ‘first pass screen’ in 104 subjects, which identified 1 or 2 variants in known LCA and EORD genes in 29 subjects. The chip was more informative for subjects with LCA than EORD. In total, the disease causing mutation was identified in 34.5% of subjects in cohort 1, using a variety of techniques including APEX analysis, direct sequencing, autozygosity mapping with positional candidate screening and exome sequencing. 35.8% of LCA subjects and 34.4% of EORD subjects had their genotype identified using these different methods. The molecular analysis and detailed phenotyping results will be further considered in the subsequent chapters.

In cohort 2, molecular analysis into *BEST1* was only carried out for the subjects with presumed autosomal recessive bestrophinopathy. Subjects with a macular phenotype similar to drusen at the macula did not undergo molecular analysis. The phenotypes of the subjects in cohort 2 will be discussed in subsequent chapters.

The molecular techniques utilised in this study were in widespread use at the time that the study was conducted. However, with the advent of next generation sequencing many of these techniques have been surpassed. The rapid detection of genes using whole genome sequencing and exome sequencing is likely to lead to the successful identification of the molecular cause in the majority of patients with LCA and EORD, in whom, in the past, the molecular diagnosis frequently remained unidentified. This is a very exciting time in the field of genetics and will hopefully produce translatable results that may help develop novel therapeutic techniques in the future.

4.3 Genotype - Phenotype Associations

Of the subjects recruited into Cohort 1 of the study a number of causative genes were identified using APEX microarray and direct sequencing. These genes have previously been identified to cause Leber Congenital Amaurosis (LCA) and Early Onset Retinal Dystrophies (EORD). A number of reports have been published describing the phenotype associated with these genes. The clinical features associated with the following genes in the subjects in cohort 1 will be briefly described here: *AIPL1*, *CEP290*, *CRB1*, *GUCY2D*, *LCA5*, *MERTK*, *RDH12*, *RPE65* and *RPGRIP1*.

4.3.1 *AIPL1* Genotype - Phenotype association

Two subjects (Subject 1 and Subject 2) from 2 families in Cohort 1 were identified to harbour mutations in *AIPL1*. The phenotype in both of these subjects was quite different, with subject 2 displaying a much milder phenotype. Subject 1 was from a consanguineous family from the UAE and was noted to have poor vision and nystagmus from 2 months of age, with photophilia. When examined at age 24 months he had perception of light vision in both eyes, amaurotic pupils, nystagmus and hypermetropia (+6.50 DS in each eye). His fundi at this age were normal. His features were consistent with a diagnosis of LCA. Subject 2, from a non-consanguineous British Caucasian family, had a much milder phenotype. She only had nystagmus, associated with head nodding, from 2 months of age. There were no visual concerns otherwise, although she did display photophilia despite her ERG findings. At 26 months of age her visual acuity was 0.50 LogMAR with both eyes open, she had

normal pupils and a myopic refraction (-8.50 DS in each eye). Aside from mild mottling at both maculae, her fundi at this age were otherwise normal (Figure 13 - A and B). OCT imaging showed disruption of the photoreceptor layer at the fovea (Figure 13 - C and D). An ERG performed at 8 months of age identified marked cone dysfunction but normal rod function. Her diagnosis was consistent with EORD, with hypomorphic features compared to the usual phenotype associated with mutations in *AIPL1*, which is typically more severe [179-181, 332, 333]. However, the residual ERG function demonstrated in subject 2 bears similarities to the very young *AIPL1* subjects with residual rod ERGs that were recently reported, and who may be human candidates for gene replacement therapy, which has been identified in animal models of *AIPL1* disease to show effective photoreceptor rescue [334, 335].

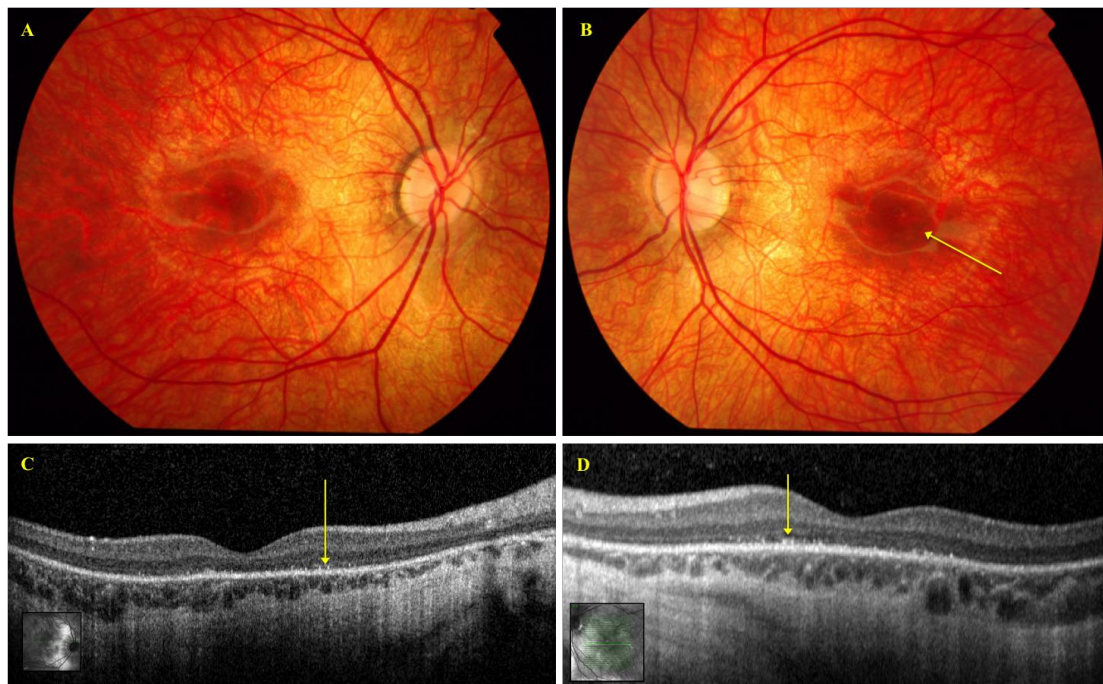


Figure 13 - Subject 2, *AIPL1*, Hypomorphic EORD. A – right eye fundus; B – left eye fundus, yellow arrow indicating subtle mottling at fovea; C – OCT right eye; D - OCT left eye, yellow arrows indicating disruption of photoreceptor layer. Images taken at age 3 years.

4.3.2 *CEP290* Genotype - Phenotype association

Eleven subjects from 11 unrelated families in cohort 1 were identified with mutations in *CEP290* (Subjects 3 -13). Eight subjects were British Caucasian, 2 were half British Caucasian and 1 was Polish. None of the *CEP290* families had consanguineous ancestries. All subjects had poor vision from birth or within the first 2 months of life, with severe nyctalopia, visual field loss and nystagmus. General health was normal in 8 of 11 *CEP290* subjects. One subject had Asperger syndrome and no renal abnormalities (Subject 3), one had a renal transplant by 12 years of age (Subject 8) and one had renal cysts by 2.75 years of age (Subject 12).

Visual acuity ranged from between 0.78 LogMAR to nil perception of light (age range 3 months to 29 years 10 months) (Figure 14). Six of 11 subjects had perception of light or nil perception of light vision. In general, the visual acuities observed in *CEP290* associated retinopathy were poor and appeared to be worse in infancy than in the third decade (Figure 14). This change in acuity might be perceived as the vision improving over time, however, it is more likely that this apparent improvement actually reflects the methods available to measure vision at an early age rather than a true improvement in vision. Due to the small number of subjects identified with *CEP290* mutations in this study, and to the lack of longitudinal data, it is not possible to reliably conclude that the vision in subjects with mutations in this gene improve with age.

Roving eye movements were present in all subjects and two displayed the oculodigital sign. Hypermetropic refractive errors were present in 9 subjects for whom refractive data were available, with a spherical equivalent ranging between +5.50 D and +7.25

D. Anterior segments and mediae were clear in all but one subject who had keratoconus and posterior subcapsular lens opacification in both eyes (Subject 3). The fundi were normal at a young age (7 subjects, age range 3 months to 33 months). In the third decade the fundi displayed widespread RPE atrophy, bone spicule and nummular pigmentary retinopathy and vascular attenuation (4 subjects, age range 20 years to 29 years 10 months) (Figure **15** - A and B, Subject 10). ERGs, performed in 9 of 11 subjects, were unrecordable (age range 3 months to 29 years). All but 2 subjects carried a diagnosis of LCA; Subjects 6 and 10 had diagnoses of EORD as their onset of visual symptoms were in infancy and visual acuities were 1.48 LogMAR (right eye) and 1.78 LogMAR (left eye) (Subject 6, age 29 years 10 months) and 0.78 logMAR in either eye (Subject 10, age 27 years).

The phenotypic findings associated with the *CEP290* subjects in this cohort are consistent with published reports [252, 255, 336]. Although there is no clear cut genotype - phenotype correlation associated with *CEP290* mutations, in LCA caused by mutations in this gene there is severe rod cone dysfunction with counting fingers or worse visual acuity and fundus changes that progress from being normal or having minimal peripheral white dots early in life to mid-peripheral nummular and specular pigmentation later in life [240, 247]. The identification of cone rich regions with corresponding normal OCTs, particularly at the fovea, has led to the suggestion that gene therapy may be possible for the restoration of central vision in these subjects [255, 337].

Subject, Family, (Gender)	Ethnicity	Consanguinity	Diagnosis	Age at Onset (Weeks)	Age at Exam	LogMAR VA RE, LE	Spherical Equivalent (Dioptres) RE, LE	General Health	Retina
3, 3, (M)	British Caucasian	Nil	LCA	Birth	21 yr 8 mth	1.78, 1.55	Moderate hypermetropia	Asperger	Peripheral RPE atrophy
4, 4, (M)	Polish	Nil	LCA	Birth	23 mth	NPL, NPL	+6.50, +6.25	Normal	Normal
5, 5, (M)	British Caucasian	Nil	LCA	8	18 mth	NPL, NPL	+6.50, +5.50	Normal	Normal
6, 6, (M)	British Caucasian	Nil	EORD	Infancy	29 yr 10 mth	1.48, 1.78	Not available	Normal	Widespread RPE atrophy, nummular & BS pigment, attenuated vessels
7, 7, (M)	1/2 British Caucasian, 1/2 Brazilian	Nil	LCA	6	3 mth	NPL, NPL	+6.50, +6.50	Normal	Normal
8, 8, (M)	British Caucasian	Nil	LCA	6	20 yr	1.00, 1.00	Not available	Renal transplant	Widespread RPE atrophy, nummular & BS pigment, attenuated vessels
9, 9, (F)	British Caucasian	Nil	LCA	6	9 mth	PL, PL	Hypermetropic astigmatism	Normal	Normal
10, 10, (M)	British Caucasian	Nil	EORD	Infancy	27 yr	0.78, 0.78	Moderate hypermetropia	Normal	'typical RP'
11, 11, (M)	British Caucasian	Nil	LCA	8	13 mth	NPL, NPL	+6.00, +6.00	Normal	Normal
12, 12, (M)	1/2 British Caucasian, 1/2 SA Caucasian	Nil	LCA	Birth	33 mth	FF, FF	+7.25, +7.25	Renal cysts	Normal
13, 13, (F)	British Caucasian	Nil	LCA	4	19 mth	PL, PL	+7.00, +6.50	Normal	Normal

Table 9 - Clinical Features of *CEP290* subjects in cohort 1.

F – Female; M – Male; SA – South African; LCA – Leber Congenital Amaurosis; EORD – Early Onset Retinal Dystrophy; yr – years; mth – months; VA – Visual Acuity; RE – Right Eye; LE – Left eye; NPL – Nil Perception of Light; PL – Perception of Light; FF – Fixing and Following; BS – Bone Spicule; RP – Retinitis Pigmentosa.

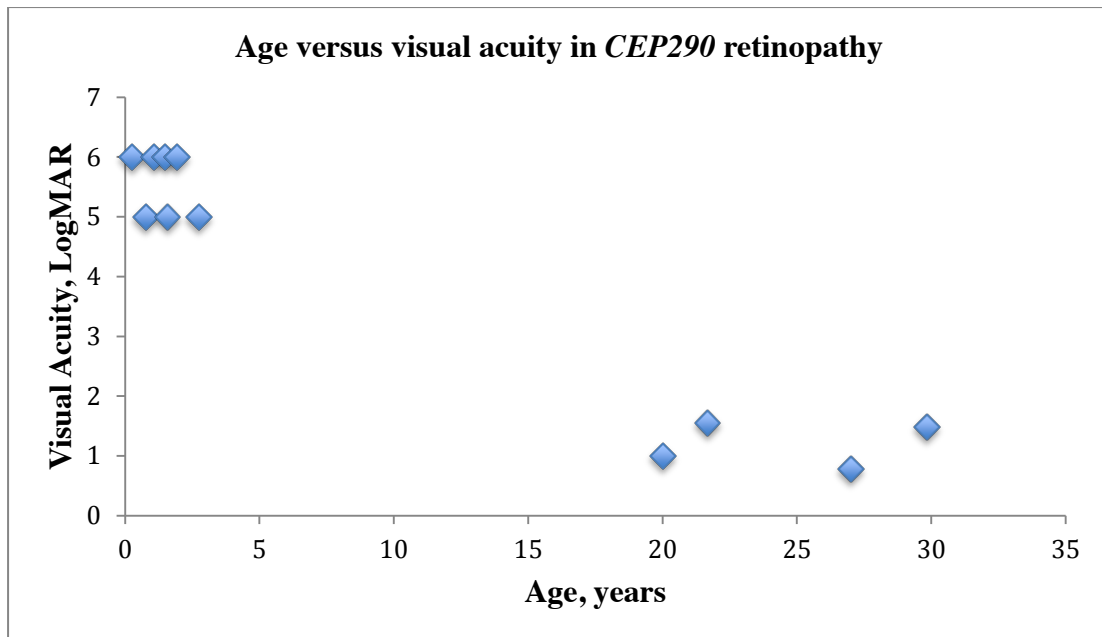


Figure 14 - Graphical representation of age versus visual acuity in *CEP290* retinopathy. In the first decade visual acuity appears to be worse than in the third decade. Visual acuities of 5 LogMAR and 6 LogMAR represent perception of light and nil perception of light vision, respectively [53].

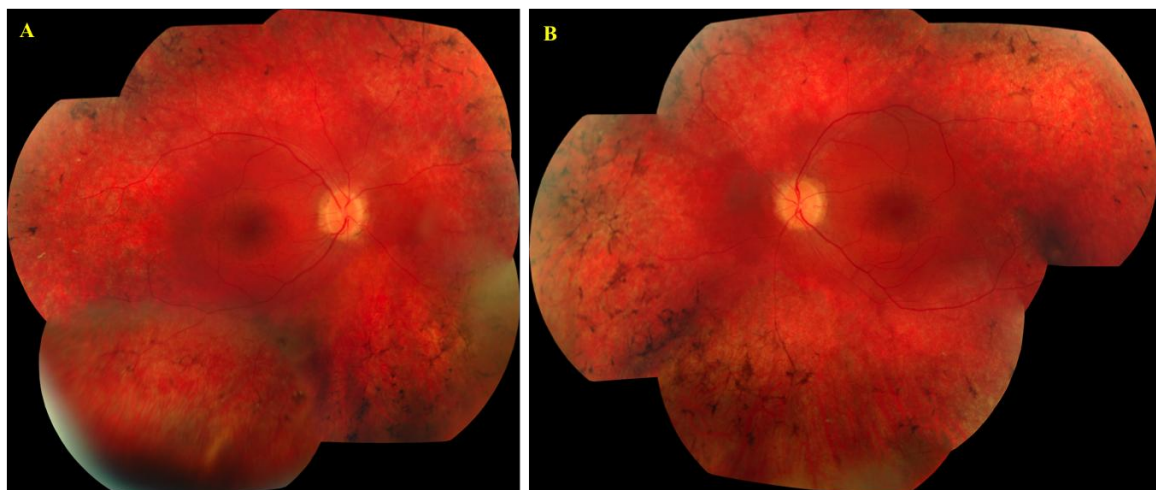


Figure 15 - Subject 10, *CEP290*, EORD. A – right eye fundus; B – left eye fundus. Both fundi show widespread RPE atrophy, vascular attenuation, and peripheral bone spicule and nummular pigmentation. Images taken at age 27 years.

4.3.3 *CRBI* Genotype - Phenotype association

Six subjects (6 families) in cohort 1 had mutations in *CRBI*. One subject carried a diagnosis of LCA (Subject 14), 4 had EORD (Subjects 15, 17, 18, 19) and 1 had rod cone dystrophy (Subject 16). Four of six subjects were British Caucasian, 1 was Indian and 1 was Italian. The only subject from a consanguineous family was subject 16 and he had compound heterozygous mutations in *CRBI*. All subjects' general health was normal.

The subject with LCA had poor vision from 6 weeks of age with nyctalopia and nystagmus. When examined at 4 months he was able to fix and follow, and he had bilateral macular atrophy with surrounding pigment. The subjects with EORD had poor vision from between 2 years and just below 5 years of age. Two of these subjects had nyctalopia and only one had nystagmus, from 10 years of age (Subject 19). Visual acuity in the subjects with EORD ranged from between 0.10 LogMAR to nil perception of light (age range 11 years 4 months to 53 years). All 4 subjects had widespread retinal pigmentation and maculopathy to varying degrees (Figure 16 – A and B, Subject 19). Subject 15 had milder retinal pigmentation at age 11 years (Figure 17 - A and B). Fundus autofluorescence (FAF) in one EORD subject identified a dense hyperautofluorescent ring at the macula at age 11 years 4 months (Subject 15) (Figure 17 - C and D). Three of 4 subjects had OCT imaging which demonstrated thickening of the retina; in 2 subjects there were intra-retinal cysts (Subjects 15 and 17) (Figure 17 – E and F, subject 15). Subject 16, diagnosed with rod cone dystrophy, had poor vision from 6 years and nyctalopia from 10 years of age. His visual acuity was 0.78 LogMAR (right eye) and 1.00 LogMAR (left eye) at 23 years of age. His fundi also displayed typical features associated with *CRBI* mutations, with

widespread RPE atrophy, coarse retinal pigmentation and macular thickening (Figure 18 - A and B). FAF demonstrated hypoautofluorescence at the macula and OCT imaging did not identify macular oedema (Figure 18 – C to F). ERGs performed in 4 of 6 *CRBI* subjects identified severe photoreceptor dysfunction with more severe rod than cone involvement (Subjects 14 – 17, age range 4 months to 23 years). In 3 subjects there was a hypermetropic refractive error with the spherical equivalent ranging between +1.88 D and +8.00 D.

These phenotypic observations correlate with the published phenotype associated with mutations in *CRBI*, which in infants is characterised by retinal white dots and macular atrophy but in later childhood is associated with deep nummular pigmentation, preservation of the para-arteriolar RPE, peripheral telangiectasia, increased retinal thickness and macular atrophy [53, 230, 233, 331]. Additionally there may be an exudative retinal detachment, seclusio pupillae and secondary glaucoma. OCT imaging in *CRBI* mutations typically displays retinal thickening, disorganised and coarse retinal lamination, loss of the outer limiting membrane with age and intra-retinal cysts [53, 234].

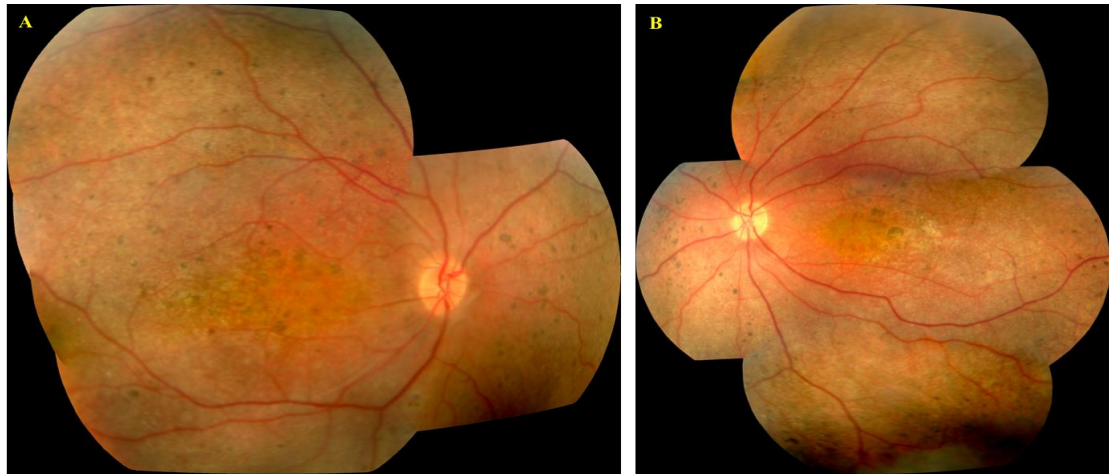


Figure 16 - Subject 19, *CRB1*. Diagnosis EORD. A – right eye fundus; B – left eye fundus. Fundi display dense macular atrophy and peripheral nummular pigmentations. Images taken at age 12 years.

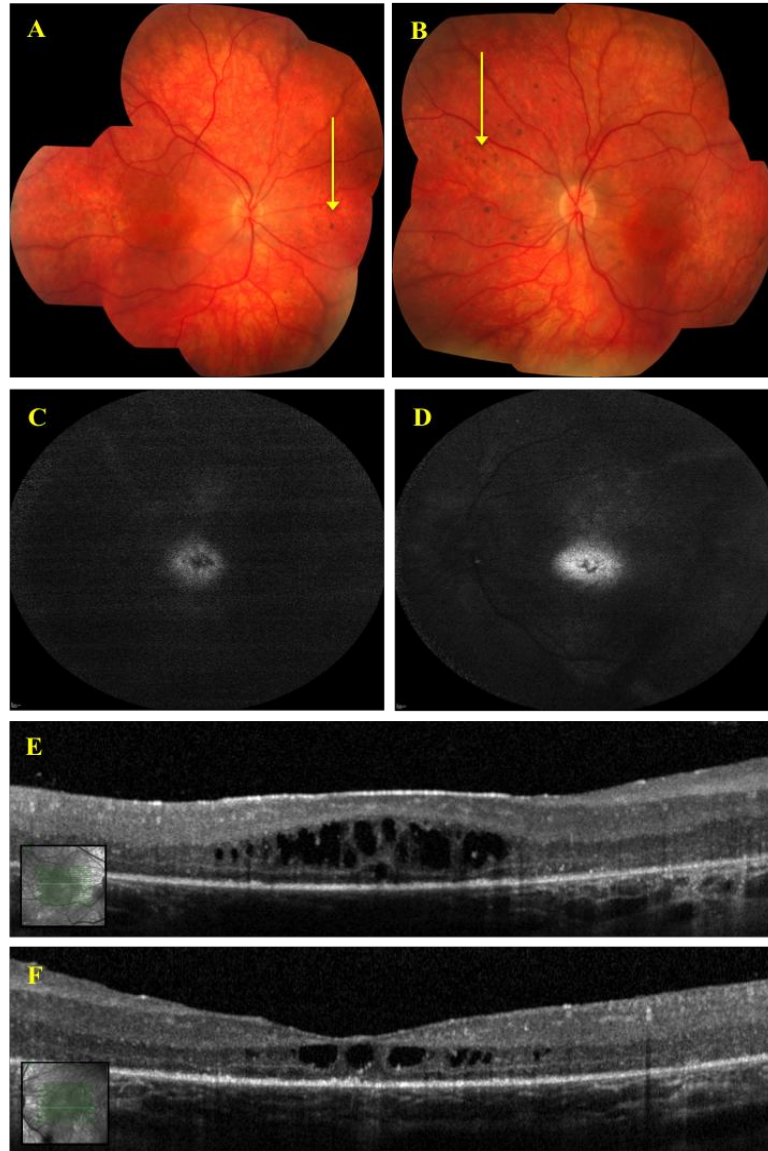


Figure 17 - Subject 15, *CRBI*, EORD. A – right eye fundus; B – left eye fundus. Fundi demonstrate mild disease with peripheral nummular retinal pigmentation (yellow arrows); C – right eye FAF; D – left eye FAF. FAF imaging shows dense hyperautofluorescence at the foveas; E – right eye OCT displaying macular thickening and intra-retinal fluid, central retinal thickness 496 microns; F – left eye OCT displaying macular thickening and intra-retinal fluid, central retinal thickness 243 microns. Images taken at age 11 years.

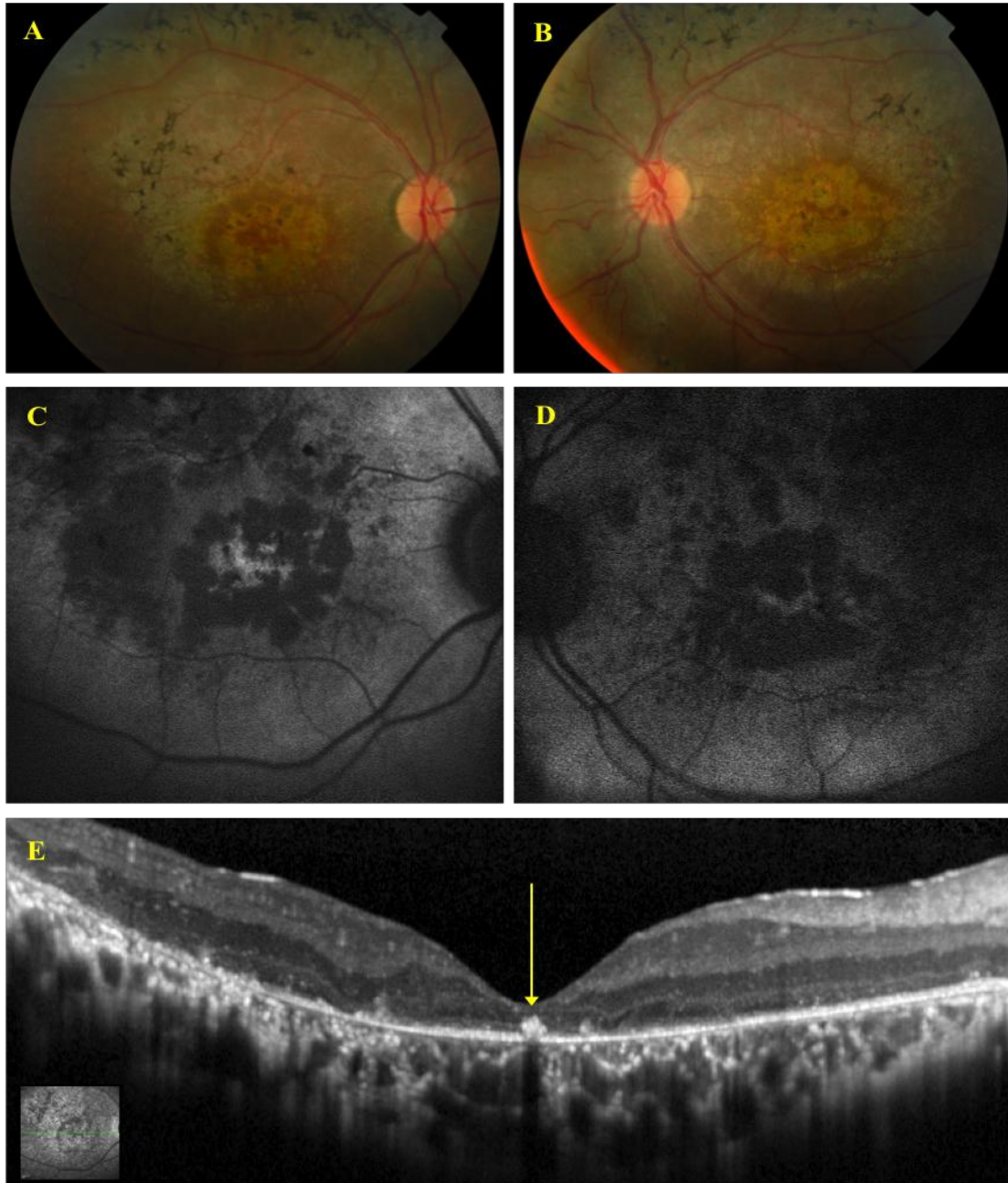


Figure 18 - Subject 16, *CRB1*. Diagnosis rod-cone dystrophy. A – right eye fundus; B – left eye fundus. Fundi display dense macular atrophy and pigmentation; C – right eye autofluorescence; D – left eye autofluorescence. Dense hypoautofluorescence corresponding with the macular atrophy; E – right eye OCT, demonstrating severe disruption of the photoreceptor layer (yellow arrow) and disrupted retinal lamination. Images taken at age 21 years.

4.3.4 *GUCY2D* Genotype - Phenotype association

In five subjects (5 families) in Cohort 1, *GUCY2D* was identified as the causative gene (Subjects 20 – 24). Three of 5 subjects were British Caucasian, 1 was Turkish and one was Khazakstani. All 5 had been diagnosed with LCA, with poor vision beginning between birth and 2 months of age. All had roving nystagmus and 2 had photoaversion. Visual acuity in the two oldest subjects was better than in the three younger subjects: perception of light to nil perception of light in subjects 21, 22 and 24 (age range 10 months to 42 months) and 0.8 LogMAR to 1.76 LogMAR in Subjects 20 and 23 (ages 16 years 4 months and 10 years 5 months respectively). Three subjects were hypermetropic with a spherical equivalent between +1.00 D and +8.00 D. However, Subject 22 was myopic with a spherical equivalent of -13.0 D. This is not in keeping with the published phenotype associated with *GUCY2D* mutations [114, 115, 338].

The fundi were normal in 4 subjects, who were examined between 10 months and 16 years of age (Subjects 20, 21, 23 and 24) (Figure 19 - A and B, Subject 20). However, in Subject 22 there was a diffuse pigmentary retinopathy, which was not in keeping with the published *GUCY2D* phenotype. The ERG was unrecordable in 4 of 5 *GUCY2D* subjects; in Subject 20 there was severe cone rod dysfunction at age 17 years.

The phenotype in Subject 22 was not typical of *GUCY2D* mutations. This subject's mother and maternal aunt had mild RP, thus it is possible that the inheritance pattern in this family is autosomal dominant. The mutation identified in this family has been reported in the heterozygous state in another family with LCA from Tunisia, but the

fundus appearance in this family was not clearly described to allow a detailed comparison with the subject in the present study [115]. In addition, Perrault *et al.* described hyperopia, while Subject 22 had myopia. It remains possible therefore, that another gene may contribute to the disease in this family, which has, as yet, not been identified.



Figure 19 - Subject 20, *GUCY2D*. A – right eye fundus; B – left eye fundus. Both fundi appear normal. Images taken at age 16 years.

4.3.5 *LCA5* Genotype - Phenotype association

Two subjects in cohort 1 were identified with *LCA5* mutations (Subjects 25 and 26). One was British Caucasian from a consanguineous family (Subject 25) and the second subject was from a non-consanguineous family of unknown ethnicity (Subject 26). Both were diagnosed with LCA, with poor vision and nystagmus from birth or early infancy. General health was normal. Visual acuity was measured at perception of light (Subject 25, age 18 years and 6 months) and 1.1 LogMAR (Subject 26, age 8 years and 6 months).

The fundus appearances were different between the two subjects. Subject 25 had atrophy at the macula, which Subject 26 did not (Figure 20 – A to D). Although both had peripheral RPE atrophy, Subject 26 had additional white dots in the periphery, which Subject 25 did not. ERGs had not been performed in these subjects. As the number of *LCA5* families ascertained in this study were small, it is not possible to make a general conclusion about the *LCA5* phenotype. However, these two subjects were included in a publication with a number of *LCA5* families ascertained worldwide, in which the clinical diagnoses were heterogeneous and the fundi frequently displayed white dots in the periphery, widespread RPE atrophy and some preserved peripheral islands of normal RPE that may indicate a potential for therapy at a very young age [339].

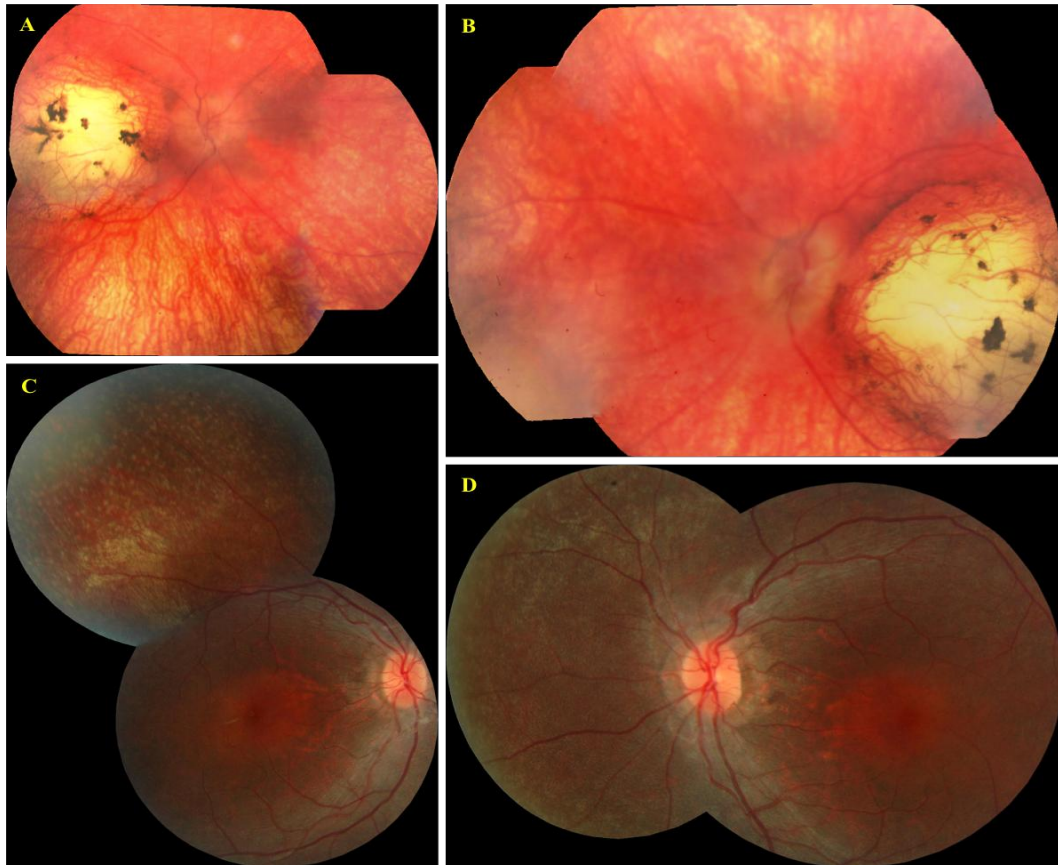


Figure 20 - Subject 25, *LCA5*: A – right eye; B – left eye. Dense macular atrophy and peripheral RPE atrophy. Images taken at age 18.5 years. Subject 26: C – right eye with white dots in the periphery; D – left eye. Images taken at age 8.5 years.

4.3.6 *MERTK* Genotype - Phenotype association

Only one subject was identified in cohort 1 with mutations in *MERTK* and a diagnosis of EORD (Subject 29). This subject was from a multiply consanguineous family from the UAE, which had 5 affected members in 2 successive generations. Subject 29 had poor vision and nyctalopia from 4 years of age, and no nystagmus. Visual acuity at 5 years and 4 months was 0.18 LogMAR in either eye, with a myopic refractive error of -4.63 D and -7.13 D spherical equivalent in the right and left eyes, respectively. Her retina appeared normal at this age (Figure 21 - A and B). FAF demonstrated a ring of hyperautofluorescence at the fovea, which corresponded to the retained photoreceptor

layer at the fovea seen on OCT imaging (Figure 21 - C and D). An ERG at age 4 years and 3 months demonstrated rod more than cone dysfunction, with sparing of the maculae. There were no other affected family members available for examination. *MERTK* subjects have been identified with macular atrophy and RPE depigmentation in a ‘bull’s eye’ configuration with corresponding hyperautofluorescence, which was seen on autofluorescence imaging in the subject in this study [340, 341]. These subjects may be amenable to treatment and a clinical trial is currently underway into gene therapy for patients with retinal disease due to *MERTK* mutations (<https://clinicaltrials.gov/ct2/show/NCT01482195>).

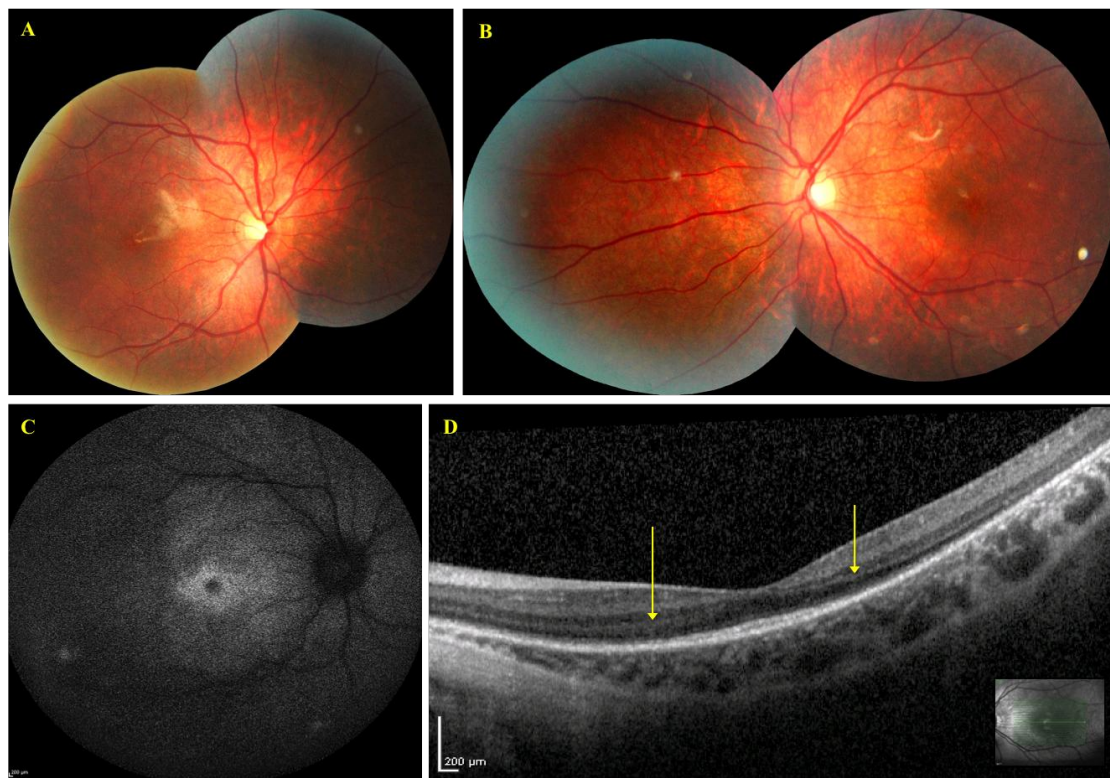


Figure 21 - Subject 29, *MERTK*, EORD. A – right eye fundus; B – left eye fundus. The fundi appeared normal at age 5 years 4 months; C – right eye fundus autofluorescence image demonstrating a ring of herperautofluorescence at the fovea; D – left eye OCT image demonstrating retention of the photoreceptor layer at the fovea, limits marked by yellow arrows.

4.3.7 *RDH12* Genotype - Phenotype association

In total, 17 subjects from 15 families were identified with causative mutations in *RDH12* (Table 10). All subjects had a diagnosis of either EORD (14 subjects) or rod cone dystrophy (3 subjects). Interestingly, the age of symptom onset varied between the two affected members of family 40, leading to subject 41 carrying a diagnosis of EORD and subject 42 carrying a diagnosis of rod cone dystrophy. Ethnicities were diverse, and included British Caucasian, Saudi Arabian, Indian, Pakistani, Kurdish, Latvian, and western European families. Symptom onset ranged from infancy to 11 years of age. Symptoms included poor vision, nyctalopia and visual field constriction. 4 subjects reported a noticeable deterioration in vision in the third and fourth decades. General health was normal in all subjects. Subjects were examined between 6 years of age and 52 years of age.

Visual acuity was best preserved at a young age – subject 39 had 0.6 LogMAR vision at 6 years of age (Figure 22). However, in general, visual acuity was poor. Only 3 subjects had 1.0 LogMAR acuity or better. In 11 subjects the acuity ranged between hand movements and perception of light. The worst visual acuity was in the oldest age at 52 years, however two subjects also had perception of light vision in their fourth decade. Due to the small numbers of subjects identified with *RDH12* associated disease and to the lack of longitudinal data it is not possible to determine how rapidly vision deteriorates with time.

Mild hypermetropia was recorded in 3 subjects. Keratoconus was present in 1 subject (Subject 31); otherwise anterior segments were normal. Posterior subcapsular lens opacification was common, affecting 10 subjects, one of whom had surgery for lens

extraction (Subject 41). The fundus appearance was easily recognisable as a severe pigmentary retinopathy with yellow macular atrophy, macular pigmentation and arteriolar attenuation (Figure 23 - A to D, Table 10). In 3 subjects the severe pigment clumping spared the para-arteriolar region. In 3 subjects in whom OCT imaging was performed, there was severe thinning of the fovea with debris visible in the photoreceptor layer (Figure 24 – C, Subject 35 and Figure 25 – B, Subject 43). In 4 subjects FAF imaging identified little to no autofluorescence at the macula, in keeping with the observed macular atrophy (Figure 24 - B, subject 35). ERGs performed in 4 subjects were unrecordable.

The phenotypic appearances of the *RDH12* subjects in this study were in keeping with the published phenotypes which have identified severe retinal pigmentation and macular atrophy with very poor vision from early childhood [270, 271, 278, 279, 282]. These subjects, and those previously recruited into the Childhood Onset Retinal Dystrophy Study, were published [284].

Subject, Family, (Gender)	Ethnicity	Consanguinity	Diagnosis	Age at Onset (Years)	Age at Exam (Years)	LogMAR VA RE, LE	Retina
30, 30, (F)	Unknown	Consanguineous	EORD	4	35	HM, HM	Pigment clumping, yellow macular atrophy, arteriolar attenuation
31, 31, (M)	Saudi Arabian	Consanguineous	EORD	2	29	HM, HM	Pigment clumping, yellow macular atrophy, arteriolar attenuation
32, 31, (M)	Saudi Arabian	Consanguineous	EORD	<5	23	HM, CF	Pigment clumping with para-arteriolar sparing, yellow macular atrophy, arteriolar attenuation
33, 32, (M)	British Caucasian	Nil	EORD	2	34	HM, HM	Pigment clumping, macular atrophy and ‘coloboma’, arteriolar attenuation
34, 33, (F)	Indian	Nil	EORD	Infancy	33	1.0, 0.78	Pigment clumping with para-arteriolar sparing, yellow macular atrophy, arteriolar attenuation
35, 34, (M)	Latvian	Nil	Rod-cone	10	40	1.78, 1.48	Pigment clumping, yellow macular atrophy, arteriolar attenuation
36, 35, (F)	European Caucasian	Nil	EORD	1.5	32	PL, PL	Pigment clumping, yellow macular atrophy, arteriolar attenuation
37, 36, (M)	Kurdish	Nil	EORD	Infancy	21	2.3, 2.3	Pigment clumping, large bilateral macular atrophic lesions, arteriolar attenuation
38, 37, (M)	British Caucasian	Nil	EORD	<5	33	1.3, 1.0	Pigment clumping, yellow macular atrophy, arteriolar attenuation
39, 38, (M)	British Caucasian	Nil	EORD	4	6	0.6, 0.6	Pigment clumping, macular atrophy, arteriolar attenuation
40, 39, (F)	Indian	Nil	EORD	1	52	PL, PL	Pigment clumping, yellow macular atrophy, arteriolar attenuation
41, 40, (M)	Pakistani	Consanguineous	EORD	4	27	HM, HM	Pigment clumping, macular atrophy, arteriolar attenuation
42, 40, (F)	Pakistani	Consanguineous	Rod-cone	8	25	HM, HM	Pigment clumping, macular atrophy, arteriolar attenuation
43, 41, (F)	Indian	Nil	EORD	2	20	1.0, 0.78	Pigment clumping with para-arteriolar sparing, yellow macular atrophy, arteriolar attenuation
44, 42, (M)	Irish Caucasian	Consanguineous	EORD	2.5	29	CF, CF	Pigment clumping, macular atrophy and ‘coloboma’, arteriolar attenuation
45, 43, (F)	Indian	Nil	Rod-cone	11	30	PL, PL	Pigment clumping, large bilateral macular atrophic lesions, arteriolar attenuation
46, 44, (M)	½ British Caucasian, ½ Portuguese	Nil	EORD	2	8	1.0, 1.3	Moderate pigment clumping, RPE atrophy, atrophic pigmented macula arteriolar attenuation

Table 10 – Clinical Features of *RDH12* subjects in cohort 1.

F – Female; M – Male; EORD – Early Onset Retinal Dystrophy; VA – Visual Acuity; RE – Right Eye; LE – Left eye; HM – Hand Movements; CF – Counting Fingers; PL – Perception of Light.

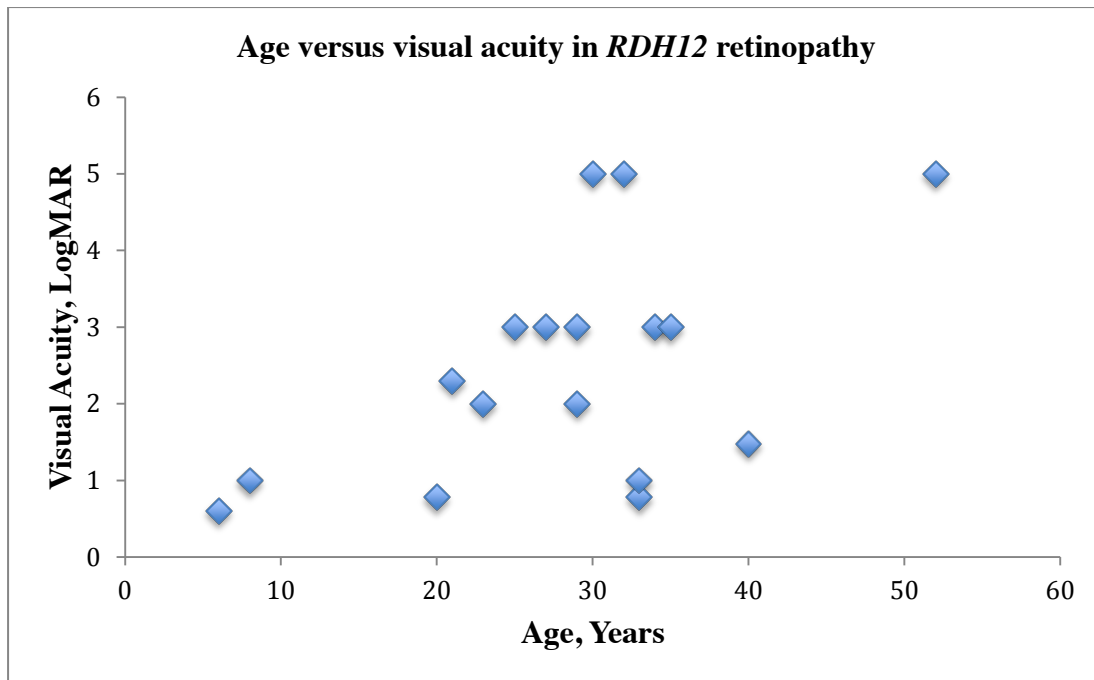


Figure 22 - Graphical representation of age versus visual acuity in *RDH12* retinopathy. In the first decade visual acuity is markedly better than in the sixth decade, however, a variety of acuities are observed in the intervening decades. Diagnoses included EORD and rod-cone dystrophy. Visual acuities of 2 LogMAR, 3 LogMAR, 5 LogMAR and 6 LogMAR represent counting fingers, hand movements, perception of light and nil perception of light vision, respectively [52, 53].

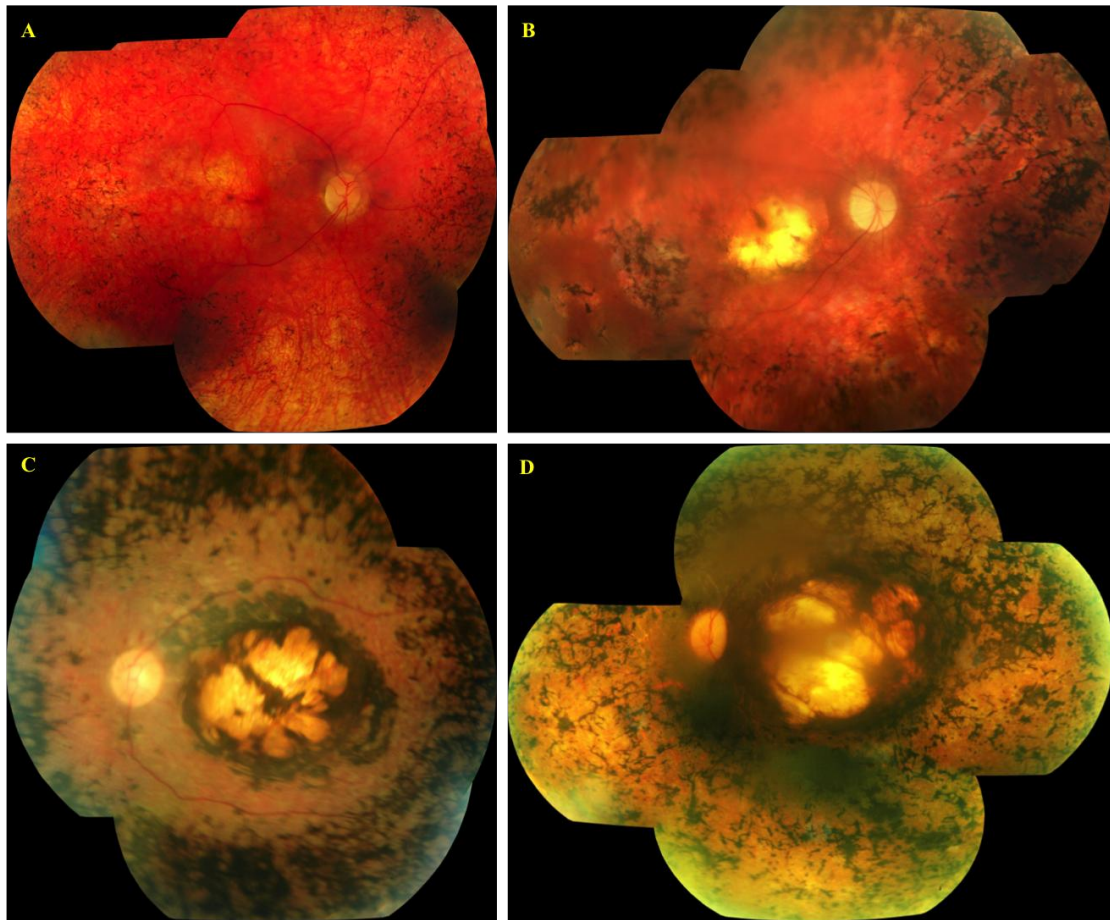


Figure 23 - *RDH12* subjects with EORD. A – Right eye fundus, Subject 39 age 6 years; B – Right eye fundus, Subject 38 age 33 years; C – Left eye fundus, Subject 31 age 29 years; D – Left eye fundus, Subject 40 age 52 years. All subjects display a severe pigmentary retinopathy and yellow macular atrophy with pigmentation that worsens with age.

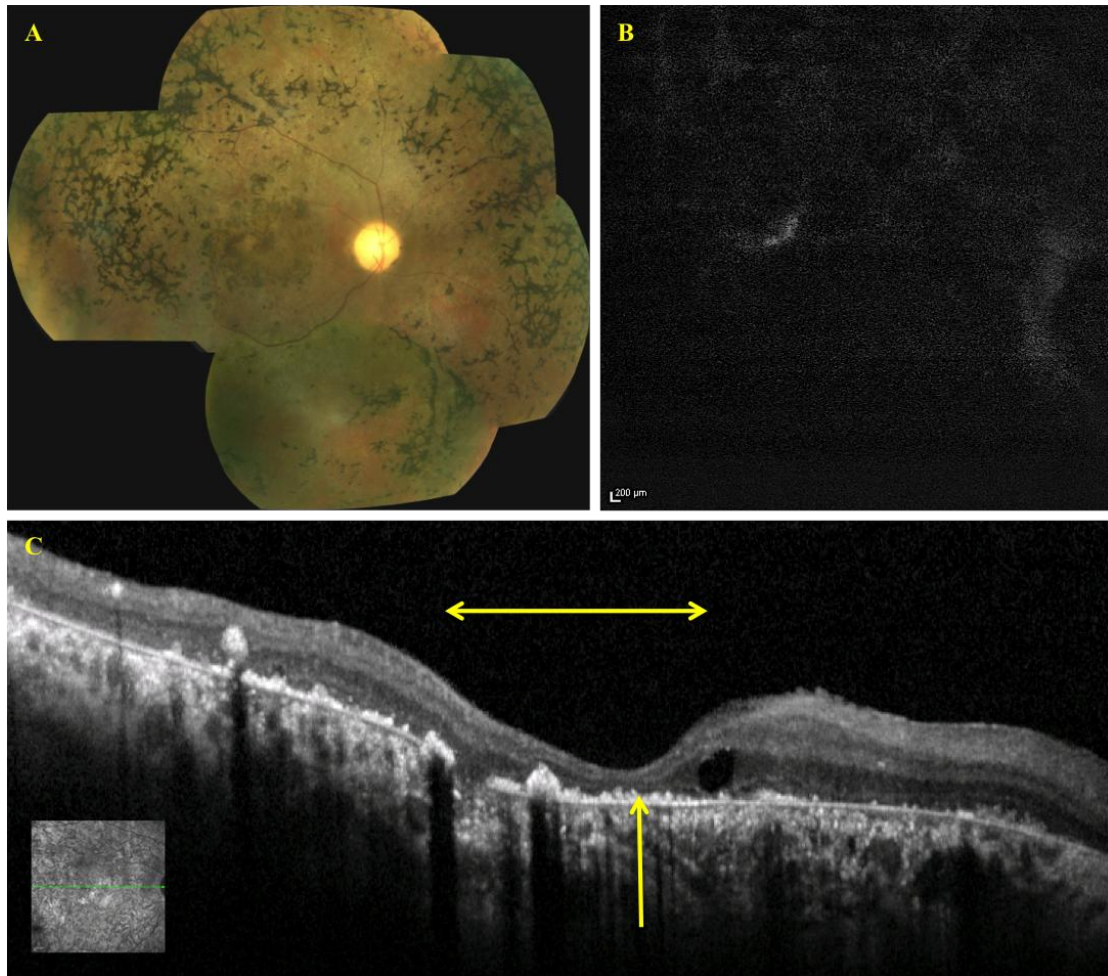


Figure 24 - Subject 35, *RDH12*, Rod-cone dystrophy. A – Right eye fundus, age 40 years displaying severe pigmentary retinopathy and yellow pigmented macular atrophy; B – corresponding right eye fundus autofluorescence image displaying only a faint autofluorescent signal at the macula; C – OCT image of the right eye displaying foveal shallowing (double ended arrow), severe photoreceptor disruption (single ended arrow) and an intra-retinal cyst.

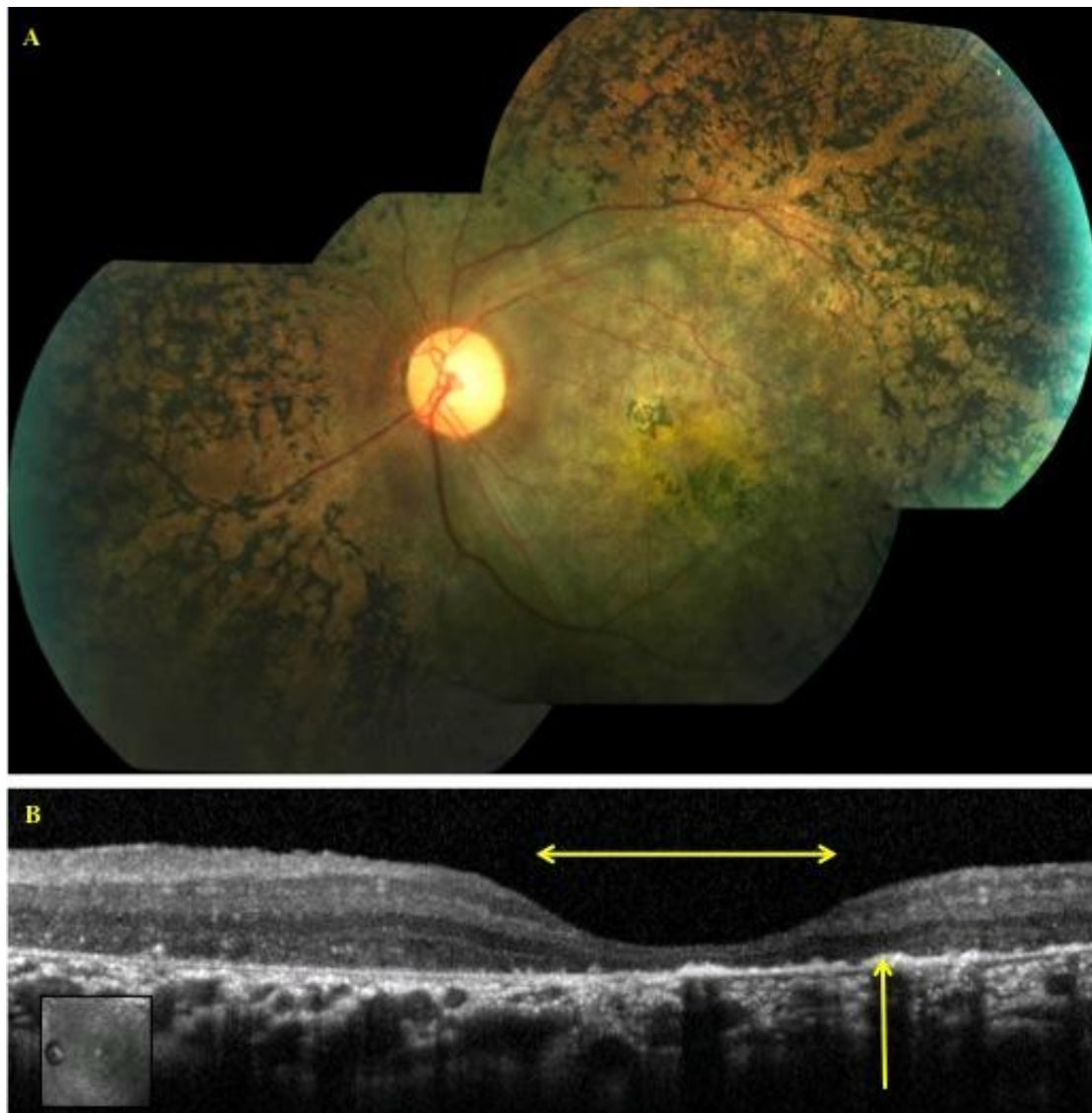


Figure 25 - Subject 43, *RDH12* EORD. A – Left eye fundus, age 20 years displaying severe pigmentary retinopathy and yellow pigmented macular atrophy; B – corresponding OCT image of left eye displaying foveal shallowing (double ended arrow) and severe photoreceptor disruption (single ended arrow).

4.3.8 *RPE65* Genotype - Phenotype association

RPE65 mutations were identified in 8 subjects from 7 families in cohort 1. Two subjects were British Caucasian, 2 were Syrian, 1 was Indian, 1 Sri Lankan and 1 from New Zealand with European ancestry; the ethnicity of one subject was unknown (Table 11). Three subjects had LCA and 5 had EORD. Those with LCA had poor

vision from birth or the first few months of life; those with EORD had symptom onset from infancy to 3.5 years of age. Photophilia, in which subjects would stare at lights, was universal. Refractive errors ranged from low hypermetropia (+2.00 D spherical equivalent) to severe myopia (-12.88 D spherical equivalent), with half of the subjects being myopic. Nystagmus was present in 3 subjects and strabismus in 2.

Reduction in visual acuity was variable (Figure 26). In the LCA subjects, visual acuity ranged from 0.7 LogMAR at age 4 years and 6 months (Subject 49), to perception of light at 33 years (Subject 51). In the EORD subjects, visual acuity ranged from 0.00 LogMAR (Subject 52, age 18 years) to 1.3 LogMAR (Subject 50, age 2 years and 3 months). Subject 52 was the most mildly affected subject with normal visual acuity and full visual fields to confrontation. His only symptom was of nyctalopia beginning at 3 years and 6 months of age. He has been diagnosed with EORD but shows hypomorphic features. In general, the visual acuity in subjects with mutations in *RPE65* was better than in other genes associated with retinal dystrophy. Although there are limited numbers of subjects with *RPE65* retinopathy in this study, these data demonstrate that the visual acuity remains stable over the first two decades of life, but may deteriorate by the fourth decade, suggesting a therapeutic window of opportunity at an early age (Figure 26).

The retina was normal in 3 subjects (Subjects 50, 53 and 55) (Table 11). In the remaining 5 subjects there was peripheral RPE atrophy with minimal pigmentation (Figure 27 – A and B, Subject 48 and Figure 28 – A, Subject 54). The only subject to have any pigment was the oldest subject, Subject 51, in whom the pigmentation was nummular and scattered in the peripheral retina at age 33 years, with focal white dots

at the macula (Figure 29 - A, arrow). Subject 52, who had hypomorphic disease, had only minimal RPE change in the retinal periphery (Figure 30 - A). FAF appearances were variable, demonstrating: retained autofluorescence at the fovea (Figure 29 – B, Subject 51); a very poor autofluorescence signal at the macula (Figure 28 – B, Subject 54); and an annulus of hyperautofluorescence at the macula in the hypomorphic patient (Figure 30 – C and D, Subject 52). OCT imaging in Subject 54 demonstrated retention of the photoreceptor layer at the fovea (Figure 28 – C) and in subject 51 demonstrated focal loss of the photoreceptor layer (Figure 29 - C). ERGs in 4 subjects were unrecordable (age range 1 year to 10 years) and in 3 subjects demonstrated severe rod and cone dysfunction (age range 4 years to 18 years), with residual cone function detected in 2 subjects (Subjects 52 and 55).

In general, the phenotype displayed in the *RPE65* subjects in this cohort are in keeping with the published phenotypes associated with *RPE65* mutations, which describe poor vision from early childhood, localised regions of RPE atrophy, vascular attenuation and bone spicule pigmentation [14, 116, 148, 149, 151, 153, 342]. Although Subject 52 has EORD, he displays hypomorphic features, which has also been identified in *RPE65* retinopathy [151, 160, 161]. In these subjects the clinical picture is milder, with onset of nyctalopia in the first or second decade, but with slower progression of disease, residual islands of vision or full visual fields, and residual ERG cone function.

Subject, Family, (Gender)	Ethnicity	Consanguinity	Diagnosis	Age at Onset (Years)	Age at Exam (Years)	LogMAR VA RE, LE	Spherical Equivalent (Dioptres) RE, LE	Retina
48, 46, (M)	Syrian	Nil	LCA	Birth	10	0.9, 1.2	-1.63, -1.63	Widespread RPE atrophy
49, 46, (M)	Syrian	Nil	LCA	Birth	4.5	0.8, 0.7	-1.13, -0.88	Peripheral RPE atrophy
50, 47, (F)	British Caucasian	Nil	EORD	1	2.25	1.3, 1.3	+2.00, +2.00	Normal
51, 48, (F)	New Zealand, European Caucasian	Nil	LCA	<3 months	33	PL, PL	Not available	Widespread RPE atrophy, scattered nummular pigment, focal white macular lesions, PPA
52, 49, (M)	Unknown	Nil	EORD	3.5	18	0.00, 0.00	0.00, 0.00	Peripheral RPE irregularity
53, 50, (F)	Sri Lankan	Nil	EORD	2	5.67	0.60, 0.70	Not available	Normal
54, 51, (M)	British Caucasian	Nil	EORD	Infancy	11.75	0.8, 0.62	Myopic	Peripheral RPE atrophy
55, 52, (M)	Indian	Nil	EORD	3 months	4	0.78, 0.78	-11.25, -12.88	Normal myopic fundus

Table 11 - Clinical Features of *RPE65* subjects in cohort 1.

F – Female; M – Male; LCA – Leber Congenital Amaurosis; EORD – Early Onset Retinal Dystrophy; VA – Visual Acuity; RE – Right Eye; LE – Left eye; PL – Perception of Light.

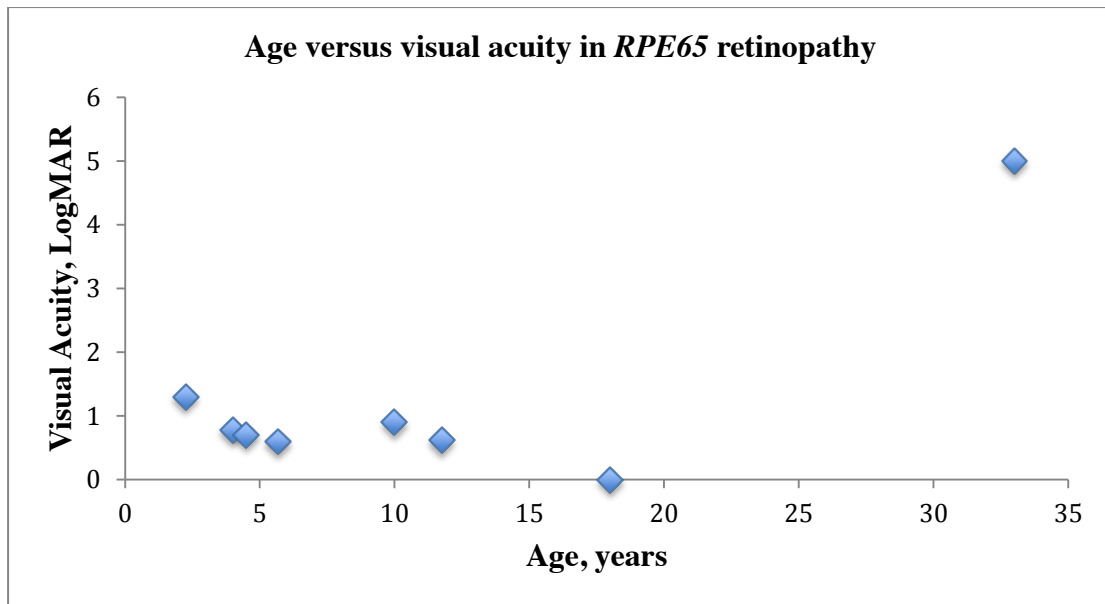


Figure 26 - Graphical representation of age versus visual acuity in *RPE65* retinopathy. Vision remains good in the first two decades and can deteriorate by the fourth decade. Visual acuity of 5 LogMAR denotes perception of light vision [53].

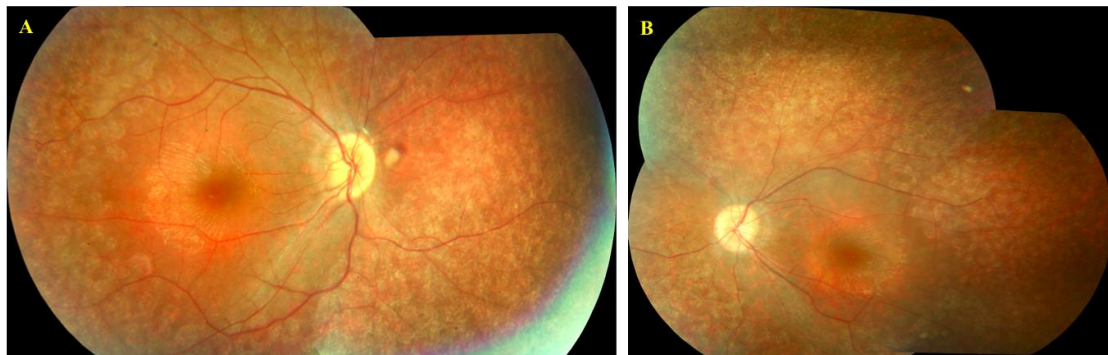


Figure 27 - Subject 48, *RPE65*, LCA. A –right eye fundus; B – left eye fundus images demonstrating widespread RPE atrophy and no retinal pigmentation. Images taken at age 10 years.

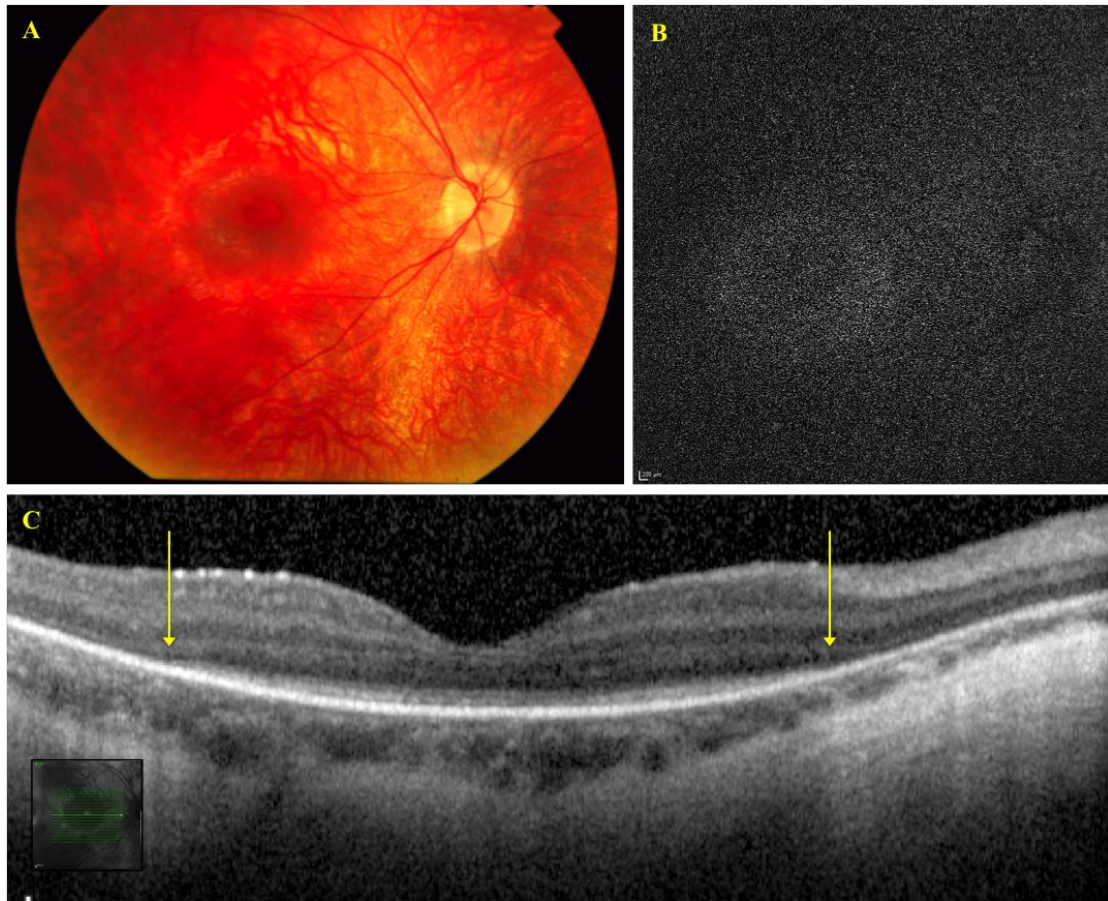


Figure 28 - Subject 54, *RPE65*, EORD. A – right eye fundus. Normal fundus at posterior pole with typical features of myopia, but peripheral retina showed RPE atrophy (not shown); B – right eye fundus autofluorescence imaging demonstrating little / no autofluorescence at the macula; C – right eye OCT image demonstrating retention of the photoreceptor layer at the fovea, demarcated by arrows. Images taken at age 11 years 9 months.

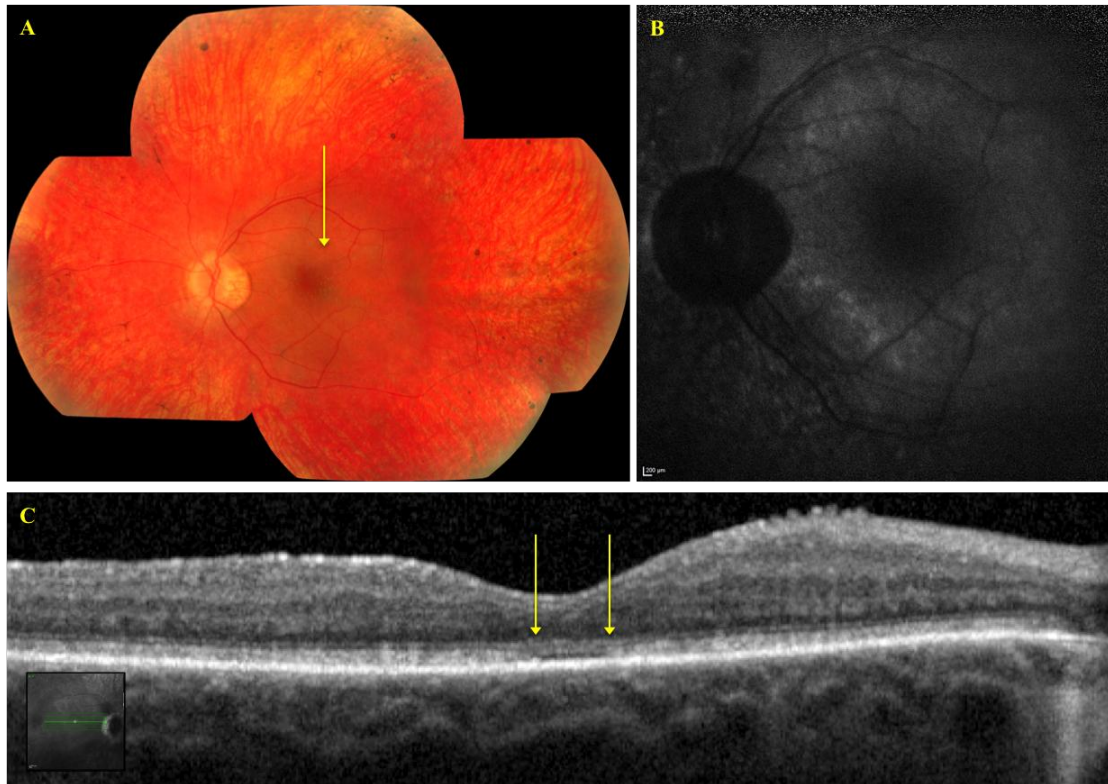


Figure 29 - Subject 51, *RPE65*, LCA. A – left eye fundus with focal white dots at the fovea (arrow) and peripheral RPE atrophy with minimal pigment in the periphery; B – left eye fundus autofluorescence image demonstrating minimal retained autofluorescence at the macula; C – left eye OCT image demonstrating focal loss of the photoreceptor layer at the fovea, delineated by arrows. Images taken at age 33 years.

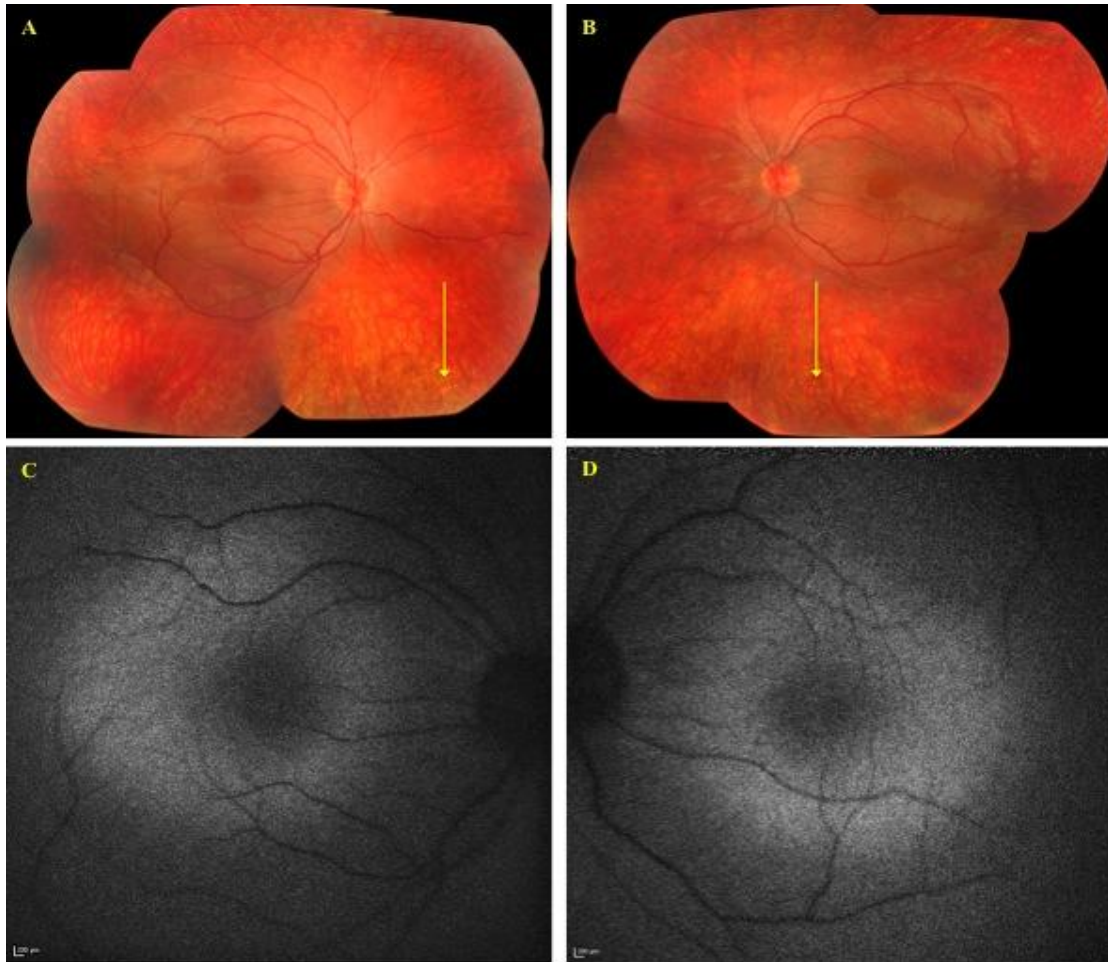


Figure 30 - Subject 52, *RPE65*, hypomorphic EORD. A – Right eye fundus; B - left eye fundus. Both fundi are essentially normal with minimal focal RPE change in the periphery (yellow arrows); C – right eye fundus autofluorescence image; D – left eye fundus autofluorescence image. Autofluorescence images indicate annuli of hyperautofluorescence at the maculae. Images taken at age 18 years.

4.3.9 *RPGRIP1* Genotype - Phenotype association

Two subjects from 2 families in cohort 1 were identified with mutations in *RPGRIP1*. The older subject was diagnosed with EORD as his age of symptom onset was described to be in childhood (Subject 56). He was British Caucasian. The younger subject had onset of poor vision and nystagmus from 3 months and was diagnosed with LCA (Subject 57). She was of Greek origin. Both subjects had very poor vision, nyctalopia and nystagmus. Subject 57 had photophilia. General health was normal.

Visual acuity was nil perception of light (right eye) and hand movements (left eye) in Subject 56, and perception of light in Subject 57. Both subjects were hypermetropic.

In the younger subject, at 2 years of age, the retinal appearances were normal aside from minimal pigmentation in the periphery. In the older subject, at 46 years of age, there was widespread RPE atrophy and bone spicule pigmentation typical of retinitis pigmentosa; the maculae appeared spared (Figure 31 - A and B). An ERG at 2 years of age in Subject 57 was unrecordable. The phenotypes observed in these two subjects correlate with the published severe phenotype associated with *RPGRIP1* mutations, which can also display a variable fundus appearance but which have been associated with vascular attenuation, a granular appearance to the retina, macular atrophy and drusen-like retinal deposits [167, 182, 183, 200, 201].

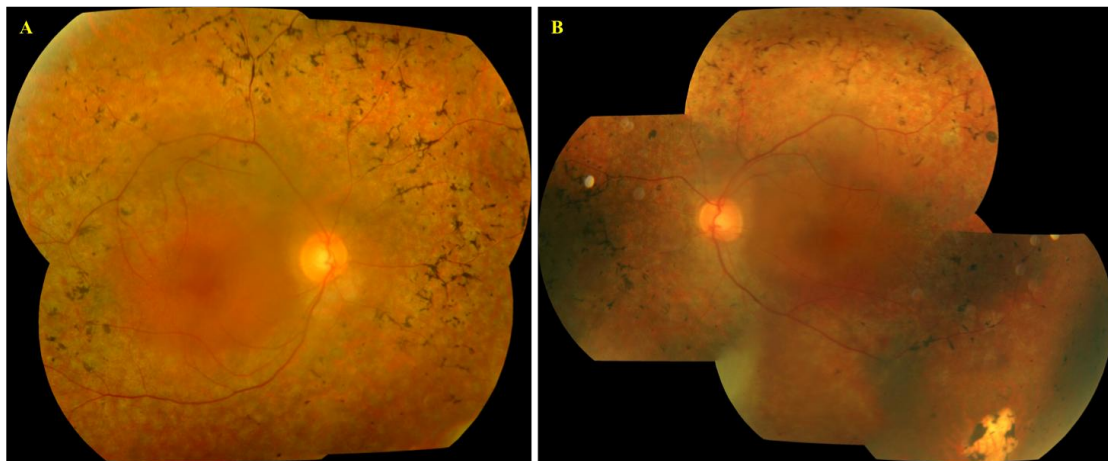


Figure 31 - Subject 56, *RPGRIP1* EORD. A – right eye fundus; B – left eye fundus. Widespread RPE atrophy and bone spicule pigmentation with macular sparing. Images taken at age 46 years.

4.4 *SPATA7* Phenotype

SPATA7 was recently identified as the causative gene at the LCA3 locus, and when this research was carried out, few studies had been published reporting the phenotype associated with this gene [163] [166]. In this study, six families were identified to harbour mutations in *SPATA7*, and their phenotypes were examined in detail. The probands of families 1-4 had been recruited into the Childhood Retinal Dystrophy Study by Mr Henderson, a previous research fellow, and the probands of families 5 and 6 were recruited by ADB during the period between Aug 2008 and Aug 2011. In total 11 subjects were identified with mutations in *SPATA7*, age range 4.5 years to 43 years when examined. The strategies used to identify the *SPATA7* variants in these families differed and will be described in this chapter. The phenotype of these subjects was explored in detail as there had been few descriptions to date regarding the *SPATA7* phenotype. The results of these phenotypic studies will be presented in this chapter, and were published [165].

4.4.1 Clinical History

All subjects affected by mutations in *SPATA7* carried a diagnosis of LCA. Onset of poor vision and nystagmus was at birth in 6 of 11 subjects (54.5%), and by 12 weeks of age in the remaining subjects. One subject had a milder phenotype (Subject 2). Although he had developed nystagmus by 8 weeks of age, he was able to fix and follow well at this age, and only developed nyctalopia and visual field constriction when older. His symptoms deteriorated from 14 years of age. In 5 of 11 subjects

photoaversion was a feature early on in the disease, and in 1 subject (Subject 2) there was photophilia. The oculodigital reflex was present from the outset in 7 subjects. General health was good in all subjects except the oldest subject, Subject 3 (family 2), who had type II diabetes mellitus, auditory dysfunction and reduced fertility due to a reduced spermatozoa count, and the two youngest members of family 3 who had renal dysfunction (Subject 6) and severe autistic spectrum disorder with auditory dysfunction (Subject 7). No other *SPATA7* subjects were identified with auditory or fertility dysfunction. In particular, Subject 1 had two children and there were no problems encountered regarding his fertility prior to having children.

Family 1, with 2 affected subjects, was a non-consanguineous British Caucasian family. Families 2-6 were of South East Asian origin; families 2-5 were consanguineous and family 6 denied consanguinity (Table 12). There were multiple affected individuals in families 1-4 (Family 1: 2 affecteds, Subjects 1 and 2; Family 2: 4 affecteds, Subject 3 only available; Family 3: 9 affecteds, Subjects 4 – 8 available; Family 4: 2 affecteds, Subject 9 only available) and the probands of families 5 (Subject 10) and 6 (Subject 11) were simplex cases. None of these families were knowingly related to each other.

4.4.2 Clinical Examination

Nine of eleven *SPATA7* subjects were male. Visual acuity was hand movements or worse in all but two subjects (Table 12). Subject 2 had a best corrected visual acuity of 0.22 logMAR in the right eye and 0.1 logMAR in the left eye at age 19 years. Subject 10 had an unaided visual acuity of 1.08 logMAR in the right eye and 1.48

logMAR in the left eye at age 17 years. Colour vision testing was only reliable in subject 2, who had a mild blue-yellow defect on HRR testing. In those subjects for whom refractive data were available, there tended to be a myopic astigmatism.

Slit lamp examination revealed keratoconus in subject 3 and mild cataract in subjects 1-3. In all but one patient the fundi had severe, widespread RPE atrophy with minimal intra-retinal pigmentation, relative parafoveal preservation, severe vascular attenuation and optic disc pallor (Figure 32, Figure 33, Figure 34 and Figure 35 – Images A, subjects 1, 2, 5 and 10). In subject 11 the posterior poles appeared to be normal and nummular pigmentation was visible in the peripheral retina superiorly. Subject 2 additionally had bilateral optic disc drusen.

4.4.3 Fundus Autofluorescence Imaging

Severe nystagmus and photoaversion precluded the acquisition of fundus autofluorescence imaging in most subjects however, in 3 subjects a parafoveal annulus of hyperautofluorescence was present (subjects 1, 2 and 4) (Figure 32, Figure 33, Figure 34 and Figure 35 - B).

4.4.4 OCT Imaging

sd-OCT imaging was only possible in subjects 2 and 10 as image acquisition was limited due to nystagmus. OCT imaging in these two subjects demonstrated retinal thinning and possible preservation of the inner segment outer segment layer at the fovea (Figure 33 and Figure 35 – C, indicated by arrows). In subject 2 this

corresponded with the centrally preserved visual field on Goldmann perimetry. Elsewhere, in both of these subjects, there was loss of the photoreceptor layer, and some loss of retinal lamination.

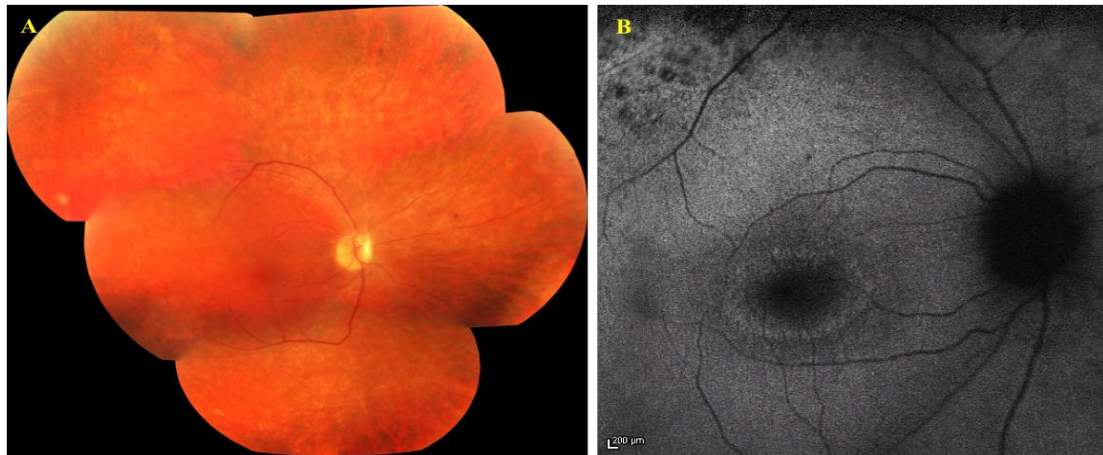


Figure 32 - Subject 1, Family 1 *SPATA7*. A – right eye fundus demonstrating widespread RPE atrophy, minimal retinal pigmentation, vascular attenuation and sparing of the fovea; B – right eye fundus autofluorescence image demonstrating an annulus of hyperautofluorescence at the fovea. Images taken at age 21 years.

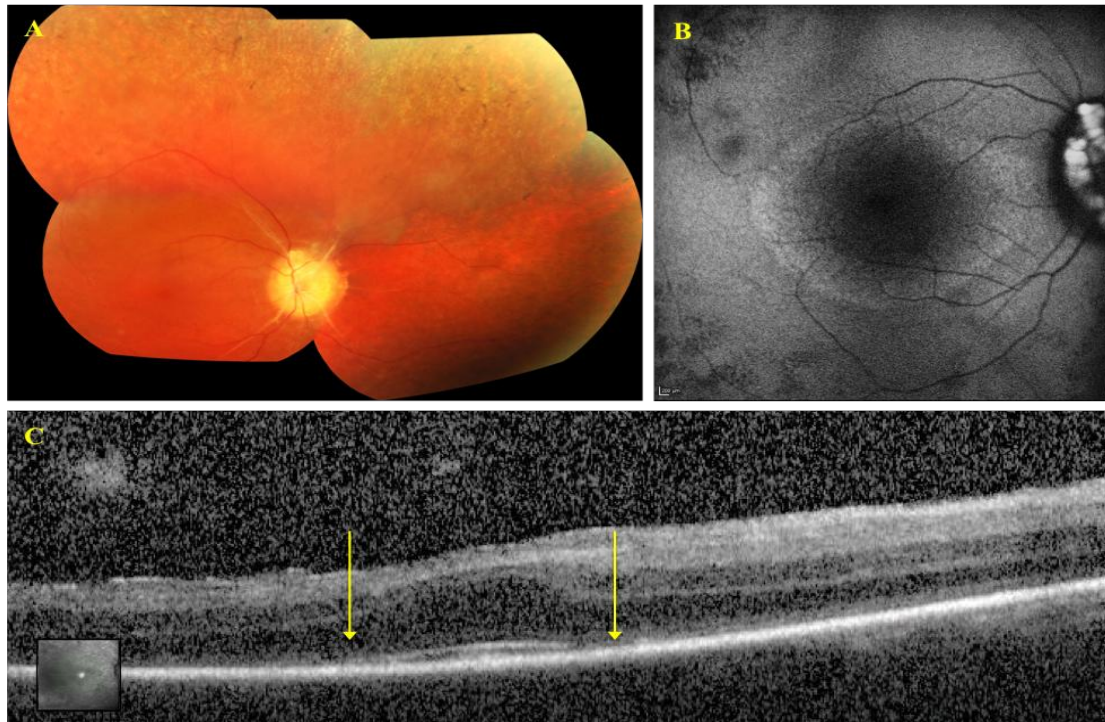


Figure 33 - Subject 2, Family 1 *SPATA7*. A – right eye fundus demonstrating widespread RPE atrophy, minimal retinal pigmentation, vascular attenuation and optic disc drusen; B – right eye fundus autofluorescence image demonstrating an annulus of hyperautofluorescence at the fovea and optic disc drusen; C – right eye OCT image demonstrating loss of retinal lamination but preservation of photoreceptors at the fovea, limits delineated by arrows. Images taken at age 19 years.

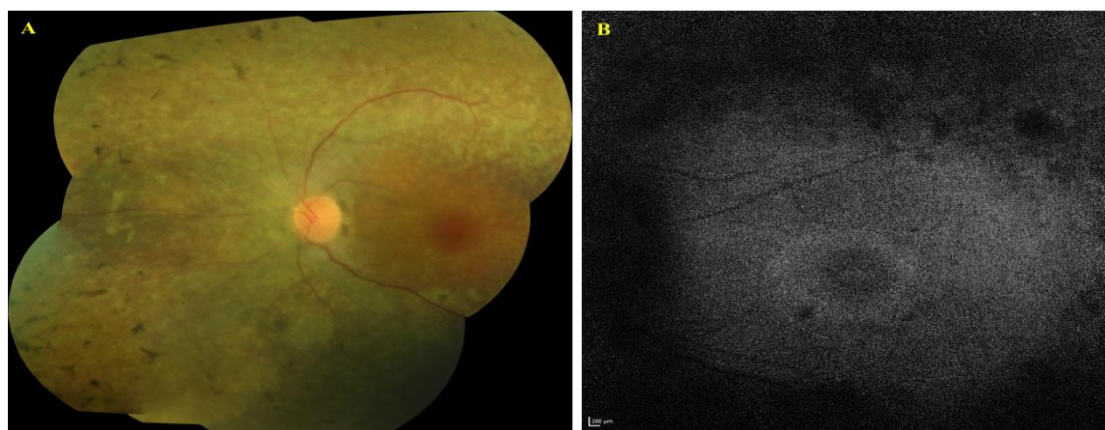


Figure 34 - Subject 5, Family 3 *SPATA7*. A – right eye fundus demonstrating widespread RPE atrophy, peripheral retinal pigmentation, vascular attenuation and sparing of the macula; B – right eye fundus autofluorescence image demonstrating an annulus of hyperautofluorescence at the fovea. Images taken at age 29 years.

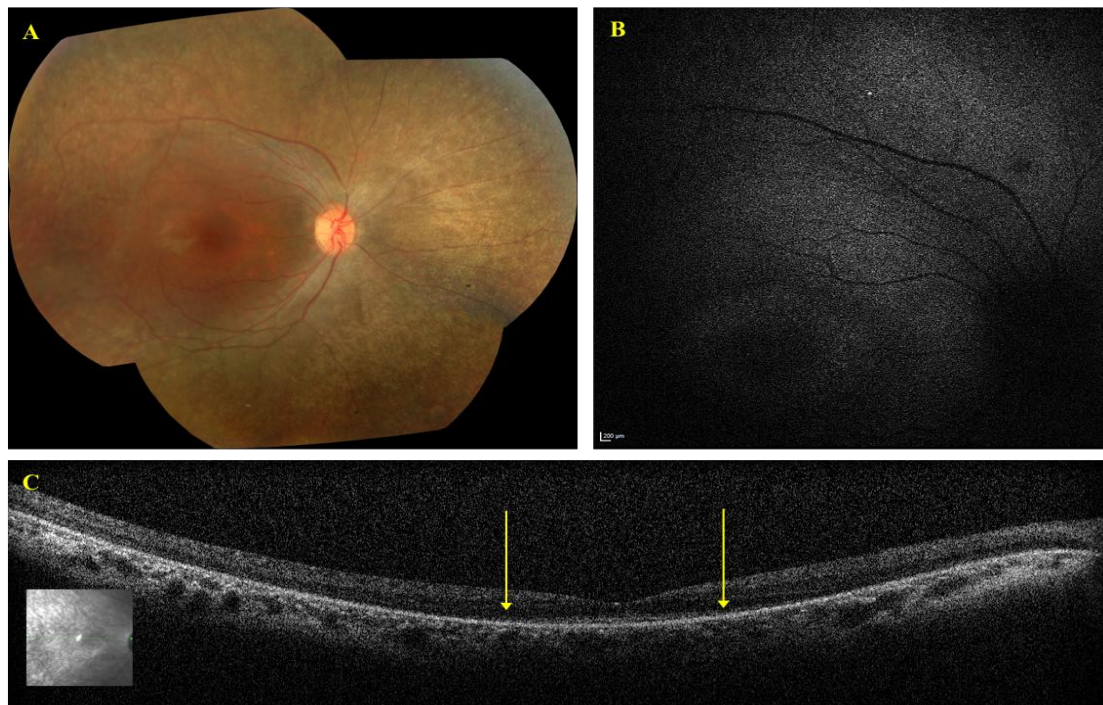


Figure 35 - Subject 10, Family 5, *SPATA7*. A – right eye fundus demonstrating widespread RPE atrophy, minimal retinal pigmentation, vascular attenuation and foveal sparing; B – right eye fundus autofluorescence image demonstrating a very faint annulus of hyperautofluorescence at the fovea; C – right eye OCT image demonstrating loss of retinal lamination but possible preservation of photoreceptors at the fovea, limits delineated by arrows. Images taken at age 17 years.

4.4.5 Psychophysical testing: Goldmann Visual Fields

Goldmann visual field testing was only reliably performed in Subject 2 and showed preservation of less than 10° of the central vision to the V4e target and less than 5° to the I4e target (Figure 36).

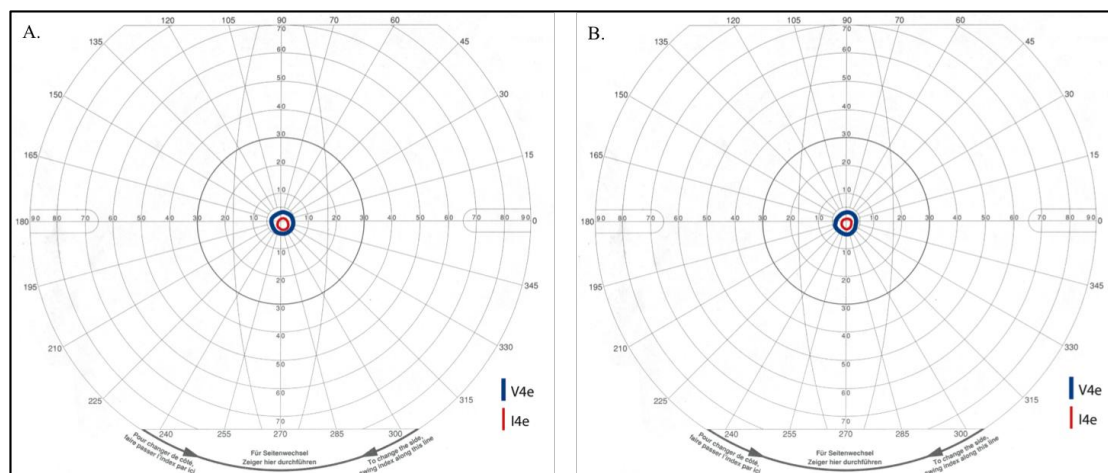


Figure 36 – Goldmann Visual Field, Subject 2, *SPATA7*. A – Left eye; B – Right eye; V4e – blue line; I4e – red line.

4.4.6 Electrophysiological Testing

ISCEV standard ERG testing was performed in Subject 9 at 18 years of age and there was no detectable full field or pattern ERG, in keeping with severe bilateral photoreceptor dysfunction. In Subjects 1 and 2, ERGs were performed at different ages in the first decade using a modified paediatric ERG protocol and skin and DTL electrodes; the methods have been described previously [64, 343]. Subject 1 was tested first at age 4 years at which time the photopic ERGs were undetectable but rod driven ERGs were detected at subnormal amplitudes. By 5 years of age the rod-ERG was also undetectable. In contrast, his younger brother, Subject 2, had normal rod driven ERG b-wave amplitudes at age 2 years, but undetectable photopic ERGs; by 4 years of age his rod driven b-wave amplitudes were subnormal; and by 9 years of age they were undetectable. This suggests that in these two subjects the condition started with predominantly cone dysfunction, progressing to cone – rod dysfunction. In Subject 11 ERGs were performed by the hospital that diagnosed his condition in India, but the results are not available.

Subject (Gender)	Family	Ethnicity	Consanguinity	Age at Onset (weeks)	Age at Examination (years)	LogMAR VA RE, LE	General Health
1 (M)	1	British Caucasian	Non-consanguineous	6	21	1.06, CF	Good
2 (M)	1	British Caucasian	Non-consanguineous	8	19	0.42, 0.66	Good
3 (M)	2	Pakistani	Consanguineous	Birth	43	HM, PL	Type II diabetes mellitus Auditory dysfunction Fertility dysfunction
4 (M)	3	Pakistani	Consanguineous	Birth	27	HM, HM	Good
5 (M)	3	Pakistani	Consanguineous	Birth	29	HM, HM	Good
6 (M)	3	Pakistani	Consanguineous	Birth	5	PL, PL	Mild renal dysfunction
7 (M)	3	Pakistani	Consanguineous	12	4.5	NPL, NPL	Autistic spectrum disorder Auditory dysfunction
8 (F)	3	Pakistani	Consanguineous	Birth	12	NPL, NPL	Good
9 (M)	4	Bangladeshi	Consanguineous	8	15	CF, CF	Good
10 (F)	5	Pakistani	Consanguineous	Birth	17	1.08, 1.48	Good
11 (M)	6	Indian	Non-consanguineous	12	5.5	PL, PL	Good

Table 12 - Clinical features of *SPATA7* subjects. M – Male; F – Female; VA – Visual Acuity; RE – Right eye; LE – left eye; CF – Counting fingers. HM – Hand movements; PL – Perception of light; NPL – Nil perception of light.

4.4.7 Molecular analysis

The molecular techniques used to identify the families with *SPATA7* mutations varied. Dr Ocaka and Dr Mackay at UCL carried out the molecular analysis on these families. Families 1-3 were identified following the screening of *SPATA7* in an enriched panel of 141 probands with LCA and EORD that had previously been screened using the LCA chip, with no variants identified; Family 4 was identified based upon the phenotype; Family 5 was identified through positional gene screening after autozygosity mapping; and family 6 was identified via analysis using the LCA chip.

The two affected brothers in Family 1 (Subjects 1 and 2) were identified by direct sequencing to harbour novel compound heterozygous variants in *SPATA7* as follows: Exon 5 c.265_268delCTCA, p.L89KfsX3 and Exon 8 c1227_1229delCAC, p.H410del. Segregation analysis in the parents identified the c.265_268delCTCA, p.L89KfsX3 variant in the unaffected mother in the heterozygous state, and the c1227_1229delCAC, p.H410del variant in the unaffected father in the heterozygous state, confirming that the variants segregate with the disease in this family. Subject 3 (the proband of family 2) was identified to harbour the novel variant c.253C>T, p.Arg85X in the homozygous state; no other family members were available for molecular analysis. The proband of family 3, Subject 4, was identified by direct screening to harbour the previously reported variant c.961dupA, p.P321TfsX5 in the homozygous state [163]. Screening of this variant in other affected family members (Subjects 5-8) also identified it in the homozygous state in these individuals. Screening of unaffected family members (parents of the affected subjects) confirmed that the mutation segregates with the disease in this family as these family members were identified to be heterozygous carriers of this variant.

Based upon the consanguineous ancestry in family 4, the proband (Subject 9) was selected for autozygosity mapping using the Affymetrix SNP 6.0 microarray (Affymetrix Inc., California, USA). This identified 11 regions of homozygosity that were greater than 10 Mb in length, the smallest of which was present on chromosome 14 (Table 13). Candidate retinal disease associated genes included *ABCA4*, *C2orf71*, *CNNM4*, *CNGA3*, *MERTK*, *RBP3*, *CEP290* and *SPATA7*. Subsequent positional screening of *SPATA7* identified the novel variant c.253C>T, p.Arg85X in the homozygous state. This subject had an affected brother but his DNA was not available; segregation analysis in the parents confirmed the variant to segregate with the disease in this family, as they were both identified to be heterozygous carriers of this mutation. This subject had previously been screened using the LCA chip, with no variants identified.

Chromosome	From	To	Size (Mb)	Retinal disease associated genes
1	83875590	99936880	16.06	<i>ABCA4</i>
2	10075000	37675050	36.67	<i>C2orf71</i>
2	67464630	130110400	62.6	<i>CNNM4</i> , <i>CNGA3</i> , <i>MERTK</i>
4	84196690	110076800	25.88	
4	162527200	180125700	17.5	
10	35104210	70084230	34.98	<i>RBP3</i>
11	91493940	103385700	11.8	
12	68292940	92857940	24.56	<i>CEP290</i>
13	21218200	38110360	16.9	
14	81267210	92342000	11	<i>SPATA7</i>
16	62435740	81326560	18.9	

Table 13 - Autozygosity data, family 4. *SPATA7* resides in the eleventh largest region of homozygosity.

Based upon the phenotype of Subject 10 (family 5), direct screening of *SPATA7* was undertaken, which identified the same novel variant that had been identified in subjects 3 and 9, c.253C>T, p.Arg85X in the homozygous state. The mother of Subject 10 was screened for this mutation, which was identified in the heterozygous

state, confirming segregation of the disease in this family. The DNA of the father was not available.

The DNA of Subject 11 (family 6) was screened using the LCA chip in 2011, which identified the previously described *SPATA7* variant c.961dupA, p.P321TfsX5, in the homozygous state. Segregation analysis was not performed for this variant as the study period had closed shortly after the variant was identified. Of note, the DNA of this subject had been screened across the LCA chip in the past, in 2007, by another research laboratory in the USA, and no variants had been identified.

The mutations identified in *SPATA7* in this study are summarised (Table 14).

Subject	Family	Mutation 1	Mutation 2	Reference
1	1	c.265_268delCTCA, p.L89KfsX3	c1227_1229delCAC, p.H410del	Novel to this study
2	1	c.265_268delCTCA, p.L89KfsX3	c1227_1229delCAC, p.H410del	Novel to this study
3	2	c.253C>T, p.Arg85X	c.253C>T, p.Arg85X	Novel to this study
4	3	c.961dupA, p.P321TfsX5	c.961dupA, p.P321TfsX5	[163]
5	3	c.961dupA, p.P321TfsX5	c.961dupA, p.P321TfsX5	[163]
6	3	c.961dupA, p.P321TfsX5	c.961dupA, p.P321TfsX5	[163]
7	3	c.961dupA, p.P321TfsX5	c.961dupA, p.P321TfsX5	[163]
8	3	c.961dupA, p.P321TfsX5	c.961dupA, p.P321TfsX5	[163]
9	4	c.253C>T, p.Arg85X	c.253C>T, p.Arg85X	Novel to this study
10	5	c.253C>T, p.Arg85X	c.253C>T, p.Arg85X	Novel to this study
11	6	c.961dupA, p.P321TfsX5	c.961dupA, p.P321TfsX5	[163]

Table 14 - Mutations identified in *SPATA7* in this study.

4.4.8 Discussion

The LCA3 locus was identified in 1998 [162] but the causative gene, *SPATA7*, was not determined until 11 years later [163]. Mutations in *SPATA7* are associated with a severe LCA phenotype. In this study 6 families were identified with pathogenic mutations in *SPATA7*, which were identified using a variety of methods. All affected subjects carried a diagnosis of LCA. Visual symptoms began at birth or within the first few months of life, with associated nystagmus and initial photoaversion. Visual field constriction was severe (less than 10° of the central vision preserved in the subject with the mildest disease). The retina displayed widespread RPE atrophy in the majority of subjects, with minimal peripheral intra-retinal pigment migration, optic disc pallor, arteriolar attenuation and foveal sparing. The fundus autofluorescence imaging demonstrated a parafoveal annulus of hyperautofluorescence, which has previously been described in RP [344]. OCT imaging suggested preservation of the photoreceptor layer at the fovea. However, although the ERG eventually showed severe photoreceptor dysfunction, there was a suggestion that this condition may present with a cone dysfunction picture, which progresses to cone – rod dysfunction.

The *SPATA7* phenotype described in this study correlates with the few published reports of families with *SPATA7* mutations, and in particular highlights the clinical heterogeneity associated with this gene, for which both severe and mild phenotypes have been reported [163, 166, 345-347]. Of note, the proband of one of the original families identified with *SPATA7* mutations had 0.00 LogMAR vision at age 7 years and retained only 5° of their central visual field, but had developed nyctalopia at age 2 years and had an unrecordable ERG [163]. Shortly after the results of the present study were published, a consanguineous family was reported with 2 affected

individuals and the same mutation identified in the present study, c.253C>T, p.Arg85X, in the homozygous state [345]. Interestingly these siblings had much later onset of visual symptoms (in one sibling nyctalopia developed at age 25 years, the other sibling was asymptomatic at age 26 years), severely reduced scotopic and photopic ERG responses in the symptomatic sibling with much milder changes in latency and amplitude in the asymptomatic sibling. It is possible that modifier alleles are responsible for the clinical heterogeneity associated with this mutation. Wang *et al.* suggested the possibility of a digenic triallelic inheritance pattern causing phenotypic heterogeneity, in which the presence of a mutation in a second gene contributes to the severity of the phenotype in an individual with two mutations in one gene, although this was not demonstrated by their study [163]. There has been a report, however, of a family with multiple affected individuals and bi-allelic mutations in *CRB1* with one sibling harbouring an additional heterozygous missense mutation in *SPATA7* that was presumed to be damaging by *in silico* analysis [348]. It is possible, though, that this variant is a rare SNP. In this family, the clinical picture was the same in all affected individuals leading to the conclusion that there was no contribution of the mutant *SPATA7* allele to the phenotype seen in this subject.

It has been hypothesised that the differential severity of mutations at a single locus may be the cause of the difference in phenotypes [163]. Mutations that occur earlier in the *SPATA7* coding region might lead to more severe protein truncation with loss of function due to nonsense mediated decay, and thus cause a more severe phenotype consistent with LCA. Conversely, mutations that occur later in the coding region, such as in the last 2 exons, may lead to less severe protein truncation and a less severe phenotype that is described as ‘juvenile RP’. Similar observations were made by

another group, who identified all six mutations in their study to cause protein truncation, and all affected subjects to display a severe phenotype consistent with LCA [166]. Of the four mutations identified in *SPATA7* in the present study, 3 are predicted to lead to premature termination of the protein (p.Arg85X, p.L89KfsX3 and p.P321TfsX5), and to be degenerated by nonsense mediated decay. The subjects with homozygosity with any of these alleles did indeed have a more severe phenotype. The compound heterozygous mutations in family 1, which has a milder phenotype in one affected sibling, involves mutations in exon 5 and exon 12, which may lead to some residual protein function. However the severity of the phenotype between the siblings who harbour the same compound heterozygous mutations is different. The reason for this is unclear but it may again be due to the influence of modifier alleles.

At the time that this study was conducted the function of *SPATA7* was unknown. *Spata7* was first cloned in the rat testis and the corresponding human cDNA was identified in the human testis [164]. The human protein had been identified to be expressed as two transcripts: one that is predominantly expressed in the retina, cerebellum and whole brain, and another that is predominantly expressed in the testis [166]. Murine *Spata7* was observed to be expressed in the mature mouse retina at day P21 (postnatal) in multiple layers including the ganglion cell layer, inner nuclear layer and inner segments of photoreceptors, and not in the mouse embryo at day E16.5 [163]. This suggested that *Spata7* is required for photoreceptor function rather than in photoreceptor development.

Recently the function of *Spata7* was further delineated [349]. It has been identified as a ciliary protein, which localises to the connecting cilium of photoreceptors. *In vitro*

and *in vivo* studies identified that a key role of SPATA7 is in its interaction with RPGRIP1 and that it binds to the N terminal coiled coil domain of RPGRIP1. In the *Spata7*^{-/-} mouse there is very little RPGRIP1 present at the connecting cilium, indicating that *Spata7* is necessary for the localisation and assembly of the RPGRIP1 protein complex, which itself is required for protein trafficking from the IS to the OS. Similarly to mutations in other ciliary genes such as *Tulp1*, *Cep290*, *Rpgrip1* and *Rpl* [243, 305, 350, 351], rhodopsin is seen to accumulate at the ISs and nuclei of photoreceptors in the *Spata7*^{-/-} mouse, leading to photoreceptor apoptosis. The retinal defects in *Spata7*^{-/-} mice are evident shortly after birth with initial thinning of the ONL and subsequent shortening and disorganisation of the OSs. Rods die by 6 months but the cones are better preserved at this age (84% of cones are still present at 6 months). Subsequent cone loss is presumed to be secondary to rod photoreceptor loss. Interestingly, in the present study, ERG testing identified initial loss of cone function with eventual rod involvement. In addition, a number of subjects in this and other studies reported transient photoaversion initially, suggesting first cone photoreceptor dysfunction [166].

Mutations in *SPATA7* have added to the spectrum of conditions known as ‘ciliopathies’. Photoreceptor dysfunction is due to degeneration rather than developmental defects. Further studies will be required to ascertain whether there are systemic associations of mutations in *SPATA7* such as infertility or hearing loss, which was observed in some of the patients in this study. The presence of less severe phenotypes and retention of photoreceptor architecture very early in the disease may provide a small window of opportunity for therapeutic options as and when they arise.

4.5 Tubby and Tubby-Like protein

Genotype - Phenotype Associations

The tubby-like proteins (TUB, TULP1, TULP2 and TULP3) are a unique family of proteins that share a highly conserved C-terminal domain (the ‘tubby domain’) that is comprised of around 260 amino acids, and is located at the carboxyl terminus of all of the members of the tubby-like protein (TULP) family [352]. TUB is the founding member of the TULPs, first identified in the tubby mouse as *Tub*, which presented with a syndrome characterised by late-onset obesity and neurosensory deficits. The causative mutation was found in the *Tub* gene [294, 295, 353]. Although human autosomal recessive mutations in *TULP1* (MIM 602280) have been identified in EORD and ARRP [299-301], no human mutations in *TUB* (MIM 601197) had been identified prior to this study. Through exome sequencing, one family in the Childhood Onset Retinal Dystrophy study was identified with a homozygous mutation in *TUB*. The subsequent phenotypic studies, and the results of collaborative studies on this family, are reported in this chapter. In addition, the phenotypes of families identified with *TULP1* mutations are described in a separate section within this chapter.

4.5.1 *TUB* Genotype - Phenotype Association

The proband of a consanguineous UK Caucasian family had previously been recruited to the Childhood Onset Retinal Dystrophy Study. His DNA had been screened across the LCA chip by previous researchers in 2008 and no mutations were identified. Due

to his consanguineous ancestry, his DNA had been analysed using autozygosity mapping by Dr Mackay, UCL, and was subsequently screened using next generation sequencing. This identified a homozygous frame-shift mutation in *TUB*, c.1194_1195delAG, p.Arg398Serfs*9. The proband and his family were invited back to MEH for phenotypic studies subsequent to this mutation being identified. Collaborators at the University of Cambridge, UK, and the University of Mainz, Germany, performed functional studies and immunohistochemistry studies on this family, and the work was published in a collaborative paper [330]. Brief descriptions of the molecular and functional studies will be presented here, but the main body of work into this family to be detailed are the phenotypic studies.

4.5.1.1 Clinical History

The male proband had reduced vision and nyctalopia from age 9 years. He was diagnosed with a unilateral retinal detachment and a retinal dystrophy at 11 years of age. Subsequent electrodiagnostic testing demonstrated undetectable full field rod and cone responses and severely reduced macular function. He was 18 years old when he attended with his parents and 2 siblings for further phenotypic studies.

General health in the proband was good, although he was noted to be overweight in his early teenage years and he had mild learning difficulties. In particular, he denied any hearing, renal or metabolic abnormalities. He had 4 siblings and there were multiple levels of consanguinity within the family (Figure 37). His older brother denied any visual symptoms and younger sister, who was obese, had been prescribed glasses at 5 years of age and had undergone intermittent occlusion therapy for

amblyopia, but had no other visual symptoms. They also denied any other systemic abnormalities. There was a family history of unilateral micro-ophthalmos, colobomata and extra digits in a male maternal cousin. The parents were asymptomatic.

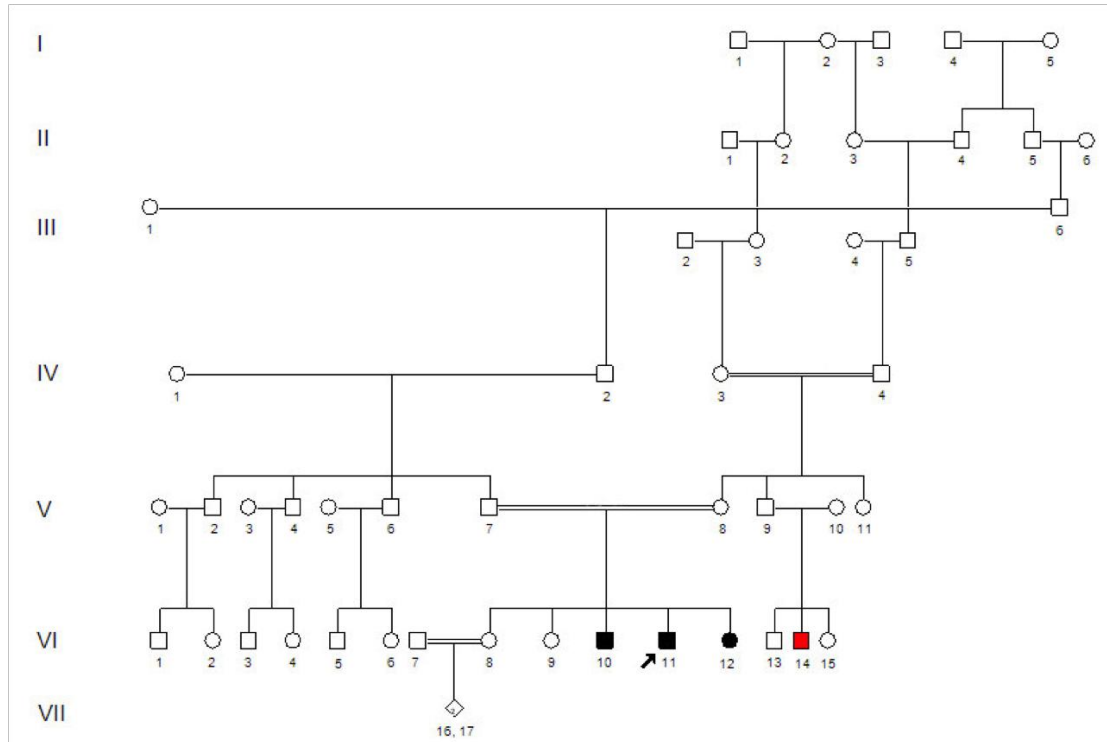


Figure 37 - Pedigree of *TUB* family. Black symbol = affected with retinal dystrophy; red symbol = affected with microphthalmos, colobomata and extra digits.

4.5.1.2 Clinical Examination

At 18 years of age BCVA in the proband (VI.11) was 0.2 LogMAR in the right eye and NPL in the left eye, with a myopic astigmatic refractive error of -1.25/-4.25, 16° in the right eye and -1.00/-4.00, 170° in the left eye. HRR colour vision testing of the right eye demonstrated a mild red - green colour deficiency and a strong blue - yellow colour deficiency. There was a left relative afferent pupillary defect and left exotropia. The anterior segments were normal and cortical lens opacities were present in the left

eye. The right fundus had widespread RPE atrophy, generalised retinal pallor, arteriolar attenuation, fine peripheral pigmentary mottling and white dots throughout, with macular sparing (Figure 38 - A). The optic nerve was normal, with peri-papillary atrophy, in keeping with myopia. The left fundus had a total retinal detachment with proliferative vitreoretinopathy. He had no syndactyly or polydactyly, although his fingers appeared to taper at the distal ends. At age 18 his BMI was 29.5kg/m², which placed him in the 'overweight' category. Biochemical investigations into glucose, triglycerides and cholesterol were normal.

Unaided visual acuity in the proband's 21 year old brother (VI.10) was 0.48 LogMAR in either eye, with no improvement with pinhole. His myopic astigmatic refractive error was -1.00/-2.00, 180° and -0.75/-1.75, 180° in the right and left eyes respectively. HRR colour plate testing revealed mild red-green and medium blue-yellow colour deficiencies. His fundus appearance, which was bilaterally symmetrical, was similar to, but less severe, than the proband (Figure 39 - A). His BMI at age 21 years was 22.9kg/ m², which is categorised as being 'normal'.

The 9-year old sister (VI.12) had a BCVA of 0.18 LogMAR right eye and 0.3 LogMAR left eye, improving to 0.18 LogMAR with pinhole. Her myopic astigmatic refractive error was +0.75/-3.50, 180° in the right eye and +0.25/-3.00, 180° in the left eye. HRR colour vision testing was normal. The fundus showed bilateral symmetrical mild peripheral RPE atrophy, generalised retinal pallor, inferior retinal pigmentary mottling with macular sparing and no retinal pigmentation (Figure 40 - A). Peri-papillary atrophy was in keeping with her myopia. Her BMI at age 9 years classified her as being 'obese', falling in the 98th centile for age and gender.

Ocular examination in the parents and oldest sister was normal. Unfortunately the family did not consent to any further phenotypic studies such as smell acuity, auditory testing and metabolic studies.

4.5.1.3 *Fundus Autofluorescence Imaging*

In the proband FAF imaging demonstrated an annulus of hyperautofluorescence centred on the fovea in the right eye (Figure 38 - B). A normal autofluorescence signal was obtained at the fovea in the brother, although there was hypoautofluorescent mottling in the posterior pole along the vascular arcades (Figure 39 - B). FAF imaging in the sister was normal (Figure 40 - B).

4.5.1.4 *OCT Imaging*

sd-OCT imaging in the proband demonstrated a preserved photoreceptor inner segment outer segment (IS/OS) junction at the fovea, with loss of this layer in the parafoveal region, corresponding to the fundus autofluorescence image (Figure 38 - C). The inner retinal layers remained intact. In the affected brother (VI.10) the IS/OS junction was preserved at the fovea, outer retinal debris was visible at the level of the RPE in the parafoveal region, and the inner retinal layers remained intact (Figure 39 - C). In the sister (VI.12) OCT imaging was normal (Figure 40 - C).



Figure 38 - TUB Family: proband (VI.11): A – right eye fundus; B – right eye fundus autofluorescence image; C – right eye sd-OCT. Yellow arrows on image B indicate nasal and temporal limits of photoreceptor inner segment outer segment layer at the fovea; beyond these arrows this layer is not visible.

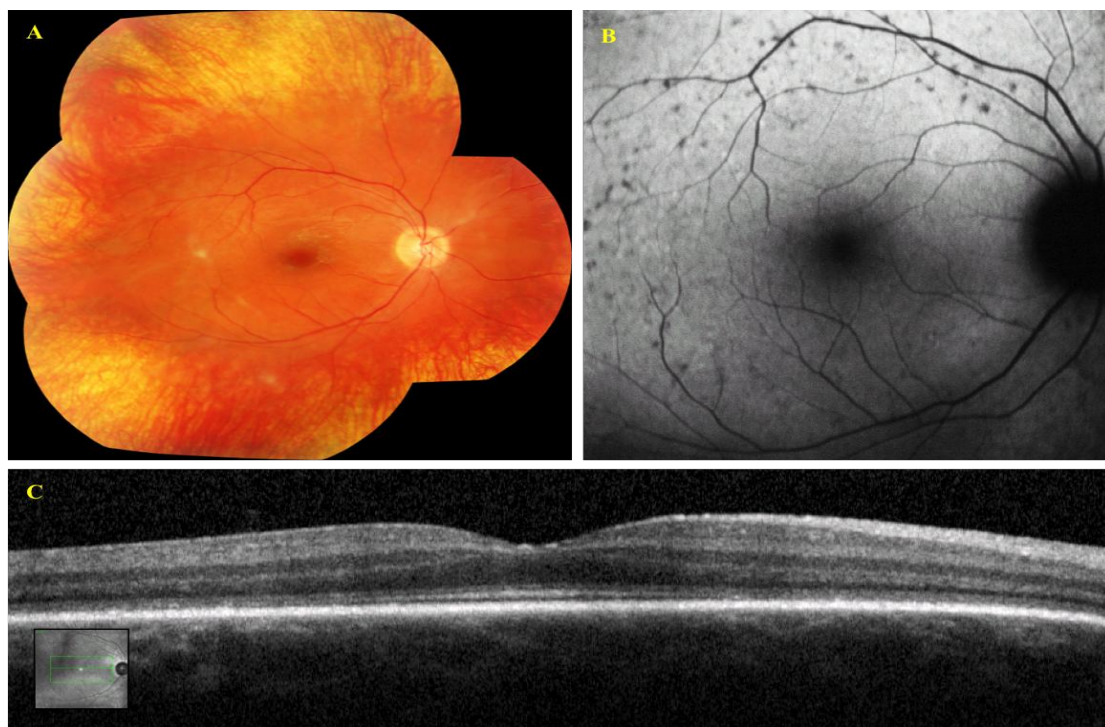


Figure 39 – TUB Family: brother (VI.10): A – right eye fundus; B – right eye fundus autofluorescence image; C – right eye sd-OCT.

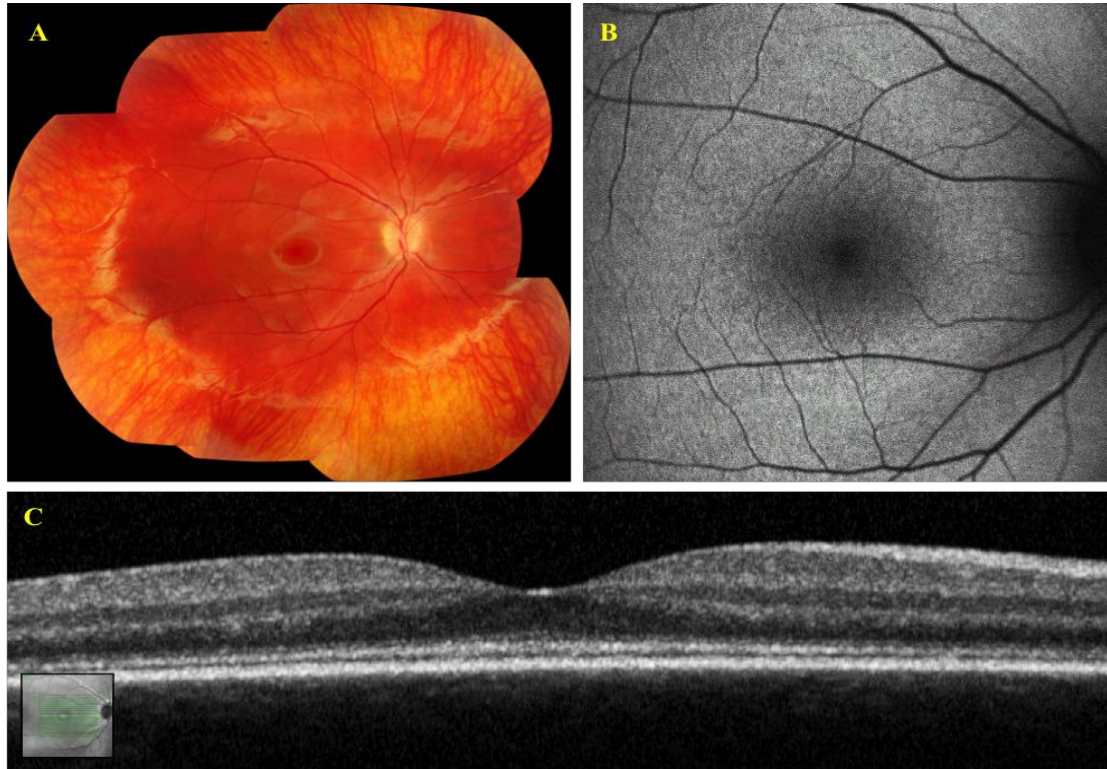


Figure 40 - TUB Family: sister (VI.12): A – right eye fundus; B – right eye fundus autofluorescence image; C – right eye sd-OCT.

4.5.1.5 Psychophysical testing: Goldmann Visual Fields

Goldmann visual field analysis was performed only for the right eye of the proband, which revealed responses in only the central 15° to the V4e target, the central 10° to the III4e target and the central 7.5° to the I4e target (Figure 41).

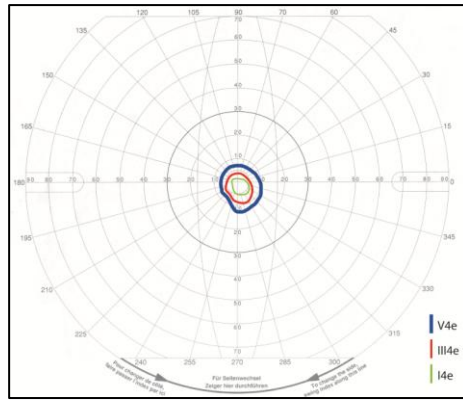


Figure 41 – Goldmann Visual Field, Subject VI.11, *TUB*. Right eye. V4e – blue line; III4e – red line; I4e – green line.

4.5.1.6 *Electrophysiological Testing*

In the proband, full-field ERGs from both eyes at age 13 years were undetectable. There was a residual 30Hz flicker response of 10 μ V in the right eye suggesting residual cone function in this eye. No further electrophysiological studies were performed in any subject as the family did not attend for any further studies.

4.5.1.7 *Molecular analysis*

Molecular analysis was performed by Dr Mackay and Dr Davidson at UCL, and the results briefly described here. More detailed information regarding the molecular analysis is available in the paper published on this family [330].

On the basis of the consanguineous ancestry in the proband, his DNA was analysed using homozygosity mapping. This identified five chromosomal segments over 5 Mb. No genes that had previously been associated with RP were found to be present within the identified regions of homozygosity. Four retinal disease associated genes that

were identified in the second largest region of homozygosity on chromosome 11 (*CTSD*, *TPPI*, *TEAD1*, *USH1C*) were screened in this subject and no disease causing variants were identified. In addition, no homozygous pathogenic copy number variants were identified.

His DNA subsequently underwent exome capture and high throughput sequencing using solution phase Agilent SureSelect 38-Mb exome capture. The average sequencing depth on target was 43 with 78.4% of the targeted region covered with a minimum read depth of 10. A homozygous frame-shift variant in *TUB*, c.1194_1195delAG, p.Arg398Serfs*9 was identified (numbered according to Ensembl transcript ENST00000299506). This variant was located in the second largest region of homozygosity and was identified in the homozygous state in his older brother and younger sister. The parents were identified as heterozygous carriers of this variant. No additional potentially pathogenic variants in *TUB* were identified on Sanger sequencing in 96 probands with childhood onset ARRP. In collaboration with the University of Cambridge Metabolic Research Laboratories, *TUB* was sequenced in 55 subjects with severe obesity and a variety of ocular phenotypes, who were part of the Genetics Of Obesity Study, and no potentially pathogenic variants were found. The *TUB* c.1194_1195delAG, p.Arg398Serfs*9 variant was not identified in over 6000 publically available exomes (NHBLI exome variant server).

4.5.1.8 Collaborative studies

In collaboration with the University of Cambridge Metabolic Research Laboratories, (Wellcome Trust-MRC Institute of Metabolic Science, Addenbrooke's Hospital, Cambridge) functional studies of the p.Arg398Serfs*9 variant identified its expression in transfected HEK293 cells and its localisation predominantly to the nucleus, in contrast to wild type TUB which was detected in the cytoplasm and plasma membrane [330]. The Department of Cell and Matrix Biology, Institute of Zoology, Johannes Gutenberg, (University of Mainz, Mainz, Germany), performed immunohistochemistry studies on retinal cryosections from eyes of a human donor, and identified strong TUB expression in the nuclei of the ganglion cell layer and in the inner segment of photoreceptor cells. TUB was identified at the base of the photoreceptor cilium and ciliary rootlet, which projects through the inner segment of the photoreceptor [330].

4.5.1.9 Summary of TUB phenotype identified in this study

The results from this study have identified that the phenotype associated with mutations in *TUB* is of a childhood onset rod cone dystrophy characterised by reduced vision, nyctalopia and visual field constriction beginning late in the first decade. There is associated myopic astigmatism, a mild red - green and a stronger blue – yellow colour deficiency, severe visual field constriction and an undetectable full field ERG. There may be residual cone function demonstrable by the ERG. The fundus displays widespread RPE atrophy, fine peripheral pigmentary mottling, and peripheral white dots. The OCT demonstrates preservation of the photoreceptors in the fovea but

loss of this layer in the parafoveal region. Autofluorescence imaging correlates with the OCT imaging. Systemically there may be obesity in childhood, but no other metabolic, auditory or olfactory abnormalities that are found in the tubby mouse can be confirmed. Further families will need to be ascertained to determine these features.

4.5.2 *TULP1* Genotype - Phenotype Association

Four individuals from 3 families were identified to harbour mutations in *TULP1*. One family with 2 affected siblings (family 1) was recruited in Cohort 1 of this study; one family with one affected member had been recruited to the study by a previous research registrar (family 2); and the final family with multiple affected individuals (family 3) was originally part of a panel of patients with ARRP that underwent autozygosity mapping and positional screening of *TULP1*. The strategies used to identify the *TULP1* variants in these families varied and will be described in this chapter, along with the results of phenotypic studies.

4.5.2.1 *Clinical History*

The age of onset of visual symptoms varied in the group of patients identified with *TULP1* mutations. Two siblings (family 1) were diagnosed with EORD, with onset of poor vision and nystagmus within the first year of life; the female proband (IV.4) was 1 year old when nyctalopia and visual field constriction were first noted but her younger brother (IV.5) was 8 months old when nystagmus developed. The probands of families 2 (V.5) and 3 (III.3) were 6 years and 12 years old respectively when they developed nyctalopia, and carried a diagnosis of rod-cone dystrophy. Current

symptoms in all subjects are of reduced vision, nyctalopia and visual field constriction. General health was good in all subjects. The children of family 1 were classified as being overweight (IV.4) and obese (IV.5) for their age and gender; subject V.5 family 2 had a normal body mass index. All 3 families are from the Asian subcontinent and are consanguineous (Figure 42 and Table 15).

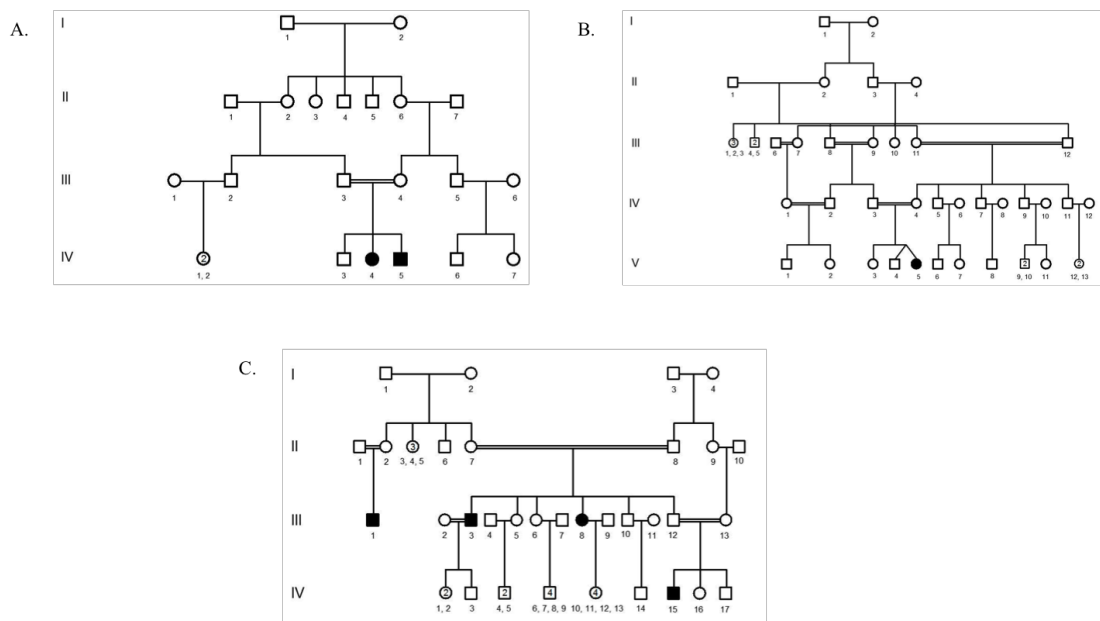


Figure 42 - Pedigrees of *TULP1* families. A. Family 1; B. Family 2; C. Family 3. Black symbols = affected individuals.

4.5.2.2 *Clinical Examination*

Visual acuity ranged from 0.6 LogMAR in the youngest subject at 6.5 years of age to 1.48 LogMAR in the oldest subject at 36.5 years of age. The refraction, where recorded, tended towards a myopic astigmatism (Table 15) and visual fields to confrontation in the two oldest subjects were constricted to the central 60° in the third

decade and central 10° in the fourth decade. Anterior segments were normal in all subjects, and lens opacities were present in the oldest subject.

Funduscopy in the youngest subjects (aged 6.5 years [IV.5 family 1] and 9 years [IV.4] family 1) showed mild RPE atrophy in the retinal periphery, vascular attenuation, macular preservation and no retinal pigmentation (Figure 43 - A). In the older subjects there was a similar picture but with more widespread RPE atrophy (V.5 family 2, age 24 years) (Figure 44 - A), which progressed to having peripheral bone spicule pigmentation and pigment clumping with a pale disc in the oldest subject (III.3 family 3, age 36.5 years) (Figure 45 - A). BMI was calculated for families 1 and 2. The children in family 1 were overweight (IV.4) and obese (IV.5) for their age and gender; the proband of family 2 had a normal BMI (Table 15).

Subject (Gender)	Family	Ethnicity	VA RE, LE (age, years)	Refraction	Visual fields	BMI (kg/m ²)
IV.4 (F)	1	Indian	0.6, 0.6 (9)	RE -0.75/-1.5, 180 LE 0/-2.0, 180	Not tested	24.1 94 th centile (over-weight)
IV.5 (M)	1	Indian	0.8, 0.6 (6.5)	RE plano LE plano	Not tested	21.1 98 th centile (obese)
V.5 (F)	2	Pakistani	0.78, 0.6 (24)	RE -5.75/-3.50, 4 LE -5.50/-4.00, 180	Central 65°	24.2 (normal)
III.3 (M)	3	Pakistani	1.3, 1.48 (36.5)	Not available	Central 10°	Not available

Table 15 - Clinical features of *TULP1* subjects. VA – visual acuity; RE – right eye; LE – left eye; M = male; F = female.

4.5.2.3 *Fundus Autofluorescence Imaging*

FAF imaging at age 9 years (IV.4 family 1) demonstrated an annulus of hyperautofluorescence in the macula with a hypoautofluorescent signal at the fovea (Figure 43 - B). In the third decade the hyperautofluorescent annulus was more diffuse and extended to the fovea (Figure 44 - B). By the fourth decade a hyperautofluorescent signal was seen at the fovea with hypoautofluorescence corresponding to atrophy and pigmentation throughout the macula and retina (**Figure 45 – B**).

4.5.2.4 *OCT Imaging*

In all subjects old enough to be tested, sd-OCT imaging showed preservation of the photoreceptor IS/OS layer at the fovea with loss of the layer in the parafoveal area (Figure 43, Figure 44 and **Figure 45 - C**). The inner retinal layers remained intact. Debris was visible in the outer retina in the oldest subject.



Figure 43 - *TULP1* Family 1: subject IV.4: A – right eye fundus; B – right eye fundus autofluorescence image; C – right eye sd-OCT. Yellow arrows indicate nasal and temporal limits of photoreceptor inner segment outer segment layer at the fovea; beyond these arrows this layer is not visible. Images taken at age 9 years.

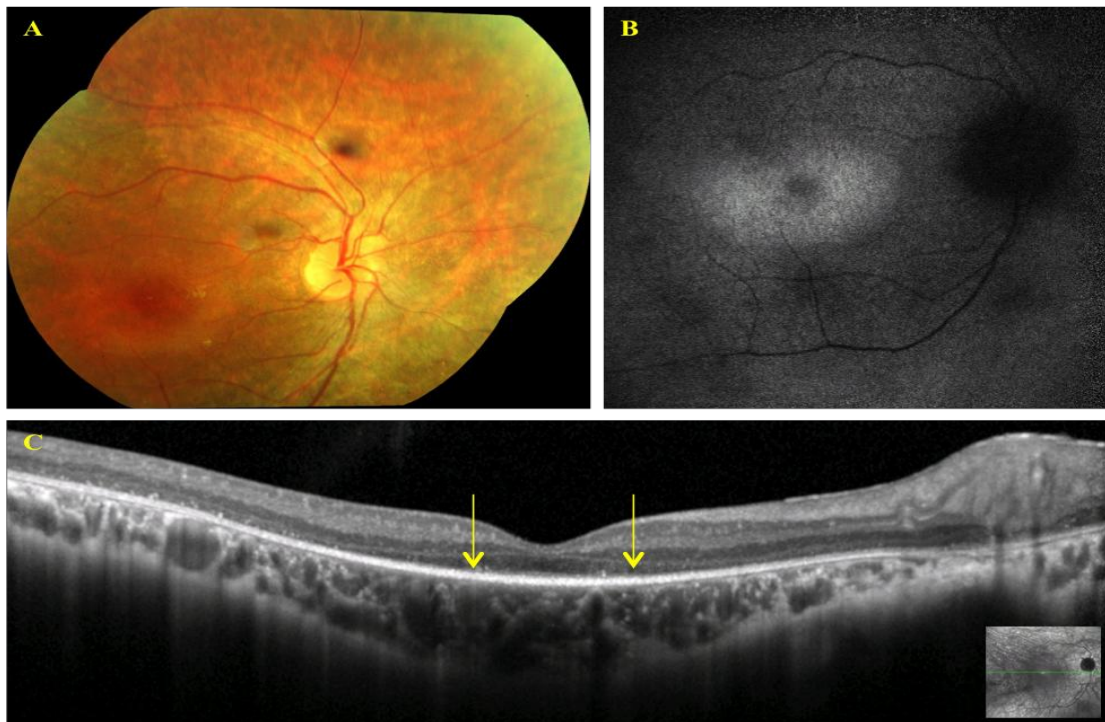


Figure 44 - *TULP1* Family 2: subject V.5: A – right eye fundus; B – right eye fundus autofluorescence image; C – right eye sd-OCT. Yellow arrows indicate nasal and temporal limits of photoreceptor inner segment outer segment layer at the fovea; beyond these arrows this layer is not visible. Images taken at age 24 years.

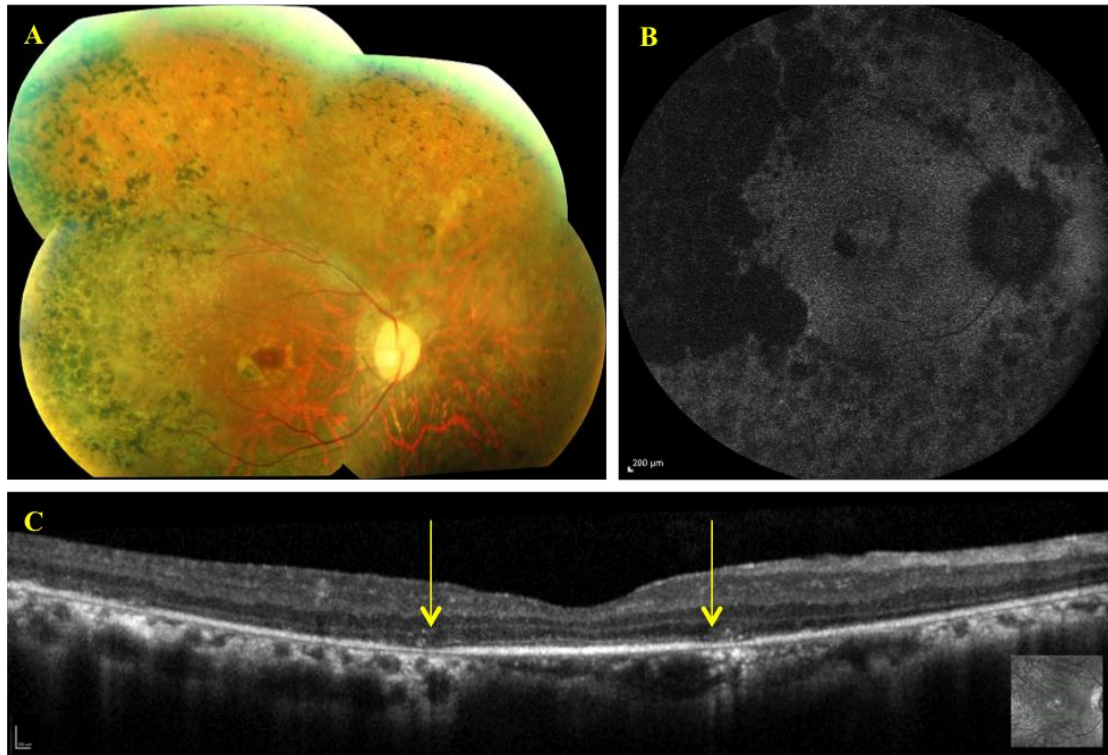


Figure 45 - *TULP1* Family 3: Subject III.3. A – right eye fundus; b – right eye fundus autofluorescence image; c – right eye sd-OCT. Yellow arrows indicate nasal and temporal limits of photoreceptor inner segment outer segment layer at the fovea; beyond these arrows this layer is not visible. Images taken at age 36.5 years.

4.5.2.5 *Psychophysical Testing: Goldmann Visual Fields*

Goldmann visual fields were performed in the proband of family 2, which showed global constriction of the visual fields in each eye. To the V4e target this was reduced in the right eye to 40-45° nasally, superiorly and inferiorly, and 60° temporally, and in the left eye to 40° nasally and superiorly, 55° inferiorly and 70° temporally (Figure 46).

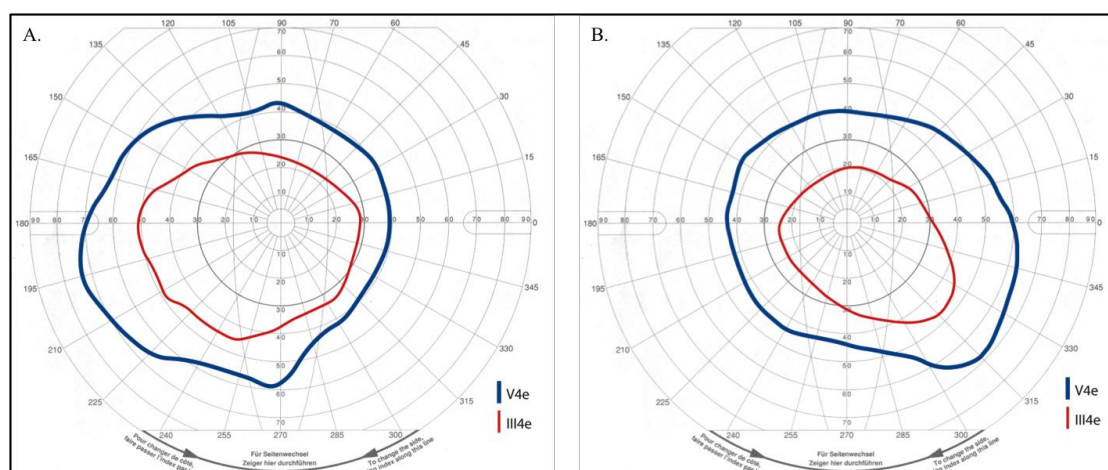


Figure 46 - *TULP1* Family 2: Subject V.5, Goldmann Visual Fields. A – Right eye; B – Left eye. V4e – blue line; III4e – red line.

4.5.2.6 *Electrophysiological Testing*

Full field and pattern ERGs were markedly reduced in subject IV.5 family 1, the youngest subject, and undetectable in 2 others (IV.4 family 1 and V.5 family 2). The oldest subject did not undergo electrophysiological testing (III.3 family 3).

4.5.2.7 *Molecular analysis*

The DNA of the proband (IV.4) of family 1 was analysed using the LCA chip, which identified the exon 15 variant c.1511_1521delTGCAGTTCGGC, p.Leu504fsX140 in the homozygous state. This variant had previously been described by den Hollander in a Surinamese family with ARRP [312]. This mutation was confirmed by ADB, and segregation checked within the family. The affected younger brother (IV.5) was also identified to harbour this variant in the homozygous state, and the parents were

identified to be heterozygous carriers of the variant, which confirms the segregation of this variant with the disease in this family (Figure 47). *TULP1* primer sequences and PCR conditions are described in the appendix (Appendix 7.2.1). This 11-bp deletion causes a frame shift and replaces the 39 C-terminal amino acids with 140 aberrant amino acid residues.

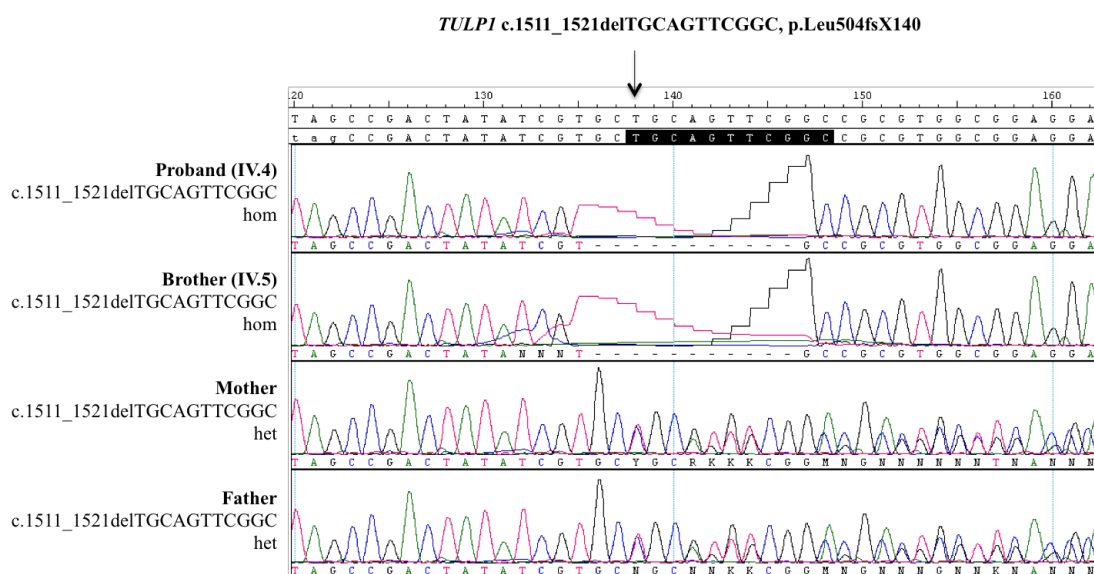


Figure 47 - *TULP1* Family 1 Electropherograms.

Due to the ancestry of families 2 and 3, autozygosity mapping was performed (family 2 by Dr Mackay, family 3 by Dr Sergouniotis). In family 2, this revealed 6 chromosomal segments over 10 Mb (Table 16), in which 4 known retinal disease associated genes resided. Based upon the phenotype in the proband of family 2, *TULP1* was selected as a positional candidate gene, and screened by ADB within a panel of 10 patients by direct sequencing. This identified the novel homozygous variant c.1035C>G, p.Ser345Arg in exon 10 in the proband. Segregation analysis identified that this variant segregates with the disease in this family as her unaffected

brother (III.2, family 2) and parents were all heterozygous for this variant (Figure 48). This variant was analysed using different *in silico* analysis programmes. SIFT gave a score of 0, indicating that this mutation is damaging (median 2.71); pMUT gave a neural network value of 0.70 and reliability value of 4 (predicting the mutation to be pathologic); and PolyPhen 2 appraised the mutation to be ‘probably damaging’ with a score of 0.992 (sensitivity 0.7, specificity 0.97). This variant was not identified in the 1000 genomes project or in the exome variant server.

Chromosome	From	To	Size (Mb)	Retinal disease associated genes
6	15062945	37547262	22.48	<i>TULP1</i>
6	130071088	155001410	24.93	<i>AHII, PEX7</i>
7	5411296	20831800	15.42	
7	110274772	141816117	31.54	
9	2615553	17987408	15.37	<i>MPDZ</i>

Table 16 - Augozygosity data, *TULP1* Family 2. *TULP1* resides in the third largest region of homozygosity.

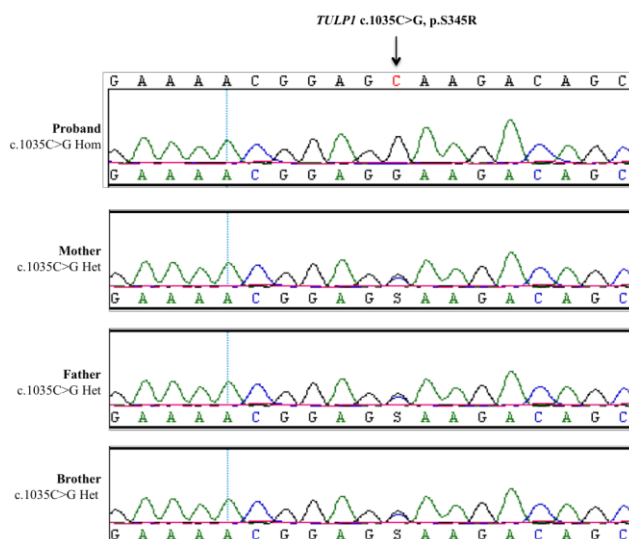


Figure 48 - *TULP1* Family 2 Electropherograms.

The autozygosity mapping data for family 3 are not available, but did identify an area of homozygosity on chromosome 6p, in which *TULP1* resides. Positional screening

(by ADB) of *TULP1* in the proband (III.3) of this family identified a novel homozygous variant in the intronic sequence as IVS3+1g>a. There were no other family members available to check the segregation of this variant, but it was confirmed in both the forward and reverse sequence (Figure 49). Splice site *in silico* analysis programmes identified that this mutation abolishes the splice acceptor site at this location (www.fruitfly.org). The mutation was not identified in the 1000 genomes project or on the exome variant server.

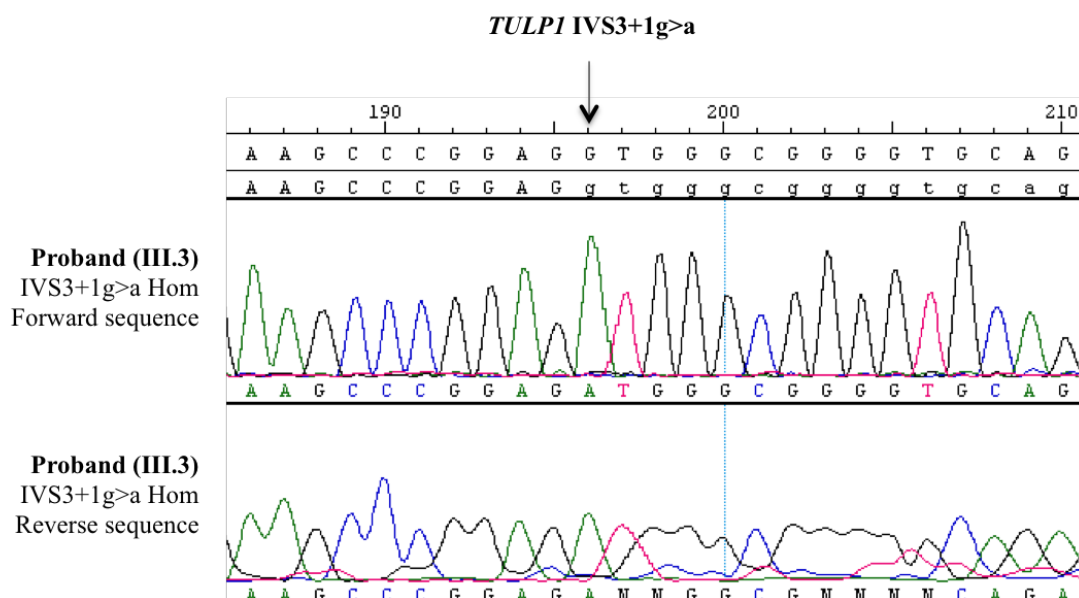


Figure 49 - *TULP1* family 3 Electropherograms.

A summary of all the *TULP1* mutations identified in this study are listed (Table 17).

Subject	Family	Mutation 1	Mutation 2	Reference
IV.4	1	c.1511_1521del p.Leu504fsX140	c.1511_1521del p.Leu504fsX140	[312]
IV.5	1	c.1511_1521del p.Leu504fsX140	c.1511_1521del p.Leu504fsX140	[312]
V.5	2	c.1035C>G p.Ser345Arg	c.1035C>G p.Ser345Arg	Novel to this study
III.3	3	IVS3+1g>a	IVS3+1g>a	Novel to this study

Table 17 - Mutations identified in *TULP1* in this study.

4.5.2.8 Summary of *TULP1* phenotype identified in this study

Onset of visual symptoms in subjects with autosomal recessive mutations in *TULP1* can occur in early childhood, giving a clinical picture of an EORD, or later in the first decade, giving a clinical picture of a rod-cone dystrophy. Subjects present with poor vision, nystagmus, nyctalopia and visual field constriction. The refraction tends towards a myopic astigmatism and colour vision is severely reduced. In the early stages the retina displays RPE atrophy, vascular attenuation and preservation of the macula with no pigmentation; with age, the RPE atrophy becomes more widespread, and peripheral retinal pigment clumping and optic disc pallor develop. The OCT shows loss of the photoreceptor layer in all areas except at the fovea and fundus autofluorescence imaging demonstrates a wide band of hyperautofluorescence around the fovea, unlike the autofluorescence imaging seen in other causes of EORD. Visual fields are constricted but may remain relatively preserved into the third decade and electroretinography shows widespread photoreceptor dysfunction including the macula. There may be obesity in childhood as observed in the affected children of *TULP1* family 1.

4.5.3 Discussion

The TULPs (including TUB) are involved in G-protein coupled receptor trafficking pathways in the cilia of neurones, and thus mutations in this family of genes add to the growing number of conditions known as ‘ciliopathies’ [354, 355]. Disease associated mutations involving the TUB family of proteins have only been identified in *Tub* (in mice) and *TULP1* (in humans) to date [294, 295, 353] [299-301]. The first human mutation in *TUB* was identified through this study, in one family, and the

phenotype published [330]. Human mutations in *TULP1* have been reported to cause both EORD and ARRP. The phenotypes associated with mutations in *TULP1* identified in this study are also described. As these genes belong to the same family of proteins, the results of the phenotypic and molecular analyses performed in this study are being considered together in this chapter.

Humans with loss of function mutations in *TUB* display a rod-cone dystrophy phenotype beginning late in the first decade of life, characterised by nyctalopia and visual field constriction. Colour vision is reduced and there is typically a myopic astigmatic refractive error. The retinal degeneration is associated with widespread atrophy of the RPE, minimal retinal pigmentation and vascular attenuation, with preservation of the photoreceptor layer at the fovea. There is associated early onset obesity. However, the effects on hearing and further effects on metabolism in humans were not determined through this study.

The tubby mouse carries an autosomal recessive loss of function mutation in *Tub* and its phenotype is characterised by neurosensory deficits and metabolic disturbances. The neurosensory deficits comprise of retinal and cochlear degeneration. The retinal degeneration is secondary to apoptotic death of photoreceptors [293]; the cochlear degeneration in the tubby mouse appears to be related to the presence of polymorphisms in the microtubule associated protein gene *Map1a*, but the biochemical sequelae of this genetic interaction is unclear [356]. The metabolic disturbances consist of obesity and insulin resistance, and are secondary to the effects on feeding behaviour and energy homeostasis controlled via the hypothalamus [357],

and to the mediating effects of *tub* on insulin and leptin signalling in the hypothalamus [358].

The childhood onset retinal dystrophy and obesity phenotype observed in the *TUB* family in this study is similar to the phenotype seen in the tubby mouse, although the obesity in this family was less severe than other genetic forms of obesity. As mentioned above, the TULPs (including TUB) are involved in G-protein coupled receptor trafficking pathways in neuronal cilia [354, 355]. The method of photoreceptor degeneration is likely due to the ineffective transport of rhodopsin to the outer segments across the connecting cilium, as observed in mice with loss of *Tulp1* function, which have an ectopic distribution of rhodopsin prior to photoreceptor degeneration [305]. This mechanism has been postulated to occur with the other TULPs [355]. The extracellular rhodopsin laden vesicles that are seen to accumulate in the interphotoreceptor space in *Tub*^{-/-} and *Tulp1*^{-/-} mice occur at a time that rhodopsin is usually rapidly synthesised to build up the outer segments, and it was hypothesised that the accumulation of these vesicles might be a hallmark of the defect of rhodopsin transport to the outer segments, a process in which the TULPs have a role [305, 307]. Mice that are doubly mutant for *tub* and *tulp1* display a more severe retinal phenotype than either mutant alone, which results in complete failure of rhodopsin trafficking and outer segment formation with rapid cell death [307].

The phenotypes associated with mutations in *TULP1* that were observed in this study were similar to other reports of *TULP1* mutations, which have described widespread loss of rod function from a young age, with only residual cone function existing at the fovea [258, 309, 311-313, 359]. Onset of visual symptoms can be very early, within

the first year of life, and thus the condition is classified as an early onset retinal dystrophy, or may begin later in childhood and so be classified as a rod-cone dystrophy. Similar to the *TUB* family, there tends to be a myopic astigmatism. RPE atrophy, vascular attenuation and preservation of the macula without pigmentation is seen in the early stages but with age, the RPE atrophy becomes more widespread, and peripheral retinal pigment clumping and optic disc pallor develop. A recent study has identified small islands of preserved RPE that is associated with better visual function at these points; these were not identified in the present cohort [359]. Fundus autofluorescence imaging in this study identified a wider band of hyperautofluorescence than that which is seen in other forms of RP. This has been observed in other studies [311]. OCT imaging in the present *TULP1* cohort demonstrates preservation of the photoreceptors only at the fovea, which may represent a small central island of residual foveal cones, but the extracentral loss of laminar architecture that has been reported in the literature was not observed [359]. Unlike *Tub*, mutations in *TULP1* appear not to be associated with obesity, hearing impairment or endocrine dysfunction [311]. Although the children in family 1 in this study were classified as being obese for their age and gender, this feature may not be related to their *TULP1* variant. From the expression profile of *TULP1* and the phenotype of the *Tulp1*^{-/-} knockout mouse, systemic features of obesity and endocrine dysfunction would not be predicted to occur, and have not been reported in human *TULP1* mutations [357].

A large number of studies have identified *TULP1* mutations in families of Middle Eastern or South East Asian descent [201, 258, 311, 313, 314, 360, 361]. Den Hollander *et al.* reported a multiply affected family from Surinam, which has a large

South East Asian population, but the ancestry in this family was not defined [312]. A small panel of 49 Spanish ARRP families had an incidence of 2% of families affected with *TULP1* mutations, although the ancestry of these families was also not defined [310]. All three families identified in this study were originally from South East Asia and were consanguineous, harbouring homozygous mutations in *TULP1*. This suggests the presence of a number of founder mutations in *TULP1* in families from these regions.

The c.1511_1521delTGCAGTTCGGC, p.Leu504fsX140 variant identified in family 1 in the homozygous state was first reported in a Surinamese family in the heterozygous state by Den Hollander, and causes a frame shift, affecting the *TULP1* C-terminal domain [312]. The novel missense mutation, c.1035C>G, p.Ser345Arg, identified in the homozygous state in family 2 is predicted to be pathological and also lies within the *TULP1* C-terminal domain. It is interesting to note that all missense mutations identified in *TULP1* and *TUB* to date affect the highly conserved C-terminal domain (tubby terminal) of this family of proteins [330, 360]. In the *TULP* family of proteins (including *TUB*) this domain contains a DNA binding region and a phosphatidylinositol-binding region, which anchors the *TULPs* to the cell membrane before they are released by phospholipase C β -mediated cleavage of phosphatidylinositol bisphosphate [302]. The crystal structure of the C-terminal domain in *Tub* was identified to comprise of a closed β barrel consisting of 12 anti-parallel strands, surrounded by a central hydrophobic α helix. An important function of this domain is in the interaction with phosphatidylinositol bisphosphate, which is disrupted in *TUB* mutations, with subsequent inability of the protein to localise to the plasma membrane, and instead remain within the nucleus [303].

It remains to be determined whether human mutations in *TUB* result in other systemic abnormalities that resemble the tubby mouse but it is known that *TULP1* families display a similar phenotype to the loss of function *Tulp1* mouse. The conditions associated with both of these genes further add to the range of conditions that are now classified as ‘ciliopathies’.

4.6 *LRAT* Phenotype

Limited reports of the phenotype associated with mutations in *LRAT* had been published by the time this study was conducted. Rather more extensive phenotypic studies of another visual cycle gene, *RPE65*, had been published, and the first human gene therapy studies undertaken into retinal dystrophies were based upon this gene [362-364]. In order to understand the phenotype associated with *LRAT* mutations, investigations into 4 families identified with variants in *LRAT* in this study were undertaken. 2 of the 4 families had been recruited to the childhood onset retinal dystrophy study by previous researchers, and two by ADB – one who was under MEH (Subject 27, cohort 1) and one who was recruited following mutation identification by the referring hospital (Subject 28, cohort 1). 3 probands were invited back to MEH and the IOO for detailed phenotypic studies. The results of the phenotypic studies and the molecular techniques utilised to ascertain the mutations in *LRAT* are described in this chapter. The results of these studies were also published [365]. In this chapter, Subject 1 refers to Subject 28 of cohort 1, Subjects 2 and 3 were recruited by previous researchers and so are not from cohort 1, and Subject 4 refers to Subject 27 of cohort 1.

4.6.1 Clinical History

The onset of visual symptoms in the four probands identified with mutations in *LRAT* was between 1 and 3 years of age (Table 18). All subjects had severe nyctalopia and visual field constriction from early childhood. A similar finding to subjects with

mutations in *RPE65* was of photophilia, which was present in 3 of the 4 *LRAT* subjects (Subjects 1, 3 and 4). Nystagmus was not reported in any subject, indicating that some visual function was preserved in infancy. Strabismus was present in 2 subjects (Subject 3 and Subject 4), with amblyopia affecting the left eye of Subject 3. The visual symptoms in all *LRAT* subjects were progressive, with deterioration of visual acuity, visual fields, nyctalopia and colour vision with age. Interestingly, 3 individuals (Subjects 1 to 3) subjectively reported deterioration of dark adaptation, specifically the time required to adapt from photopic to mesopic lighting conditions with age. General health was normal in all subjects except Subject 2 who had unilateral acquired conductive auditory dysfunction secondary to otosclerosis.

All affected subjects were simplex cases, with no other affected family members. Subject 1 (Family 1) was from a multiply consanguineous South East Asian family; his parents were first cousins. Subject 2 (Family 2) was British Caucasian whose parents were first cousins. Subject 3 (Family 3) was Scandinavian from a non-consanguineous family. Subject 4 (Family 4) was from the Caribbean, from a non-consanguineous family.

4.6.2 Clinical Examination

Two of four *LRAT* subjects were male. They were all examined in adulthood (Subject 1 – age 27 years; Subject 2 – age 54 years; Subject 3 – age 41 years; Subject 4 – age 31 years). Best corrected monocular visual acuity ranged from 0.22 LogMAR to hand movements (Table 18). Subject 3 had hand movements vision in the left eye, which was an amblyopic eye. There was no particular trend to the refractive errors: in the

right eye the spherical equivalent ranged from -1.00 DS to +3.63 DS and in the left eye it ranged from -1.00 DS to +3.33 DS. Colour vision was severely reduced in all subjects: none were able to identify any correct plates on Ishihara testing; low colour discrimination was recorded on the Farnsworth-Munsell 100 hue test in Subjects 1, 2 and 3; and Nagel anomaloscope matches suggested poor red – green colour discrimination in Subjects 1, 2 and 3.

Ocular motility examination identified torsional nystagmus in Subject 1; no other subjects had nystagmus. Subjects 3 and 4 had a left and right esotropia respectively. Anterior segments were normal in all subjects and mild nuclear sclerotic cataracts were evident in Subject 2 (unilateral, left eye) and Subject 4 (bilateral). All subjects had bilateral widespread RPE atrophy involving the macula, arteriolar attenuation and minimal retinal pigmentation, which was confined to the mid-peripheral retina (Figure 50, Figure 51, Figure 52 and Figure 53 - A). Subject 1 also displayed an annulus of retinal pallor extending to the vascular arcades within the macula (Figure 50). In Subject 3 the macula appeared relatively spared with hypopigmentation superior to the foveae. In Subject 4 there were bilateral epiretinal membranes. Asteroid hyalosis was evident in Subject 2 (bilateral) and Subject 3 (unilateral, right eye). A core vitrectomy had been performed in the left eye of Subject 2 with the aim of visual improvement from symptomatic asteroid hyalosis but there was no subsequent subjective or objective improvement in vision following this procedure.

4.6.3 Fundus Autofluorescence Imaging

Fundus autofluorescence imaging revealed a reduced autofluorescence signal in all subjects. It had been necessary to utilise a number of frames to obtain a mean image at the highest sensitivity of signal detection, which resulted in the optic nerve head and large retinal vessels appearing artefactually brighter than normal subjects. In those subjects in whom an autofluorescence signal was detected, there was a very small hypoautofluorescent signal at the foveolae (Figure 50 - B), poor autofluorescence at the macula (Figure 51, Figure 52 and Figure 53 – images B) and a diffuse annulus of hyperautofluorescence at the macula (Figure 52 - B).

4.6.4 OCT Imaging

sd-OCT imaging was performed in Subjects 1-3. The quality of the images acquired was affected by poor vision, which limited the subjects' ability to maintain central and steady fixation. The inner retinal layers appeared intact in these three subjects and the foveal thickness was relatively well preserved, although in the oldest subjects there was shallowing and broadening of the foveal depression (Figure 51 and Figure 52 – image C). The inner segment outer segment junction appeared to be preserved throughout the macula in the youngest subject, Subject 1, with preservation of the external limiting membrane and intact retinal lamination (Figure 50 - C). The outer retina was disrupted at the fovea in the two oldest subjects, Subjects 2 and 3, and there was no clear photoreceptor layer visible (Figure 51 and Figure 52 – images C). In these two subjects the outer nuclear layer was absent centrally but was preserved in the parafoveal region (Figure 50, Figure 51 and Figure 52 - images C, yellow arrows indicate the beginning of the ONL in left eyes). A faint line, presumed to represent the

external limiting membrane, was visible in these two subjects. In subjects 1-3 the nerve fibre layer was irregular but there was no evidence of vitreo-retinal traction. Subject 4 had undergone time-domain OCT imaging, which showed loss of the foveal inner segment outer segment junction, preserved retinal thickness and bilateral extra-foveal epi-retinal membranes with no loss of the foveal contour (Figure **53** - C).

Subject (Gender)	Family	Ethnicity	Consanguinity	Age at Onset (years)	Age at examination (years)	LogMAR VA RE, LE	Refraction
1 (M)	1	Indian	Consanguineous	3	27	0.22, 0.90	RE Plano LE Plano
2 (F)	2	British Caucasian	Consanguineous	1	54	0.66, HM	RE +0.75/+2.63, 162 LE +2.75/+1.13, 34
3 (M)	3	Swedish	Non-consanguineous	1	41	HM, 1.80	RE +4.25/-1.25, 22 LE +4.0/-1.75, 159
4 (F)	4	Caribbean	Non-consanguineous	2	31	0.80, 0.50	RE plano/-2.00, 20 LE -0.75/-0.50, 25

Table 18 - Demographic and clinical data of *LRAT* subjects. M – Male; F – Female; RE – right eye; LE – left eye; HM – hand movements vision.

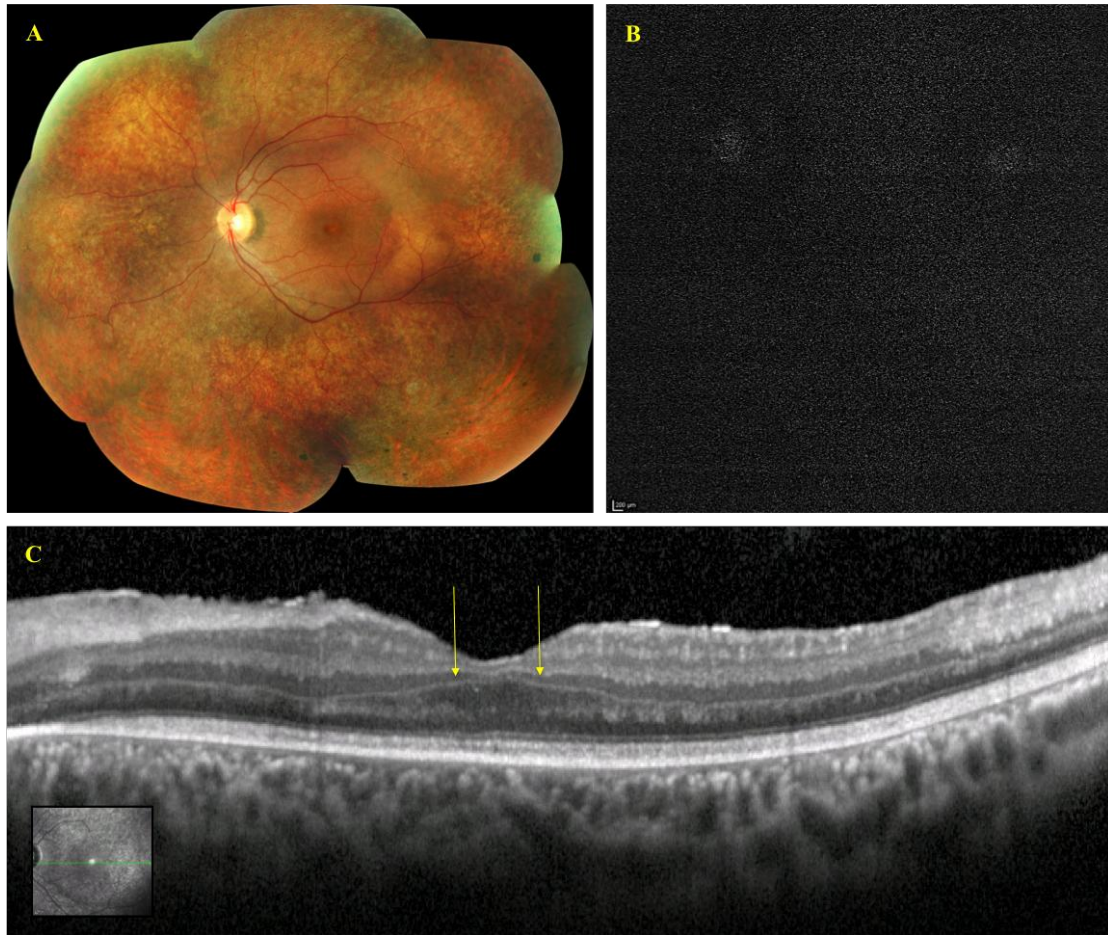


Figure 50 - Subject 1, *LRA*. A – Left eye fundus image displaying widespread RPE atrophy involving the macula but sparing the fovea, arteriolar attenuation and minimal retinal pigmentation. There is an annulus of retinal pallor extending to the temporal vascular arcade; B – left eye fundus autofluorescence image demonstrating a very weak hyperautofluorescent signal at the fovea; C – OCT image of the left macula demonstrating intact lamination and retention of a disrupted photoreceptor layer at the macula, and of the external limiting membrane. Arrows indicate the outer nuclear layer which appears preserved but severely diminished at the fovea. Images taken at age 27 years.

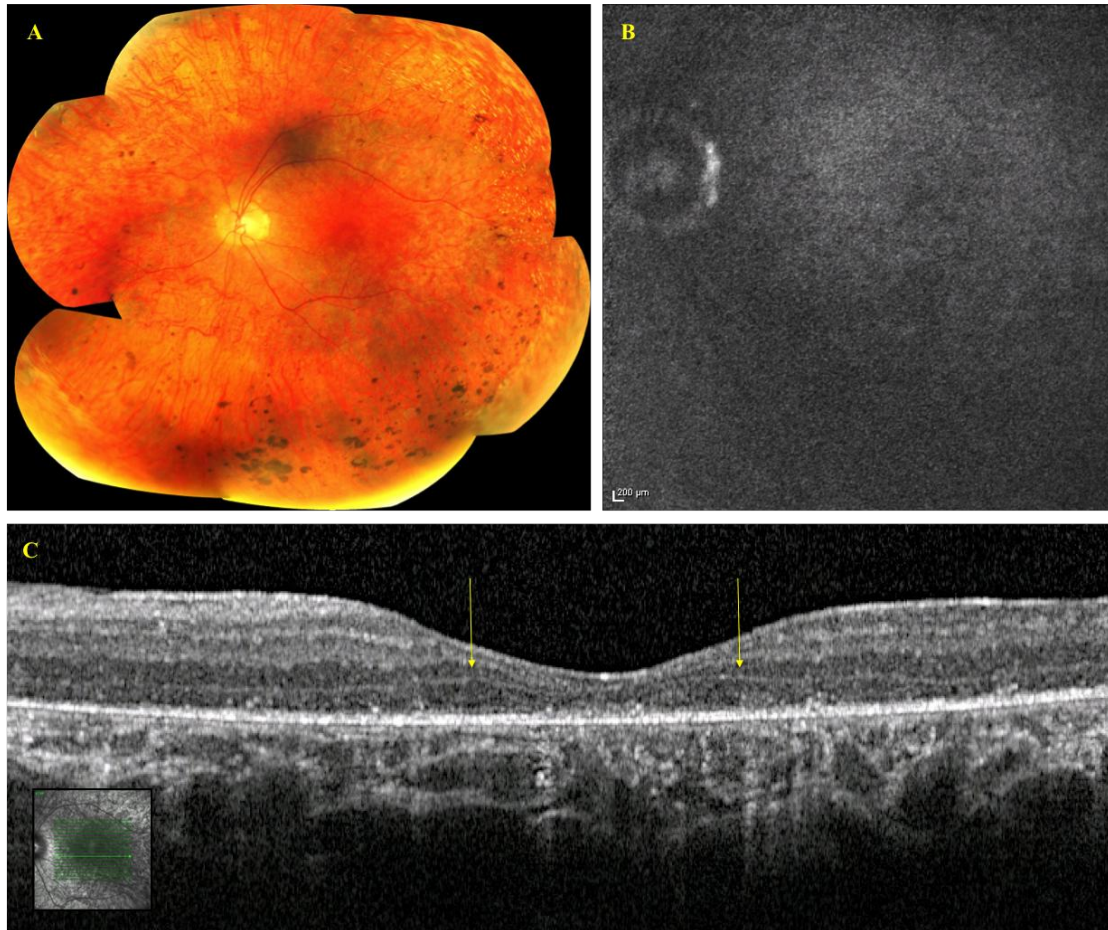


Figure 51 - Subject 2, *LRA*. A – Left eye fundus image displaying widespread RPE atrophy involving the macula, arteriolar attenuation and peripheral retinal pigmentation. A core vitrectomy has been performed and the vitreous base is visible in the inferior retinal periphery; B – left eye fundus autofluorescence image demonstrating a very weak autofluorescence signal at the fovea; C – OCT image of the left macula demonstrating preservation of the retinal lamination and external limiting membrane but severe disruption and loss of the photoreceptor layer. Arrows indicate the outer nuclear layer, which is lost at the fovea. The foveal contour is broad and shallow. Images taken at age 54 years.

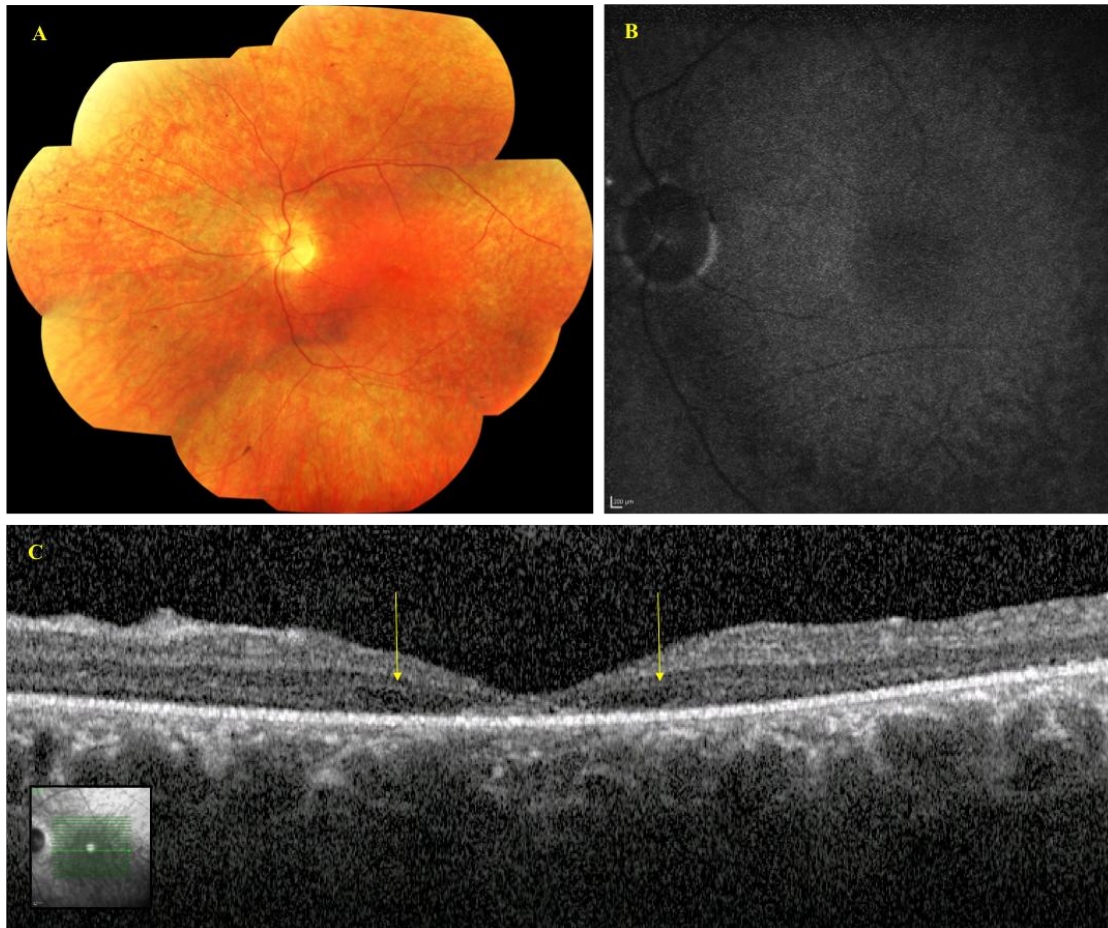


Figure 52 - Subject 3, *LRAT*. A – Left eye fundus image displaying widespread RPE atrophy involving the macula but sparing the fovea, arteriolar attenuation and minimal retinal pigmentation; B – left eye fundus autofluorescence image demonstrating a diffuse hyperautofluorescent signal at the macula; C – OCT image of the left macula demonstrating preservation of the retinal lamination and external limiting membrane, but severe disruption and loss of the photoreceptor layer. Arrows indicate the outer nuclear layer, which is lost at the fovea. The foveal contour is broad and shallow. Images taken at age 41 years.

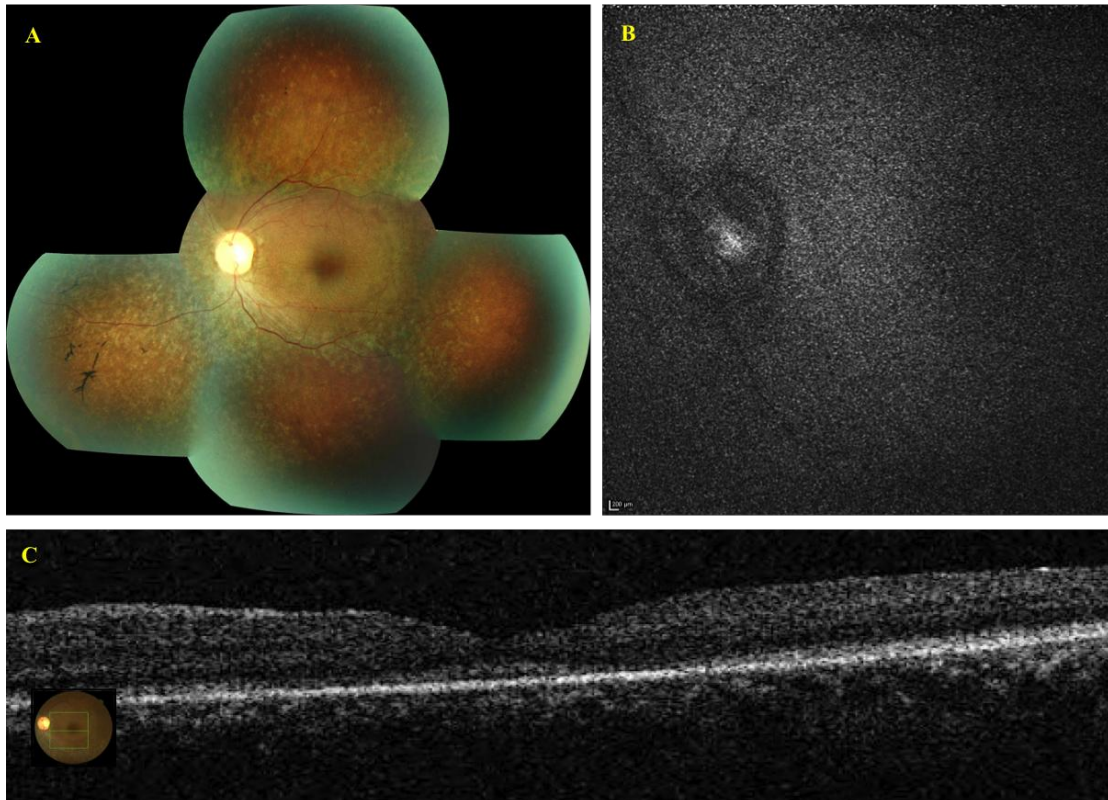


Figure 53 - Subject 4, *LRAT*. A – Left eye fundus image displaying widespread RPE atrophy sparing the macula, arteriolar attenuation and peripheral retinal pigmentation; B – left eye fundus autofluorescence image demonstrating a very weak autofluorescence signal at the fovea; C – OCT image of the left macula demonstrating preservation of the retinal lamination and photoreceptor layer at the fovea, and epiretinal membranes. Images taken at age 31 years.

4.6.5 Electrophysiological Testing

ISCEV standard electrophysiological studies were performed in subjects 1-3. The youngest subject, Subject 1, had residual PERGs detectable bilaterally, suggesting minimal residual macular function. PERGs were not detectable in Subjects 2 and 3. In all 3 subjects, the rod-mediated full field ERGs were undetectable following the standard period of 25 minutes of dark adaptation. Following overnight dark adaptation of the left eye in Subject 3, no discernable inter-ocular asymmetry was demonstrated in the full field ERG responses, indicating no recovery of rod function after prolonged

dark adaptation. Light adapted cone-mediated ERGs were not detectable in Subject 1, however in Subjects 2 and 3 they were present but delayed and small.

4.6.6 Psychophysical Testing

4.6.6.1 Goldmann Visual Fields

Goldmann perimetry was performed in subjects 1-3 but the only reliable responses were to the V4e target (Figure 54). Perimetry was difficult and time consuming due to variable abilities to maintain central and steady fixation. Circumferentially constricted visual fields were present in 2 subjects to between 15° and 40° of central fixation (Subjects 1 and 2). Subject 3 had inconsistent responses within the visual field. As has been previously described in individuals with RP, in addition to circumferential constriction of the visual field, there may be residual ‘islands’ of retained vision within apparent ‘non seeing’ areas that can be difficult to plot consistently [57]. All three subjects demonstrated this. In Subject 1 the central 30° was retained with additional far peripheral crescents of vision in the infero-temporal quadrants measuring 10° (Figure 54 – A and B). Subject 2 had retention of the central 15° and 40° in the left and right eyes respectively, with additional 20° crescents in the inferior and temporal quadrants (Figure 54 – C and D). The visual field was difficult to plot in Subject 3 and appeared to demonstrate retained fields to 50-55° nasally and 80-90° temporally. Although he had small additional islands of visual loss within this area, these were not consistently recordable and so are not included in the plots (Figure 54 – E and F).

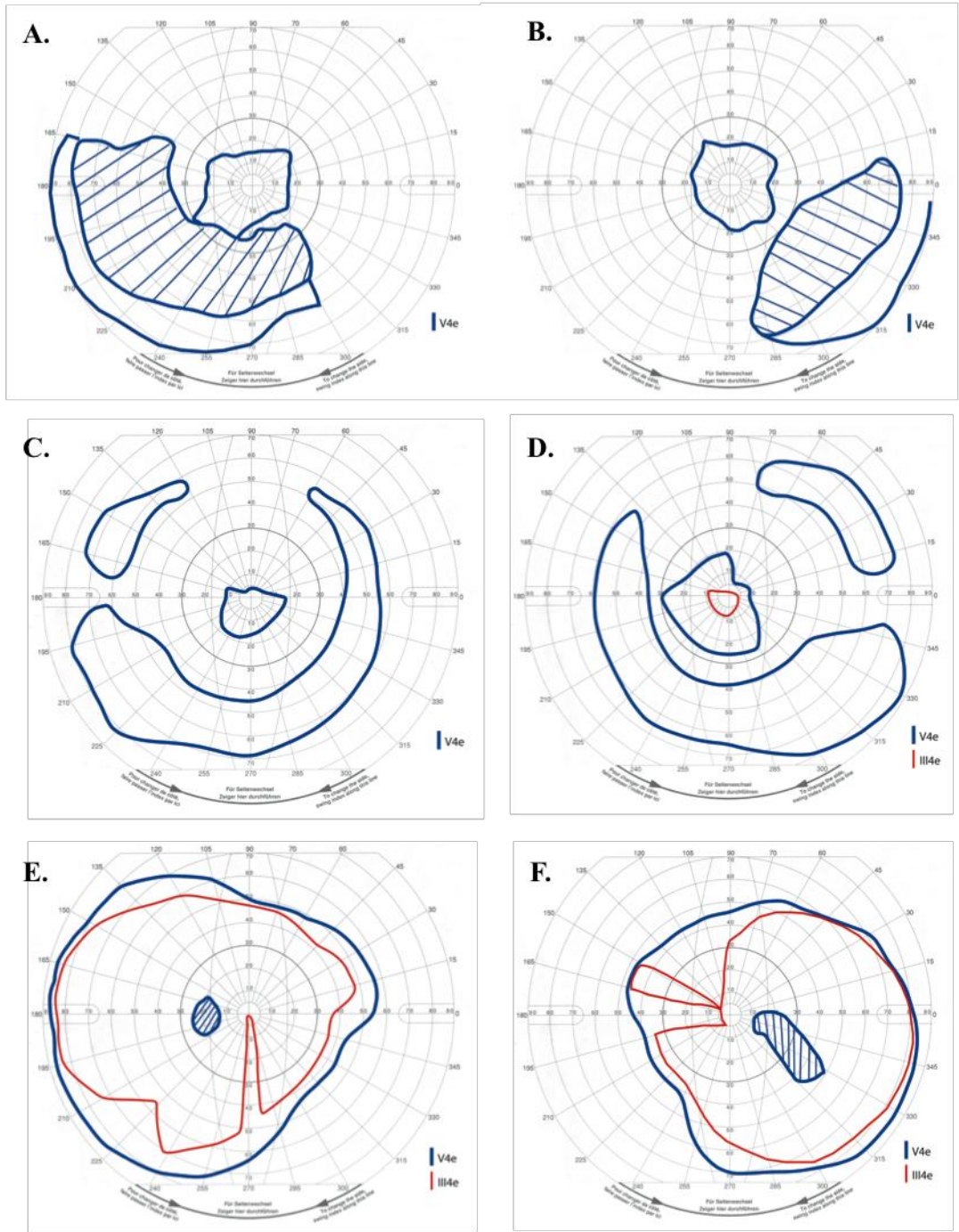


Figure 54 – Goldmann Visual Field plots, *LRAT* subjects. A – Left eye, Subject 1 and B – Right eye Subject 1, demonstrating retention of the central 15° with additional peripheral crescents in the visual fields of both eyes to the V4e target; C – Left eye, Subject 2 and D – Right eye, Subject 3, demonstrating retention of the central 15° in the visual field of the left eye and central 40° in the visual field of the right eye to the V4e target; E – Left eye, Subject 3 and F – Right eye, Subject 3, demonstrating retained visual fields across the central 120° to the V4e target, although islands of visual loss within these fields are not plotted as they were inconsistent. V4e target – blue line; III4e target - red line; hashed areas correspond to islands of reduced vision.

4.6.6.2 *Dark Adapted Perimetry*

Photopic and dark adapted static threshold perimetry was performed by Professor Fitzke's laboratory at UCL in Subjects 1-3 using a modified Humphrey visual field analyser (Allergan Humphrey, Hertford, UK). Dark adapted perimetry was performed following pupillary dilatation using guttae tropicamide 1% and guttae phenylephrine 2.5% in each eye and following 45 minutes of dark adaptation. The Humphrey visual field analyser had been modified for dark adapted conditions as previously described [366, 367] and controlled by a customised computer programme (PS/2 model 50; International Business Machines, Armonk, New York, USA) [368]. Testing was performed in the light adapted state with a white light stimulus and, after dark adaptation, with red (608 nm) and blue stimuli (506 nm). The blue stimulus reflects rod function and red stimulus reflects cone function.

In subjects 1-3 photopic static threshold perimetry demonstrated severely elevated thresholds of 10 to 30 decibels (dB) across the central 30° (Figure 55 - A shows an example in Subject 3). There was severe loss of sensitivity of 30 dB to 40 dB in all subjects with dark adapted perimetry. In subject 1 there were no recordable responses to scotopic red and blue stimuli in the dark adapted state, indicating absent rod function. Subjects 2 and 3 showed measurable responses in only a few locations in the central 9° of fixation, to scotopic red and blue stimuli, indicating severe loss of rod function (Figure 55 – B and C show an example in Subject 3). It is likely that the sensitivities in these locations are mediated by dark adapted cones, which themselves have reduced sensitivity. This is consistent with the findings of abnormal cone function from the critical flicker fusion measurements performed in Professor Stockman's laboratory (see section 4.5.6.4).

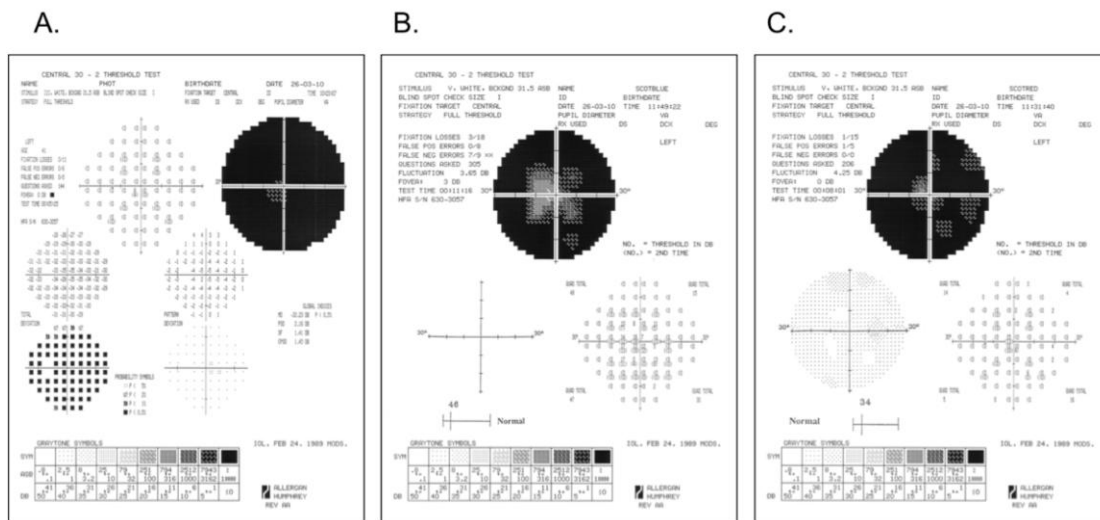


Figure 55 - Full static threshold central 30° photopic and dark adapted perimetry, LRAT Subject 3. A – photopic static threshold perimetry; B – dark adapted static threshold perimetry, blue stimulus; C – dark adapted static threshold perimetry, red stimulus. Severe threshold elevations are evident throughout with generally some central function, but elevated by 20–30 dB even at the most sensitive locations.

4.6.6.3 Dark adapted spectral sensitivities

The dark adapted spectral sensitivities were measured in Subjects 1-3 by Dr Ripamonti in the laboratory of Professor Stockman at UCL. The methods have previously been described [369]. Subjects were dark adapted for 40 minutes prior to measurements being taken. The target stimulus was 3.5° in visual diameter, presented at 10° in the superior retina and sinusoidally flickered at 1 Hz. Target wavelengths of 400, 500, 550, 600 and 650 nm were used to make the measurements. The observer adjusted the radiance of the target at each wavelength, until the flicker at 1 Hz was just at threshold.

Evidence of rod function was present in Subjects 2 (green diamonds) and 3 (yellow circles), as demonstrated by the dark adapted spectral sensitivity data, which followed

the shape of rod, or scotopic, luminosity function (black lines) (Figure 56). However in both subjects the rod sensitivity was reduced compared to normal subjects (red squares). The data for Subject 1 (blue circles) were more consistent in shape with cone, or photopic, luminosity function (dashed red line). They were also reduced in sensitivity, which suggested that this Subject had little or no rod function. Compared to normal subjects, there was a reduction of cone sensitivity by approximately 3 log units, which was consistent with the cone critical flicker fusion loss in this subject.

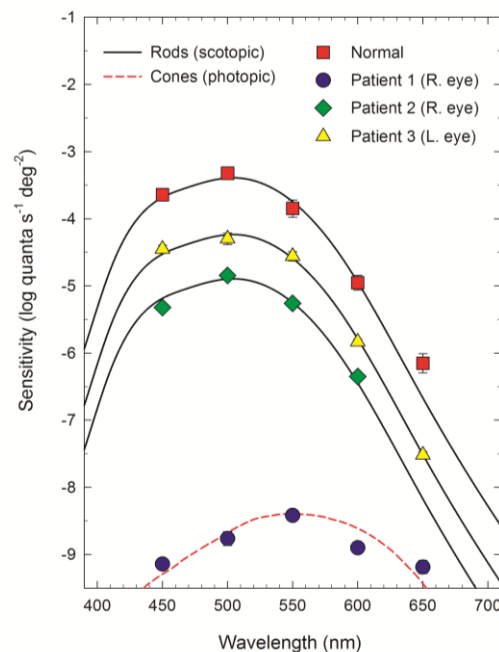


Figure 56 - Dark adapted spectral sensitivities, *LRAT* subjects. Blue circles - Subject 1; Green diamonds – Subject 2; Yellow triangles – Subject 3; Red squares – normative data. The curves are standard spectral sensitivity functions vertically shifted to least squares fit each data set. The continuous black lines are shifted versions of the rod or scotopic $V^0(k)$ luminosity function, and the red dashed line is a shifted version of the cone or photopic $V(k)$ luminosity function adopted by the Commission Internationale de l'éclairage (CIE) [370]. Agreement with $V^0(k)$ indicates rod function in Subjects 2 and 3, but agreement with $V(k)$ suggests mainly cone function and no rod function in Subject 1.

4.6.6.4 *Critical Flicker Fusion*

Defects in light adaptation caused by variants in visual cycle or phototransduction genes can be characterised by measuring the changes in temporal sensitivity that accompany changes in light levels. This can be undertaken by measuring changes in temporal acuity or resolution (also known as the critical flicker frequency, c.f.f.) as a function of light level [371]. These tests were performed in Subjects 1-3 by Professor Stockman's laboratory at UCL.

A Maxwellian-view optical system with a 2-mm entrance pupil illuminated by a 900 W xenon arc lamp was used for the c.f.f. measurements. Wavelengths were selected with interference filters with full-width at half-maximum bandwidths of between 7 nm and 11 nm (Ealing or Oriel). Other details were the same as the spectral sensitivity measurements. Fixation was central. A flickering target of 4° in diameter and 650 nm in wavelength was presented in the centre of a 9° diameter background field of 481 nm in order to measure L-cone c.f.f. This background served to suppress the rods, but also selectively desensitised the M-cones at lower target radiances. The 650 nm target was chosen to favour flicker detection mainly by L-cones over most of the intensity range. It was varied in intensity from 6.5 to 11.0 \log_{10} quanta s^{-1} deg^{-1} (-0.63 – 3.87 \log_{10} photopic trolands). At higher target intensities M-cones are also likely to contribute to flicker detection. At each target intensity the subject adjusted the flicker frequency to identify the frequency at which the flicker just disappeared (the c.f.f.). S-cone c.f.f. measurements were made by presenting a flickering target of 4° diameter and 440 nm wavelength in the centre of a 9° diameter field of background 620 nm, which selectively desensitises the M- and L-cones with comparatively little effect on the S-cones. In normal subjects a 620 nm field of 11.51 \log_{10} quanta s^{-1} deg^{-1} isolates

the S-cone response up to a target radiance of approximately $10.5 \log_{10} \text{ quanta s}^{-1} \text{ deg}^{-1}$ [372].

All 3 subjects had substantially reduced L-cone c.f.f. measurements compared to normal subjects (red squares) (Figure 57). Subject 2 (green diamonds) showed the best temporal resolution, which suggested reduced but moderately good L-cone function. Subjects 1 (blue circles) and 3 (yellow triangles) had devastating loss of temporal resolution compared with normal subjects. For these two subjects, flicker is seen clearly first at target radiances above $9.0 \log_{10} \text{ quanta s}^{-1} \text{ deg}^{-1}$, which is approximately 250 times higher than normal subjects. However, resolution reached to less than 20 Hz even at the highest radiances, suggesting severely reduced L-cone function. No measurable S-cone function was detected in any of these three subjects by S-cone c.f.f. measurements.

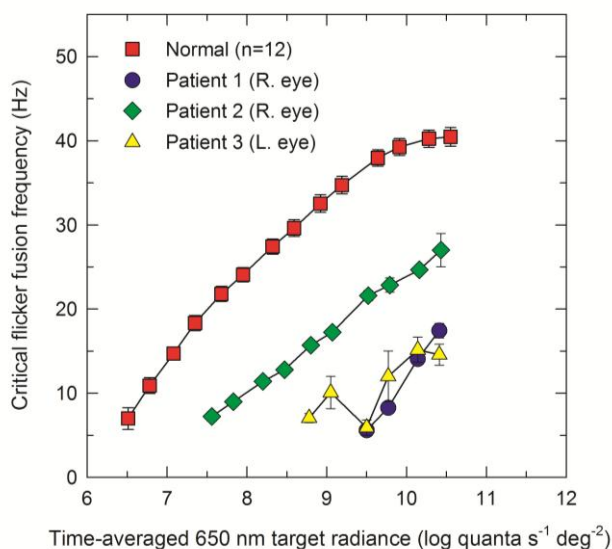


Figure 57 - Critical flicker fusion frequencies in *LRAT* subjects. Blue circles - Subject 1; Green diamonds – Subject 2; Yellow triangles – Subject 3; Red squares – mean data for 12 normal observers. Subjects 1 and 3 show a substantial loss of cone temporal sensitivity, while Subject 2 shows more moderate loss.

4.6.7 Molecular analysis

The molecular techniques used to identify *LRAT* mutations in these 4 subjects varied.

All direct sequencing was performed by Dr Ocaka, UCL.

Subject 1 (Subject 28, cohort 1), referred by colleagues at the University of Manchester, had undergone screening using the LCA chip, which identified the previously reported *LRAT* missense variant c.525T>A, p.Ser175Arg, in exon 2, in the homozygous state [285]. The variant was confirmed by direct sequencing and was identified to segregate with the disease in the family, as his unaffected parents were both heterozygous for this variant.

The mutations in subjects 2-4 were identified by direct sequencing of *LRAT* in a panel of LCA and EORD patients that had previously been screened using the LCA chip, without any variants being identified (Table 19). Subject 2 was identified to harbour the novel 2- base pair deletion/insertion, c.40-41delGAinsTT, p.Glu14Leu. Both unaffected parents were heterozygous for this variant, confirming segregation of the disease in this family. Subject 3 harboured the novel variant c.181T>A, p.Tyr61Asp, in the homozygous state. His unaffected father was heterozygous for this variant; his mother was not available for testing. Subject 4 had previously undergone screening of *RPE65* as she had some phenotypic similarities to individuals with mutations in this gene; this screening did not identify any pathogenic variants. She was subsequently identified to harbour the novel *LRAT* variant c.316G>A, p.Ala106Thr, in the homozygous state. No family members were available to check segregation of this mutation.

Subject	Family	Mutation 1	Mutation 2	Reference
1	1	c.525T>A, p.Ser175Arg	c.525T>A, p.Ser175Arg	[285]
2	2	c.40-41delGAinsTT, p.Glu14Leu	c.40-41delGAinsTT, p.Glu14Leu	Novel to this study
3	3	c.181T>A, p.Tyr61Asp	c.181T>A, p.Tyr61Asp	Novel to this study
4	4	c.316G>A, p.Ala106Thr	c.316G>A, p.Ala106Thr	Novel to this study

Table 19 – Mutations identified in *LRAT* in this study. All are homozygous.

All four variants were not identified in 96 ECACC control DNAs or any other probands in the panel of 148 LCA and EORD patients. All four mutations were analysed using the *in silico* analysis programmes SIFT and PolyPhen2. SIFT predicted all four mutations to be damaging, with a probability score of 0 for each mutation (probability scores less than 0.05 are predicted to be deleterious) and a median range between 2.51 and 3.00 (this is used to measure the diversity of the sequences used for prediction; this value ranges between 0 and 4.32 and should ideally be between 2.75 and 3.5). PolyPhen2 predicted all four mutations to be probably damaging (c.525T>A, c.40-41delGAinsTT and c.316G>A in subjects 1, 2 and 4 respectively) or possibly damaging (c.181T>A in subject 3), with scores ranging between 0.95 and 1.00.

4.6.8 Discussion

Mutations in *LRAT* lead to a severe EORD phenotype that consists of poor vision, nyctalopia and visual field constriction from early childhood; photophilia is a consistently described feature. With time, visual acuity, contrast sensitivity and colour discrimination deteriorate. Electrophysiological data support the clinical findings and

are in keeping with severe generalised photoreceptor dysfunction affecting rods more severely than cones. At the time that this study was conducted there had only been a handful of reports describing the phenotype associated with mutations in *LRAT*, in which in the majority of subjects, poor vision, nyctalopia and nystagmus commenced in childhood, the retinal dystrophy was severe with an undetectable ERG, and the diagnoses carried were of LCA or juvenile RP [26, 285, 290, 291]. Photophobia had been reported in a number of cases [26, 290]. In these studies, visual acuity ranged from 0.6 LogMAR (age 6 years) to hand motion vision (age 23 years), with a predominantly hypermetropic refractive error. The retinal appearances have been reported to be normal in infancy [291], and in adult life to consist of peripheral RPE atrophy, optic disc pallor and ‘perimacular retinal surface wrinkling’. In the present study, and in agreement with these other studies, RPE atrophy was widespread but there was little retinal pigmentation until later age, suggesting that photoreceptor cell death occurs late in *LRAT* mutations [373]. Epi-retinal membranes were present in 25% of eyes in this study, which is more common than the 1.2% reported prevalence of epi-retinal membranes in RP [374]. In addition, asteroid hyalosis was more common in *LRAT* retinopathy, with 37.5% of eyes in this study affected, compared to only 3.1% in RP in general [375].

Detailed retinal imaging in humans with *LRAT* mutations had not been previously reported. Although the ability to acquire clear sd-OCT images in the subjects in this study was affected by instability of fixation, reasonable images were obtained. In the youngest subject (age 27 years) there was retention of the external limiting membrane, the outer nuclear layer was visible throughout the macula but markedly diminished in the very centre of the fovea and photoreceptor inner segment outer

segment layer was present at the fovea. In the oldest subjects (age 41 and 54 years) there was disruption of the outer retina and loss of the outer nuclear layer at the fovea, with possible retention of this layer in the extra-foveal region. There was no photoreceptor layer discernable in these two subjects, but there was a faint line corresponding to the external limiting membrane. An irregular nerve fibre layer, with no overlying vitreo-macular traction, was observed in all three subjects, which may correspond to early retinal fibrosis. This has not been reported in OCT imaging of *Lrat*^{-/-} mice, however loss of the external limiting membrane and diminution of the outer nuclear layer has been observed in these and in *Rpe65*^{-/-} mice who were treated with control compounds ('vehicle' and all-*trans*-retinyl acetate) in a study evaluating the effects of prodrugs that generate 9-*cis*-retinal in vivo [376]. A reduced autofluorescence signal was obtained in all *LRAT* subjects, in keeping with the reduced autofluorescence signal seen in mutations in genes encoding other visual cycle enzymes [158, 377, 378]. *Lrat*^{-/-} and *Rpe65*^{-/-} mice have also been identified by scanning laser ophthalmoscopy to have little to no autofluorescence, and reduced retinal fluorophore production has also been identified in humans with *RPE65* mutations, however autofluorescence in humans with *LRAT* mutations has not been reported [158, 379, 380].

The *LRAT* subjects in this study displayed severe photopic kinetic visual field constriction with preserved islands of vision in the mid- and far retinal periphery, and elevated thresholds measured by static perimetry, but they were able to maintain useful navigational vision that was subjectively reported to be better in daylight or ambient lighting conditions. Dark-adapted spectral sensitivity measurements demonstrated reduced to undetectable rod function, and perimetric and critical flicker

fusion measurements demonstrated severely reduced, but persistent, cone function in *LRAT* mutations. Similar psychophysical analysis using full field stimulus testing of subjects with *RPE65* related LCA has been undertaken [381]. This identified more than half of the subjects tested to have rod mediation of a blue stimulus, indicating that there is severely reduced but detectable residual rod function in these subjects. The remaining subjects had only residual cone mediated vision. The authors suggested that psychophysical methods are able to detect both rod and cone mediated vision in these patients. In the present study we were able to identify areas of retina with residual but abnormal rod function. In other areas cones were mediating responses at threshold.

Phenotypic variability has been reported in disease associated with mutations in visual cycle genes, in particular *RPE65* [14, 15, 161]. Recently two families have been reported with the same homozygous frame-shifting mutation in *LRAT*, c.12delC, p.M5CfsX53, with a phenotype suggestive of retinitis punctata albescens, a slowly progressive retinal dystrophy characterised by nyctalopia, tiny yellow-white dots throughout the retina, and mutations in *RLBP1* [45]. As with the mutations identified in the present study, this frame shifting mutation occurs in exon 2, but why it leads to a very different phenotype remains unknown. It may be that these white dots are present transiently in the disease process and may be replaced by photoreceptor degeneration and loss, and thus not be detected if the patient is not examined in time [382]. All but one *LRAT* mutation identified to date reside in exon 2 [26, 45, 285, 290, 291, 365], suggesting that this exon may be targeted in the screening of this gene in LCA and EORD.

The N1pC/P60 proteins, of which LRAT is one, are cell-wall peptidases, with 3 conserved residues: a cysteine, a histidine and a polar residue [383]. As it had not been possible to extract and purify full length LRAT, a recombinant truncated form of LRAT, t-LRAT, has been expressed in bacteria and purified fully, and has been demonstrated to be catalytically active despite it not containing the N- and C- terminal hydrophobic segments [384]. The triad of the LRAT-family specific conserved residues, cysteine-161, tyrosine-154 and histidine-60, have been identified in this truncated protein, and the tyrosine-154 residue has been identified to be essential for catalytic activity [385]. It is possible that the novel p.Tyr61Asp mutation identified in the present study interferes with the conserved histidine-60 residue and affects the catalytic activity of this enzyme. The p.Ser175Arg mutation was originally identified by Thompson *et al.*, and it was postulated to cause disease by the loss of an essential nucleophilic residue at the catalytically active site of the enzyme [285]. However, the effect of this mutation on the function of t-LRAT was recently studied, and although no enzymatic activity was found with this mutant, the global tertiary structure of t-LRAT and its membrane binding properties remained unchanged with this mutation [386]. It was suggested instead that as the serine-175 residue lies close to the catalytically active site of LRAT, this mutation, resulting in the insertion of an arginine residue, could obstruct the entrance of the substrate at this site, leading to loss of catalytic activity.

The retinal dysfunction in *Lrat*^{-/-} and *Rpe65*^{-/-} murine models is similar, with slow rod degeneration, rapid cone degeneration and mislocalisation of cone opsins [288, 289, 380, 387, 388]. Hypomorphic allele function has been hypothesised to be the reason for the continued isomerisation activity in some *Rpe65* mutant models and in the

milder phenotypes that have been observed in humans [147, 161]. The alternative visual pathway involving Müller cells and cone regeneration may be another reason for the less severe phenotypes in visual cycle related mutations [139].

Lrat^{-/-} murine models have led to the identification of two therapeutic interventions that restore retinal function: oral pharmacologic treatments with novel retinoid compounds such as 9-*cis*-retinyl acetate and 9-*cis*-retinyl succinate, and intraocular gene therapy [389]. Both of these treatments have resulted in improvements in electrophysiological and pupillary responses, and to the levels of visual pigment observed in these mice.

The pharmacologic agent QLT091001, manufactured by QLT, Inc. (Vancouver, Canada), contains 9-*cis*-retinyl acetate, a prodrug that generates 9-*cis*-retinal in vivo [390], which has been shown to be safe in mice [376] and humans [391]. In *Lrat*^{-/-} and *Rpe65*^{-/-} mice administered with prolonged high dose oral QLT091001, retinal thickness and morphology were well maintained, no significant increases in autofluorescence suggestive of toxic retinoid by-products were seen, and scotopic ERG responses were improved compared to wild-type mice who were also treated with QLT091001 [376]. Results of the first human oral retinoid trial in patients with *RPE65* and *LRAT* mutations were published very recently [392]. In this trial, patients received an oral dose of QLT091001 once daily for 7 days. They were examined at baseline and followed up over a period of at least 2 months. 10 of 14 patients (71%) were reported to have at least 20% improvement in visual field areas, 6 of 14 patients (43%) had an improvement in visual acuity of at least 5 letters. No improvements in ERG or colour vision were reported and the majority of patients returned to baseline

by 2 years. Side effects included headache and photophobia. However, the inter-test variability, test-retest variability, wide range of visual field results at baseline due to young participant age (64% of patients were under 16 years old) and lack of ERG evidence to support the reported large increases in visual field areas in response to treatment, mean that the reported improvements following this treatment should be taken with caution [58]. Although these results are promising, further more robust studies are required.

Advances have been made in the field of retinal gene therapy, with the first human trials of *RPE65* gene replacement therapy and *CHM* gene therapy for choroideraemia being reported recently [362, 363, 393, 394]. Studies into differentiated RPE cells obtained from human induced pluripotent stem cells have identified the expression of functional visual cycle enzymes, and transplantation of mouse primary RPE cells into *Lrat*^{-/-} and *Rpe65*^{-/-} mice has resulted in recovery of the visual function, including improvement of visual acuity, improvements in the ERG and endogenous 11-*cis*-retinal production [395]. These results are promising and human trials into RPE stem cell therapy for Stargardt disease and age related macular degeneration have begun, with the results of safety studies recently published [396, 397].

This detailed phenotypic study into families with mutations in *LRAT* has demonstrated residual photoreceptor function in adulthood despite there being significant visual dysfunction from early childhood. This suggests that there may be a window of opportunity for a variety of therapeutic interventions that can extend into late childhood.

4.7 *RGR* Phenotype

The proband of one family was referred for enrolment into the Childhood Onset Retinal Dystrophy Study. He had been diagnosed with EORD in Italy and his DNA had been sent for screening using the LCA chip by his referring team. He was identified to harbour a homozygous mutation in *RGR*, as follows: c.196A>C, p.Ser66Arg [319]. As there had been little description of the phenotype associated with mutations in *RGR*, the family was invited to participate in the Study and the proband was extensively phenotyped, along with other family members, at Moorfields Eye Hospital (MEH) and at the Institute of Ophthalmology (IOO).

4.7.1 Clinical History

The male proband (Subject 47, Family 45 of Cohort 1) was aged 16 years and 7 months when he attended for phenotypic studies. He had been diagnosed with an EORD at age 13 years following electrophysiological testing in Italy. The family is originally from Albania and moved to Italy when the proband was 8 years old. He had been noted by his parents to have reduced vision from birth, with nystagmus and a convergent squint from 5 months of age. As a toddler he was noted to be clumsy and to frequently bump into objects. At age 2 years he was prescribed glasses and commenced amblyopia therapy in Albania. A visiting ophthalmologist from Russia diagnosed strabismus and ‘a retinal abnormality’ and subsequently performed unilateral strabismus surgery in Russia when the proband was 5 years old. This improved his ocular alignment and nystagmus, but his symptoms of poor vision and

nyctalopia persisted. At age 11 years he noticed significant constriction of his visual fields and had difficulty seeing moving objects. He had mild photophobia but no photophilia.

His general health was good aside from having renal calculi removed at age 2 years. He was born at full term and there had been no problems in pregnancy. There were no other affected family members and his younger male sibling and parents denied any ocular abnormalities. There is no history of consanguinity in his family.

4.7.2 Clinical Examination

Best corrected visual acuity at age 16 years was 0.48 LogMAR in the right eye, with no improvement with pinhole, and 0.30 LogMAR in the left eye, improving to 0.18 LogMAR with pinhole. Refractive error was right eye +1.00/+2.25, 90° (spherical equivalent +2.75D) and left eye +0.75/+1.75, 100° (spherical equivalent +1.3D). The right eye is likely to be amblyopic. He failed the screening tests on HRR colour vision testing. Pupil examination was normal. He had a mild roving nystagmus and right esotropia.

Slit lamp biomicroscopy identified normal anterior segments and clear lenses. Funduscopy demonstrated bilateral symmetrical widespread RPE atrophy with peripheral retinal white dots, bilateral macular atrophic changes, vascular attenuation and minimal retinal pigmentation (Figure 58 - A and B).

Visual acuity in his brother and parents was normal (-0.10 LogMAR in each eye), as were their retinal examinations. Blood samples were obtained from the proband, his brother and parents for molecular analysis.

4.7.3 Fundus Autofluorescence Imaging

Fundus autofluorescence imaging in both eyes demonstrated a ring of diffuse hyperautofluorescence in the macula centred on the fovea, which itself had a normal autofluorescent signal (Figure 58 - C and D).

4.7.4 OCT Imaging

sd-OCT imaging identified relative preservation of the inner retinal layers and the foveal contour. There was loss of the inner segment outer segment layer throughout the macula except for a small area at the fovea, which may represent preserved photoreceptors in this region. (Figure 58 - E and F, arrows demarcate the preserved photoreceptor inner segment outer segment layer at the fovea in right and left eye).

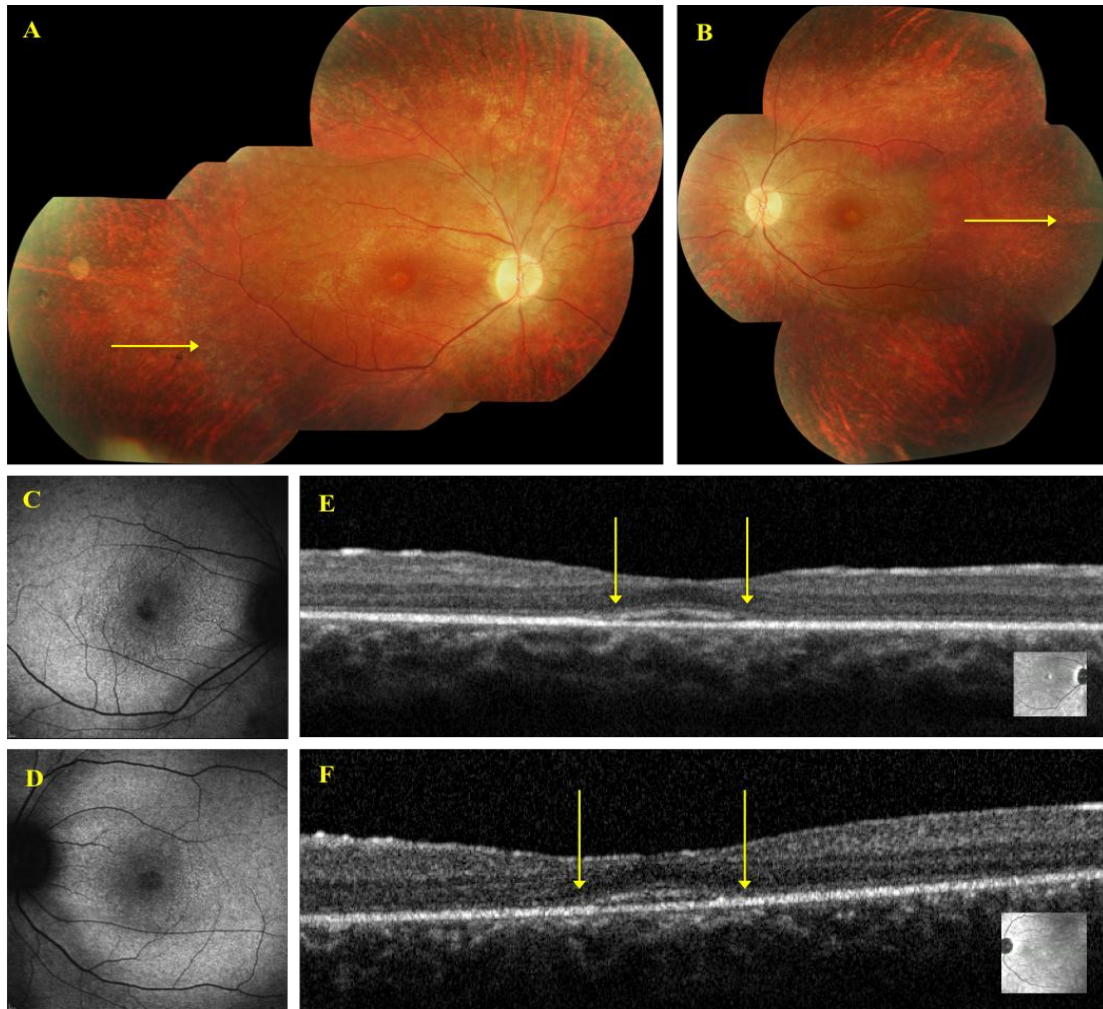


Figure 58 - Retinal imaging of Subject 47, *RGR* with EORD. A - Right eye fundus; B - Left eye fundus, both retinas have widespread RPE atrophy, peripheral retinal white dots (arrows), minimal retinal pigmentation, bilateral macular atrophy and arteriolar attenuation; C - Right eye sd-OCT image; D. Left eye sd-OCT image; OCT images demonstrate intact retinal lamination, the arrows demarcate the preserved photoreceptor inner segment outer segment layer at the fovea; E - Right eye fundus autofluorescence image; F - Left eye fundus autofluorescence image. Autofluorescence images demonstrate a diffuse area of hyperautofluorescence at the macula in each eye.

4.7.5 Psychophysical Testing – Goldmann Visual Fields

Goldmann visual fields, performed in the proband, were only reliably performed to the V4e and III4e targets in each eye. To the III4e target his visual fields were constricted to the central 20° although there were additional nasal and peripheral

islands of vision present. To the V4e target there was constriction of the superior visual field to between 35° to 10°, but the nasal and temporal fields were maintained to 60° and 80° respectively. However, there was a mid-peripheral ring scotoma bilaterally between 10° to 30° from fixation in the right eye and between 10° to 20° from fixation in the left eye to the V4e target (Figure 59).

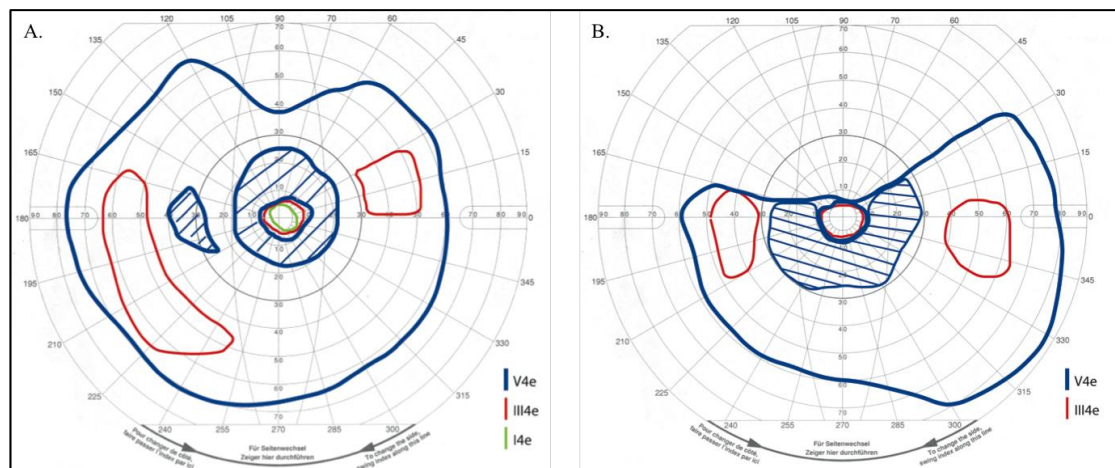


Figure 59 - Goldmann visual fields, Subject 47, RGR. A. Right eye; B. Left eye; V4e blue line, III4e stimulus – red line.

4.7.6 Electrophysiological Testing

ISCEV standard electrophysiological studies in the proband carried out at MEH demonstrated undetectable full field ERGs, in keeping with severe loss of generalised rod and cone function at the level of the photoreceptor. PERGs were poor and demonstrated residual function in both eyes, in keeping with bilateral macular dysfunction.

4.7.7 Molecular analysis

DNA was obtained for molecular analysis from blood samples provided by the proband, his unaffected brother and unaffected parents. All subjects underwent direct Sanger sequencing of exon 2 of *RGR* (by ADB). The primer sequences and PCR conditions are listed in the Appendix (Appendix 7.2.2). The pathogenic variant that had been identified by the LCA Chip analysis was confirmed in the proband in the homozygous state as: c.196A>C, p.Ser66Arg. This variant has been previously reported in a family with RP [319]. Sequencing of the DNA in family members identified that this variant was present in the heterozygous state in each parent and that the unaffected brother was a wild type homozygote, confirming segregation of this variant with the disease in this family (Figure 60). In *silico* analysis using SIFT predicts this mutation to be damaging (SIFT Score 0.04) and using PolyPhen2 to be probably damaging (Score 0.984, Sensitivity 0.74, Specificity 0.96). The variant was not identified in the exon variant server or in the 1000 genomes project.

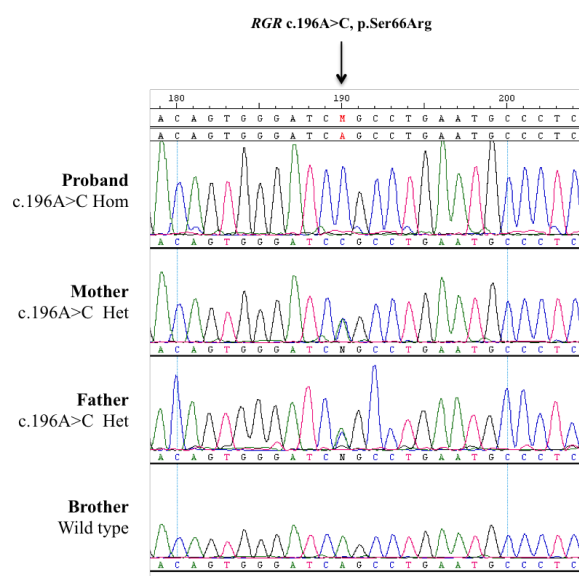


Figure 60 - *RGR* sequencing in Family 45. Proband: c.196A>C, p.Ser66Arg homozygous; unaffected parents are heterozygous (Het) carriers of the change and unaffected brother has the wild type alleles (WT).

4.7.8 Discussion

Mutations in *RGR* are rare. Only two families have previously been reported with biallelic mutations in *RGR* and both had homozygous c.196A>C, p.Ser66Arg variants [292, 319]. Screening of *RGR* in panels of 331 and 91 RP subjects, respectively, identified no other pathogenic variants [320, 321]. The retinal phenotype in the original *RGR* family was of diffuse depigmentation of the RPE involving the macula, pigmentation in the retinal periphery and vascular attenuation. The subjects were examined in their 4th and 5th decades and had a visual acuity of 1.00 LogMAR or worse, severely constricted visual fields and widespread loss of photoreceptor function on electrophysiological testing. The individual described by Collin *et al.* had ARRP, diagnosed at age 6 years. He was Serbian in origin and in the 4th decade had perception of light vision, RPE atrophy involving the macula, peripheral retinal paving stone-like retinal changes, vascular attenuation and pale optic discs. In comparison to these two families, the subject described in the present study, who had symptom onset from the first few months of age, was examined in his second decade and had better preservation of his central vision, although he had severe constriction of his visual fields and severe generalised photoreceptor dysfunction on electrophysiological testing. The retina had widespread RPE atrophy with white dots in the periphery, atrophy at the macula involving the fovea and vascular attenuation. There was minimal peripheral pigmentation visible in one eye. His OCT demonstrated preservation of the photoreceptor layer at the fovea, but loss of this layer from the parafovea and remaining macula, and this could be correlated with the FAF images which showed an annulus of hypoautofluorescence corresponding to the loss of photoreceptors on OCT, as seen in subjects with RP [344].

RGR, retinal G protein-coupled receptor, is an intracellular membrane bound protein located in the RPE and Müller cells, that plays a role in the visual cycle [315]. However, the specific role of RGR in the visual cycle is not clear. It was initially proposed to function in an ‘alternative’ visual cycle, in which there is regeneration of 11-*cis*-retinal from all-*trans*-retinal under photopic conditions [316]. This would ensure availability of 11-*cis* retinal under conditions of prolonged light exposure. Further studies have suggested that RGR also plays a role in the classical visual cycle and that its effects may be independent of light. [317]. It has also been identified that RGR mediates the mobilisation of all-*trans* retinyl esters in RPE cells in response to light, and *in vitro* studies have shown that in the dark, RGR inhibits LRAT and all-*trans*-retinyl ester hydrolase, but in the light this inhibition is reversed [318]. Work is ongoing but the specific role for RGR remains to be elucidated.

Although the p.Ser66Arg *RGR* mutation in this and other families has segregated in an autosomal recessive manner, an *RGR* mutation in an autosomal dominant RP family has been described, with a phenotype similar to choroidal sclerosis [319]. This mutation, a 1-bp insertion at codon Gly275, at the 3’ end of the coding region, creates a protein that is 21% longer than that encoded by wild type RGR. The homologous region in rhodopsin is a frequent target of mutations in ADRP. It is unclear why dominant and recessive mutations in *RGR* lead to disease, which have different phenotypes. However there are also other genes, for example *NR2E3*, *BEST-1*, and *Rhodopsin* where both recessive and dominant mutations cause variable retinal phenotypes [398-403]. This may be seen to be more common as next generation sequencing becomes more available in molecular diagnostic investigation.

4.8 Childhood Onset Autosomal Recessive Bestrophinopathy

The clinical heterogeneity associated with mutations in the Bestrophin-1 (*BEST1*) gene has recently been expanded and these conditions are now considered under the umbrella term: ‘bestrophinopathies’. Autosomal dominant inheritance classically leads to the condition ‘Best disease’ (Best’s vitelliform macular dystrophy, BVMD) (OMIM 153700) [400], but other rare dominantly inherited conditions also occur, including Autosomal Dominant Vitreochorioretinopathy (ADVIRC) (OMIM 193220) [404] and retinitis pigmentosa (OMIM 613194) [405]. Recently, autosomal recessive inheritance, with bi-allelic mutations in *BEST1* was reported in adults, a condition termed Autosomal Recessive Bestrophinopathy (ARB) (OMIM 611809) [401].

Subjects recruited into this study presented in childhood with clinical features suggestive of a bestrophinopathy, and subsequent molecular analysis of *BEST1* was performed. A paper has been published with some of the results of this cohort of subjects, and since then, further families have been identified [406]. This chapter describes the phenotype associated with childhood onset autosomal recessive bestrophinopathy (ARB) for those subjects that were phenotyped at MEH, and describes the results of the molecular analyses performed in these families.

4.8.1 Clinical History

Six probands of six families were included in this sub-category of the ‘macular phenotype’ cohort of subjects in this study. Three of six (50%) probands presented with strabismus (Subjects 1, 3 and 5), 2 with reduced vision (Subjects 2 and 6) and 1 with leucocoria that had been identified on a photograph (Subject 4) (Table 20). Age at presentation ranged between 2 years and 6 years. No subjects reported nyctalopia, photophobia or ocular pain, and nystagmus was not a feature. Subject 1 was reported to be amblyopic in the right eye but she also had macular scarring; Subject 5 underwent strabismus surgery at age 13 years. General health was unremarkable in all subjects.

Of the 11 parents that were available for clinical testing, all were asymptomatic. The male cousin of Subject 3 (Family 3) carried a diagnosis of Best disease. There was no other family history of ocular disease in the other families. All probands except Subject 5 were from non-consanguineous families. The parents of Subject 5 were second cousins. Families 1-5 were British Caucasian, and family 6 was Greek.

4.8.2 Clinical Examination

Four of six subjects were male. They were examined at different ages: Subject 1 at 7.7 years; Subject 2 at 19.0 years; Subject 3 at 12.5 years; Subject 4 at 5.5 years; Subject 5 at 17.8 years; and Subject 6 at 6.5 years (Table 20). The two subjects that were examined in early adulthood (Subjects 2 and 5) had been previously examined in childhood. Visual acuity at presentation was generally good, and ranged between 0.00 LogMAR and 1.10 LogMAR. Subject 1 had amblyopia and macular scarring due to

sub-retinal neovascular membrane in the right eye; visual acuity in this eye was 1.10 LogMAR. If this measurement is excluded, the worst visual acuity at presentation was in the left eye of Subject 2, at 0.48 LogMAR. No subjects showed deterioration of vision over time unless there was choroidal neovascularisation (Subject 1). As with adults with ARB, hypermetropia predominated; the spherical equivalent ranged between +1.50 dioptres and +8.00 dioptres. Anterior segments were normal in all subjects.

The affected subjects all had bilateral symmetrical macular changes with characteristic sub-retinal yellow deposits that either had the appearance of 'classical' Best disease (Subject 1), or a variable multi-focal pattern (Subjects 2-6), or a combination of the two (Subject 6, left eye). In subject 1 the macular lesions extended to the inferior vascular arcades and contained, bilaterally, a para-foveal cicatricial component (Figure 61 - A and B). This subject developed a right sub-retinal neovascular membrane by age 7.5 years. The multi-focal yellow deposits were more subtle in subject 2, and appeared on a background of macular oedema and confluent yellow sub-retinal change located along and beyond the temporal vascular arcades (Figure 62 - A and B). In subjects 3 to 6 the multi-focal round yellow deposits were more prominent, surrounding an area of neurosensory detachment, with similar additional areas superior to the optic discs (Figure 63, Figure 64, Figure 65 and Figure 66 - A and B). Subject 3 had a similar area inferior to the discs of approximately 1 disc diameter. Subject 5, at age 17.8 years additionally had bilateral macular scarring which spared the foveae, and very fine yellow dots in the peripheral retina at the equators. In Subject 6 there was a foveal yellow lesion that resembled the vitelliform

lesion classically seen in Best disease – this was more prominent in the left macula than in the right. All parents examined (11 of 12) had normal fundi.

4.8.3 Fundus Autofluorescence Imaging

Fundus autofluorescence imaging displayed marked hyperautofluorescence corresponding to the round yellow lesions seen on funduscopy (Figure 61, Figure 62, Figure 63, Figure 64, Figure 65 – images C and D, and Figure 66 - C). In Subject 1 the hyperautofluorescence corresponded to the focal macular lesions, which extended to the inferior vascular arcades. In subject 2 the hyperautofluorescence was more diffuse but there were additional foci of hyperautofluorescence corresponding to the yellow lesions.

4.8.4 OCT Imaging

sd-OCT imaging demonstrated sub-retinal hyporeflective areas in the maculae of all subjects (Figure 61, Figure 62, Figure 63, Figure 64, Figure 65 – images E and Figure 66 - D). Discrete hyperreflective dome-shaped sub-retinal elevations were present in all subjects except Subject 2. A prominent photoreceptor outer segment layer bordering the sub-retinal hyporeflectivity was seen in Subjects 1, 3, 4 and 6, but in the two oldest subjects this layer appeared to be disrupted and more irregular (Subjects 2 and 5). The inner retinal layers were intact with normal laminar architecture in Subjects 1, 3, 4 and 5. Multiple intra-retinal hyporeflective areas were present in Subject 2; in Subject 6 there was one focal intra-retinal hyporeflective spot.

Subject, Family (Gender)	Presenting symptoms	Presenting VA, LogMAR (RE; LE) (Age, yr)	Latest VA, LogMAR (RE; LE) (Age, yr)	Refraction (RE; LE)	EOG light rise (RE; LE)	PERG (RE; LE) (Age, yr)	ffERG (RE; LE) (Age, yr)
1, 1 (F)	Strabismus	1.10; 0.10 (4.8)	1.18; 0.18 (7.7)	+8.00 DS; +7.00/-1.00, 20	Undetectable; Undetectable	Normal; Subnormal (7.5)	Normal; Normal (7.5)
2, 2 (F)	Reduced vision	0.18; 0.48 (6)	0.00; 0.30 (19)	+2.50/-0.75, 170; +2.50/-0.75, 170	Undetectable; Undetectable	Normal (9.5), Subnormal (17.5); Normal (9.5), Subnormal (17.5)	Normal (9.5), Subnormal (17.5); Normal (9.5), Subnormal (17.5)
3, 3 (M)	Strabismus	0.40; 0.00 (2)	0.4; 0.00 (12.5)	+7.00/-0.25, 90; +5.00/-0.50, 90	Undetectable; Undetectable	Normal; Normal (12.5)	Normal; Normal (12.5)
4, 4 (M)	Leucocoria (on photograph)	0.12; 0.12 (2)	0.12; 0.08 (5.5)	+5.25/-0.75, 10; +4.25/-0.75, 170	Not tested; Not tested	Normal; Normal (3.5) ^a	Normal; Normal (3.5) ^a
5, 5 (M)	Strabismus	0.3; 0.2 (12)	0.2; 0.2 (17.8)	+3.50/-3.00, 180; +2.50/-2.00, 15	Undetectable; Undetectable	Not tested; Not tested	Normal; Normal (13)
6, 6 (M)	Reduced vision	0.1; 0.1 (6.5)	0.1; 0.1 (6.5)	+3.00/+3.00, 100; +3.25/+2.50, 80	Undetectable; Undetectable	Normal; Normal (6.5)	Normal; Normal (6.5)

Table 20 - Clinical Features of Paediatric ARB subjects. F – Female; M – Male; VA – Visual Acuity; RE – Right Eye; LE – Left Eye; yr – year; DS – Dioptre Sphere; EOG – Electro-Oculogram; PERG – Pattern Electroretinogram; ffERG – full field Electroretinogram.

a. ERGs performed using paediatric protocol and peri-orbital skin electrodes with non-Ganzfeld stimulation.

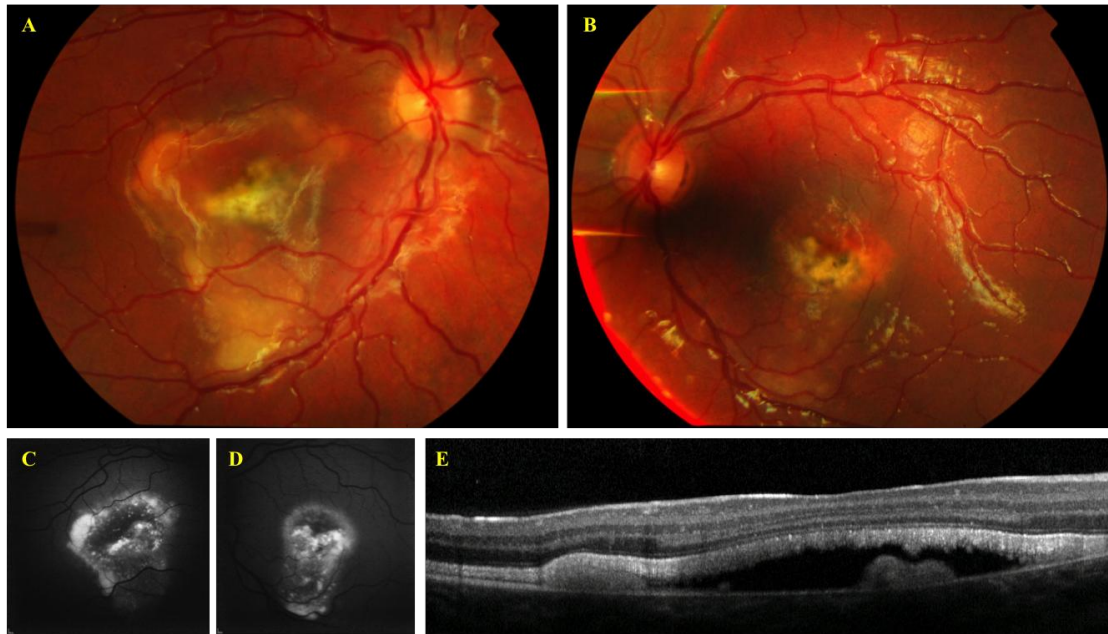


Figure 61 - Subject 1 ARB. A – Right eye fundus; B – Left eye fundus; C – Right eye fundus autofluorescence image; D – Left eye fundus autofluorescence image; E – Right eye OCT image.



Figure 62 - Subject 2 ARB. A – Right eye fundus; B – Left eye fundus; C – Right eye fundus autofluorescence image; D – Left eye fundus autofluorescence image; E – Right eye OCT image.

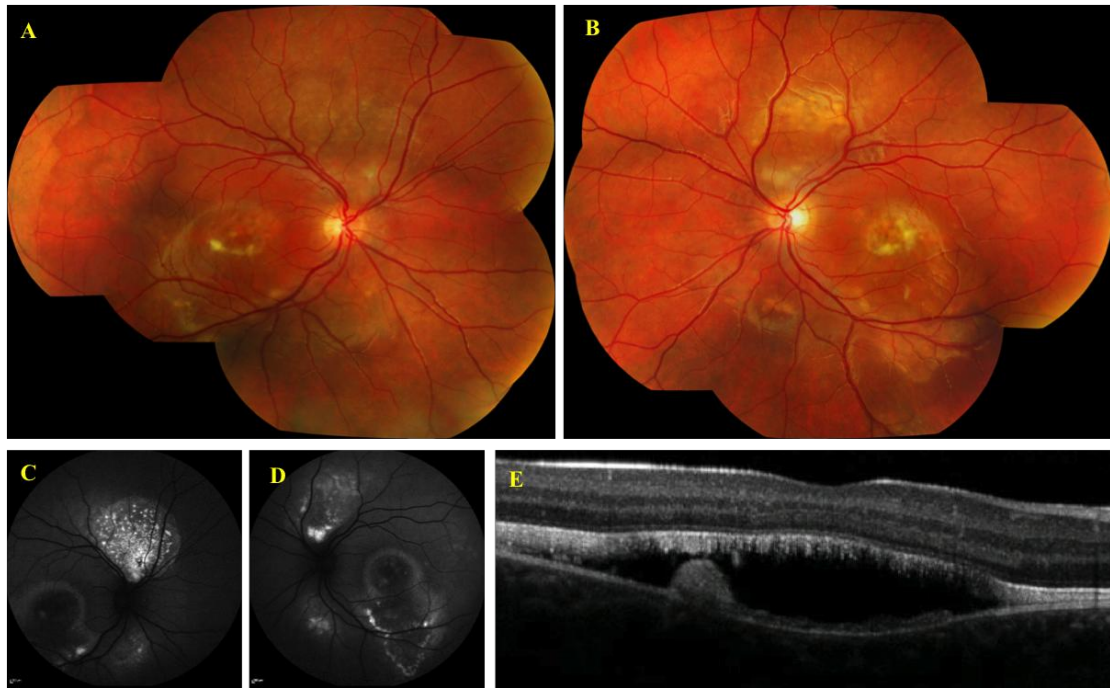


Figure 63 - Subject 3 ARB. A – Right eye fundus; B – Left eye fundus; C – Right eye fundus autofluorescence image; D – Left eye fundus autofluorescence image; E – Right eye OCT image.

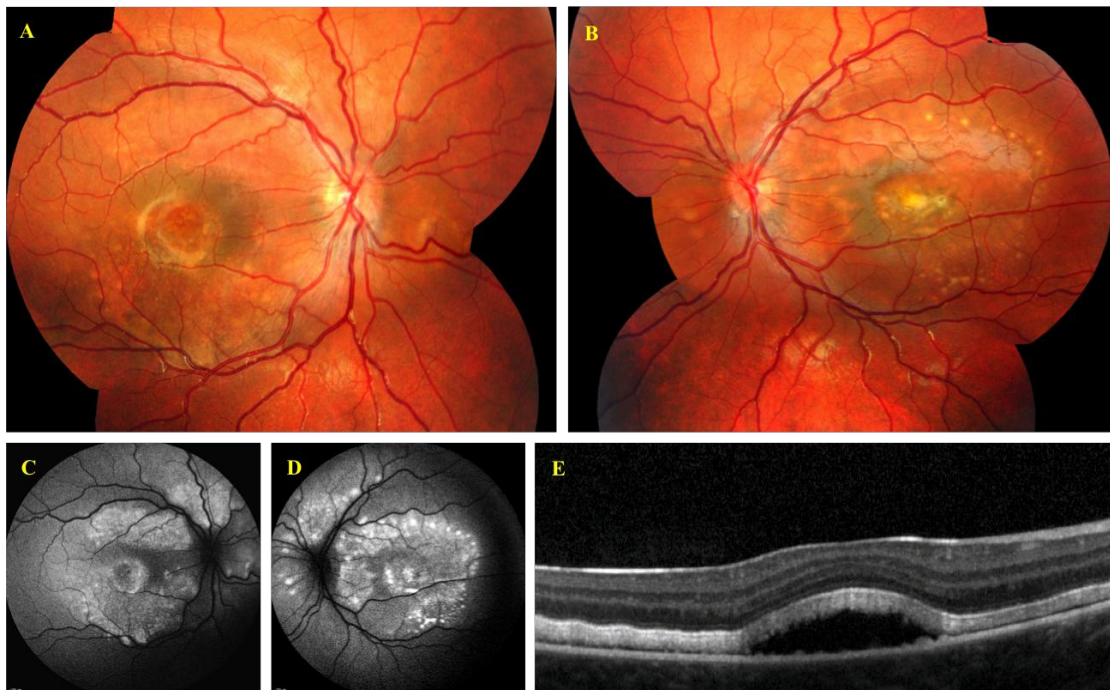


Figure 64 - Subject 4 ARB. A – Right eye fundus; B – Left eye fundus; C – Right eye fundus autofluorescence image; D – Left eye fundus autofluorescence image; E – Right eye OCT image.

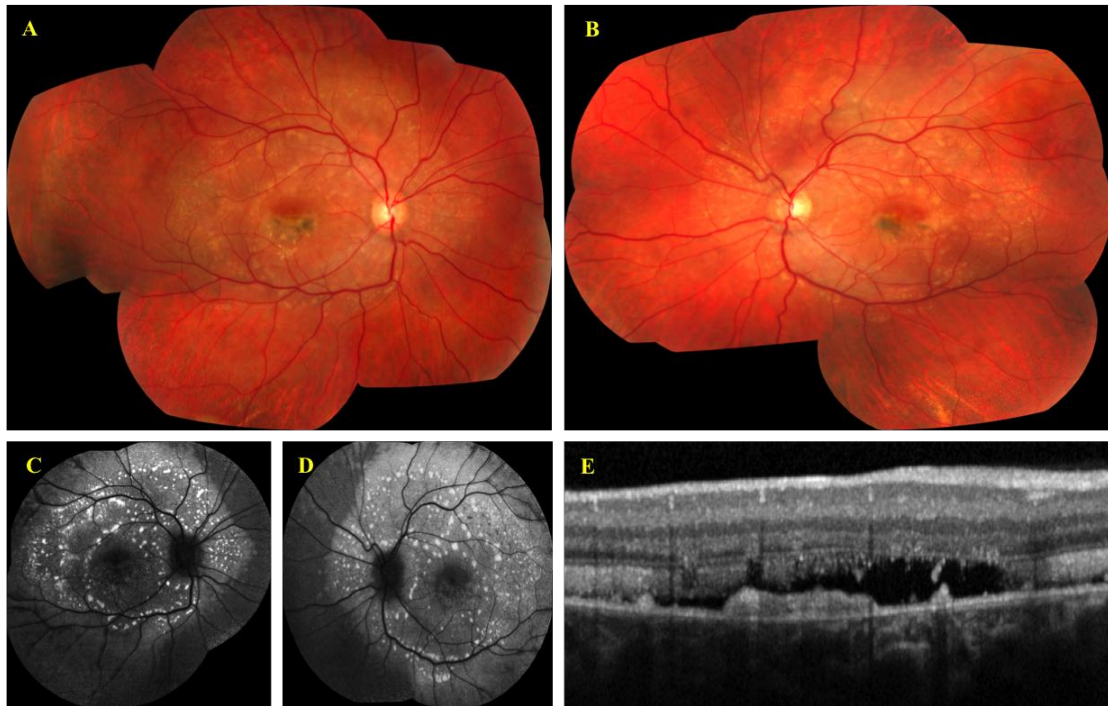


Figure 65 - Subject 5 ARB. A – Right eye fundus; B – Left eye fundus; C – Right eye fundus autofluorescence image; D – Left eye fundus autofluorescence image; E – Right eye OCT image.

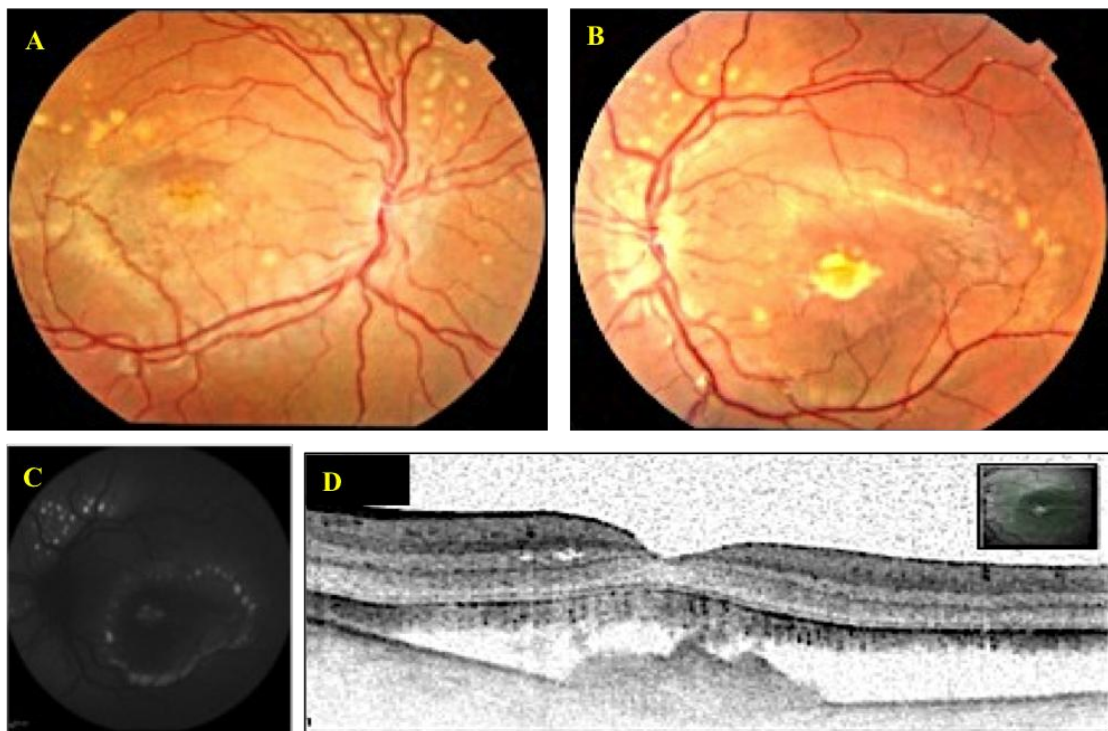


Figure 66 - Subject 6 ARB. A – Right eye fundus; B – Left eye fundus; C – Left eye fundus autofluorescence image; D - Left eye OCT image.

4.8.5 Electrophysiological Studies

Electrophysiological testing was undertaken in all subjects using ISCEV standards or using a modified paediatric protocol with peri-orbital skin recording electrodes. Flash or full-field ERGs (ffERGs), pattern ERGs (PERGs) and electro-oculograms (EOGs) were performed where possible. All available parents underwent EOG testing.

There was no light rise in either eye on EOG in all subjects who underwent testing (Subjects 1-3, 5 and 6). Subject 4 was too young to perform the test reliably. These findings are in keeping with severe generalised RPE dysfunction. Both of the parents of Subjects 1, 2, 4 and 5 had normal EOG light rises. Only the mother of Subject 3 was available and she also had a normal EOG light rise. The mother of Subject 6 had a normal EOG light rise but his father had a mildly subnormal light rise at 155% in both eyes (a light rise less than 150% is considered abnormally low and above 200% is considered to be normal; between 150% and 200% is considered to be borderline). The EOG result in the father of Subject 6 was considered not to be typical of a carrier of autosomal dominant Best disease, as in asymptomatic gene carriers there is minimal light rise, if any.

Except for Subject 2, the ffERGs were normal in all probands (age 7.5 years, Subject 1; 12.5 years, Subject 3; 4.0 years, Subject 4; 13.0 years, Subject 5; 6.5 years, Subject 6). Longitudinal ffERG data were available for Subject 2. At age 9.5 years she had normal flash ERGs but at age 17.5 years full field ERG abnormalities were evident, consistent with mild generalised rod and cone dysfunction.

The pattern ERG (PERG), a measure of macular function, was mildly subnormal in the eye with a subretinal neovascular membrane, but normal in the fellow eye, of Subject 1. In subject 2, at age 9.5 years, the PERG was normal but at 17.5 years the P50 component of the PERG was reduced, consistent with macular involvement. In Subjects 3, 4 and 6 the PERGs were normal. PERGs were not performed in Subject 5.

In summary, the electrophysiology findings in subjects 1-3 and 5-6 are of severe generalised dysfunction at the level of the RPE / photoreceptor interface. There is additional generalised photoreceptor dysfunction with macular involvement in the oldest subject, in whom serial electrophysiology demonstrates progression over an 8-year period. An important finding is that all but one parent of the affected children had normal EOGs.

4.8.6 Molecular Analysis

Molecular analysis of *BEST1* was performed by Dr Davidson, University of Manchester, in Families 1-4 and by ADB in Families 5 and 6. All ten coding exons and flanking intronic boundaries were analysed by direct sequencing from PCR amplicons for subjects 1,2,3,5 and 6. DNA was only available for the parents of Subject 4 and was screened for mutations in *BEST1*. Otherwise, only the relevant exons containing sequence alterations were sequenced in the parents (Table 21). PCR conditions and primer sequences are listed in the Appendix (Appendix 7.2.3).

Subject 1 harboured one previously reported heterozygous missense mutation c.422G>A p.Arg141His [401, 407] [408] and one novel heterozygous nonsense

mutation, c.475C>T p.Gln159X, in *BEST1*. Her father carried the c.422G>A p.Arg141His variant in the heterozygous state and mother carried the c.475C>T p.Gln159X variant in the heterozygous state.

Subject 2 harboured a novel missense mutation, c.533A>C p.His178Pro, and a novel duplication mutation, c.1038dupC p.Tyr347LeufsX54, in *BEST1*. Her father carried the c.533A>C p.His178Pro variant in the heterozygous state and mother carried the c.1038dupC p.Tyr347LeufsX54 variant in the heterozygous state.

Subject 3 had one novel heterozygous missense mutation and one novel heterozygous nonsense mutation in *BEST1*: c.550C>T p.Pro184Ser and c.1066C>T p.Arg356X. His mother carried the c.550C>T p.Pro184Ser variant in the heterozygous state. His father was not available for testing.

DNA was unavailable from subject 4. However, both of the unaffected parents of this subject carried the following previously reported heterozygous missense mutations in *BEST1*: c.584C>T, p.Ala195Val [409, 410] (mother) and c.974T>C, p.Met325Thr [401] (father).

Subject 5 harboured the novel intronic homozygous mutation c.1740-3t>g, p.Asp581SerfsX85 in *BEST1* (mutation identified by direct sequencing by ADB, protein change identified by RT-PCR by Dr Davidson). This was the only consanguineous family in this cohort. His unaffected parents and unaffected sister were each identified to carry this mutation in the heterozygous state (Figure 67). This mutation occurs 3 nucleotides before the first base of exon 11. In *silico* prediction

software (www.fruitfly.org) predicts that this mutation abolishes the acceptor splice site. It is likely that the transcript does not undergo nonsense mediated decay, but that it produces a non functional isoform of bestrophin-1 that may affect the function of the calcium channel (direct communication from Dr Davidson, UCL).

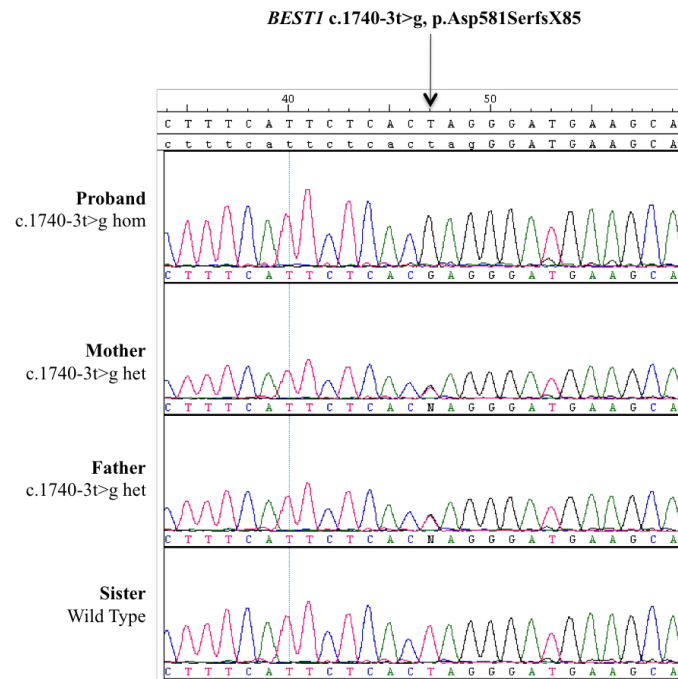


Figure 67 – Electropherograms ARB Family 5. *BEST1* c.1740-3t>g, p.Asp581SerfsX85.

Subject 6 harboured the novel duplication c.171-172dupAC, p.Glu58GlufsX4 and the previously reported missense mutation c.653G>A, p.Arg218His [410-412] in *BEST1* (Figure 68). His mother harboured the c.171-172dupAC, p.Glu58GlufsX4 variant in the heterozygous state and father harboured the c.653G>A, p.Arg218His variant in the heterozygous state. The frame shifting mutation is likely to be a null variant as it occurs early in the protein.

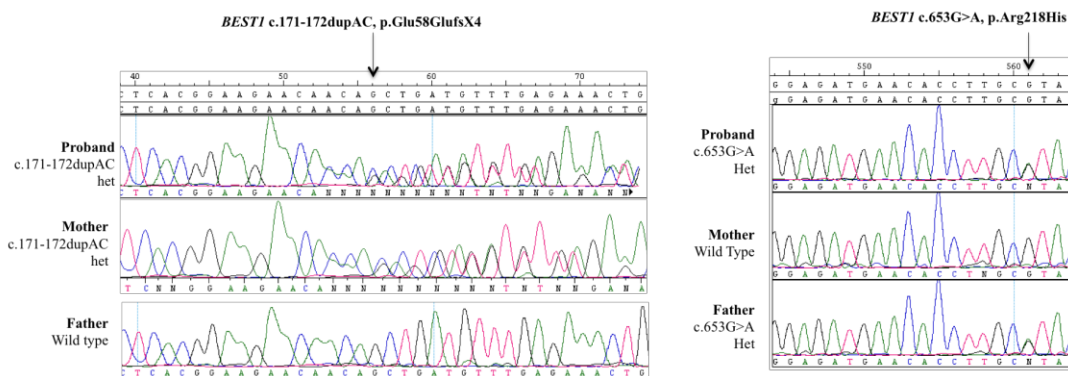


Figure 68 - Electropherograms ARB Family 6. *BEST1* c.171-172dupAC, p.Glu58GlufsX4 and c.653G>A, p.Arg218His.

Screening of DNA from the unaffected parents of subjects 1, 2, 3, 5 and 6 demonstrated that, in each instance, the *BEST1* mutations identified in the children were present in *trans*, one being inherited from each parent on separate alleles (Table 21). The absence of the putative novel pathogenic sequence alterations that had been found in families 1-4 in 210 control chromosomes was confirmed by either single stranded conformation polymorphism analysis or by direct sequencing (Dr Davidson). Five of 7 novel mutations identified in this study (c.475C>T p.Gln159X, c.533A>C p.His178Pro, c.550C>T p.Pro184Ser, c.1038dupC p.Tyr347LeufsX54 and c.1066C>T p.Arg356X) were absent from 210 ethnically matched control chromosomes. The novel variants c.1740-3t>g, p.Asp581SerfsX85 and c.171-172dupAC, p.Glu58GlufsX4, identified in subjects 5 and 6 respectively, were not identified on different variant databases including dbSNP (<http://www.ncbi.nlm.nih.gov/>), the exome variant server (<http://evs.gs.washington.edu/EVS/>), the 1000 genomes variant database (<http://browser.1000genomes.org/index.html>) or the Leiden Open Variation Database (http://www-huge.uni-regensburg.de/BEST1_database/).

Family	Subject	<i>BEST1</i> Allele 1				<i>BEST1</i> Allele 2			
		Nucleotide	Amino Acid	Type	Ref.	Nucleotide	Amino Acid	Type	Ref.
1	1	c.422G>A	p.Arg141His	Missense	[401, 407, 408, 410]	c.475C>T	p.Gln159X	Nonsense	Novel to this study
	Mother	WT	WT			c.475C>T	p.Gln159X		
	Father	c.422G>A	p.Arg141His			WT	WT		
2	2	c.533A>C	p.His178Pro	Missense	Novel to this study	c.1038dupC	p.Tyr347LeufsX54	Duplication, Frame shift, Null	Novel to this study
	Mother	WT	WT			c.1038dupC	p.Tyr347LeufsX54		
	Father	c.533A>C	p.His178Pro			WT	WT		
3	3	c.550C>T	p.Pro184Ser	Missense	Novel to this study	c.1066C>T	p.Arg356X	Nonsense	Novel to this study
	Mother	c.550C>T	p.Pro184Ser			WT	NA		
	Father	NA	NA			NA	WT		
4	4	NA	NA	Missense	[408, 410]	NA	NA	Missense	[401]
	Mother	c.584C>T	p.Ala195Val			WT	WT		
	Father	WT	WT			c.974T>C	p.Met325Thr		
5	5	c.1740-3t>g	p.Asp581SerfsX85	Frame shift, Null	Novel to this study	c.1740-3t>g	p.Asp581SerfsX85	Frame shift, Null	Novel to this study
	Mother	c.1740-3t>g	p.Asp581SerfsX85			WT	WT		
	Father	WT	WT			c.1740-3t>g	p.Asp581SerfsX85		
6	6	c.171-172dupAC	p.Glu58GlufsX4	Duplication, Frame shift, Null	Novel to this study	c.653G>A	p.Arg218His	Missense	[410-412]
	Mother	c.171-172dupAC	p.Glu58GlufsX4			WT	WT		
	Father	WT	WT			c.653G>A	p.Arg218His		

Table 21 - *BEST1* molecular analysis in affected Subjects and unaffected parents in ARB families. WT – Wild Type; NA – Not Available. Compound heterozygous and homozygous mutations identified in the probands are indicated in bold.

4.8.7 Discussion

At the time that this study was conducted, ARB had been a recently described disorder caused by bi-allelic, or compound heterozygous, mutations in *BEST1* [401, 405, 413]. Most of the reports were of individuals who were diagnosed in adulthood, and only 12 molecularly confirmed individuals from 7 families had been reported. An additional family reported with ‘atypical’ Best disease with compound heterozygous mutations was also likely to have ARB [407]. The phenotype associated with ARB had predominantly been described in adults who had central visual loss, hypermetropia, irregularity of the RPE and deep scattered hyperautofluorescent sub-retinal deposits [401]. The *BEST1* gene was initially mapped to chromosome 11q13 in 1992 [414, 415] and was later characterised in 1998 [400]. *BEST1* encodes a 585 amino acid protein product, bestrophin-1, which is thought to function as a calcium activated chloride channel in the basolateral plasma membrane of RPE cells [405, 416]. An additional role of bestrophin-1 as a regulator of voltage dependent calcium channels has been suggested [417]. The reduced/absent EOG light rise in conditions caused by mutations in *BEST1*, which are grouped under the umbrella term ‘bestrophinopathies’, is believed to be generated by a reduced influx of chloride ions into the RPE [417-420].

In this study the paediatric phenotype of ARB was sought in order to expand understanding of this condition in a young age group. In all affected subjects compound heterozygous mutations in *BEST1* were identified, with symptoms or signs being present by 6 years of age. Hypermetropia was frequent, in keeping with other disorders associated with mutations in *BEST1* [401, 404]. Overall, visual loss was mild and there was little change in the visual acuity unless choroidal

neovascularisation developed. Sub-retinal yellow deposits with sub-retinal fluid were evident in the posterior pole of all subjects. Similar changes were reported in adults with ARB [401, 407, 413], but the fundus appearances were more variable in the present paediatric cohort, ranging from subtle multi-focal deposits to a more ‘classical’ Best disease appearance. In addition to the macular deposits, similar lesions could be seen to extend beyond the vascular arcades or to localise to the peripapillary regions, predominantly superior to the optic discs. The deposits were highly autofluorescent and appeared as discrete hyper-reflective dome-shaped sub-retinal elevations. It is unclear whether these elevations lie above, below or within the RPE. Similar appearances were described in a previous report and were thought to localise to within the RPE [413]. In multi-focal vitelliform macular dystrophy [421] and Best disease [76], similar lesions have been proposed to lie at the level of the RPE/photoreceptor complex.

Sd-OCT imaging in the younger subjects (5 subjects, age range 5.5 – 17.8 years) suggested that the inner retinal layers remain intact, but with age, intra-retinal hyporeflective areas, presumed to be intra-retinal cysts, may develop (demonstrated by Subject 2, age 19 years). Comparison of the OCT imaging in this older subject with time domain OCT images obtained in other adult series’ suggests that in ARB, intra-retinal cystic changes develop with age [401, 407]. The neurosensory retina was detached in all affected subjects, with sub-retinal hyporeflective areas that are presumed to represent sub-retinal fluid. The photoreceptor layer appeared more prominent than normal, giving the appearance of extensions into the sub-retinal space. These extensions may represent an unmasking of the normal tight inter-digitations that exist between the photoreceptor outer segments and the RPE apical microvilli

[422]. They may also represent prolongations of the photoreceptor outer segments that do not become phagocytosed by the RPE due to the neurosensory detachment. Thickening and elongation of the photoreceptor outer segments with small filament-like bridges connecting the outer segment layer and the RPE, proposed to represent unshedded outer segment discs that in turn may lead to outer segment elongation, have been reported in ARB [413]. Such bridges were not identified in the present study.

Electrophysiological investigation is paramount to the diagnosis of ARB. The absent EOG light rise suggests that the defect localises to the RPE. However, EOG testing is difficult to perform in young children and may not be possible. In dominant *BEST1* disease the EOG is abnormal in heterozygotes. Thus, investigation of other family members may help distinguish dominant from recessive disease, allowing clinicians to provide appropriate genetic counselling to the family. If both parents have a normal EOG light rise, the disease is almost certainly recessive in inheritance.

In the present study the EOG light rise was undetectable in all subjects that were old enough to comply with the test. In the younger subjects, PERGs were normal in all but one eye of one child (subject 1, age 7.5 years), who clinically had a sub-retinal neovascular membrane and strabismus that could account for the subnormal PERG. In the oldest subject the PERG became subnormal at an older age (subject 2, at age 17.5 years), having been normal at a younger age, suggesting progressive macular dysfunction. All subjects tested in childhood had normal flash or full-field ERGs (age 3.5 to 13 years).

Of the previously described cases in the literature, all adults were identified to have abnormal full-field ERGs with mild to severely reduced PERGs, in keeping with generalised retinal dysfunction with macular involvement [401]. Of the data published in children, full-field ERGs were reported to show reduced rod and cone b-waves, and multi-focal ERG responses were reduced and delayed within the central 10° [401] [413]. The limited longitudinal data available suggest that there is deterioration of the full-field ERG with time [401].

Molecular analysis of the 6 ARB families in this study, performed by Dr Davidson and ADB, identified 5 families to harbour compound heterozygous mutations and 1 consanguineous family to harbour a homozygous mutation in *BEST1*. Of the seven novel mutations identified, 2 were missense mutations (c.553A>C p.His178Pro and c.550C>T p.Pro184Ser), 2 were nonsense mutations (c.475C>T p.Gln159X and c.1066C>T p.Arg356X), 2 were duplications that lead to frameshifts and premature stop codons that are presumed to produce transcripts that are degraded by nonsense mediated decay (c.1038dupC p.Tyr347LeufsX54 and c.171-172dupAC, p.Glu58GlufsX4), and one was an intronic variant occurring 3 bases before the start of exon 11, causing a frame shift that produces a non-functioning isoform of bestrophin-1 (c.1740-3t>g, p.Asp581SerfsX85). The novel missense mutations identified lie in highly conserved regions of the protein product, suggesting that these regions have an important functional role.

The original paper describing ARB proposed that the phenotype results from null *BEST1* mutations, with affected individuals having either null or missense mutations that are non-functional [401]. Three subjects in the present cohort had compound

heterozygous null mutations (Subjects 2, 5 and 6), 2 had a combination of nonsense and missense mutations (Subjects 1 and 3) and 1 had two missense mutations (Subject 4). Three variants were present that have been described in both autosomal dominant Best disease and ARB (p.Arg141His, p.Ala195Val and p.Arg218His) [407, 408, 410, 412]. However, an affected subject reported with the p.Arg141His mutation had a further nonsense mutation in *trans* and it is likely that they have ARB [407]. Moreover, a p.Arg141His / wild type heterozygous parent of a subject with ARB reported by Burgess *et al.* had a normal examination and electrophysiology [401] and the p.Arg141His heterozygote reported by Schatz *et al.* also had a normal EOG light rise (although the ERG was reported to be reduced at age 59 years) [407], suggesting that the variants in these two reports are more likely to be recessive mutations. There have been further reports of the bestrophin-1 codon 141 being affected in ARB indicating that the p.Arg141His mutation is predominantly an ARB mutation and that it is likely to be the most frequently identified mutation associated with ARB to date [401, 406, 407, 423-427]. The probands with p.Ala195Val reported by Lotery *et al.* and Kramer *et al.* have no family or clinical data described in either study, leaving open the possibility that these, too, had ARB, in which a second allele was undiscovered [408, 410].

Interestingly, family 6 in the present cohort harboured compound heterozygous mutations, one of which has been reported in a number of families with [autosomal dominant] Best disease (c.653G>A, p.Arg218His) [411] [410, 412, 428]. In fact, codon 218 has been implicated in a number of unrelated families with Best disease, and the Arginine that normally resides in this position has been mutated to Histidine and Cysteine in different families [410, 412]. This residue is highly conserved and

codon 218 is a key residue in the bestrophin-1 protein that may represent a mutational ‘hotspot’ in Best disease. In a number of French studies this codon was the target of various missense mutations in unrelated families, leading the authors to conclude that this may correspond to a founder effect in French and other western European families [411, 412]. The clinical data in reports of mutations affecting the 218 codon are variable, and the cases included are both isolated and familial [410, 412]. In one family with a p.Arg218His mutation, the phenotype was described to be highly heterogeneous within the family, with the proband being severely affected and her father having very mild disease [412]. Although this may represent variable expressivity within this family, it is possible that this family had recessive disease in which the second allele was not found in the proband and that the father was an unaffected heterozygous carrier [411].

Alternatively, the mutations identified in family 6 in the present study may indicate both dominant and recessive inheritance within the same family. Aside from in the proband, there is no clinical history of *BEST1* related disease in this family. However, his father, who carried the p.Arg218His mutation in the heterozygous state had normal fundi and very mild reduction in the EOG. It can be postulated that either he has a mild phenotype of dominant disease (detectable only on EOG testing), or that he is phenotypically normal, and that the variant he carries is truly recessive. If this mutation behaves in a dominant manner, then when inherited along with the variant inherited from the mother, the combination may lead to a mixed inheritance pattern. If this mutation behaves in a recessive manner then the affected child has truly recessive disease and the clinical picture in the child is due to bi-allelic mutations. The correct

inheritance pattern is important to distinguish in this family, as it will help towards genetic counselling if other offspring are planned.

Around the time that some of the data from this study were published, a number of other reports of ARB families were also published, with descriptions made of the phenotype in both adults and children [406, 423, 424, 426, 429-435]. There is general agreement with the present study regarding the clinical features and electrophysiological findings in ARB. The phenotype is milder in children unless sub-retinal neovascularisation develops, and the full field ERG remains normal until late childhood / early adulthood, when the flicker (cone) ERG and PERG (macular) first become reduced and delayed, with eventual full field rod and cone dysfunction developing in adulthood [423, 426, 429, 430, 433, 434]. In agreement with the findings of the present study, the deterioration in the ERG appears to occur when intra-retinal cysts or neovascularisation develop [401, 413, 426, 430, 433]. More recently, further families have been described and the phenotype widely recognised to be associated with choroidal neovascularisation and angle closure glaucoma, that may be resistant to conventional treatment with laser iridotomy due to a plateau iris configuration and peripheral anterior synechiae [425, 427, 428, 436-441].

There is currently no treatment available for the bestrophinopathies, although complications such as choroidal neovascularisation and angle closure glaucoma do benefit from therapeutic intervention. As with all conditions affecting young children, management of amblyopia is important. There have been recent reports of success with anti-vascular endothelial growth factor (anti-VEGF) treatment for individuals with choroidal neovascularisation in ARB, with improvement of the visual acuity

(especially if combined with amblyopia therapy) [426, 427, 437]. Other options for management of intra-retinal fluid include carbonic anhydrase inhibitors, although there has been a recent report of reduction of the dose of this treatment leading to sub-acute angle closure [425, 439]. The management of angle closure in ARB may be difficult due to the configuration of the iris; the options include laser peripheral iridotomy and lens extraction.

A naturally occurring dog model of ARB exists (a disorder termed canine multi-focal retinopathy, *cmr*) [442]. Multi-focal areas of retinal elevation containing sub-retinal serous or pink-tan fluid occur, which are more clearly visible superiorly in the canine retina. In the more densely pigmented inferior canine retina the lesions are fewer and appear white, lying adjacent to the inferior retinal vessels. Histopathologic examination of *cmr* revealed autofluorescent cytoplasmic granules within hypertrophic RPE cells. As there are phenotypic similarities with humans, the study of *cmr* may help improve understanding of the disease mechanism and serve as a useful model for the future testing of novel therapies, including gene replacement therapy. Most recently, advances have been made in the recombinant adeno-associated virus based gene augmentation therapy of *BEST1* in dogs, which may pave the way for future human therapies for bestrophinopathies [443].

To conclude, the childhood phenotype of ARB has been determined in this study, demonstrating that the clinical features, results of electrophysiological studies and retinal imaging distinguish ARB from Best disease. The normal ERG in childhood suggests that there may be a window of opportunity for gene replacement therapy or other therapeutic intervention at an early age.

4.9 Benign Yellow Dot Dystrophy

A subset of individuals in Cohort 2 had been identified with an unusual phenotype that affected the macula, which was associated with good visual function. This subset was comprised of 18 individuals (Subjects 7 – 24 from Cohort 2) from 14 families (Families 7 – 20 from Cohort 2). Their phenotypes were ascertained and the results reported in this chapter. Molecular analysis is outstanding on this group of patients. The condition has been termed ‘Benign Yellow Dot Dystrophy’.

4.9.1 Clinical History

Of the 18 subjects identified with this phenotype, 16 were asymptomatic (88.9% of subjects with yellow dot dystrophy; 66.7% of subjects of cohort 2). Subjects were either referred from a community optometrist (13/18), from another ophthalmologist (1/18) or following screening due to a positive family history (4/18). Reduced vision was the presenting complaint in the two symptomatic subjects (Subjects 7 and 14). No cause was found for the reduced vision in Subject 7, who presented at age 16 years, and in whom multiple electrophysiological studies over a number of years were normal. A diagnosis of ‘functional’ visual loss was subsequently made. In Subject 14, who presented to another ophthalmologist at age 4 years but whose macular yellow dots were not apparent until age 6 years, the reduced vision was attributed to bilateral ametropic amblyopia due to hypermetropic astigmatism; there was also a partially accommodative esotropia. His vision eventually improved with spectacle wear and occlusion therapy.

Refractive error (identified in 5 subjects) was the predominant feature in the 7 subjects who had any past ocular history (Table 22). One of these 7 subjects had been treated for strabismus and 3 of 7 had been treated for amblyopia. One subject was diagnosed with functional visual loss (Subject 7). One subject had bilateral optic neuropathy of unknown cause 4½ years after presentation with the maculopathy; the optic neuropathy resolved spontaneously (Subject 16). General health was good in all, except for subject 24, who was taking antidepressants.

Of the 14 families identified in this sub-group, 2 families had multiple affected members (Family 7 and Family 8) and 12 families had only one affected member. Family 7 had 4 affected members in 2 successive generations. Family 8 had 2 affected members in 2 successive generations. The ethnic distribution was as follows: 12 families were British Caucasian; 1 was West African (Subject 21, Family 17); and 1 was South East Asian (Subject 24, Family 20). There was no history of consanguinity in any family.

4.9.2 Clinical Examination

Five subjects in the yellow dot dystrophy sub-group of cohort 2 were male, 13 were female. The age at presentation ranged between 5 years and 45 years, median 14.5 years. Visual acuity at presentation was 0.00 LogMAR or better in both eyes in 13 of 18 subjects (72.2% of yellow dot dystrophy subjects) (Table 22). Subject 7, with functional visual loss, had a presenting visual acuity of 0.78 LogMAR in either eye at age 15 years. Pattern appearance VEPs were consistent with normal visual acuity. Amblyopia affected subjects 14 (bilateral), 18 (unilateral right eye) and 19 (unilateral

left eye), whose acuities are listed (Table **22**). Colour vision was normal in 12 of 13 subjects examined using Ishihara or HRR colour plates. Only in subject 7 was the colour vision abnormal - she failed the HRR screening plates II and III at age 16 years. Anterior segments and ocular mediae were normal in all patients.

Characteristic bilateral macular changes consisting of yellow dots at the level of the retinal pigment epithelium, concentrated around the fovea, were present in all subjects (Table **23**). These were symmetrical between each eye and resembled drusen-like deposits. In the majority of subjects these were fine discrete lesions (Figure **69**, Figure **70** and Figure **71**), however, in 7 subjects some of the dots were confluent (subjects 7, 9, 10, 12, 13, 19, 22) (Figure **69** and Figure **72**). In 11 subjects the yellow dots were distributed evenly around the fovea (Figure **70**); in 7 subjects they were concentrated in the nasal parafoveal region (Figure **71**). In subjects 13 and 15 dots were visible outside the temporal vascular arcades in the right eye. These were minimal in number. In all but 1 subject (subject 14) for whom detailed images were available, a yellow crescent was visible to varying degrees around the optic disc, which was otherwise normal in all (Table **23**). In some cases this took on the appearance of a 'yellow halo' around the disc; in others the change was more consistent with peri-papillary atrophy. The retinal periphery and vasculature were otherwise normal in all subjects. In all parents of the sporadic cases that were examined, funduscopy was normal.

Subject (Gender)	Family	Ethnicity	Relation to Proband	Age at presentation (years)	Presenting symptoms	Family history	Visual Acuity (LogMAR) RE, LE (Age, years)	Past Ocular History
7 (F)	7	British Caucasian	Proband	15	Reduced vision	Dominant	0.78, 0.78 (15)	Functional visual loss
8 (F)	7	British Caucasian	Sister	18	Asymptomatic ¹	Dominant	0.00, 0.00 (18)	Nil
9 (F)	7	British Caucasian	Mother	45	Asymptomatic ¹	Dominant	0.18, 0.18 (45)	Nil
10 (M)	7	British Caucasian	Maternal first cousin	10	Asymptomatic ¹	Dominant	-0.08, -0.08 (10)	Nil
11 (F)	8	British Caucasian	Proband	22	Asymptomatic ²	Dominant	-0.08, -0.08 (22)	Myopic astigmatism
12 (F)	8	British Caucasian	Mother	Unknown	Asymptomatic ¹	Dominant	0.00, 0.00	Nil
13 (F)	9	British Caucasian	Proband	8	Asymptomatic ²	Sporadic	0.00, 0.00 (8)	Nil
14 (M)	10	British Caucasian	Proband	6	Reduced vision, strabismus	Sporadic	0.18, 0.26 (14)	Hypermetropic astigmatism, Partially accommodative ET, bilateral amblyopia
15 (F)	11	British Caucasian	Proband	10	Asymptomatic ²	Sporadic	0.00, 0.00 (10)	Nil
16 (F)	12	British Caucasian	Proband	5	Asymptomatic ²	Sporadic	0.00, 0.00 (10)	Bilateral optic neuropathy
17 (F)	13	British Caucasian	Proband	10	Asymptomatic ²	Sporadic	0.00, 0.00 (10)	Nil
18 (F)	14	British Caucasian	Proband	12	Asymptomatic ²	Sporadic	0.40, 0.00 (14)	Hypermetropia, RE amblyopia
19 (M)	15	British Caucasian	Proband	14	Asymptomatic ²	Sporadic	0.08, 0.14 (14)	Hypermetropia, LE amblyopia
20 (F)	16	British Caucasian	Proband	15	Asymptomatic ²	Sporadic	0.00, 0.00 (15)	Hypermetropia
21 (M)	17	West African	Proband	15	Asymptomatic ²	Sporadic	0.00, 0.00 (15)	Nil
22 (M)	18	British Caucasian	Proband	28	Asymptomatic ²	Sporadic	0.00, 0.00 (29)	Nil
23 (F)	19	British Caucasian	Proband	28	Asymptomatic ²	Sporadic	-0.08, -0.08 (29)	Nil
24 (F)	20	South East Asian	Proband	29	Asymptomatic ²	Sporadic	0.00, 0.00 (29)	Nil

Table 22 - Clinical features of subjects with Benign Yellow Dot Dystrophy. M – Male; F – Female, RE – right eye; LE – left eye; ET – Esotropia. ¹Family history; ²Referred from the Community.

Subject	Family	Appearance of yellow dots at the macula		Autofluorescence	
7	7	Discrete, drusen-like, some confluent	Even distribution	HyperAF dots	Crescent not visible
8	7	Discrete, fine, drusen-like	Even distribution	HyperAF dots	HypoAF crescent
9	7	Discrete, drusen-like, large	Even distribution	HyperAF dots	Crescent not visible
10	7	Discrete, drusen-like, some confluent	Even distribution	HyperAF dots	HyperAF crescent
11	8	Discrete, fine, drusen-like	Nasal parafovea	N/A	N/A
12	8	Discrete, drusen-like, some confluent	Nasal parafovea	N/A	N/A
13	9	Discrete, drusen-like, some confluent	Even, some outside macula	HyperAF dots	Crescent not visible
14	10	Discrete, fine, drusen-like	Even distribution	HyperAF dots	Crescent not visible
15	11	Discrete, fine, drusen-like	Even, some outside macula	HyperAF dots	HypoAF crescent
16	12	Discrete, fine, drusen-like	Even distribution	N/A	N/A
17	13	Discrete, fine, drusen-like	Nasal parafovea	HyperAF dots	HyperAF crescent
18	14	Discrete, fine, drusen-like	Nasal parafovea	HyperAF dots	HyperAF crescent
19	15	Discrete, drusen-like, many confluent	Nasal parafovea	HyperAF dots	HyperAF crescent
20	16	Discrete, fine, drusen-like	Even distribution	HyperAF dots	Crescent not visible
21	17	Discrete, fine, drusen-like	Nasal parafovea	HyperAF dots	HypoAF crescent
22	18	Discrete, drusen-like, some confluent	Nasal parafovea	HyperAF dots	HyperAF crescent
23	19	Discrete, fine, drusen-like	Even distribution	N/A	N/A
24	20	Discrete, fine, drusen-like	Even distribution	N/A	N/A

Table 23 - Features of yellow dots at the fundus in Benign Yellow Dot Dystrophy Subjects.

HyperAF – hyperautofluorescent; HypoAF – hypoautofluorescent; N/A – not available.

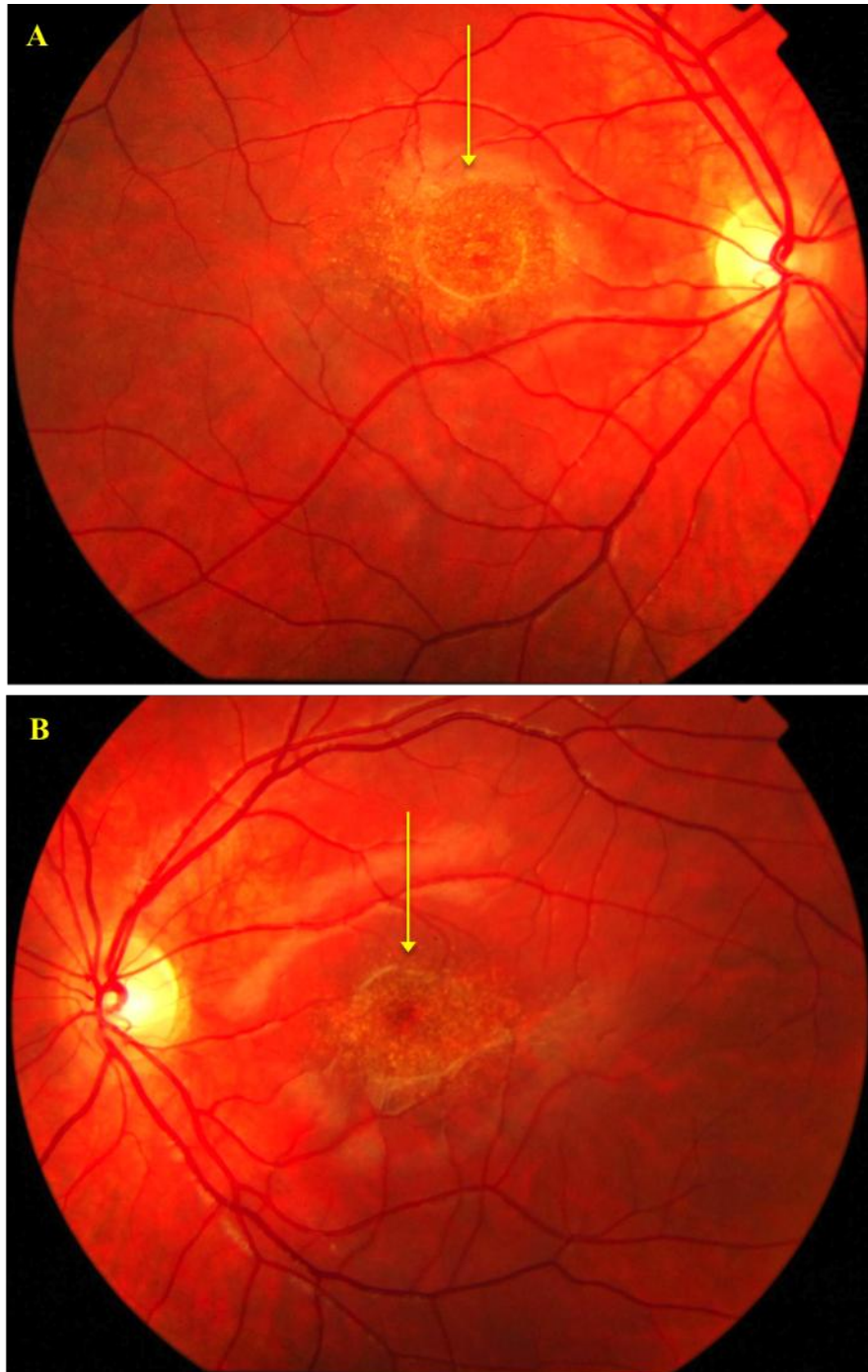


Figure 69 - Subject 10, Family benign yellow dot dystrophy. A – right eye fundus; B – left eye fundus. Discrete, fine drusen-like yellow dots are distributed evenly at each fovea. Some are confluent. Arrows indicate the location of the dots. A faint yellow crescent is seen around the optic discs in both eyes.

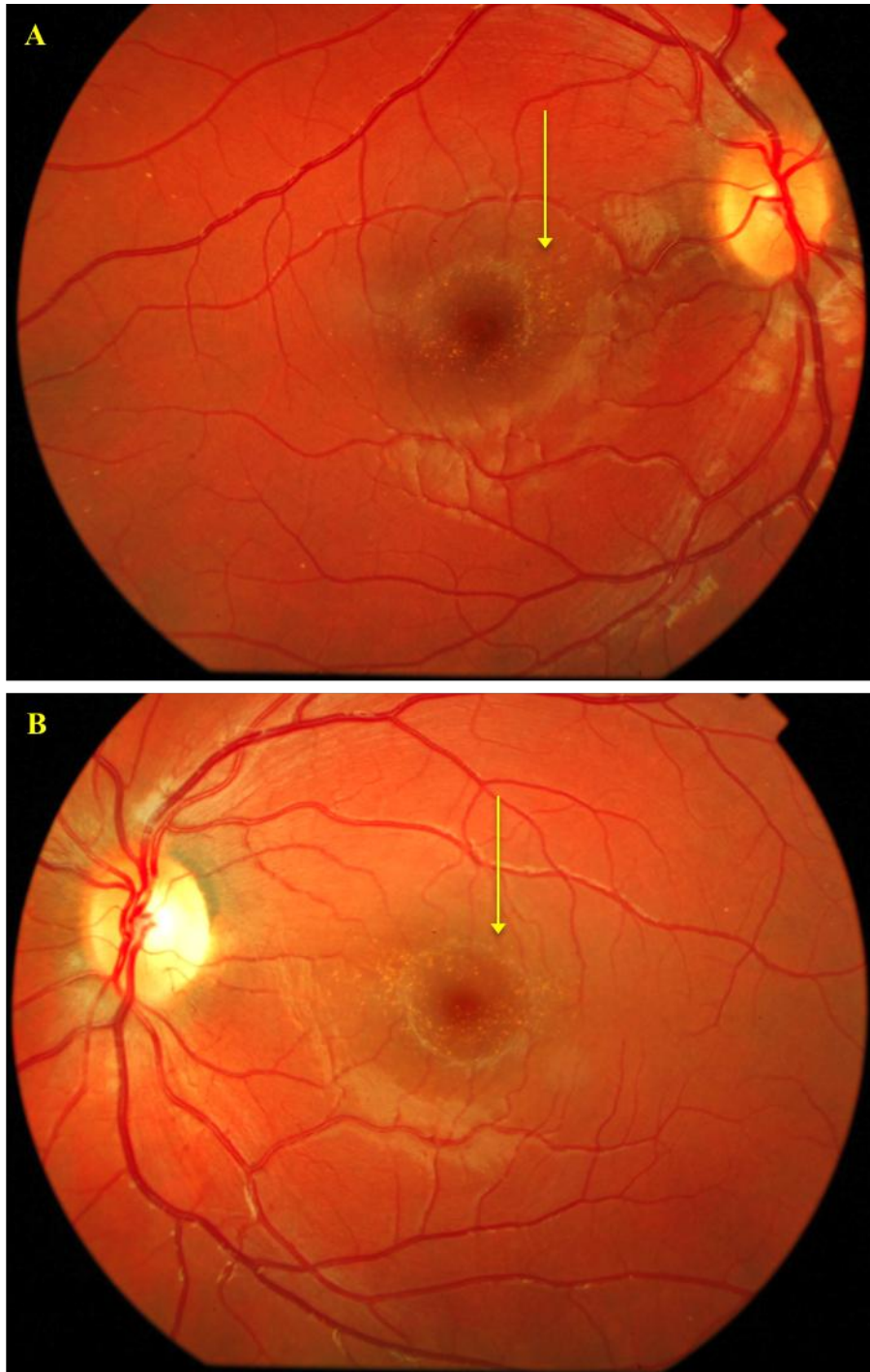


Figure 70 - Subject 15, Sporadic benign yellow dot dystrophy. A – right eye fundus; B – left eye fundus. Discrete, fine drusen-like yellow dots are distributed evenly at each fovea. Arrows indicate the location of the dots. Some dots are evident outside the macula area in the right eye. A faint yellow crescent is seen around the optic discs in both eyes.

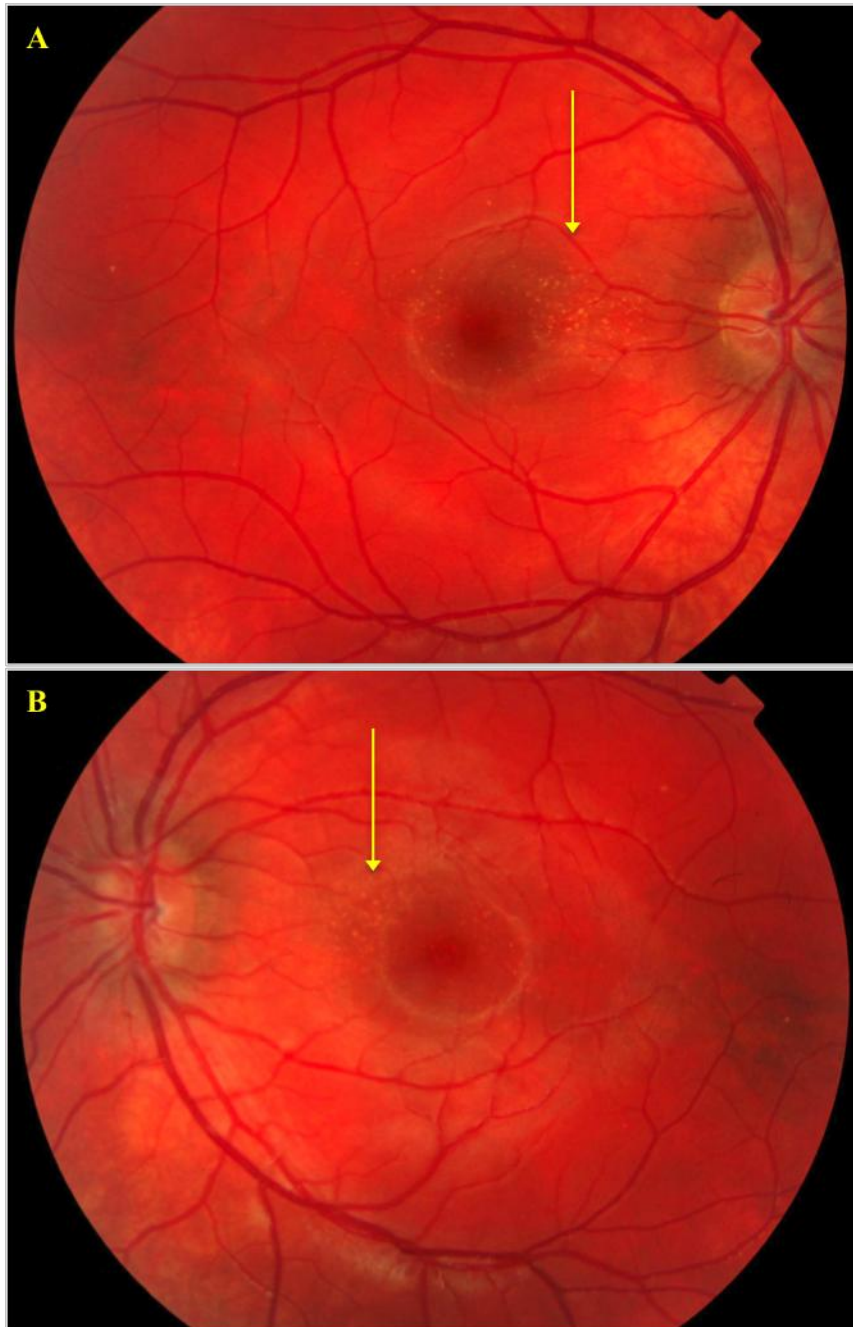


Figure 71 - Subject 17, Sporadic benign yellow dot dystrophy. A – right eye fundus; B – left eye fundus. Discrete fine drusen-like yellow dots are concentrated in the nasal parafoveal regions of both eyes. Arrows indicate the location of the dots. A faint yellow crescent is seen around the optic discs temporally in both eyes.

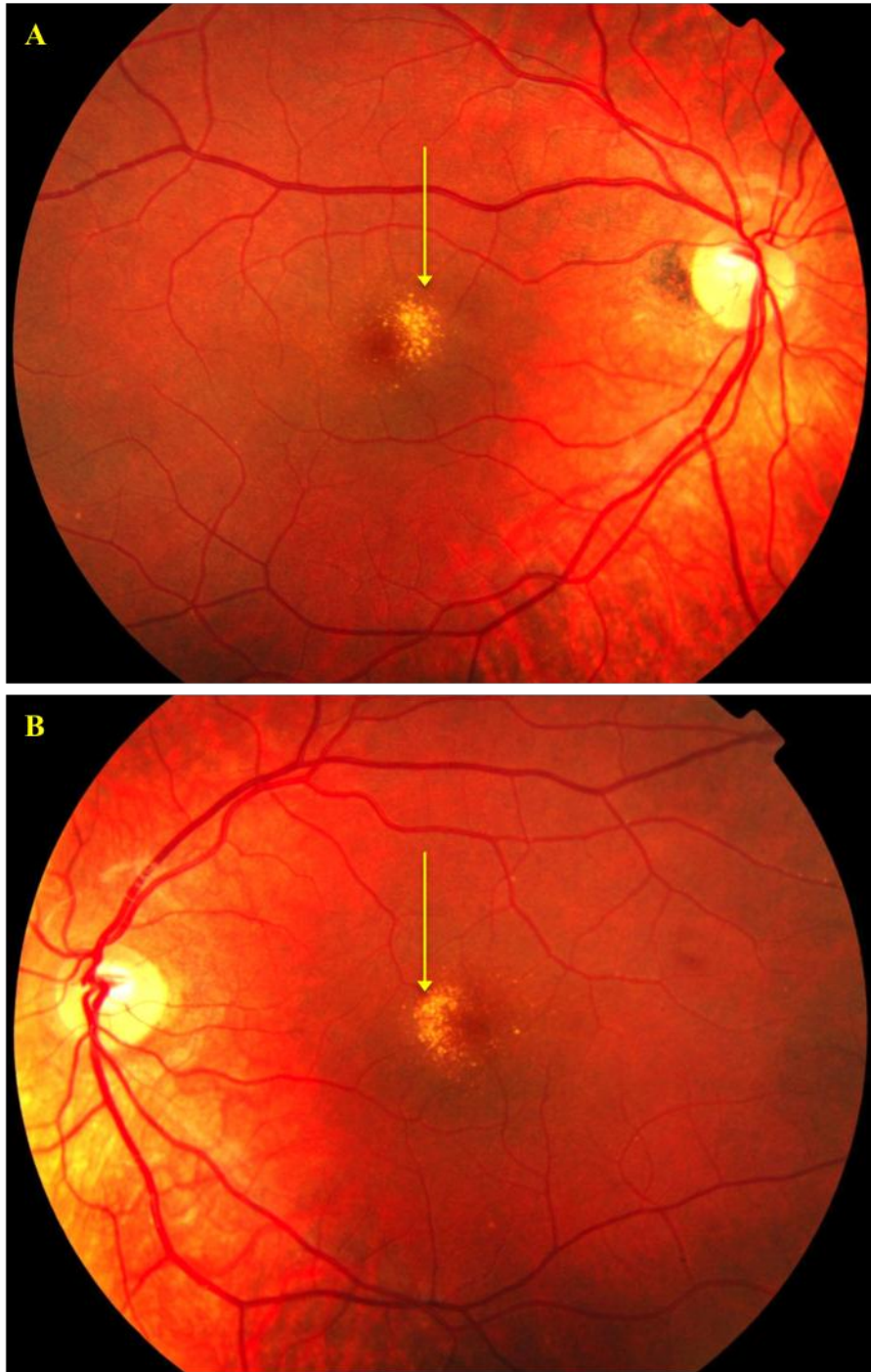


Figure 72 - Subject 19, Sporadic benign yellow dot dystrophy. A – right eye fundus; B – left eye fundus. The discrete drusen-like yellow dots are more confluent and are concentrated in the nasal parafoveal region in both eyes. Arrows indicate the location of the dots. A faint yellow crescent is seen around the optic discs resembling peripapillary atrophy in both eyes.

4.9.3 Fundus Autofluorescence Imaging

Fundus autofluorescence imaging, available for 13 of 18 subjects, revealed foci of hyperautofluorescence corresponding to the yellow dots, on an otherwise normal background autofluorescence signal in all (Figure **73**). In 5 of these there was a hyperautofluorescent signal corresponding with the crescent seen around the optic disc (Subjects 10, 17, 18, 19 and 22). In 3 subjects this crescent displayed a hypoautofluorescent signal (Subjects 8, 15 and 22). In no subjects did the fundus autofluorescence imaging identify further yellow dots than were visible on funduscopy.

4.9.4 OCT Imaging

Sd-OCT imaging performed in 7 of 18 subjects identified no subretinal hyper- or hypo-reflectivity, and the inner retinal layers remained intact. OCT imaging in 3 subjects was normal (Subjects 13, 15 and 18). In 3 subjects a slight irregularity of the inner segment / outer segment junction was seen (Subjects 10, 14 and 17), which corresponded with the locations of the yellow dots, as observed on the infra-red reflectance image taken during OCT image acquisition (Figure **74**). In 1 subject (Subject 19) only a slight irregularity of the RPE layer was seen (Figure **74**).

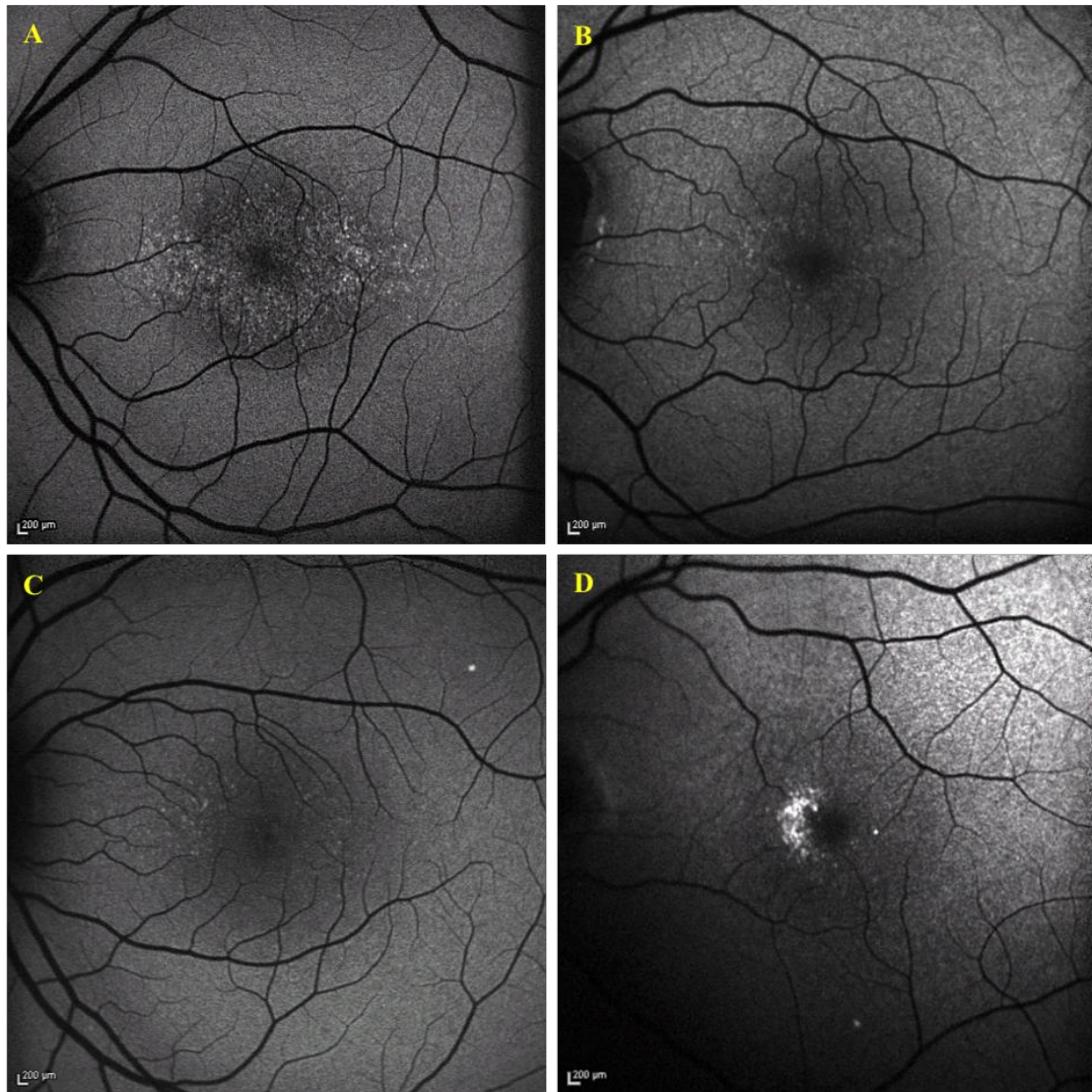


Figure 73 - Fundus autofluorescence images of benign yellow dot dystrophy Subjects. A – subject 10; B – Subject 15; C – Subject 17; D – Subject 19. In all subjects the yellow dots are hyperautofluorescent. In subjects 10, 17 and 19 there is hyperautofluorescence corresponding to the yellow crescent at the optic disc (A, C and D) and in subject 15 there is hypoautofluorescence corresponding to the yellow crescent (B).

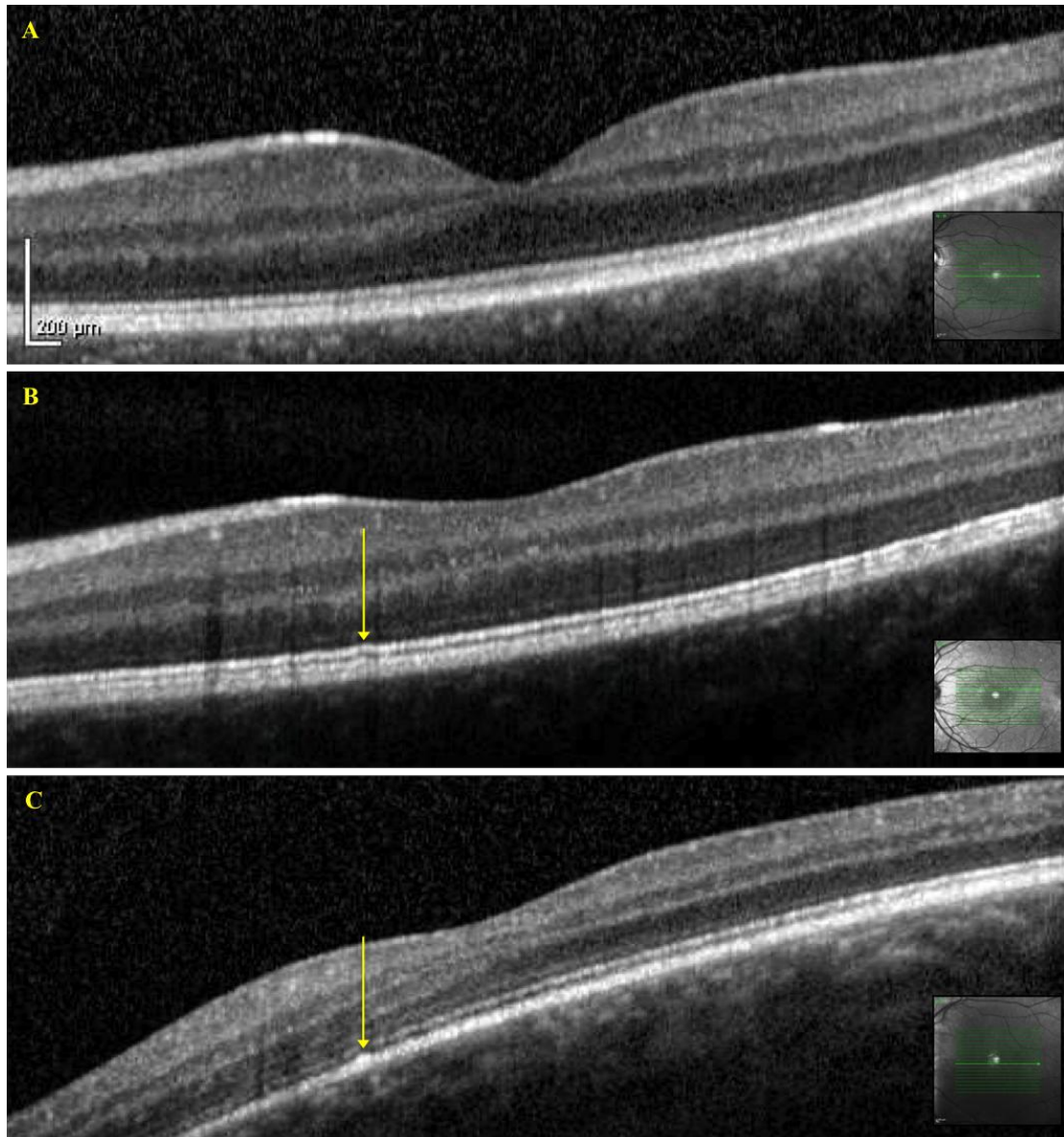


Figure 74 - OCT of Subjects with benign yellow dot dystrophy. A – Subject 15, normal OCT; B – subject 17 – slight irregularity of the inner segment outer segment line, indicated by the arrow; C – subject 19 – slight irregularity of the RPE layer, indicated by the arrow.

4.9.5 Electrophysiological Studies

Electroretinography was performed in 13 subjects. In 12, the PERG and full field ERGs were normal (age range 6-45 years). In subject 19 the PERG and cone ERGs were slightly delayed and of reduced amplitude. This was attributed to his hypermetropic refractive error. Of the 2 subjects with subjectively reduced vision (subjects 7 and 14), the PERGs and ffERGs, were normal. In subject 14 the pattern reversal VEP was slightly reduced in the left eye, consistent with strabismus. EOGs performed in 4 of 5 subjects demonstrated a normal light rise. In subject 19 the EOG was mildly subnormal in both eyes, at age 18 years.

4.9.6 Discussion

The subjects in this group were identified to have a previously unreported macular phenotype that is associated with excellent visual function. The condition is commonly sporadic, although it may also segregate in an autosomal dominant manner. In the majority of subjects, identification is an incidental finding or discovered after examination of family members of affected individuals.

Macular dystrophies may occur in isolation or in association with a variety of systemic abnormalities. Considerable clinical and genetic heterogeneity exists for this group of disorders and all of the Mendelian inheritance patterns have been described, as well as mitochondrial inheritance [444, 445]. A rare sub-group of disorders presenting in infancy have also been described, termed ‘developmental macular dystrophies’, which may be further sub-classified to include a condition known as North Carolina Macular dystrophy (NCMD) [446].

There are a number of conditions with systemic associations that have been identified with drusen-like deposits at the macula. These include: membranoproliferative glomerulonephritis type 2, in which there are electron dense deposits in glomerular basement membranes and in Bruch's membrane, with associated renal failure [447]; Alport's syndrome, a predominantly X-linked condition associated with renal failure, deafness, anterior lenticonus and macular flecks [448]; Sjögren-Larsson syndrome, associated with a 'crystalline' maculopathy, spastic diplegia / tetraplegia and congenital ichthyosis [449]; and hereditary oxalosis due to multi-system calcium oxalate crystal deposition including the retina [450]. However, none of the subjects in this study had any such systemic associations. Purely ocular conditions with drusen-like deposits include: autosomal dominant drusen [451]; Bietti's crystalline maculopathy, characterised by crystalline deposits at the macula with areas of geographic atrophy; and Sorsby dystrophy which has autosomal dominant inheritance and marked loss of vision with extensive macular drusen and choroidal neovascularisation [452]. However the macular appearances described in this study appear quite different to these.

The phenotype associated with benign yellow dot dystrophy shares some similarities with the mildest cases of NCMD. This autosomal dominant condition, with variable expressivity, was first described by Lefler *et al*, who reported a single family that settled in North Carolina in the early 19th century, with amino aciduria and a macular dystrophy [453]. A number of families with NCMD without systemic associations have subsequently been reported and the phenotype extensively documented [454-462]. The macular appearances associated with NCMD demonstrate both inter- and

intra-familial variability, and have been categorised into 3 grades: Grade 1 - bilaterally symmetrical central macular yellow 'specks' less than 50 microns in diameter, associated with good visual acuity of 0.00 to 0.18 logMAR; Grade 2 – bilaterally symmetrical confluent yellow specks at the central macula with vision of 0.10 to 0.48 logMAR; Grade 3 – bilaterally symmetrical large colobomatous central macular lesions with visual acuity of 0.30 to 1.00 logMAR [67, 454, 463]. Grade 1 NCMD patients bear the most resemblance to the benign yellow dot dystrophy subjects reported in this study. However, the majority of the subjects in this study were sporadic. Those that were familial displayed none of the other clinical characteristics associated with NCMD.

The phenotype described here is mild and associated with excellent visual function. Fine hyperautofluorescent yellow dots, similar to drusen, are visible at the macula, which rarely extend beyond this area, unlike in NCMD [462]. The dots are distributed in the parafoveal areas, and may concentrate in the nasal parafovea. The underlying RPE and vasculature appear normal. In all subjects the optic disc appearance was within normal limits. However, in 96% of patients a yellow 'halo' surrounding the optic disc was observed, which in some resembled peripapillary atrophy, and which was associated with both hyper- and hypoautofluorescence on fundus autofluorescence imaging. Although myopia is associated with peripapillary atrophy, it was not a feature identified in these subjects. OCT imaging showed a subtle irregularity of the IS/OS junction. The inner retinal layers were normal, no drusen were seen and no serous detachments between the RPE and Bruch's membrane were visible. Electrophysiological studies of macular and full field retinal function were normal.

Through linkage analysis two loci have been identified that segregate with NCMD. Chromosome 6q was the first region identified to harbour the MCDR1 locus, the first area to be mapped to NCMD families [144, 464, 465]. Further refinement has identified a 1.86 million bp region between D6S1716 to D6S1671 [459] and a second locus, MCDR3, has been identified on chromosome 5p in subjects with a phenotype typical of NCMD [378, 466]. Despite a vast amount of work performed into this condition, the causative gene(s) remains to be identified.

It is possible that benign yellow dot dystrophy represents a variation of the phenotypic spectrum that has been described in NCMD. However, due to the sporadic nature of the majority of patients that have been identified and the fact that in the familial cases there are no cases with an atrophic macular phenotype, it is considered to be a separate clinical entity. Although two families identified in this study suggested an autosomal dominant mode of inheritance to their ocular condition, their phenotypes are not typical of NCMD. The precise aetiology for the condition described in this study remains to be determined. However, subjects can be reassured of the excellent visual function that is associated with this phenotype.

5.0 Discussion and Conclusions

5.1 The Childhood Onset Retinal

Dystrophy Study

The aims and objectives of this study were to recruit subjects with childhood onset retinal dystrophies to an on going investigation into the molecular genetic basis and phenotypic characteristics of inherited retinal disease in childhood. This study specifically aimed to characterise the phenotypes associated with variants in specific genes identified in these cohorts and of those previously recruited into the study, and to characterise any novel phenotypes among the subjects included in these cohorts. The overall aim was to undertake genotype – phenotype studies in order to enable more accurate information for prognostic and genetic counselling, that may, in turn, identify potential candidates who may be amenable to future therapeutic options.

Over a 3-year period, I recruited 201 subjects from 186 families into the Study. Subjects were categorised into two cohorts: (i) Cohort 1 - generalised retinal dystrophies that encompassed Leber congenital amaurosis (LCA), Early Onset Retinal Dystrophy (EORD), rod-cone dystrophies, cone-rod dystrophies and cone dystrophies, and (ii) Cohort 2 - childhood onset macular phenotypes that included Autosomal Recessive Bestrophinopathy (ARB) and benign Yellow Dot Dystrophy. 177 subjects from 166 families were recruited into cohort 1 and 24 subjects from 20 families into cohort 2. Access was also available to a database of patients that had been previously recruited into the study in order to re-investigate them if their molecular cause was identified. A number of subjects were recalled for phenotypic

studies based upon their molecular diagnosis, and this project succeeded in its aim of exploring, expanding and refining our understanding of the phenotypes associated with variants in specific genes.

The genetic heterogeneity that is associated with LCA and EORD was evident from the phenotypic and molecular studies undertaken in this project. The predominant molecular strategies utilised in this study were apex microarray using the Asper Biotech LCA chip and direct sequencing of candidate genes. These techniques were in widespread use at the time that this study was conducted, although they have now been surpassed by the next generation sequencing technologies. Apex microarray via the LCA chip was used as a 'first pass' screen in 107 subjects in cohort 1, which identified the causative gene in 29.9% of subjects that were sent from UCL to be screened with this technique. Of all the subjects in cohort 1 whose causative gene was identified using a variety of techniques, the LCA chip was responsible for 52.5%. It was a useful strategy to ascertain previously reported variants in genes that have been identified to cause LCA and EORD. New mutations in these genes would be missed using this technique. The efficacy of this technique has previously been investigated, with mutation identification in approximately 30% – 35% of patients analysed, and a higher rate of identification in LCA than EORD [109, 110, 122]. Despite a newer generation of this chip being used in this study, the overall success rate of gene identification was slightly less than these reports, and this is likely to reflect the higher percentage of EORD subjects analysed with this technology than LCA (47 LCA and 51 EORD subjects from UCL). However, in agreement with Henderson *et al.*, the chip was more informative for those carrying a diagnosis of LCA than EORD.

Molecular analysis using a variety of techniques identified the causative gene in 34.5% of all subjects in cohort 1. These genes were all previously known to be associated with LCA and EORD. However, using next generation sequencing, a family that had been previously recruited to the study was found to harbour a pathogenic mutation in a gene previously unreported in humans to cause early onset retinal dystrophy: *TUB*. The phenotype associated with this gene was investigated in detail in this study and adds to the clinical heterogeneity observed in LCA and EORD. To date it remains the only family in the literature with mutations in this gene [330]. The gene had long been thought to be a strong candidate for human retinal disease as there is a well characterised mouse model that has a severe retinal dystrophy [293, 295]. This thesis also reports the results of detailed phenotypic studies in a number of other genes including *LRAT*, *SPATA7*, *RGR* and *BEST1*; some of which only had limited descriptions prior to this study. In addition, this study revealed some new insights into the phenotype associated with other causative genes such as *LCA5* and *RDH12*. This will help inform affected individuals of their prognoses, aid clinicians in reaching diagnoses and provide information to aid in genetic counselling.

A large proportion of the families identified with mutations in this study were from consanguineous pedigrees. From some of the earliest studies into inherited diseases, the increased incidence of autosomal recessive disease in consanguineous families has been recognised [8, 467]. Molecular techniques have evolved to analyse regions of autozygosity that are presumed to harbour causative genes [104] and inbred populations are recognised to be very informative for gene identification in recessive diseases [468]. Four families reported in this study underwent autozygosity mapping that subsequently led to successful candidate gene screening in *LCA5*, *TULP1* and

SPATA7. The incidence of consanguinity was high in this study, with 10 families in cohort 1 whose mutations were identified and 7 other families who were recalled for phenotyping being consanguineous. In one consanguineous family (Subject 16, family 16), compound heterozygous mutations in *CRBI* were identified, highlighting the importance of avoiding the presumption that individuals will be homozygous if they have a consanguineous ancestry [469]. This individual underwent autozygosity mapping which failed to identify the causative gene. This was eventually identified to be *CRBI*, in the compound heterozygous state, by exome sequencing. On revisiting the phenotype in this individual, the clinical characteristics were typical of a rod-cone dystrophy due to mutations in *CRBI*. The incidence of consanguinity in the molecularly identified families was higher in those from South East Asia (11 families) and Middle Eastern countries (2 families), which reflects the high proportion of first and second cousin marriages that are traditional in these communities [103]. Consanguinity was also observed in European families, with 3 British Caucasian and 1 Irish consanguineous family among the molecularly identified families in this study.

5.2 Phenotypic heterogeneity in childhood onset retinal dystrophies

Phenotypic heterogeneity was identified in 5 genes that were identified in this study: *RDH12*, *RPE65*, *LCA5*, *AIPL1* and *BEST1*. The largest sub-group of subjects

identified had *RDH12* mutations (17 subjects, 15 families in cohort 1). This may be due to the easily recognisable fundus features, which allowed direct selection for *RDH12* screening. The phenotype varied with respect to the age of symptom onset, and therefore diagnosis, with 14 affected with EORD (symptom onset less than 5 years of age) and 3 with a rod cone dystrophy (symptom onset of at least 5 years of age). This heterogeneity was evident within families, with one family carrying two diagnoses based on the age of symptom onset. Although the retinal features were similar amongst those with *RDH12* retinopathy, with severe pigment clumping, dense macular atrophy and yellowing of the macula, some variability was present, such as para-arteriolar sparing of the pigmentation and a ‘colobomatous’ appearance to the macular atrophy. No genotype phenotype correlation was identified for the retinal features or age of symptom onset in *RDH12*.

RPE65 was also well represented in cohort 1. Again, this is likely to be due to the recognisable clinical signs, such as photophilia and minimal retinal changes, and the subsequent selective screening of *RPE65*. However, a spectrum of retinal features was noted in *RPE65*, including some with normal fundi, some with RPE atrophy and only one (the oldest subject) with retinal pigmentation and white dots at the macula. One subject displayed hypomorphic features with nyctalopia, normal vision, full visual fields and essentially normal retinas aside from peripheral RPE disturbance. He was a compound heterozygote, as were 5 of the 7 families identified with *RPE65* mutations, but the only subject to harbour a duplication on one allele. His c.1543C>T, p.Arg525Trp variant occurs late in the transcript, and his duplication, c.1067dupA, p.Asn356Lysfs*8 occurs beyond halfway in the transcript. Presumably this compound heterozygous mutation leads to some functional protein product. However,

comparison of the location of these variants to the other milder cases reported in the literature, which have occurred much earlier in the transcript, do not identify any true correlation between the location of the mutations and the severity of the phenotype [151, 161].

The small numbers of cases identified with mutations in both *AIPL1* and *LCA5* mean that no generalisations should be made from this study regarding the phenotypes associated with mutations in these genes. However, both of the subjects affected with mutations in each of these genes displayed quite different phenotypes to each other. In the two *LCA5* subjects this difference in retinal appearance may have been due to the different ages at which the subjects were examined – one was 8 years and the other 18 years old. Although *LCA5* mutations are frequently associated with widespread RPE atrophy, white dots in the retinal periphery and macular atrophy, other cases reported in the literature have also suggested that there is some degree of variability to the phenotype, with a similar disparity between young and older individuals to those individuals in this study [185, 339]. The fundi of both of the *AIPL1* subjects identified in this study were essentially normal, but their clinical features were quite different – one had typical LCA, the other was much more mildly affected with an EORD with cone rod dysfunction, again reflecting the clinical heterogeneity associated with EORDs.

The studies of subjects with mutations in *LRAT*, *RGR* and *SPATA7* have made a significant contribution to our knowledge of the phenotypes associated with these genes. Prior to this there were few detailed descriptions of these phenotypes. Mutations in the visual cycle gene *LRAT* are associated with a severe EORD with

poor vision, visual field constriction and nyctalopia from early childhood. Similarly to *RPE65*, there is photophilia in childhood. With age, there is deterioration in visual acuity, colour vision and contrast sensitivity. The retina is characterised by widespread RPE atrophy but little pigment migration, suggesting that photoreceptor cell death is a late feature [373]. Epi-retinal membrane formation and asteroid hyalosis are also more common. There is a severely reduced autofluorescence signal, which is a feature of retinal dystrophies due to visual cycle genes [158, 377, 378]. At a young age the OCT can identify a preserved photoreceptor layer and outer nuclear layer at the fovea, but these are lost with age. The nerve fibre layer is frequently irregular without any overlying vitreo-retinal traction. Kinetic perimetry identifies severe visual field constriction with preserved islands of vision. Dark-adapted psychophysical testing demonstrates reduced to undetectable rod function, with reduced but better preserved, cone function. The results of such detailed investigations had not been reported in *LRAT* retinopathy prior to this study. This study has demonstrated that the phenotype associated with mutations in *LRAT* is similar to that associated with mutations in *RPE65*, with an extended window for therapeutic intervention. *LRAT* and *RPE65* are both key proteins in the visual cycle that are both expressed in the RPE. Successful gene replacement therapies have been carried out in *RPE65* disease, which suggests that *LRAT* retinopathy is also a good candidate for gene replacement therapy [362, 363, 392, 393].

The phenotype in a family with mutations in another visual cycle gene, *RGR*, was investigated in this study. Mutations in this gene are very rare and there are only 2 reported families in the literature to date with mutations in this gene [292, 319]. This study has identified that *RGR* mutations are characterised by an EORD with

nyctalopia and visual field constriction, but with preservation of the central vision until the second decade. The retina displays widespread RPE atrophy with white dots in the periphery, minimal retinal pigmentation and macular atrophy involving the fovea. The OCT demonstrates preservation of the photoreceptor layer only at the fovea, and this correlates with the autofluorescence images, which show an annulus of hyperautofluorescence typical of RP [344].

This study identified that mutations in *SPATA7*, a ciliary gene, usually display a severe LCA phenotype, although milder features can occur [165, 166]. This heterogeneity was evident in this study within the same family, in which 2 brothers were affected to different degrees, with one displaying better preservation of his central vision, albeit with severe visual field constriction. The vision is generally extremely poor from infancy and progressively deteriorates. The retina displays widespread RPE atrophy, minimal retinal pigmentation and foveal sparing. The OCT can identify preserved photoreceptors at the fovea and autofluorescence imaging reflects this by demonstrating a hyperautofluorescent annulus. *SPATA7* represents another LCA / EORD gene that is associated with phenotypic variability as differences between individuals within a family harbouring the same mutation were observed. Although the cause for this was not clearly identified, it may be due to the influence of modifier alleles.

A number of genes identified in this study are important in the structure or function of cilia, and thus mutations in them contribute to the spectrum of conditions known as ‘ciliopathies’. Of the subjects that were phenotyped more closely, these included *TUB*, *TULP1* and *SPATA7*. The *TUB* family had systemic features of childhood

obesity, but no other systemic effects that have been identified in the Tubby mouse were identified in the affected family members. Unfortunately no other studies were possible in this family to ascertain smell acuity, hearing and other metabolic abnormalities. Further families will need to be identified and studied for this to be ascertained. The *TULP1* individuals in this study, in agreement with other studies, did not display any systemic features. This is to be expected, as the *TULP1* expression profile is purely retinal. The individuals with *SPATA7* mutations might have been expected to have infertility as the human protein has been identified as two transcripts – one predominantly expressed in the retina, cerebellum and whole brain, and another that is predominantly expressed in the testis. Although there were 3 affected males in the *SPATA7* group who had planned to have children, two did not have any difficulties conceiving, and only one had infertility due to a low spermatozoa count. It is possible that this may be due to a wider ‘ciliopathy’ secondary to his *SPATA7* mutations. Further studies would be required to ascertain this. The association of the ocular phenotype with fertility in these individuals is important to ascertain as this may influence choices to plan for families in the future. Clearly the association with systemic abnormalities in different ciliopathies, such as renal and neurological function in *CEP290* mutations, is important to recognise, manage and counsel patients about, once their causative mutation has been identified.

The ARB phenotypes in children identified in this study were interesting. Although there was some variability in the retinal features in that some displayed characteristic multifocal yellow sub-retinal deposits on a background of confluent sub-retinal change, and some had a more ‘classical’ Best disease appearance, the phenotype was clearly identifiable and differed from adults reported with the condition. The

electrodiagnostic findings observed in ARB children and their parents are fundamental to their diagnosis and allow distinction between the different *BEST1* related conditions, which will provide information both for prognosis and for accurate genetic counselling to these families.

One novel phenotype associated with fine drusen-like deposits at the macula was identified in this study, and the condition termed ‘benign yellow dot dystrophy’. As the name suggests, this condition appears to have a benign course and ocular function remains normal. Although it is predominantly a sporadic condition, some families have been identified, in whom the condition appears to segregate in an autosomal dominant manner. Although the condition bears some resemblance to mild North Carolina Macular Dystrophy, there are a number of differences that suggest that the phenotype described in this study is a novel entity. The causative gene is yet to be determined in these families.

5.3 Therapeutic options for childhood onset retinal dystrophies

One aim of this study was to identify subjects that may be amenable to new therapies for retinal dystrophies. These diseases, until recently, have been considered to be incurable. During the past few years exciting progress has been made into new

therapeutic techniques, predominantly into gene augmentation therapies, but also into oral pharmacologic therapies. As discussed in chapter 4.6, the first human phase 1b trials of an oral retinoid replacement therapy have been undertaken and promising initial results of improvements in visual fields and visual acuity were reported by the trial authors [392]. Two of the four *LRAT* subjects identified in the present study took part in this trial and their results are due to be published in a subsequent report. It will be interesting to see whether these compounds have an effect and are sustainable in these subjects, in whom the retinal degeneration is well established with significant, potentially irreversible, retinal damage.

Gene augmentation therapies in humans have become possible due to animal models of recessive retinal disease, through which proof-of-concept, safety and efficacy studies have been performed. In this regard, rodents provide a useful model as the effects of therapy can be ascertained fairly rapidly. The primary disadvantages of mouse models compared to humans are that they lack a well-defined cone dominated central retinal region, and due to the small size of the murine eye, different surgical approaches are required for gene delivery. Large animal models such as dogs and cats, many of which have naturally occurring mutations in retinal dystrophy genes, such as the Briard dog with an *RPE65* mutation and the Abyssinian cat with a *CEP290* splice defect, serve as useful models as they are anatomically more similar to humans than rodents [46]. Gene augmentation therapies utilise vectors to deliver DNA to target tissues, and a number of viral and non-viral vectors have been used in retinal gene therapy proof-of-concept studies [470]. Viral vectors include recombinant adeno-associated viruses (rAAVs) and lentiviruses. rAAVs generally target photoreceptors more efficiently than other vectors and induce a relatively benign

immune response; they are non-integrating and the transgene expression persists only for a few months. Lentiviruses are integrating vectors and mediate stable transgene expression, but there is a risk of insertional mutagenesis [46].

The first human gene augmentation therapies were carried out in subjects with LCA and *RPE65* mutations [362-364, 393, 471]. Subjects demonstrated both objective and subjective improvements in vision, and the extent of recovery was age dependent, with children having the greatest improvement. Further trials into *RPE65* gene therapy are on going, and human gene therapy trials into *MERTK* have begun (ClinicalTrials.gov Identifier: NCT01482195) [472]. However, one challenge is in ascertaining the stage of the disease process that intervention is most likely to be beneficial. In this regard, detailed phenotyping of the different genes that underlie retinal dystrophies is important as it can identify the extent of the degeneration and the age at which this degeneration occurs – if the gene is involved in photoreceptor differentiation then therapy may be required in infancy to maximise the chance of restoring and preserving vision [46]. In fact, treatment might be optimal in children below 3 years of age as the plasticity of the retinal and neurological pathways deteriorates beyond this age. It is predicted that the less severe the retinal phenotype in terms of structural damage, the more chance that gene therapy would be successful. However, promisingly, studies into gene therapy for other causes of retinal dystrophy, for example into *AIPL1*, have suggested that there may be rescue of photoreceptor degeneration in a more severe phenotype [335].

Another approach to gene augmentation therapy is in stem cell therapy for retinal degenerative disease, and a number of trials are currently recruiting subjects [473]. In

pre-clinical studies, both embryonic stem cells and induced pluripotent stem cells have been used to guide differentiation into cells that display many similarities to RPE cells, that can be transplanted to replace this monolayer which is frequently damaged in retinal diseases such as RP, Stargardt disease and age related macular degeneration. Childhood onset retinal dystrophies caused by genes that reside in the RPE, such as *RPE65*, *LRAT*, *RGR* and *BEST1* may be amenable to treatment with stem cell derived RPE in the future. The results from the first human clinical trials into RPE stem cell transplantation, including those using autologous human induced pluripotent stem cells, and the subsequent applications, are keenly anticipated.

5.4 Advances since this study was conducted

The most significant advances since this study was conducted have been in molecular analysis. Next generation sequencing technology has surpassed the molecular techniques that were routinely utilised to identify the molecular cause of disease in individuals with childhood onset retinal dystrophies. This has led the genetic cause being ‘solved’ in a number of families, and has identified novel genes.

The causative gene at the LCA9 locus remained undiscovered for many years, but was eventually identified in 2012, simultaneously by different groups using whole exome sequencing, to be *NMNAT1* [236-239]. *NMNAT1* encodes a rate-limiting enzyme that

generates NAD⁺ both in a biosynthetic pathway from nicotinic acid mononucleotide, and in a salvage pathway from nicotinamide mononucleotide [236]. It is involved in the nuclear NAD⁺ homeostasis that is necessary for both DNA metabolism and cell signalling. The phenotype is of severe LCA, with vision in the majority of patients of between hand movements and nil perception of light. There is dense pigmented macular atrophy, widespread RPE atrophy and peripheral pigment migration. Nine subjects from the childhood onset retinal dystrophy study from UCL were subsequently identified with mutations in *NMNAT1*, of which 4 were from cohort 1 in this study, and they contributed to one of the original *NMNAT1* LCA publications [236].

A second gene, *KCNJ13*, was also recently identified using a combination of homozygosity mapping and exome sequencing, to cause LCA in two families [327]. The proband of one of these families was in cohort 1 of the present study. *KCNJ13* encodes an inwardly rectifying potassium channel subunit, Kir7.1, which localises to the plasma membrane of a number of ion-transporting epithelia [327]. In the retina it primarily localises to the apical membrane of the RPE. Mutations in this gene have also been reported to cause another retinal dystrophy known as ‘snowflake vitreo-retinal degeneration’, but the phenotype associated with this and that associated with *KCNJ13* related LCA are quite different, once again highlighting the clinical heterogeneity associated with genes causing childhood onset retinal dystrophies.

The next generation sequencing technologies have vastly improved the ability and speed of identification of the molecular causes of genetic disease. As the costs of these technologies are rapidly falling they will lead to the discovery of a number of

novel genes and will quickly ‘solve’ many undetermined cases. Despite these predicted advances, accurate phenotyping of affected families still remains very important in these conditions.

The other major advance has been in therapeutics for retinal dystrophies. Some of the advances in gene augmentation therapy have been discussed in the previous section. However it is important not to ‘oversell’ the potential of gene therapy to patients who may wish to participate in future studies of gene therapy for retinal degeneration [46]. The successes of the *RPE65* trials were influenced by the mild retinal changes, presence of some useful vision early in life in some of these individuals and the location of the defective gene; in the future, gene augmentation therapy may not be as successful if the defect leads to severe functional and/or structural retinal changes or if it primarily affects the photoreceptors. In this situation, there is a fine balance between effective ‘dosage’ and toxicity, and the target therapy needs to involve as many photoreceptors as possible, which may prove to be technically challenging.

As the landscape of molecular technologies continues to evolve, next generation sequencing will provide many answers and lead to many more families having their molecular cause identified. In addition, advances in gene augmentation therapy are entering an exciting era in which effective treatments will become available for these, previously ‘incurable’ blinding conditions.

5.5 Conclusions and further work

Since Donders' and Leber's first descriptions of childhood onset retinal dystrophies, a vast body of work has been conducted to elucidate the molecular causes, clinical features and possible therapies for this heterogeneous group of conditions. Although the specific conditions that comprise this spectrum of diseases have been, and continue to be, characterised, confusion can lie in the specific clinical diagnoses, as there is often significant overlap between them. It is likely that, as the molecular causes are being identified, the classification of these conditions will progress to reflect the genetic cause, such as that which has occurred for the bestrophinopathies. Phenotypic studies have become invaluable at characterising these conditions, and allow accurate prognostic and genetic counselling to affected individuals and their families. Careful phenotyping is also very important in ascertaining disorders that may be suitable for clinical trials of novel therapies, and in identifying the optimal point in the disease process for which intervention is likely to have the greatest success.

Future research and clinical diagnostic work on the childhood onset retinal dystrophies will undoubtedly involve next generation sequencing technologies. These technologies, including whole exome sequencing, will identify novel mutations in known genes, novel genes for isolated retinal dystrophies and for retinal dystrophies with systemic associations. Although expected to be higher, it has been predicted that whole exome sequencing will lead to the molecular diagnosis in 55% of non-syndromic retinal dystrophies and 80% of syndromic retinal dystrophies [474]. Whole genome sequencing is likely to be adopted as the gold standard as costs come down.

This technique has better read depths of exomes and allows the identification of intronic variants that affect gene transcription. Phenotypic studies will become necessary once these genes have been identified. Detailed phenotyping, or ‘deep phenotyping’, involving conventional phenotypic techniques utilised in the present study, along with additional psychophysical testing such as microperimetry and adaptive optics, will be useful for selecting subjects for therapeutic trials and in identifying treatment effects. Such future molecular and phenotypic investigations are likely to benefit from large-scale collaborations, such as those that are currently underway into rare genetic diseases.

6.0 References

1. Donders, F.C., *Beiträge zur pathologischen Anatomie des Auges*. Archiv für Ophthalmologie, 1855. **2**(1): p. 106-118.
2. Franceschetti, A., J. Francois, and J. Babel, *Chorioretinal Heredodegenerations (An updated report of La Societe Francaise d'Ophthalmologie)*. 1974, Springfield, Illinois: Charles C Thomas. 1371.
3. von Graefe, A., *Vereinzelte Beobachtungen und Bemerkungen*. Archiv für Ophthalmologie, 1858. **4**(2): p. 250-253.
4. Duke-Elder, S. and J.H. Dobree, *Diseases of the Retina*. 1 ed. System of Ophthalmology, ed. S. Duke-Elder. Vol. X. 1967, London: Henry Kimpton. 878.
5. Daiger, S.P., L.S. Sullivan, and S.J. Bowne, *Genes and mutations causing retinitis pigmentosa*. Clin Genet, 2013. **84**(2): p. 132-41.
6. Hamel, C., *Retinitis pigmentosa*. Orphanet J Rare Dis, 2006. **1**: p. 40.
7. Daiger, S.P., S.J. Bowne, and L.S. Sullivan, *Perspective on genes and mutations causing retinitis pigmentosa*. Archives of ophthalmology, 2007. **125**(2): p. 151-8.
8. Garrod, A.E., *About Alkaptonuria*. Med Chir Trans, 1902. **85**: p. 69-78.
9. Freund, C.L., et al., *De novo mutations in the CRX homeobox gene associated with Leber congenital amaurosis*. Nature genetics, 1998. **18**(4): p. 311-2.
10. Branham, K., et al., *Mutations in RPGR and RP2 account for 15% of males with simplex retinal degenerative disease*. Investigative ophthalmology & visual science, 2012. **53**(13): p. 8232-7.
11. Mansergh, F.C., et al., *Retinitis pigmentosa and progressive sensorineural hearing loss caused by a C12258A mutation in the mitochondrial MTT2 gene*. American journal of human genetics, 1999. **64**(4): p. 971-85.
12. Crimi, M., et al., *A mitochondrial tRNA(His) gene mutation causing pigmentary retinopathy and neurosensorial deafness*. Neurology, 2003. **60**(7): p. 1200-3.
13. Moraes, C.T., et al., *Mitochondrial DNA deletions in progressive external ophthalmoplegia and Kearns-Sayre syndrome*. The New England journal of medicine, 1989. **320**(20): p. 1293-9.
14. Weleber, R.G., et al., *The phenotype of Severe Early Childhood Onset Retinal Dystrophy (SECORD) from mutation of RPE65 and differentiation from Leber congenital amaurosis*. Investigative ophthalmology & visual science, 2011. **52**(1): p. 292-302.
15. Schatz, P., et al., *Fundus albipunctatus associated with compound heterozygous mutations in RPE65*. Ophthalmology, 2011. **118**(5): p. 888-94.
16. von Leber, T., *Ueber Refinitis pigmentosa und angeborene Amaurose*. Graefe's archive for clinical and experimental ophthalmology = Albrecht von Graefes Archiv fur klinische und experimentelle Ophthalmologie, 1869. **15**(3): p. 1-25.
17. Waardenburg, P.J., *Congenital and Early Infantile Retinal Dysfunction (high-graded amblyopia and amaurosis Leber)*, in *Genetics and Ophthalmology*. 1963, Royal VanGorcum: Assen, Netherlands. p. 1567-1604.

18. Franceschetti, A. and P. Dieterle, [*Differential diagnostic significance of electroretinogram in tapeto-retinal degeneration*]. Bibliotheca ophthalmologica : supplementa ad ophthalmologica, 1957(48): p. 161-82.
19. Schappert-Kimmijser, J., H.E. Henkes, and J. Van Den Bosch, *Amaurosis congenita (Leber)*. AMA Arch Ophthalmol, 1959. **61**(2): p. 211-8.
20. Waardenburg, P.J., *Does agenesis or dysgenesis neuroepithelialis retinae, whether or not related to keratoglobus, exist?* Ophthalmologica. Journal international d'ophthalmologie. International journal of ophthalmology. Zeitschrift fur Augenheilkunde, 1957. **133**(6): p. 454-60; discussion, 460-1.
21. Alström, C.H. and O. Olson, *Heredo-retinopathia congenitalis monohybrida recessiva autosomalis*. Hereditas, 1957. **43**: p. 1-177.
22. Waardenburg, P.J. and J. Schappert-Kimmijser, *On Various Recessive Biotypes of Leber's Congenital Amaurosis*. Acta Ophthalmol (Copenh), 1963. **41**: p. 317-20.
23. Sorsby, A. and C.E. Williams, *Retinal Aplasia as a Clinical Entity*. Br Med J, 1960. **1**(5169): p. 293-7.
24. den Hollander, A.I., et al., *Leber congenital amaurosis: genes, proteins and disease mechanisms*. Progress in retinal and eye research, 2008. **27**(4): p. 391-419.
25. Rahi, J.S., N. Cable, and G. British Childhood Visual Impairment Study, *Severe visual impairment and blindness in children in the UK*. Lancet, 2003. **362**(9393): p. 1359-65.
26. den Hollander, A.I., et al., *Identification of novel mutations in patients with Leber congenital amaurosis and juvenile RP by genome-wide homozygosity mapping with SNP microarrays*. Investigative ophthalmology & visual science, 2007. **48**(12): p. 5690-8.
27. Paunescu, K., et al., *Longitudinal and cross-sectional study of patients with early-onset severe retinal dystrophy associated with RPE65 mutations*. Graefes archive for clinical and experimental ophthalmology = Albrecht von Graefes Archiv fur klinische und experimentelle Ophthalmologie, 2005. **243**(5): p. 417-26.
28. Ek, J., et al., *Peroxisomal dysfunction in a boy with neurologic symptoms and amaurosis (Leber disease): clinical and biochemical findings similar to those observed in Zellweger syndrome*. J Pediatr, 1986. **108**(1): p. 19-24.
29. De Laey, J.J., *The eye of Vesalius*. Acta ophthalmologica, 2011. **89**(3): p. 293-300.
30. Kolb, H. *Simple anatomy of the retina*. 2015 [26.04.2015]; Available from: <http://webvision.med.utah.edu/book/part-i-foundations/simple-anatomy-of-the-retina/>.
31. Anstis, S., *The Purkinje rod-cone shift as a function of luminance and retinal eccentricity*. Vision research, 2002. **42**(22): p. 2485-91.
32. Liu, Q., et al., *The proteome of the mouse photoreceptor sensory cilium complex*. Mol Cell Proteomics, 2007. **6**(8): p. 1299-317.
33. Rachel, R.A., T. Li, and A. Swaroop, *Photoreceptor sensory cilia and ciliopathies: focus on CEP290, RPGR and their interacting proteins*. Cilia, 2012. **1**(1): p. 22.
34. Westheimer, G., *Directional sensitivity of the retina: 75 years of Stiles-Crawford effect*. Proc Biol Sci, 2008. **275**(1653): p. 2777-86.
35. Kevany, B.M. and K. Palczewski, *Phagocytosis of retinal rod and cone photoreceptors*. Physiology, 2010. **25**(1): p. 8-15.

36. Masland, R.H., *The neuronal organization of the retina*. Neuron, 2012. **76**(2): p. 266-80.
37. Reichenbach, A. and A. Bringmann, *New functions of Muller cells*. Glia, 2013. **61**(5): p. 651-78.
38. Strauss, O., *The retinal pigment epithelium in visual function*. Physiol Rev, 2005. **85**(3): p. 845-81.
39. Fain, G.L., *Why photoreceptors die (and why they don't)*. BioEssays : news and reviews in molecular, cellular and developmental biology, 2006. **28**(4): p. 344-54.
40. Kefalov, V.J., *Rod and cone visual pigments and phototransduction through pharmacological, genetic, and physiological approaches*. The Journal of biological chemistry, 2012. **287**(3): p. 1635-41.
41. Wang, J.S. and V.J. Kefalov, *The cone-specific visual cycle*. Progress in retinal and eye research, 2011. **30**(2): p. 115-28.
42. Lamb, T.D. and E.N. Pugh, Jr., *Phototransduction, dark adaptation, and rhodopsin regeneration the proctor lecture*. Investigative ophthalmology & visual science, 2006. **47**(12): p. 5137-52.
43. Parker, R.O. and R.K. Crouch, *Retinol dehydrogenases (RDHs) in the visual cycle*. Experimental eye research, 2010. **91**(6): p. 788-92.
44. Chen, C., D.A. Thompson, and Y. Koutalos, *Reduction of all-trans-retinal in vertebrate rod photoreceptors requires the combined action of RDH8 and RDH12*. The Journal of biological chemistry, 2012. **287**(29): p. 24662-70.
45. Littink, K.W., et al., *A homozygous frameshift mutation in LRAT causes retinitis punctata albescens*. Ophthalmology, 2012. **119**(9): p. 1899-906.
46. den Hollander, A.I., et al., *Lighting a candle in the dark: advances in genetics and gene therapy of recessive retinal dystrophies*. The Journal of clinical investigation, 2010. **120**(9): p. 3042-53.
47. Fleisch, V.C. and S.C. Neuhauss, *Parallel visual cycles in the zebrafish retina*. Progress in retinal and eye research, 2010. **29**(6): p. 476-86.
48. Jones, G.J., et al., *Retinoid requirements for recovery of sensitivity after visual-pigment bleaching in isolated photoreceptors*. Proceedings of the National Academy of Sciences of the United States of America, 1989. **86**(23): p. 9606-10.
49. Mata, N.L., et al., *Isomerization and oxidation of vitamin a in cone-dominant retinas: a novel pathway for visual-pigment regeneration in daylight*. Neuron, 2002. **36**(1): p. 69-80.
50. Miyazono, S., et al., *Highly efficient retinal metabolism in cones*. Proceedings of the National Academy of Sciences of the United States of America, 2008. **105**(41): p. 16051-6.
51. Bailey, I.L. and J.E. Lovie, *New design principles for visual acuity letter charts*. Am J Optom Physiol Opt, 1976. **53**(11): p. 740-5.
52. Holladay, J.T., *Visual acuity measurements*. J Cataract Refract Surg, 2004. **30**(2): p. 287-90.
53. Henderson, R.H., et al., *Phenotypic variability in patients with retinal dystrophies due to mutations in CRB1*. The British journal of ophthalmology, 2010.
54. Cole, B.L., *Assessment of inherited colour vision defects in clinical practice*. Clin Exp Optom, 2007. **90**(3): p. 157-75.
55. Birch, J., *Diagnosis of Defective Colour Vision*. Second ed. 2001, Oxford: Reed Educational and Professional Publishing Ltd. 149.

56. Wright, W.D., *Diagnostic tests for colour vision*. Ann R Coll Surg Engl, 1957. **20**(3): p. 177-91.
57. Grover, S., G.A. Fishman, and J. Brown, Jr., *Patterns of visual field progression in patients with retinitis pigmentosa*. Ophthalmology, 1998. **105**(6): p. 1069-75.
58. Iannaccone, A. and M.A. Zarbin, *A new era in medical therapy for retinal degenerative disease?* Lancet, 2014. **384**(9953): p. 1482-4.
59. Marmor, M.F., et al., *ISCEV standard for clinical electro-oculography (2010 update)*. Documenta ophthalmologica. Advances in ophthalmology, 2011. **122**(1): p. 1-7.
60. Marmor, M.F., et al., *ISCEV Standard for full-field clinical electroretinography (2008 update)*. Documenta ophthalmologica. Advances in ophthalmology, 2009. **118**(1): p. 69-77.
61. Bach, M., et al., *ISCEV standard for clinical pattern electroretinography (PERG): 2012 update*. Documenta ophthalmologica. Advances in ophthalmology, 2013. **126**(1): p. 1-7.
62. Odom, J.V., et al., *ISCEV standard for clinical visual evoked potentials (2009 update)*. Documenta ophthalmologica. Advances in ophthalmology, 2010. **120**(1): p. 111-9.
63. Hood, D.C., et al., *ISCEV standard for clinical multifocal electroretinography (mfERG) (2011 edition)*. Documenta ophthalmologica. Advances in ophthalmology, 2012. **124**(1): p. 1-13.
64. Kriss, A., *Skin ERGs: their effectiveness in paediatric visual assessment, confounding factors, and comparison with ERGs recorded using various types of corneal electrode*. Int J Psychophysiol, 1994. **16**(2-3): p. 137-46.
65. Kriss, A. and I. Russell-Eggitt, *Electrophysiological assessment of visual pathway function in infants*. Eye, 1992. **6** (Pt 2): p. 145-53.
66. Lambert, S.R., et al., *Follow-up and diagnostic reappraisal of 75 patients with Leber's congenital amaurosis*. American journal of ophthalmology, 1989. **107**(6): p. 624-31.
67. Huang, D., et al., *Optical coherence tomography*. Science, 1991. **254**(5035): p. 1178-81.
68. Drexler, W., et al., *In vivo ultrahigh-resolution optical coherence tomography*. Optics letters, 1999. **24**(17): p. 1221-3.
69. Drexler, W., et al., *Ultrahigh-resolution ophthalmic optical coherence tomography*. Nature medicine, 2001. **7**(4): p. 502-7.
70. Wojtkowski, M., et al., *Three-dimensional retinal imaging with high-speed ultrahigh-resolution optical coherence tomography*. Ophthalmology, 2005. **112**(10): p. 1734-46.
71. HeidelbergEngineering. [cited 2015 24.01.2015]; Available from: <http://www.heidelbergengineering.com/international/products/spectralis/technology/spectral-domain-oct/>.
72. Castro Lima, V., et al., *Simultaneous confocal scanning laser ophthalmoscopy combined with high-resolution spectral-domain optical coherence tomography: a review*. J Ophthalmol, 2011. **2011**: p. 743670.
73. Delori, F.C., D.G. Goger, and C.K. Dorey, *Age-related accumulation and spatial distribution of lipofuscin in RPE of normal subjects*. Investigative ophthalmology & visual science, 2001. **42**(8): p. 1855-66.

74. Feeney, L., *Lipofuscin and melanin of human retinal pigment epithelium. Fluorescence, enzyme cytochemical, and ultrastructural studies*. Investigative ophthalmology & visual science, 1978. **17**(7): p. 583-600.
75. Kellner, S., et al., *Lipofuscin- and melanin-related fundus autofluorescence in patients with ABCA4-associated retinal dystrophies*. American journal of ophthalmology, 2009. **147**(5): p. 895-902, 902 e1.
76. Ferrara, D.C., et al., *Multimodal fundus imaging in Best vitelliform macular dystrophy*. Graefes archive for clinical and experimental ophthalmology = Albrecht von Graefes Archiv fur klinische und experimentelle Ophthalmologie, 2010. **248**(10): p. 1377-86.
77. Eldred, G.E. and M.L. Katz, *Fluorophores of the human retinal pigment epithelium: separation and spectral characterization*. Experimental eye research, 1988. **47**(1): p. 71-86.
78. Schutt, F., et al., *Photodamage to human RPE cells by A2-E, a retinoid component of lipofuscin*. Investigative ophthalmology & visual science, 2000. **41**(8): p. 2303-8.
79. Delori, F.C., et al., *In vivo fluorescence of the ocular fundus exhibits retinal pigment epithelium lipofuscin characteristics*. Investigative ophthalmology & visual science, 1995. **36**(3): p. 718-29.
80. von Ruckmann, A., F.W. Fitzke, and A.C. Bird, *Distribution of fundus autofluorescence with a scanning laser ophthalmoscope*. The British journal of ophthalmology, 1995. **79**(5): p. 407-12.
81. Jorzik, J.J., et al., *Digital simultaneous fluorescein and indocyanine green angiography, autofluorescence, and red-free imaging with a solid-state laser-based confocal scanning laser ophthalmoscope*. Retina, 2005. **25**(4): p. 405-16.
82. Schmitz-Valckenberg, S., et al., *Fundus autofluorescence imaging: review and perspectives*. Retina, 2008. **28**(3): p. 385-409.
83. Abramoff, M.D., M.K. Garvin, and M. Sonka, *Retinal Imaging and Image Analysis*. IEEE Trans Med Imaging, 2010. **3**: p. 169-208.
84. Allen, L., *Ocular Fundus Photography: Suggestions for Achieving Consistently Good Pictures and Instructions for Stereoscopic Photography*. American journal of ophthalmology, 1964. **57**: p. 13-28.
85. Mendel, G., *Versuche über Pflanzenhybriden*. Verhandlungen des naturforschenden Vereines in Brünn, Bd. IV für das Jahr 1865, 1865: p. 3-47.
86. Bateson, W., E.R. Saunders, and R.C. Punnett, *Experimental studies in the physiology of heredity*. Reports to the Evolution Committee of the Royal Society, 1905. **2**: p. 1-55, 80-99.
87. Morgan, T.H., *Sex Limited Inheritance in Drosophila*. Science, 1910. **32**(812): p. 120-2.
88. Morgan, T.H., *Random Segregation Versus Coupling in Mendelian Inheritance*. Science, 1911. **34**(873): p. 384.
89. Sturtevant, A.H., *The linear arrangement of six sex-linked factors in Drosophila, as shown by their mode of association* Journal of Experimental Zoology, 1913. **14**(1): p. 43-59.
90. Pulst, S.M., *Genetic linkage analysis*. Arch Neurol, 1999. **56**(6): p. 667-72.
91. Sachidanandam, R., et al., *A map of human genome sequence variation containing 1.42 million single nucleotide polymorphisms*. Nature, 2001. **409**(6822): p. 928-33.

92. Saiki, R.K., et al., *Enzymatic amplification of beta-globin genomic sequences and restriction site analysis for diagnosis of sickle cell anemia*. Science, 1985. **230**(4732): p. 1350-4.
93. Mullis, K.B. and F.A. Faloona, *Specific synthesis of DNA in vitro via a polymerase-catalyzed chain reaction*. Methods in enzymology, 1987. **155**: p. 335-50.
94. Saiki, R.K., et al., *Primer-directed enzymatic amplification of DNA with a thermostable DNA polymerase*. Science, 1988. **239**(4839): p. 487-91.
95. Sanger, F., S. Nicklen, and A.R. Coulson, *DNA sequencing with chain-terminating inhibitors*. Proceedings of the National Academy of Sciences of the United States of America, 1977. **74**(12): p. 5463-7.
96. Smith, L.M., et al., *Fluorescence detection in automated DNA sequence analysis*. Nature, 1986. **321**(6071): p. 674-9.
97. Dovichi, N.J., *DNA sequencing by capillary electrophoresis*. Electrophoresis, 1997. **18**(12-13): p. 2393-9.
98. Fodor, S.P., et al., *Multiplexed biochemical assays with biological chips*. Nature, 1993. **364**(6437): p. 555-6.
99. Pease, A.C., et al., *Light-generated oligonucleotide arrays for rapid DNA sequence analysis*. Proceedings of the National Academy of Sciences of the United States of America, 1994. **91**(11): p. 5022-6.
100. Chee, M., et al., *Accessing genetic information with high-density DNA arrays*. Science, 1996. **274**(5287): p. 610-4.
101. Lockhart, D.J., et al., *Expression monitoring by hybridization to high-density oligonucleotide arrays*. Nat Biotechnol, 1996. **14**(13): p. 1675-80.
102. Schena, M., et al., *Quantitative monitoring of gene expression patterns with a complementary DNA microarray*. Science, 1995. **270**(5235): p. 467-70.
103. Alkuraya, F.S., *Autozygome decoded*. Genet Med, 2010. **12**(12): p. 765-71.
104. Lander, E.S. and D. Botstein, *Homozygosity mapping: a way to map human recessive traits with the DNA of inbred children*. Science, 1987. **236**(4808): p. 1567-70.
105. Weber, J.L. and P.E. May, *Abundant class of human DNA polymorphisms which can be typed using the polymerase chain reaction*. American journal of human genetics, 1989. **44**(3): p. 388-96.
106. Woods, C.G., et al., *A new method for autozygosity mapping using single nucleotide polymorphisms (SNPs) and EXCLUDEAR*. Journal of medical genetics, 2004. **41**(8): p. e101.
107. Pastinen, T., et al., *Minisequencing: a specific tool for DNA analysis and diagnostics on oligonucleotide arrays*. Genome research, 1997. **7**(6): p. 606-14.
108. Shumaker, J.M., A. Metspalu, and C.T. Caskey, *Mutation detection by solid phase primer extension*. Human mutation, 1996. **7**(4): p. 346-54.
109. Zernant, J., et al., *Genotyping microarray (disease chip) for Leber congenital amaurosis: detection of modifier alleles*. Investigative ophthalmology & visual science, 2005. **46**(9): p. 3052-9.
110. Henderson, R.H., et al., *An assessment of the apex microarray technology in genotyping patients with Leber congenital amaurosis and early-onset severe retinal dystrophy*. Investigative ophthalmology & visual science, 2007. **48**(12): p. 5684-9.
111. International Human Genome Sequencing, C., *Finishing the euchromatic sequence of the human genome*. Nature, 2004. **431**(7011): p. 931-45.

112. Mardis, E.R., *Next-generation sequencing platforms*. Annu Rev Anal Chem (Palo Alto Calif), 2013. **6**: p. 287-303.
113. Camuzat, A., et al., *A gene for Leber's congenital amaurosis maps to chromosome 17p*. Human molecular genetics, 1995. **4**(8): p. 1447-52.
114. Perrault, I., et al., *Retinal-specific guanylate cyclase gene mutations in Leber's congenital amaurosis*. Nature genetics, 1996. **14**(4): p. 461-4.
115. Perrault, I., et al., *Spectrum of retGCI mutations in Leber's congenital amaurosis*. European journal of human genetics : EJHG, 2000. **8**(8): p. 578-82.
116. Perrault, I., et al., *Different functional outcome of RetGCI and RPE65 gene mutations in Leber congenital amaurosis*. American journal of human genetics, 1999. **64**(4): p. 1225-8.
117. Sitorus, R.S., B. Lorenz, and M.N. Preising, *Analysis of three genes in Leber congenital amaurosis in Indonesian patients*. Vision research, 2003. **43**(28): p. 3087-93.
118. Vallespin, E., et al., *Mutation screening of 299 Spanish families with retinal dystrophies by Leber congenital amaurosis genotyping microarray*. Investigative ophthalmology & visual science, 2007. **48**(12): p. 5653-61.
119. Simonelli, F., et al., *Clinical and molecular genetics of Leber's congenital amaurosis: a multicenter study of Italian patients*. Investigative ophthalmology & visual science, 2007. **48**(9): p. 4284-90.
120. Dharmaraj, S.R., et al., *Mutational analysis and clinical correlation in Leber congenital amaurosis*. Ophthalmic genetics, 2000. **21**(3): p. 135-50.
121. Lotery, A.J., et al., *Mutation analysis of 3 genes in patients with Leber congenital amaurosis*. Archives of ophthalmology, 2000. **118**(4): p. 538-43.
122. Yzer, S., et al., *Microarray-based mutation detection and phenotypic characterization of patients with Leber congenital amaurosis*. Investigative ophthalmology & visual science, 2006. **47**(3): p. 1167-76.
123. Booij, J.C., et al., *Identification of mutations in the AIPL1, CRB1, GUCY2D, RPE65, and RPGRIP1 genes in patients with juvenile retinitis pigmentosa*. Journal of medical genetics, 2005. **42**(11): p. e67.
124. Hanein, S., et al., *Leber congenital amaurosis: comprehensive survey of the genetic heterogeneity, refinement of the clinical definition, and genotype-phenotype correlations as a strategy for molecular diagnosis*. Human mutation, 2004. **23**(4): p. 306-17.
125. Smith, M., et al., *Phenotype of autosomal dominant cone-rod dystrophy due to the R838C mutation of the GUCY2D gene encoding retinal guanylate cyclase-1*. Eye, 2007. **21**(9): p. 1220-5.
126. Downes, S.M., et al., *Autosomal dominant cone-rod dystrophy with mutations in the guanylate cyclase 2D gene encoding retinal guanylate cyclase-1*. Archives of ophthalmology, 2001. **119**(11): p. 1667-73.
127. Gregory-Evans, K., et al., *Autosomal dominant cone-rod retinal dystrophy (CORD6) from heterozygous mutation of GUCY2D, which encodes retinal guanylate cyclase*. Ophthalmology, 2000. **107**(1): p. 55-61.
128. Payne, A.M., et al., *Clustering and frequency of mutations in the retinal guanylate cyclase (GUCY2D) gene in patients with dominant cone-rod dystrophies*. Journal of medical genetics, 2001. **38**(9): p. 611-4.
129. Tucker, C.L., et al., *Functional analyses of mutant recessive GUCY2D alleles identified in Leber congenital amaurosis patients: protein domain*

- comparisons and dominant negative effects*. *Molecular vision*, 2004. **10**: p. 297-303.
130. Hamel, C.P., et al., *A developmentally regulated microsomal protein specific for the pigment epithelium of the vertebrate retina*. *Journal of neuroscience research*, 1993. **34**(4): p. 414-25.
 131. Hamel, C.P., et al., *Molecular cloning and expression of RPE65, a novel retinal pigment epithelium-specific microsomal protein that is post-transcriptionally regulated in vitro*. *The Journal of biological chemistry*, 1993. **268**(21): p. 15751-7.
 132. Hamel, C.P., et al., *The gene for the retinal pigment epithelium-specific protein RPE65 is localized to human 1p31 and mouse 3*. *Genomics*, 1994. **20**(3): p. 509-12.
 133. Nicoletti, A., et al., *Molecular characterization of the human gene encoding an abundant 61 kDa protein specific to the retinal pigment epithelium*. *Human molecular genetics*, 1995. **4**(4): p. 641-9.
 134. Moiseyev, G., et al., *RPE65 is the isomerohydrolase in the retinoid visual cycle*. *Proceedings of the National Academy of Sciences of the United States of America*, 2005. **102**(35): p. 12413-8.
 135. Jin, M., et al., *Rpe65 is the retinoid isomerase in bovine retinal pigment epithelium*. *Cell*, 2005. **122**(3): p. 449-59.
 136. Redmond, T.M., et al., *Mutation of key residues of RPE65 abolishes its enzymatic role as isomerohydrolase in the visual cycle*. *Proceedings of the National Academy of Sciences of the United States of America*, 2005. **102**(38): p. 13658-63.
 137. Znoiko, S.L., et al., *Identification of the RPE65 protein in mammalian cone photoreceptors*. *Investigative ophthalmology & visual science*, 2002. **43**(5): p. 1604-9.
 138. Takahashi, Y., et al., *An alternative isomerohydrolase in the retinal Muller cells of a cone-dominant species*. *The FEBS journal*, 2011.
 139. Parker, R., et al., *Interphotoreceptor retinoid-binding protein as the physiologically relevant carrier of 11-cis-retinol in the cone visual cycle*. *The Journal of neuroscience : the official journal of the Society for Neuroscience*, 2011. **31**(12): p. 4714-9.
 140. Pang, J.J., et al., *Retinal degeneration 12 (rd12): a new, spontaneously arising mouse model for human Leber congenital amaurosis (LCA)*. *Molecular vision*, 2005. **11**: p. 152-62.
 141. Aguirre, G.D., et al., *Congenital stationary night blindness in the dog: common mutation in the RPE65 gene indicates founder effect*. *Molecular vision*, 1998. **4**: p. 23.
 142. Narfstrom, K., A. Wrigstad, and S.E. Nilsson, *The Briard dog: a new animal model of congenital stationary night blindness*. *The British journal of ophthalmology*, 1989. **73**(9): p. 750-6.
 143. Redmond, T.M., et al., *Rpe65 is necessary for production of 11-cis-vitamin A in the retinal visual cycle*. *Nature genetics*, 1998. **20**(4): p. 344-51.
 144. Nilsson, S.E., A. Wrigstad, and K. Narfstrom, *Changes in the DC electroretinogram in Briard dogs with hereditary congenital night blindness and partial day blindness*. *Experimental eye research*, 1992. **54**(2): p. 291-6.
 145. Wrigstad, A., S.E. Nilsson, and K. Narfstrom, *Ultrastructural changes of the retina and the retinal pigment epithelium in Briard dogs with hereditary*

- congenital night blindness and partial day blindness*. Experimental eye research, 1992. **55**(6): p. 805-18.
146. Veske, A., et al., *Retinal dystrophy of Swedish briard/briard-beagle dogs is due to a 4-bp deletion in RPE65*. Genomics, 1999. **57**(1): p. 57-61.
 147. Samardzija, M., et al., *R91W mutation in Rpe65 leads to milder early-onset retinal dystrophy due to the generation of low levels of 11-cis-retinal*. Human molecular genetics, 2008. **17**(2): p. 281-92.
 148. Marlhens, F., et al., *Mutations in RPE65 cause Leber's congenital amaurosis*. Nature genetics, 1997. **17**(2): p. 139-41.
 149. Gu, S.M., et al., *Mutations in RPE65 cause autosomal recessive childhood-onset severe retinal dystrophy*. Nature genetics, 1997. **17**(2): p. 194-7.
 150. Morimura, H., et al., *Mutations in the RPE65 gene in patients with autosomal recessive retinitis pigmentosa or leber congenital amaurosis*. Proceedings of the National Academy of Sciences of the United States of America, 1998. **95**(6): p. 3088-93.
 151. Thompson, D.A., et al., *Genetics and phenotypes of RPE65 mutations in inherited retinal degeneration*. Investigative ophthalmology & visual science, 2000. **41**(13): p. 4293-9.
 152. Thompson, D.A. and A. Gal, *Vitamin A metabolism in the retinal pigment epithelium: genes, mutations, and diseases*. Progress in retinal and eye research, 2003. **22**(5): p. 683-703.
 153. Lorenz, B., et al., *Early-onset severe rod-cone dystrophy in young children with RPE65 mutations*. Investigative ophthalmology & visual science, 2000. **41**(9): p. 2735-42.
 154. Hamel, C.P., et al., *Retinal dystrophies caused by mutations in RPE65: assessment of visual functions*. The British journal of ophthalmology, 2001. **85**(4): p. 424-7.
 155. Yzer, S., et al., *A Tyr368His RPE65 founder mutation is associated with variable expression and progression of early onset retinal dystrophy in 10 families of a genetically isolated population*. Journal of medical genetics, 2003. **40**(9): p. 709-13.
 156. El Matri, L., et al., *Phenotype of three consanguineous Tunisian families with early-onset retinal degeneration caused by an R91W homozygous mutation in the RPE65 gene*. Graefe's archive for clinical and experimental ophthalmology = Albrecht von Graefes Archiv fur klinische und experimentelle Ophthalmologie, 2006. **244**(9): p. 1104-12.
 157. Felius, J., et al., *Clinical course and visual function in a family with mutations in the RPE65 gene*. Archives of ophthalmology, 2002. **120**(1): p. 55-61.
 158. Lorenz, B., et al., *Lack of fundus autofluorescence to 488 nanometers from childhood on in patients with early-onset severe retinal dystrophy associated with mutations in RPE65*. Ophthalmology, 2004. **111**(8): p. 1585-94.
 159. Jacobson, S.G., et al., *Photoreceptor layer topography in children with leber congenital amaurosis caused by RPE65 mutations*. Investigative ophthalmology & visual science, 2008. **49**(10): p. 4573-7.
 160. Marlhens, F., et al., *Autosomal recessive retinal dystrophy associated with two novel mutations in the RPE65 gene*. European journal of human genetics : EJHG, 1998. **6**(5): p. 527-31.
 161. Lorenz, B., et al., *A comprehensive clinical and biochemical functional study of a novel RPE65 hypomorphic mutation*. Investigative ophthalmology & visual science, 2008. **49**(12): p. 5235-42.

162. Stockton, D.W., et al., *A novel locus for Leber congenital amaurosis on chromosome 14q24*. Human genetics, 1998. **103**(3): p. 328-33.
163. Wang, H., et al., *Mutations in SPATA7 cause Leber congenital amaurosis and juvenile retinitis pigmentosa*. American journal of human genetics, 2009. **84**(3): p. 380-7.
164. Zhang, X., et al., *A novel gene, RSD-3/HSD-3.1, encodes a meiotic-related protein expressed in rat and human testis*. Journal of molecular medicine, 2003. **81**(6): p. 380-7.
165. Mackay, D.S., et al., *Screening of SPATA7 in patients with Leber congenital amaurosis and severe childhood-onset retinal dystrophy reveals disease-causing mutations*. Investigative ophthalmology & visual science, 2011. **52**(6): p. 3032-8.
166. Perrault, I., et al., *Spectrum of SPATA7 mutations in Leber congenital amaurosis and delineation of the associated phenotype*. Human mutation, 2010. **31**(3): p. E1241-50.
167. Hameed, A., et al., *A novel locus for Leber congenital amaurosis (LCA4) with anterior keratoconus mapping to chromosome 17p13*. Investigative ophthalmology & visual science, 2000. **41**(3): p. 629-33.
168. Sohocki, M.M., et al., *Mutations in a new photoreceptor-pineal gene on 17p cause Leber congenital amaurosis*. Nature genetics, 2000. **24**(1): p. 79-83.
169. Ma, Q. and J.P. Whitlock, Jr., *A novel cytoplasmic protein that interacts with the Ah receptor, contains tetratricopeptide repeat motifs, and augments the transcriptional response to 2,3,7,8-tetrachlorodibenzo-p-dioxin*. The Journal of biological chemistry, 1997. **272**(14): p. 8878-84.
170. van der Spuy, J., et al., *The Leber congenital amaurosis gene product AIPL1 is localized exclusively in rod photoreceptors of the adult human retina*. Human molecular genetics, 2002. **11**(7): p. 823-31.
171. van der Spuy, J., et al., *The expression of the Leber congenital amaurosis protein AIPL1 coincides with rod and cone photoreceptor development*. Investigative ophthalmology & visual science, 2003. **44**(12): p. 5396-403.
172. van der Spuy, J. and M.E. Cheetham, *Role of AIP and its homologue the blindness-associated protein AIPL1 in regulating client protein nuclear translocation*. Biochemical Society transactions, 2004. **32**(Pt 4): p. 643-5.
173. Ramamurthy, V., et al., *AIPL1, a protein implicated in Leber's congenital amaurosis, interacts with and aids in processing of farnesylated proteins*. Proceedings of the National Academy of Sciences of the United States of America, 2003. **100**(22): p. 12630-5.
174. van der Spuy, J., *Focus on molecules: the aryl hydrocarbon receptor interacting protein-like 1 (AIPL1)*. Experimental eye research, 2006. **83**(6): p. 1307-8.
175. Liu, X., et al., *AIPL1, the protein that is defective in Leber congenital amaurosis, is essential for the biosynthesis of retinal rod cGMP phosphodiesterase*. Proceedings of the National Academy of Sciences of the United States of America, 2004. **101**(38): p. 13903-8.
176. Ramamurthy, V., et al., *Leber congenital amaurosis linked to AIPL1: a mouse model reveals destabilization of cGMP phosphodiesterase*. Proceedings of the National Academy of Sciences of the United States of America, 2004. **101**(38): p. 13897-902.

177. Hidalgo-de-Quintana, J., et al., *The Leber congenital amaurosis protein AIPL1 functions as part of a chaperone heterocomplex*. Investigative ophthalmology & visual science, 2008. **49**(7): p. 2878-87.
178. Kirschman, L.T., et al., *The Leber congenital amaurosis protein, AIPL1, is needed for the viability and functioning of cone photoreceptor cells*. Human molecular genetics, 2010. **19**(6): p. 1076-87.
179. Jacobson, S.G., et al., *Human retinal disease from AIPL1 gene mutations: foveal cone loss with minimal macular photoreceptors and rod function remaining*. Investigative ophthalmology & visual science, 2011. **52**(1): p. 70-9.
180. Testa, F., et al., *Evaluation of Italian Patients with Leber Congenital Amaurosis due to AIPL1 Mutations Highlights the Potential Applicability of Gene Therapy*. Investigative ophthalmology & visual science, 2011. **52**(8): p. 5618-24.
181. Dharmaraj, S., et al., *The phenotype of Leber congenital amaurosis in patients with AIPL1 mutations*. Archives of ophthalmology, 2004. **122**(7): p. 1029-37.
182. Galvin, J.A., et al., *Evaluation of genotype-phenotype associations in leber congenital amaurosis*. Retina, 2005. **25**(7): p. 919-29.
183. Walia, S., et al., *Visual acuity in patients with Leber's congenital amaurosis and early childhood-onset retinitis pigmentosa*. Ophthalmology, 2010. **117**(6): p. 1190-8.
184. Dharmaraj, S., et al., *A novel locus for Leber congenital amaurosis maps to chromosome 6q*. American journal of human genetics, 2000. **66**(1): p. 319-26.
185. Mohamed, M.D., et al., *Progression of phenotype in Leber's congenital amaurosis with a mutation at the LCA5 locus*. The British journal of ophthalmology, 2003. **87**(4): p. 473-5.
186. den Hollander, A.I., et al., *Mutations in LCA5, encoding the ciliary protein lebercilin, cause Leber congenital amaurosis*. Nature genetics, 2007. **39**(7): p. 889-95.
187. Boldt, K., et al., *Disruption of intraflagellar protein transport in photoreceptor cilia causes Leber congenital amaurosis in humans and mice*. The Journal of clinical investigation, 2011. **121**(6): p. 2169-80.
188. Gerber, S., et al., *Mutations in LCA5 are an uncommon cause of Leber congenital amaurosis (LCA) type II*. Human mutation, 2007. **28**(12): p. 1245.
189. Ramprasad, V.L., et al., *Identification of a novel splice-site mutation in the Lebercilin (LCA5) gene causing Leber congenital amaurosis*. Molecular vision, 2008. **14**: p. 481-6.
190. Jacobson, S.G., et al., *Leber congenital amaurosis caused by Lebercilin (LCA5) mutation: retained photoreceptors adjacent to retinal disorganization*. Molecular vision, 2009. **15**: p. 1098-106.
191. Ahmad, A., et al., *Identification of a novel LCA5 mutation in a Pakistani family with Leber congenital amaurosis and cataracts*. Molecular vision, 2011. **17**: p. 1940-5.
192. Meindl, A., et al., *A gene (RPGR) with homology to the RCC1 guanine nucleotide exchange factor is mutated in X-linked retinitis pigmentosa (RP3)*. Nature genetics, 1996. **13**(1): p. 35-42.
193. Breuer, D.K., et al., *A comprehensive mutation analysis of RP2 and RPGR in a North American cohort of families with X-linked retinitis pigmentosa*. American journal of human genetics, 2002. **70**(6): p. 1545-54.

194. Vervoort, R., et al., *Mutational hot spot within a new RPGR exon in X-linked retinitis pigmentosa*. Nature genetics, 2000. **25**(4): p. 462-6.
195. Yang, Z., et al., *Mutations in the RPGR gene cause X-linked cone dystrophy*. Human molecular genetics, 2002. **11**(5): p. 605-11.
196. Demirci, F.Y., et al., *X-linked cone-rod dystrophy (locus COD1): identification of mutations in RPGR exon ORF15*. American journal of human genetics, 2002. **70**(4): p. 1049-53.
197. Boylan, J.P. and A.F. Wright, *Identification of a novel protein interacting with RPGR*. Human molecular genetics, 2000. **9**(14): p. 2085-93.
198. Hong, D.H., et al., *Retinitis pigmentosa GTPase regulator (RPGR)-interacting protein is stably associated with the photoreceptor ciliary axoneme and anchors RPGR to the connecting cilium*. The Journal of biological chemistry, 2001. **276**(15): p. 12091-9.
199. Roepman, R., et al., *The retinitis pigmentosa GTPase regulator (RPGR) interacts with novel transport-like proteins in the outer segments of rod photoreceptors*. Human molecular genetics, 2000. **9**(14): p. 2095-105.
200. Dryja, T.P., et al., *Null RPGRIP1 alleles in patients with Leber congenital amaurosis*. American journal of human genetics, 2001. **68**(5): p. 1295-8.
201. McKibbin, M., et al., *Genotype-phenotype correlation for leber congenital amaurosis in Northern Pakistan*. Archives of ophthalmology, 2010. **128**(1): p. 107-13.
202. Hameed, A., et al., *Evidence of RPGRIP1 gene mutations associated with recessive cone-rod dystrophy*. Journal of medical genetics, 2003. **40**(8): p. 616-9.
203. Furukawa, T., E.M. Morrow, and C.L. Cepko, *Crx, a novel otx-like homeobox gene, shows photoreceptor-specific expression and regulates photoreceptor differentiation*. Cell, 1997. **91**(4): p. 531-41.
204. Freund, C.L., et al., *Cone-rod dystrophy due to mutations in a novel photoreceptor-specific homeobox gene (CRX) essential for maintenance of the photoreceptor*. Cell, 1997. **91**(4): p. 543-53.
205. Chen, S., et al., *Crx, a novel Otx-like paired-homeodomain protein, binds to and transactivates photoreceptor cell-specific genes*. Neuron, 1997. **19**(5): p. 1017-30.
206. Mitton, K.P., et al., *The leucine zipper of NRL interacts with the CRX homeodomain. A possible mechanism of transcriptional synergy in rhodopsin regulation*. The Journal of biological chemistry, 2000. **275**(38): p. 29794-9.
207. Hodges, M.D., et al., *Characterization of the genomic and transcriptional structure of the CRX gene: substantial differences between human and mouse*. Genomics, 2002. **80**(5): p. 531-42.
208. Chow, R.L. and R.A. Lang, *Early eye development in vertebrates*. Annual review of cell and developmental biology, 2001. **17**: p. 255-96.
209. Furukawa, T., et al., *Retinopathy and attenuated circadian entrainment in Crx-deficient mice*. Nature genetics, 1999. **23**(4): p. 466-70.
210. Swain, P.K., et al., *Mutations in the cone-rod homeobox gene are associated with the cone-rod dystrophy photoreceptor degeneration*. Neuron, 1997. **19**(6): p. 1329-36.
211. Sohocki, M.M., et al., *A range of clinical phenotypes associated with mutations in CRX, a photoreceptor transcription-factor gene*. American journal of human genetics, 1998. **63**(5): p. 1307-15.

212. Jacobson, S.G., et al., *Retinal degenerations with truncation mutations in the cone-rod homeobox (CRX) gene*. Investigative ophthalmology & visual science, 1998. **39**(12): p. 2417-26.
213. Tzekov, R.T., et al., *Autosomal dominant retinal degeneration and bone loss in patients with a 12-bp deletion in the CRX gene*. Investigative ophthalmology & visual science, 2001. **42**(6): p. 1319-27.
214. Rivolta, C., et al., *Novel frameshift mutations in CRX associated with Leber congenital amaurosis*. Human mutation, 2001. **18**(6): p. 550-1.
215. Perrault, I., et al., *Evidence of autosomal dominant Leber congenital amaurosis (LCA) underlain by a CRX heterozygous null allele*. Journal of medical genetics, 2003. **40**(7): p. e90.
216. Nakamura, M., S. Ito, and Y. Miyake, *Novel de novo mutation in CRX gene in a Japanese patient with leber congenital amaurosis*. American journal of ophthalmology, 2002. **134**(3): p. 465-7.
217. Koenekoop, R.K., et al., *Visual improvement in Leber congenital amaurosis and the CRX genotype*. Ophthalmic genetics, 2002. **23**(1): p. 49-59.
218. Wang, P., X. Guo, and Q. Zhang, *Further evidence of autosomal-dominant Leber congenital amaurosis caused by heterozygous CRX mutation*. Graefes' archive for clinical and experimental ophthalmology = Albrecht von Graefes Archiv fur klinische und experimentelle Ophthalmologie, 2007. **245**(9): p. 1401-2.
219. Nichols, L.L., 2nd, et al., *Two novel CRX mutant proteins causing autosomal dominant Leber congenital amaurosis interact differently with NRL*. Human mutation, 2010. **31**(6): p. E1472-83.
220. Silva, E., et al., *A CRX null mutation is associated with both Leber congenital amaurosis and a normal ocular phenotype*. Investigative ophthalmology & visual science, 2000. **41**(8): p. 2076-9.
221. Rivolta, C., E.L. Berson, and T.P. Dryja, *Dominant Leber congenital amaurosis, cone-rod degeneration, and retinitis pigmentosa caused by mutant versions of the transcription factor CRX*. Human mutation, 2001. **18**(6): p. 488-98.
222. Swaroop, A., et al., *Leber congenital amaurosis caused by a homozygous mutation (R90W) in the homeodomain of the retinal transcription factor CRX: direct evidence for the involvement of CRX in the development of photoreceptor function*. Human molecular genetics, 1999. **8**(2): p. 299-305.
223. van Soest, S., et al., *Assignment of a gene for autosomal recessive retinitis pigmentosa (RP12) to chromosome 1q31-q32.1 in an inbred and genetically heterogeneous disease population*. Genomics, 1994. **22**(3): p. 499-504.
224. den Hollander, A.I., et al., *Mutations in a human homologue of Drosophila crumbs cause retinitis pigmentosa (RP12)*. Nature genetics, 1999. **23**(2): p. 217-21.
225. Tepass, U., C. Theres, and E. Knust, *crumbs encodes an EGF-like protein expressed on apical membranes of Drosophila epithelial cells and required for organization of epithelia*. Cell, 1990. **61**(5): p. 787-99.
226. Tepass, U., *Crumbs, a component of the apical membrane, is required for zonula adherens formation in primary epithelia of Drosophila*. Developmental biology, 1996. **177**(1): p. 217-25.
227. van de Pavert, S.A., et al., *Crb1 is a determinant of retinal apical Muller glia cell features*. Glia, 2007. **55**(14): p. 1486-97.

228. Pellikka, M., et al., *Crumbs, the Drosophila homologue of human CRB1/RP12, is essential for photoreceptor morphogenesis*. *Nature*, 2002. **416**(6877): p. 143-9.
229. Heckenlively, J.R., *Preserved para-arteriole retinal pigment epithelium (PPRPE) in retinitis pigmentosa*. *The British journal of ophthalmology*, 1982. **66**(1): p. 26-30.
230. den Hollander, A.I., et al., *Leber congenital amaurosis and retinitis pigmentosa with Coats-like exudative vasculopathy are associated with mutations in the crumbs homologue 1 (CRB1) gene*. *American journal of human genetics*, 2001. **69**(1): p. 198-203.
231. Lotery, A.J., et al., *Mutations in the CRB1 gene cause Leber congenital amaurosis*. *Archives of ophthalmology*, 2001. **119**(3): p. 415-20.
232. Lotery, A.J., et al., *CRB1 mutations may result in retinitis pigmentosa without para-arteriolar RPE preservation*. *Ophthalmic genetics*, 2001. **22**(3): p. 163-9.
233. McKay, G.J., et al., *Pigmented paravenous chorioretinal atrophy is associated with a mutation within the crumbs homolog 1 (CRB1) gene*. *Investigative ophthalmology & visual science*, 2005. **46**(1): p. 322-8.
234. Jacobson, S.G., et al., *Crumbs homolog 1 (CRB1) mutations result in a thick human retina with abnormal lamination*. *Human molecular genetics*, 2003. **12**(9): p. 1073-8.
235. Keen, T.J., et al., *Identification of a locus (LCA9) for Leber's congenital amaurosis on chromosome 1p36*. *European journal of human genetics : EJHG*, 2003. **11**(5): p. 420-3.
236. Falk, M.J., et al., *NMNAT1 mutations cause Leber congenital amaurosis*. *Nature genetics*, 2012. **44**(9): p. 1040-5.
237. Koenekoop, R.K., et al., *Mutations in NMNAT1 cause Leber congenital amaurosis and identify a new disease pathway for retinal degeneration*. *Nature genetics*, 2012. **44**(9): p. 1035-9.
238. Perrault, I., et al., *Mutations in NMNAT1 cause Leber congenital amaurosis with early-onset severe macular and optic atrophy*. *Nature genetics*, 2012. **44**(9): p. 975-7.
239. Chiang, P.W., et al., *Exome sequencing identifies NMNAT1 mutations as a cause of Leber congenital amaurosis*. *Nature genetics*, 2012. **44**(9): p. 972-4.
240. den Hollander, A.I., et al., *Mutations in the CEP290 (NPHP6) gene are a frequent cause of Leber congenital amaurosis*. *American journal of human genetics*, 2006. **79**(3): p. 556-61.
241. Valente, E.M., et al., *Mutations in CEP290, which encodes a centrosomal protein, cause pleiotropic forms of Joubert syndrome*. *Nature genetics*, 2006. **38**(6): p. 623-5.
242. Sayer, J.A., et al., *The centrosomal protein nephrocystin-6 is mutated in Joubert syndrome and activates transcription factor ATF4*. *Nature genetics*, 2006. **38**(6): p. 674-81.
243. Chang, B., et al., *In-frame deletion in a novel centrosomal/ciliary protein CEP290/NPHP6 perturbs its interaction with RPGR and results in early-onset retinal degeneration in the rd16 mouse*. *Human molecular genetics*, 2006. **15**(11): p. 1847-57.
244. McEwen, D.P., et al., *Hypomorphic CEP290/NPHP6 mutations result in anosmia caused by the selective loss of G proteins in cilia of olfactory sensory neurons*. *Proceedings of the National Academy of Sciences of the United States of America*, 2007. **104**(40): p. 15917-22.

245. Craige, B., et al., *CEP290 tethers flagellar transition zone microtubules to the membrane and regulates flagellar protein content*. The Journal of cell biology, 2010. **190**(5): p. 927-40.
246. Betleja, E. and D.G. Cole, *Ciliary trafficking: CEP290 guards a gated community*. Current biology : CB, 2010. **20**(21): p. R928-31.
247. Coppieters, F., et al., *CEP290, a gene with many faces: mutation overview and presentation of CEP290base*. Human mutation, 2010. **31**(10): p. 1097-108.
248. Frank, V., et al., *Mutations of the CEP290 gene encoding a centrosomal protein cause Meckel-Gruber syndrome*. Human mutation, 2008. **29**(1): p. 45-52.
249. Helou, J., et al., *Mutation analysis of NPHP6/CEP290 in patients with Joubert syndrome and Senior-Loken syndrome*. Journal of medical genetics, 2007. **44**(10): p. 657-63.
250. Stone, E.M., et al., *Variations in NPHP5 in patients with nonsyndromic leber congenital amaurosis and Senior-Loken syndrome*. Archives of ophthalmology, 2011. **129**(1): p. 81-7.
251. Perrault, I., et al., *Spectrum of NPHP6/CEP290 mutations in Leber congenital amaurosis and delineation of the associated phenotype*. Human mutation, 2007. **28**(4): p. 416.
252. Coppieters, F., et al., *Genetic screening of LCA in Belgium: predominance of CEP290 and identification of potential modifier alleles in AH1 of CEP290-related phenotypes*. Human mutation, 2010. **31**(10): p. E1709-66.
253. Pasadhika, S., et al., *Differential macular morphology in patients with RPE65-, CEP290-, GUCY2D-, and AIPL1-related Leber congenital amaurosis*. Investigative ophthalmology & visual science, 2010. **51**(5): p. 2608-14.
254. Littink, K.W., et al., *A novel nonsense mutation in CEP290 induces exon skipping and leads to a relatively mild retinal phenotype*. Investigative ophthalmology & visual science, 2010. **51**(7): p. 3646-52.
255. Cideciyan, A.V., et al., *Centrosomal-ciliary gene CEP290/NPHP6 mutations result in blindness with unexpected sparing of photoreceptors and visual brain: implications for therapy of Leber congenital amaurosis*. Human mutation, 2007. **28**(11): p. 1074-83.
256. Papon, J.F., et al., *Abnormal respiratory cilia in non-syndromic Leber congenital amaurosis with CEP290 mutations*. Journal of medical genetics, 2010. **47**(12): p. 829-34.
257. Vallespin, E., et al., *Frequency of CEP290 c.2991_1655A>G mutation in 175 Spanish families affected with Leber congenital amaurosis and early-onset retinitis pigmentosa*. Molecular vision, 2007. **13**: p. 2160-2.
258. Li, Y., et al., *Mutation survey of known LCA genes and loci in the Saudi Arabian population*. Investigative ophthalmology & visual science, 2009. **50**(3): p. 1336-43.
259. Sundaresan, P., et al., *Mutations that are a common cause of Leber congenital amaurosis in northern America are rare in southern India*. Molecular vision, 2009. **15**: p. 1781-7.
260. Seong, M.W., et al., *Molecular characterization of Leber congenital amaurosis in Koreans*. Molecular vision, 2008. **14**: p. 1429-36.
261. Kennan, A., et al., *Identification of an IMPDH1 mutation in autosomal dominant retinitis pigmentosa (RP10) revealed following comparative microarray analysis of transcripts derived from retinas of wild-type and Rho(-/-) mice*. Human molecular genetics, 2002. **11**(5): p. 547-57.

262. Bowne, S.J., et al., *Mutations in the inosine monophosphate dehydrogenase 1 gene (IMPDH1) cause the RP10 form of autosomal dominant retinitis pigmentosa*. Human molecular genetics, 2002. **11**(5): p. 559-68.
263. Bowne, S.J., et al., *Spectrum and frequency of mutations in IMPDH1 associated with autosomal dominant retinitis pigmentosa and leber congenital amaurosis*. Investigative ophthalmology & visual science, 2006. **47**(1): p. 34-42.
264. Bowne, S.J., et al., *Why do mutations in the ubiquitously expressed housekeeping gene IMPDH1 cause retina-specific photoreceptor degeneration?* Investigative ophthalmology & visual science, 2006. **47**(9): p. 3754-65.
265. Friedman, J.S., et al., *Premature truncation of a novel protein, RD3, exhibiting subnuclear localization is associated with retinal degeneration*. American journal of human genetics, 2006. **79**(6): p. 1059-70.
266. Azadi, S., L.L. Molday, and R.S. Molday, *RD3, the protein associated with Leber congenital amaurosis type 12, is required for guanylate cyclase trafficking in photoreceptor cells*. Proceedings of the National Academy of Sciences of the United States of America, 2010. **107**(49): p. 21158-63.
267. Peshenko, I.V., et al., *Retinal degeneration 3 (RD3) protein inhibits catalytic activity of retinal membrane guanylyl cyclase (RetGC) and its stimulation by activating proteins*. Biochemistry, 2011. **50**(44): p. 9511-9.
268. Preising, M.N., et al., *Mutations in RD3 are associated with an extremely rare and severe form of early onset retinal dystrophy*. Investigative ophthalmology & visual science, 2012. **53**(7): p. 3463-72.
269. Perrault, I., et al., *Union makes strength: a worldwide collaborative genetic and clinical study to provide a comprehensive survey of RD3 mutations and delineate the associated phenotype*. PloS one, 2013. **8**(1): p. e51622.
270. Janecke, A.R., et al., *Mutations in RDH12 encoding a photoreceptor cell retinol dehydrogenase cause childhood-onset severe retinal dystrophy*. Nature genetics, 2004. **36**(8): p. 850-4.
271. Perrault, I., et al., *Retinal dehydrogenase 12 (RDH12) mutations in leber congenital amaurosis*. American journal of human genetics, 2004. **75**(4): p. 639-46.
272. Thompson, D.A., et al., *Retinal degeneration associated with RDH12 mutations results from decreased 11-cis retinal synthesis due to disruption of the visual cycle*. Human molecular genetics, 2005. **14**(24): p. 3865-75.
273. Haeseleer, F., et al., *Dual-substrate specificity short chain retinol dehydrogenases from the vertebrate retina*. The Journal of biological chemistry, 2002. **277**(47): p. 45537-46.
274. Belyaeva, O.V., et al., *Biochemical properties of purified human retinol dehydrogenase 12 (RDH12): catalytic efficiency toward retinoids and C9 aldehydes and effects of cellular retinol-binding protein type I (CRBPI) and cellular retinaldehyde-binding protein (CRALBP) on the oxidation and reduction of retinoids*. Biochemistry, 2005. **44**(18): p. 7035-47.
275. Maeda, A., et al., *Retinol dehydrogenase (RDH12) protects photoreceptors from light-induced degeneration in mice*. The Journal of biological chemistry, 2006. **281**(49): p. 37697-704.
276. Maeda, A., et al., *Redundant and unique roles of retinol dehydrogenases in the mouse retina*. Proceedings of the National Academy of Sciences of the United States of America, 2007. **104**(49): p. 19565-70.

277. Mata, N.L., et al., *Chicken retinas contain a retinoid isomerase activity that catalyzes the direct conversion of all-trans-retinol to 11-cis-retinol*. *Biochemistry*, 2005. **44**(35): p. 11715-21.
278. Schuster, A., et al., *The phenotype of early-onset retinal degeneration in persons with RDH12 mutations*. *Investigative ophthalmology & visual science*, 2007. **48**(4): p. 1824-31.
279. Sun, W., et al., *Novel RDH12 mutations associated with Leber congenital amaurosis and cone-rod dystrophy: biochemical and clinical evaluations*. *Vision research*, 2007. **47**(15): p. 2055-66.
280. Jacobson, S.G., et al., *RDH12 and RPE65, visual cycle genes causing leber congenital amaurosis, differ in disease expression*. *Investigative ophthalmology & visual science*, 2007. **48**(1): p. 332-8.
281. Sodi, A., et al., *Novel RDH12 sequence variations in Leber congenital amaurosis*. *Journal of AAPOS : the official publication of the American Association for Pediatric Ophthalmology and Strabismus / American Association for Pediatric Ophthalmology and Strabismus*, 2010. **14**(4): p. 349-51.
282. Valverde, D., et al., *Complexity of phenotype-genotype correlations in Spanish patients with RDH12 mutations*. *Investigative ophthalmology & visual science*, 2009. **50**(3): p. 1065-8.
283. Avila-Fernandez, A., et al., *Mutation analysis of 272 Spanish families affected by autosomal recessive retinitis pigmentosa using a genotyping microarray*. *Molecular vision*, 2010. **16**: p. 2550-8.
284. Mackay, D.S., et al., *RDH12 retinopathy: novel mutations and phenotypic description*. *Molecular vision*, 2011. **17**: p. 2706-16.
285. Thompson, D.A., et al., *Mutations in the gene encoding lecithin retinol acyltransferase are associated with early-onset severe retinal dystrophy*. *Nature genetics*, 2001. **28**(2): p. 123-4.
286. Ruiz, A., et al., *Genomic organization and mutation analysis of the gene encoding lecithin retinol acyltransferase in human retinal pigment epithelium*. *Investigative ophthalmology & visual science*, 2001. **42**(1): p. 31-7.
287. Ruiz, A., et al., *Molecular and biochemical characterization of lecithin retinol acyltransferase*. *The Journal of biological chemistry*, 1999. **274**(6): p. 3834-41.
288. Batten, M.L., et al., *Lecithin-retinol acyltransferase is essential for accumulation of all-trans-retinyl esters in the eye and in the liver*. *The Journal of biological chemistry*, 2004. **279**(11): p. 10422-32.
289. Fan, J., et al., *Rpe65^{-/-} and Lrat^{-/-} mice: comparable models of leber congenital amaurosis*. *Investigative ophthalmology & visual science*, 2008. **49**(6): p. 2384-9.
290. Preising, M.N., et al., *[Genetic and clinical heterogeneity in LCA patients. The end of uniformity]*. *Der Ophthalmologe : Zeitschrift der Deutschen Ophthalmologischen Gesellschaft*, 2007. **104**(6): p. 490-8.
291. Senechal, A., et al., *Screening genes of the retinoid metabolism: novel LRAT mutation in leber congenital amaurosis*. *American journal of ophthalmology*, 2006. **142**(4): p. 702-4.
292. Collin, R.W., et al., *High-resolution homozygosity mapping is a powerful tool to detect novel mutations causative of autosomal recessive RP in the Dutch population*. *Investigative ophthalmology & visual science*, 2011. **52**(5): p. 2227-39.

293. Ohlemiller, K.K., et al., *Cochlear and retinal degeneration in the tubby mouse*. *Neuroreport*, 1995. **6**(6): p. 845-9.
294. Kleyn, P.W., et al., *Identification and characterization of the mouse obesity gene tubby: a member of a novel gene family*. *Cell*, 1996. **85**(2): p. 281-90.
295. Noben-Trauth, K., et al., *A candidate gene for the mouse mutation tubby*. *Nature*, 1996. **380**(6574): p. 534-8.
296. North, M.A., et al., *Molecular characterization of TUB, TULP1, and TULP2, members of the novel tubby gene family and their possible relation to ocular diseases*. *Proceedings of the National Academy of Sciences of the United States of America*, 1997. **94**(7): p. 3128-33.
297. Nishina, P.M., et al., *Molecular characterization of a novel tubby gene family member, TULP3, in mouse and humans*. *Genomics*, 1998. **54**(2): p. 215-20.
298. Li, Q.Z., et al., *Molecular cloning and characterization of the mouse and human TUSP gene, a novel member of the tubby superfamily*. *Gene*, 2001. **273**(2): p. 275-84.
299. Banerjee, P., et al., *TULP1 mutation in two extended Dominican kindreds with autosomal recessive retinitis pigmentosa*. *Nature genetics*, 1998. **18**(2): p. 177-9.
300. Hagstrom, S.A., et al., *Recessive mutations in the gene encoding the tubby-like protein TULP1 in patients with retinitis pigmentosa*. *Nature genetics*, 1998. **18**(2): p. 174-6.
301. Gu, S., et al., *Tubby-like protein-1 mutations in autosomal recessive retinitis pigmentosa*. *Lancet*, 1998. **351**(9109): p. 1103-4.
302. Boggon, T.J., et al., *Implication of tubby proteins as transcription factors by structure-based functional analysis*. *Science*, 1999. **286**(5447): p. 2119-25.
303. Santagata, S., et al., *G-protein signaling through tubby proteins*. *Science*, 2001. **292**(5524): p. 2041-50.
304. Ikeda, S., et al., *Cell-specific expression of tubby gene family members (tub, Tulp1,2, and 3) in the retina*. *Investigative ophthalmology & visual science*, 1999. **40**(11): p. 2706-12.
305. Hagstrom, S.A., et al., *Retinal degeneration in tulp1^{-/-} mice: vesicular accumulation in the interphotoreceptor matrix*. *Investigative ophthalmology & visual science*, 1999. **40**(12): p. 2795-802.
306. Ikeda, A., P.M. Nishina, and J.K. Naggert, *The tubby-like proteins, a family with roles in neuronal development and function*. *Journal of cell science*, 2002. **115**(Pt 1): p. 9-14.
307. Hagstrom, S.A., et al., *A role for the Tubby-like protein 1 in rhodopsin transport*. *Investigative ophthalmology & visual science*, 2001. **42**(9): p. 1955-62.
308. Grossman, G.H., et al., *Early synaptic defects in tulp1^{-/-} mice*. *Investigative ophthalmology & visual science*, 2009. **50**(7): p. 3074-83.
309. Lewis, C.A., et al., *Tubby-like protein 1 homozygous splice-site mutation causes early-onset severe retinal degeneration*. *Investigative ophthalmology & visual science*, 1999. **40**(9): p. 2106-14.
310. Paloma, E., et al., *Novel mutations in the TULP1 gene causing autosomal recessive retinitis pigmentosa*. *Investigative ophthalmology & visual science*, 2000. **41**(3): p. 656-9.
311. Mataftsi, A., et al., *Novel TULP1 mutation causing leber congenital amaurosis or early onset retinal degeneration*. *Investigative ophthalmology & visual science*, 2007. **48**(11): p. 5160-7.

312. den Hollander, A.I., et al., *Novel compound heterozygous TULP1 mutations in a family with severe early-onset retinitis pigmentosa*. Archives of ophthalmology, 2007. **125**(7): p. 932-5.
313. Abbasi, A.H., H.J. Garzosi, and T. Ben-Yosef, *A novel splice-site mutation of TULP1 underlies severe early-onset retinitis pigmentosa in a consanguineous Israeli Muslim Arab family*. Molecular vision, 2008. **14**: p. 675-82.
314. Iqbal, M., et al., *Association of pathogenic mutations in TULP1 with retinitis pigmentosa in consanguineous Pakistani families*. Archives of ophthalmology, 2011. **129**(10): p. 1351-7.
315. Chen, X.N., et al., *Localization of the human RGR opsin gene to chromosome 10q23*. Human genetics, 1996. **97**(6): p. 720-2.
316. Chen, P., et al., *A photic visual cycle of rhodopsin regeneration is dependent on Rgr*. Nature genetics, 2001. **28**(3): p. 256-60.
317. Wenzel, A., et al., *The retinal G protein-coupled receptor (RGR) enhances isomerohydrolase activity independent of light*. The Journal of biological chemistry, 2005. **280**(33): p. 29874-84.
318. Radu, R.A., et al., *Retinal pigment epithelium-retinal G protein receptor-opsin mediates light-dependent translocation of all-trans-retinyl esters for synthesis of visual chromophore in retinal pigment epithelial cells*. The Journal of biological chemistry, 2008. **283**(28): p. 19730-8.
319. Morimura, H., et al., *Mutations in RGR, encoding a light-sensitive opsin homologue, in patients with retinitis pigmentosa*. Nature genetics, 1999. **23**(4): p. 393-4.
320. Bernal, S., et al., *Study of the involvement of the RGR, CRPBI, and CRBI genes in the pathogenesis of autosomal recessive retinitis pigmentosa*. Journal of medical genetics, 2003. **40**(7): p. e89.
321. Ksantini, M., et al., *Screening genes of the visual cycle RGR, RBP1 and RBP3 identifies rare sequence variations*. Ophthalmic genetics, 2010. **31**(4): p. 200-4.
322. Estrada-Cuzcano, A., et al., *IQCB1 mutations in patients with leber congenital amaurosis*. Investigative ophthalmology & visual science, 2011. **52**(2): p. 834-9.
323. Otto, E.A., et al., *Nephrocystin-5, a ciliary IQ domain protein, is mutated in Senior-Loken syndrome and interacts with RPGR and calmodulin*. Nature genetics, 2005. **37**(3): p. 282-8.
324. Schafer, T., et al., *Genetic and physical interaction between the NPHP5 and NPHP6 gene products*. Human molecular genetics, 2008. **17**(23): p. 3655-62.
325. Wang, X., et al., *Whole-exome sequencing identifies ALMS1, IQCB1, CNGA3, and MYO7A mutations in patients with Leber congenital amaurosis*. Human mutation, 2011. **32**(12): p. 1450-9.
326. Cideciyan, A.V., et al., *Cone photoreceptors are the main targets for gene therapy of NPHP5 (IQCB1) or NPHP6 (CEP290) blindness: generation of an all-cone Nphp6 hypomorph mouse that mimics the human retinal ciliopathy*. Human molecular genetics, 2011. **20**(7): p. 1411-23.
327. Sergouniotis, P.I., et al., *Recessive mutations in KCNJ13, encoding an inwardly rectifying potassium channel subunit, cause leber congenital amaurosis*. American journal of human genetics, 2011. **89**(1): p. 183-90.
328. Sellick, G.S., et al., *Genomewide linkage searches for Mendelian disease loci can be efficiently conducted using high-density SNP genotyping arrays*. Nucleic acids research, 2004. **32**(20): p. e164.

329. Carr, I.M., et al., *Interactive visual analysis of SNP data for rapid autozygosity mapping in consanguineous families*. Human mutation, 2006. **27**(10): p. 1041-6.
330. Borman, A.D., et al., *A homozygous mutation in the TUB gene associated with retinal dystrophy and obesity*. Human mutation, 2014. **35**(3): p. 289-93.
331. den Hollander, A.I., et al., *CRB1 mutation spectrum in inherited retinal dystrophies*. Human mutation, 2004. **24**(5): p. 355-69.
332. Tan, M.H., et al., *Leber congenital amaurosis associated with AIPL1: challenges in ascribing disease causation, clinical findings, and implications for gene therapy*. PloS one, 2012. **7**(3): p. e32330.
333. Aboshiha, J., et al., *Preserved Outer Retina in AIPL1 Leber's Congenital Amaurosis: Implications for Gene Therapy*. Ophthalmology, 2015. **122**(4): p. 862-4.
334. Pennesi, M.E., et al., *Residual electroretinograms in young Leber congenital amaurosis patients with mutations of AIPL1*. Investigative ophthalmology & visual science, 2011. **52**(11): p. 8166-73.
335. Tan, M.H., et al., *Gene therapy for retinitis pigmentosa and Leber congenital amaurosis caused by defects in AIPL1: effective rescue of mouse models of partial and complete Aipl1 deficiency using AAV2/2 and AAV2/8 vectors*. Human molecular genetics, 2009. **18**(12): p. 2099-114.
336. Yzer, S., et al., *Ocular and extra-ocular features of patients with Leber congenital amaurosis and mutations in CEP290*. Molecular vision, 2012. **18**: p. 412-25.
337. Burnight, E.R., et al., *CEP290 gene transfer rescues Leber congenital amaurosis cellular phenotype*. Gene therapy, 2014. **21**(7): p. 662-72.
338. Milam, A.H., et al., *Clinicopathologic effects of mutant GUCY2D in Leber congenital amaurosis*. Ophthalmology, 2003. **110**(3): p. 549-58.
339. Mackay, D.S., et al., *Screening of a large cohort of leber congenital amaurosis and retinitis pigmentosa patients identifies novel LCA5 mutations and new genotype-phenotype correlations*. Human mutation, 2013. **34**(11): p. 1537-46.
340. Tschernutter, M., et al., *Clinical characterisation of a family with retinal dystrophy caused by mutation in the Mertk gene*. The British journal of ophthalmology, 2006. **90**(6): p. 718-23.
341. Mackay, D.S., et al., *Novel mutations in MERTK associated with childhood onset rod-cone dystrophy*. Molecular vision, 2010. **16**: p. 369-77.
342. Cideciyan, A.V., *Leber congenital amaurosis due to RPE65 mutations and its treatment with gene therapy*. Progress in retinal and eye research, 2010. **29**(5): p. 398-427.
343. Flitcroft, D.I., et al., *Retinal dysfunction and refractive errors: an electrophysiological study of children*. The British journal of ophthalmology, 2005. **89**(4): p. 484-8.
344. Robson, A.G., et al., *Serial Imaging and Structure-Function Correlates of High-Density Rings of Fundus Autofluorescence in Retinitis Pigmentosa*. Retina, 2011.
345. Avila-Fernandez, A., et al., *Late onset retinitis pigmentosa*. Ophthalmology, 2011. **118**(12): p. 2523-4.
346. Kannabiran, C., L. Palavalli, and S. Jalali, *Mutation of SPATA7 in a family with autosomal recessive early-onset retinitis pigmentosa*. J Mol Genet Med, 2012. **6**: p. 301-3.

347. Li, L., et al., *Detection of variants in 15 genes in 87 unrelated Chinese patients with Leber congenital amaurosis*. PloS one, 2011. **6**(5): p. e19458.
348. Li, L., et al., *Lack of phenotypic effect of triallelic variation in SPATA7 in a family with Leber congenital amaurosis resulting from CRB1 mutations*. Molecular vision, 2011. **17**: p. 3326-32.
349. Eblimit, A., et al., *Spata7 is a retinal ciliopathy gene critical for correct RPGRIP1 localization and protein trafficking in the retina*. Human molecular genetics, 2015. **24**(6): p. 1584-601.
350. Gao, J., et al., *Progressive photoreceptor degeneration, outer segment dysplasia, and rhodopsin mislocalization in mice with targeted disruption of the retinitis pigmentosa-1 (Rp1) gene*. Proceedings of the National Academy of Sciences of the United States of America, 2002. **99**(8): p. 5698-703.
351. Zhao, Y., et al., *The retinitis pigmentosa GTPase regulator (RPGR)-interacting protein: subserving RPGR function and participating in disk morphogenesis*. Proceedings of the National Academy of Sciences of the United States of America, 2003. **100**(7): p. 3965-70.
352. Carroll, K., C. Gomez, and L. Shapiro, *Tubby proteins: the plot thickens*. Nat Rev Mol Cell Biol, 2004. **5**(1): p. 55-63.
353. Coleman, D.L. and E.M. Eicher, *Fat (fat) and tubby (tub): two autosomal recessive mutations causing obesity syndromes in the mouse*. The Journal of heredity, 1990. **81**(6): p. 424-7.
354. Mukhopadhyay, S. and P.K. Jackson, *The tubby family proteins*. Genome Biol, 2011. **12**(6): p. 225.
355. Sun, X., et al., *Tubby is required for trafficking G protein-coupled receptors to neuronal cilia*. Cilia, 2012. **1**(1): p. 21.
356. Ikeda, A., et al., *Microtubule-associated protein 1A is a modifier of tubby hearing (moth1)*. Nature genetics, 2002. **30**(4): p. 401-5.
357. Ikeda, S., et al., *Retinal degeneration but not obesity is observed in null mutants of the tubby-like protein 1 gene*. Human molecular genetics, 2000. **9**(2): p. 155-63.
358. Prada, P.O., et al., *Tub has a key role in insulin and leptin signaling and action in vivo in hypothalamic nuclei*. Diabetes, 2013. **62**(1): p. 137-48.
359. Jacobson, S.G., et al., *TULP1 mutations causing early-onset retinal degeneration: preserved but insensitive macular cones*. Investigative ophthalmology & visual science, 2014. **55**(8): p. 5354-64.
360. Ajmal, M., et al., *Identification of recurrent and novel mutations in TULP1 in Pakistani families with early-onset retinitis pigmentosa*. Molecular vision, 2012. **18**: p. 1226-37.
361. Kannabiran, C., et al., *Mutations in TULP1, NR2E3, and MFRP genes in Indian families with autosomal recessive retinitis pigmentosa*. Molecular vision, 2012. **18**: p. 1165-74.
362. Bainbridge, J.W., et al., *Effect of gene therapy on visual function in Leber's congenital amaurosis*. The New England journal of medicine, 2008. **358**(21): p. 2231-9.
363. Cideciyan, A.V., et al., *Human gene therapy for RPE65 isomerase deficiency activates the retinoid cycle of vision but with slow rod kinetics*. Proceedings of the National Academy of Sciences of the United States of America, 2008. **105**(39): p. 15112-7.

364. Maguire, A.M., et al., *Age-dependent effects of RPE65 gene therapy for Leber's congenital amaurosis: a phase I dose-escalation trial*. *Lancet*, 2009. **374**(9701): p. 1597-605.
365. Dev Borman, A., et al., *Early onset retinal dystrophy due to mutations in LRAT: molecular analysis and detailed phenotypic study*. *Investigative ophthalmology & visual science*, 2012. **53**(7): p. 3927-38.
366. Jacobson, S.G., et al., *Automated light- and dark-adapted perimetry for evaluating retinitis pigmentosa*. *Ophthalmology*, 1986. **93**(12): p. 1604-11.
367. Steinmetz, R.L., et al., *Symptomatic abnormalities of dark adaptation in patients with age-related Bruch's membrane change*. *The British journal of ophthalmology*, 1993. **77**(9): p. 549-54.
368. Chen, J.C., et al., *Functional loss in age-related Bruch's membrane change with choroidal perfusion defect*. *Investigative ophthalmology & visual science*, 1992. **33**(2): p. 334-40.
369. Stockman, A., D.J. Plummer, and E.D. Montag, *Spectrally opponent inputs to the human luminance pathway: slow +M and -L cone inputs revealed by intense long-wavelength adaptation*. *The Journal of physiology*, 2005. **566**(Pt 1): p. 61-76.
370. l'eclairge, C.I.d., *Fundamental Chromacity Diagram With Physiological Axes - Part 1*. 2006.
371. Hecht, S. and C.D. Verrijp, *The Influence of Intensity, Color and Retinal Location on the Fusion Frequency of Intermittent Illumination*. *Proceedings of the National Academy of Sciences of the United States of America*, 1933. **19**(5): p. 522-35.
372. Stockman, A., D.I. MacLeod, and D.D. DePriest, *The temporal properties of the human short-wave photoreceptors and their associated pathways*. *Vision research*, 1991. **31**(2): p. 189-208.
373. Jaissle, G.B., et al., *Bone spicule pigment formation in retinitis pigmentosa: insights from a mouse model*. *Graefe's archive for clinical and experimental ophthalmology = Albrecht von Graefes Archiv fur klinische und experimentelle Ophthalmologie*, 2010. **248**(8): p. 1063-70.
374. Hagiwara, A., et al., *Macular abnormalities in patients with retinitis pigmentosa: prevalence on OCT examination and outcomes of vitreoretinal surgery*. *Acta ophthalmologica*, 2011. **89**(2): p. e122-5.
375. Ikeda, Y., et al., *Retinitis pigmentosa associated with asteroid hyalosis*. *Retina*, 2010. **30**(8): p. 1278-81.
376. Maeda, T., et al., *QLT091001, a 9-cis-retinal analog, is well-tolerated by retinas of mice with impaired visual cycles*. *Investigative ophthalmology & visual science*, 2013. **54**(1): p. 455-66.
377. Sergouniotis, P.I., et al., *Phenotypic Variability in RDH5 Retinopathy (Fundus Albipunctatus)*. *Ophthalmology*, 2011.
378. Schatz, P., et al., *Lack of autofluorescence in fundus albipunctatus associated with mutations in RDH5*. *Retina*, 2010. **30**(10): p. 1704-13.
379. Palczewska, G., et al., *Noninvasive multiphoton fluorescence microscopy resolves retinol and retinal condensation products in mouse eyes*. *Nature medicine*, 2010. **16**(12): p. 1444-9.
380. Katz, M.L. and T.M. Redmond, *Effect of Rpe65 knockout on accumulation of lipofuscin fluorophores in the retinal pigment epithelium*. *Investigative ophthalmology & visual science*, 2001. **42**(12): p. 3023-30.

381. Jacobson, S.G., et al., *Defining the residual vision in leber congenital amaurosis caused by RPE65 mutations*. Investigative ophthalmology & visual science, 2009. **50**(5): p. 2368-75.
382. Marmor, M.F., *Fundus albipunctatus: a clinical study of the fundus lesions, the physiologic deficit, and the vitamin A metabolism*. Documenta ophthalmologica. Advances in ophthalmology, 1977. **43**(2): p. 277-302.
383. Anantharaman, V. and L. Aravind, *Evolutionary history, structural features and biochemical diversity of the NlpC/P60 superfamily of enzymes*. Genome Biol, 2003. **4**(2): p. R11.
384. Bok, D., et al., *Purification and characterization of a transmembrane domain-deleted form of lecithin retinol acyltransferase*. Biochemistry, 2003. **42**(20): p. 6090-8.
385. Xue, L. and R.R. Rando, *Roles of cysteine 161 and tyrosine 154 in the lecithin-retinol acyltransferase mechanism*. Biochemistry, 2004. **43**(20): p. 6120-6.
386. Bussieres, S., L. Cantin, and C. Salesses, *Lecithin retinol acyltransferase and its S175R mutant have a similar secondary structure content and maximum insertion pressure but different enzyme activities*. Experimental eye research, 2011. **93**(5): p. 778-81.
387. Huber, G., et al., *Spectral domain optical coherence tomography in mouse models of retinal degeneration*. Investigative ophthalmology & visual science, 2009. **50**(12): p. 5888-95.
388. Zhang, T., et al., *Cone opsin determines the time course of cone photoreceptor degeneration in Leber congenital amaurosis*. Proceedings of the National Academy of Sciences of the United States of America, 2011.
389. Batten, M.L., et al., *Pharmacological and rAAV gene therapy rescue of visual functions in a blind mouse model of Leber congenital amaurosis*. PLoS medicine, 2005. **2**(11): p. e333.
390. Maeda, T., et al., *Evaluation of 9-cis-retinyl acetate therapy in Rpe65^{-/-} mice*. Investigative ophthalmology & visual science, 2009. **50**(9): p. 4368-78.
391. Koenekoop, R.K., et al., *Oral Synthetic cis-Retinoid Therapy in Subjects with Leber Congenital Amaurosis (LCA) due to Lecithin: Retinol Acyltransferase (LRAT) or Retinal Pigment Epithelial 65 Protein (RPE65) mutations: Preliminary Results of a Phase Ib Open Label Trial*. ARVO Meeting Abstracts, 2011. **52**(6): p. 3323.
392. Koenekoop, R.K., et al., *Oral 9-cis retinoid for childhood blindness due to Leber congenital amaurosis caused by RPE65 or LRAT mutations: an open-label phase Ib trial*. Lancet, 2014. **384**(9953): p. 1513-20.
393. Maguire, A.M., et al., *Safety and efficacy of gene transfer for Leber's congenital amaurosis*. The New England journal of medicine, 2008. **358**(21): p. 2240-8.
394. MacLaren, R.E., et al., *Retinal gene therapy in patients with choroideremia: initial findings from a phase I/2 clinical trial*. Lancet, 2014. **383**(9923): p. 1129-37.
395. Maeda, T., et al., *Retinal pigmented epithelial cells obtained from human induced pluripotent stem cells possess functional visual cycle enzymes in vitro and in vivo*. The Journal of biological chemistry, 2013. **288**(48): p. 34484-93.
396. Schwartz, S.D., et al., *Human embryonic stem cell-derived retinal pigment epithelium in patients with age-related macular degeneration and Stargardt's*

- macular dystrophy: follow-up of two open-label phase 1/2 studies*. Lancet, 2015. **385**(9967): p. 509-16.
397. Schwartz, S.D., et al., *Embryonic stem cell trials for macular degeneration: a preliminary report*. Lancet, 2012. **379**(9817): p. 713-20.
398. Dryja, T.P., et al., *Mutations within the rhodopsin gene in patients with autosomal dominant retinitis pigmentosa*. The New England journal of medicine, 1990. **323**(19): p. 1302-7.
399. Rosenfeld, P.J., et al., *A null mutation in the rhodopsin gene causes rod photoreceptor dysfunction and autosomal recessive retinitis pigmentosa*. Nature genetics, 1992. **1**(3): p. 209-13.
400. Petrukhin, K., et al., *Identification of the gene responsible for Best macular dystrophy*. Nature genetics, 1998. **19**(3): p. 241-7.
401. Burgess, R., et al., *Biallelic mutation of BEST1 causes a distinct retinopathy in humans*. American journal of human genetics, 2008. **82**(1): p. 19-31.
402. Bernal, S., et al., *Analysis of the involvement of the NR2E3 gene in autosomal recessive retinal dystrophies*. Clin Genet, 2008. **73**(4): p. 360-6.
403. Coppieters, F., et al., *Recurrent mutation in the first zinc finger of the orphan nuclear receptor NR2E3 causes autosomal dominant retinitis pigmentosa*. American journal of human genetics, 2007. **81**(1): p. 147-57.
404. Yardley, J., et al., *Mutations of VMD2 splicing regulators cause nanophthalmos and autosomal dominant vitreoretinopathopathy (ADVIRC)*. Investigative ophthalmology & visual science, 2004. **45**(10): p. 3683-9.
405. Davidson, A.E., et al., *Missense mutations in a retinal pigment epithelium protein, bestrophin-1, cause retinitis pigmentosa*. American journal of human genetics, 2009. **85**(5): p. 581-92.
406. Borman, A.D., et al., *Childhood-onset autosomal recessive bestrophinopathy*. Archives of ophthalmology, 2011. **129**(8): p. 1088-93.
407. Schatz, P., et al., *Variant phenotype of Best vitelliform macular dystrophy associated with compound heterozygous mutations in VMD2*. Ophthalmic genetics, 2006. **27**(2): p. 51-6.
408. Kramer, F., et al., *Mutations in the VMD2 gene are associated with juvenile-onset vitelliform macular dystrophy (Best disease) and adult vitelliform macular dystrophy but not age-related macular degeneration*. European journal of human genetics : EJHG, 2000. **8**(4): p. 286-92.
409. Kramer, F., et al., *Ten novel mutations in VMD2 associated with Best macular dystrophy (BMD)*. Human mutation, 2003. **22**(5): p. 418.
410. Lotery, A.J., et al., *Allelic variation in the VMD2 gene in best disease and age-related macular degeneration*. Investigative ophthalmology & visual science, 2000. **41**(6): p. 1291-6.
411. Marchant, D., et al., *Identification of novel VMD2 gene mutations in patients with best vitelliform macular dystrophy*. Human mutation, 2001. **17**(3): p. 235.
412. Marchant, D., et al., *New VMD2 gene mutations identified in patients affected by Best vitelliform macular dystrophy*. Journal of medical genetics, 2007. **44**(3): p. e70.
413. Gerth, C., et al., *Detailed analysis of retinal function and morphology in a patient with autosomal recessive bestrophinopathy (ARB)*. Documenta ophthalmologica. Advances in ophthalmology, 2009. **118**(3): p. 239-46.
414. Stone, E.M., et al., *Genetic linkage of vitelliform macular degeneration (Best's disease) to chromosome 11q13*. Nature genetics, 1992. **1**(4): p. 246-50.

415. Forsman, K., et al., *The gene for Best's macular dystrophy is located at 11q13 in a Swedish family*. Clin Genet, 1992. **42**(3): p. 156-9.
416. Marmorstein, A.D., et al., *Bestrophin, the product of the Best vitelliform macular dystrophy gene (VMD2), localizes to the basolateral plasma membrane of the retinal pigment epithelium*. Proceedings of the National Academy of Sciences of the United States of America, 2000. **97**(23): p. 12758-63.
417. Rosenthal, R., et al., *Expression of bestrophin-1, the product of the VMD2 gene, modulates voltage-dependent Ca²⁺ channels in retinal pigment epithelial cells*. The FASEB journal : official publication of the Federation of American Societies for Experimental Biology, 2006. **20**(1): p. 178-80.
418. Arden, G.B., A. Barrada, and J.H. Kelsey, *New clinical test of retinal function based upon the standing potential of the eye*. The British journal of ophthalmology, 1962. **46**(8): p. 449-67.
419. Deutman, A.F., *Electro-oculography in families with vitelliform dystrophy of the fovea. Detection of the carrier state*. Archives of ophthalmology, 1969. **81**(3): p. 305-16.
420. Cross, H.E. and L. Bard, *Electro-oculography in Best's macular dystrophy*. American journal of ophthalmology, 1974. **77**(1): p. 46-50.
421. Querques, G., et al., *High-resolution spectral domain optical coherence tomography findings in multifocal vitelliform macular dystrophy*. Survey of ophthalmology, 2009. **54**(2): p. 311-6.
422. Sonoda, S., et al., *A protocol for the culture and differentiation of highly polarized human retinal pigment epithelial cells*. Nature protocols, 2009. **4**(5): p. 662-73.
423. Wittstrom, E., et al., *Morphological and functional changes in multifocal vitelliform retinopathy and biallelic mutations in BEST1*. Ophthalmic genetics, 2011. **32**(2): p. 83-96.
424. MacDonald, I.M., et al., *Phenotype and genotype of patients with autosomal recessive bestrophinopathy*. Ophthalmic genetics, 2012. **33**(3): p. 123-9.
425. Boon, C.J., et al., *Autosomal recessive bestrophinopathy: differential diagnosis and treatment options*. Ophthalmology, 2013. **120**(4): p. 809-20.
426. Iannaccone, A., et al., *Autosomal recessive best vitelliform macular dystrophy: report of a family and management of early-onset neovascular complications*. Archives of ophthalmology, 2011. **129**(2): p. 211-7.
427. Madhusudhan, S., A. Hussain, and J.N. Sahni, *Value of anti-VEGF treatment in choroidal neovascularization associated with autosomal recessive bestrophinopathy*. Digit J Ophthalmol, 2013. **19**(4): p. 59-63.
428. Tian, R., et al., *Screening for BEST1 gene mutations in Chinese patients with bestrophinopathy*. Molecular vision, 2014. **20**: p. 1594-604.
429. Guerriero, S., et al., *Autosomal recessive bestrophinopathy: new observations on the retinal phenotype - clinical and molecular report of an Italian family*. Ophthalmologica. Journal international d'ophtalmologie. International journal of ophthalmology. Zeitschrift fur Augenheilkunde, 2011. **225**(4): p. 228-35.
430. Pineiro-Gallego, T., et al., *Clinical evaluation of two consanguineous families with homozygous mutations in BEST1*. Molecular vision, 2011. **17**: p. 1607-17.
431. Kinnick, T.R., et al., *Autosomal recessive vitelliform macular dystrophy in a large cohort of vitelliform macular dystrophy patients*. Retina, 2011. **31**(3): p. 581-95.

432. Sodi, A., et al., *Ocular phenotypes associated with biallelic mutations in BEST1 in Italian patients*. *Molecular vision*, 2011. **17**: p. 3078-87.
433. Pomares, E., et al., *Nonsense-mediated decay as the molecular cause for autosomal recessive bestrophinopathy in two unrelated families*. *Investigative ophthalmology & visual science*, 2012. **53**(1): p. 532-7.
434. Cascavilla, M.L., et al., *Unilateral vitelliform phenotype in autosomal recessive bestrophinopathy*. *Ophthalmic Res*, 2012. **48**(3): p. 146-50.
435. Preising, M.N., et al., [*Autosomal recessive bestrophinopathy (ARB): a clinical and molecular description of two patients at childhood*]. *Klinische Monatsblätter für Augenheilkunde*, 2012. **229**(10): p. 1009-17.
436. Fung, A., S. Yzer, and R. Allikmets, *Clinical and genetic misdiagnosis of autosomal recessive bestrophinopathy*. *JAMA Ophthalmol*, 2013. **131**(12): p. 1651.
437. Hussain, R.N., et al., *Use of Intravitreal Bevacizumab in a 9-year-old Child with Choroidal Neovascularization Associated with Autosomal Recessive Bestrophinopathy*. *Ophthalmic genetics*, 2014: p. 1-5.
438. Sharon, D., et al., *Ocular phenotype analysis of a family with biallelic mutations in the BEST1 gene*. *American journal of ophthalmology*, 2014. **157**(3): p. 697-709 e1-2.
439. Crowley, C., et al., *Autosomal recessive bestrophinopathy associated with angle-closure glaucoma*. *Documenta ophthalmologica. Advances in ophthalmology*, 2014. **129**(1): p. 57-63.
440. Fung, A.T., et al., *New best1 mutations in autosomal recessive bestrophinopathy*. *Retina*, 2015. **35**(4): p. 773-82.
441. Pichi, F., et al., *Multimodal imaging in hereditary retinal diseases*. *J Ophthalmol*, 2013. **2013**: p. 634351.
442. Guziewicz, K.E., et al., *Bestrophin gene mutations cause canine multifocal retinopathy: a novel animal model for best disease*. *Investigative ophthalmology & visual science*, 2007. **48**(5): p. 1959-67.
443. Guziewicz, K.E., et al., *Recombinant AAV-mediated BEST1 transfer to the retinal pigment epithelium: analysis of serotype-dependent retinal effects*. *PloS one*, 2013. **8**(10): p. e75666.
444. Musarella, M.A., *Molecular genetics of macular degeneration*. *Documenta ophthalmologica. Advances in ophthalmology*, 2001. **102**(3): p. 165-77.
445. Scullica, L. and B. Falsini, *Diagnosis and classification of macular degenerations: an approach based on retinal function testing*. *Documenta ophthalmologica. Advances in ophthalmology*, 2001. **102**(3): p. 237-50.
446. Moore, A.T., *Childhood macular dystrophies*. *Current opinion in ophthalmology*, 2009. **20**(5): p. 363-8.
447. McAvoy, C.E. and G. Silvestri, *Retinal changes associated with type 2 glomerulonephritis*. *Eye*, 2005. **19**(9): p. 985-9.
448. Colville, D.J. and J. Savage, *Alport syndrome. A review of the ocular manifestations*. *Ophthalmic genetics*, 1997. **18**(4): p. 161-73.
449. Willemsen, M.A., et al., *Juvenile macular dystrophy associated with deficient activity of fatty aldehyde dehydrogenase in Sjogren-Larsson syndrome*. *American journal of ophthalmology*, 2000. **130**(6): p. 782-9.
450. Zak, T.A. and R. Buncic, *Primary hereditary oxalosis retinopathy*. *Archives of ophthalmology*, 1983. **101**(1): p. 78-80.
451. Tarttelin, E.E., et al., *Molecular genetic heterogeneity in autosomal dominant drusen*. *Journal of medical genetics*, 2001. **38**(6): p. 381-4.

452. Sivaprasad, S., et al., *Clinical course and treatment outcomes of Sorsby fundus dystrophy*. American journal of ophthalmology, 2008. **146**(2): p. 228-234.
453. Lefler, W.H., J.A. Wadsworth, and J.B. Sidbury, Jr., *Hereditary macular degeneration and amino-aciduria*. American journal of ophthalmology, 1971. **71**(1 Pt 2): p. 224-30.
454. Small, K.W., *North Carolina macular dystrophy: clinical features, genealogy, and genetic linkage analysis*. Trans Am Ophthalmol Soc, 1998. **96**: p. 925-61.
455. Small, K.W., et al., *North Carolina macular dystrophy (MCDRI) locus: a fine resolution genetic map and haplotype analysis*. Molecular vision, 1999. **5**: p. 38.
456. den Hollander, A.I., et al., *CRBI has a cytoplasmic domain that is functionally conserved between human and Drosophila*. Human molecular genetics, 2001. **10**(24): p. 2767-73.
457. Rohrschneider, K., et al., *Macular function testing in a German pedigree with North Carolina macular dystrophy*. Retina, 1998. **18**(5): p. 453-9.
458. Pauleikhoff, D., et al., *Clinical and genetic evidence for autosomal dominant North Carolina macular dystrophy in a German family*. American journal of ophthalmology, 1997. **124**(3): p. 412-5.
459. Yang, Z., et al., *Clinical characterization and genetic mapping of North Carolina macular dystrophy*. Vision research, 2008. **48**(3): p. 470-7.
460. Szlyk, J.P., et al., *Comprehensive functional vision assessment of patients with North Carolina macular dystrophy (MCDRI)*. Retina, 2005. **25**(4): p. 489-97.
461. Khurana, R.N., et al., *A reappraisal of the clinical spectrum of North Carolina macular dystrophy*. Ophthalmology, 2009. **116**(10): p. 1976-83.
462. Kiernan, D.F., et al., *Thirty-Year follow-up of an African American family with macular dystrophy of the retina, locus 1 (North Carolina macular dystrophy)*. Ophthalmology, 2011. **118**(7): p. 1435-43.
463. Small, K.W., *North Carolina macular dystrophy, revisited*. Ophthalmology, 1989. **96**(12): p. 1747-54.
464. Lu, X., et al., *Limited proteolysis differentially modulates the stability and subcellular localization of domains of RPGRIP1 that are distinctly affected by mutations in Leber's congenital amaurosis*. Human molecular genetics, 2005. **14**(10): p. 1327-40.
465. Liu, S.Y. and T.M. Redmond, *Role of the 3'-untranslated region of RPE65 mRNA in the translational regulation of the RPE65 gene: identification of a specific translation inhibitory element*. Archives of biochemistry and biophysics, 1998. **357**(1): p. 37-44.
466. Michaelides, M., et al., *An early-onset autosomal dominant macular dystrophy (MCDR3) resembling North Carolina macular dystrophy maps to chromosome 5*. Investigative ophthalmology & visual science, 2003. **44**(5): p. 2178-83.
467. Woods, C.G., et al., *Quantification of homozygosity in consanguineous individuals with autosomal recessive disease*. American journal of human genetics, 2006. **78**(5): p. 889-96.
468. Sheffield, V.C., E.M. Stone, and R. Carmi, *Use of isolated inbred human populations for identification of disease genes*. Trends Genet, 1998. **14**(10): p. 391-6.
469. Petukhova, L., et al., *The effect of inbreeding on the distribution of compound heterozygotes: a lesson from Lipase H mutations in autosomal recessive woolly hair/hypotrichosis*. Human heredity, 2009. **68**(2): p. 117-30.

470. Bainbridge, J.W., M.H. Tan, and R.R. Ali, *Gene therapy progress and prospects: the eye*. Gene therapy, 2006. **13**(16): p. 1191-7.
471. Cideciyan, A.V., et al., *Human RPE65 gene therapy for Leber congenital amaurosis: persistence of early visual improvements and safety at 1 year*. Human gene therapy, 2009. **20**(9): p. 999-1004.
472. Boye, S.E., et al., *A comprehensive review of retinal gene therapy*. Molecular therapy : the journal of the American Society of Gene Therapy, 2013. **21**(3): p. 509-19.
473. Ramsden, C.M., et al., *Stem cells in retinal regeneration: past, present and future*. Development, 2013. **140**(12): p. 2576-85.
474. Glockle, N., et al., *Panel-based next generation sequencing as a reliable and efficient technique to detect mutations in unselected patients with retinal dystrophies*. European journal of human genetics : EJHG, 2014. **22**(1): p. 99-104.

7.0 Appendices

7.1 Patient Documents

7.1.1 Patient Information Leaflet

A clinical and molecular genetic investigation of childhood retinal dystrophies

INFORMATION LEAFLET

PLEASE CONTACT US IF YOU WOULD LIKE THIS LEAFLET IN LARGER TYPE OR THE INFORMATION PROVIDED ON AUDIO CASSETTE TAPE

You are invited to take part in this research study. Before you decide it is important for you to understand why the research is being done and what's involved. Please take time to read the following information carefully and discuss it with your family, friends, hospital specialist or GP if you wish. If you need more information please contact the research team whose telephone number is at the end of this leaflet.

Why the study is being done?

Inherited retinal disorders are an important cause of childhood visual impairment and this research study aims to discover the causes of the retinal problem and to understand the reasons why the retina fails to function normally. Vision is dependent upon the functioning of the cone and rod cells of the retina, a thin membrane at the back of the eye. There are two groups of cells in the retina that detect light. The cones cells are used when light levels are high, and the rods are used when light levels are low. From the way in which night vision, colour vision, central vision and the electrical responses from the retina are changed we can learn how a condition has affected the cells in the retina. We are able to use this information together with knowledge of the genetic faults causing an eye disorder to build up a picture of what is causing the retinal dysfunction and which approach would be best used in the future to slow down disease progression.

Research has shown that genetic factors have an effect on the risk of someone developing this group of disorders. In other words, some people are at higher risk than others because of their genetic make-up.

This research study is being carried out for two important reasons:

1. We want to find out more about the genetic factors in childhood retinal dystrophies
2. We want to find the genes that affect the risk of developing childhood retinal dystrophies

If we can find which genes affect the risk of childhood retinal dystrophies it would help us understand why the disease occurs and could in the longer term lead to better treatment.

How will the study be carried out?

To find out more about genetic factors in childhood retinal dystrophies we need the help of patients with childhood retinal dystrophies and their relatives. By comparing the genetic make-up of those with childhood retinal dystrophies we can see what genes they have in common and start to work out which genes affect the risk of developing childhood retinal dystrophies. We can also obtain additional information if we have the opportunity of studying unaffected relatives as well.

Why you are being invited to take part

You are being invited to take part because you or your relative has a childhood retinal dystrophy. To give us a good chance of success, we need to study a large number of cases. We hope to recruit at least 60 patients with the disorder and their close relatives.

Do I have to take part?

It is up to you to decide whether or not to take part. If you do decide to take part you will be given this information sheet to keep and be asked to sign a consent form. If you decide to take part you are still free to withdraw at any time and without giving a reason. A decision to withdraw at any time, or a decision not to take part, will not affect the standard of care you receive.

What will happen to me if I take part?

If you decide to take part and have signed a consent form you will be asked to give a 30 ml blood sample (that's about 6 teaspoon-fulls) which will be used to extract DNA (the chemical containing your genetic information) which will be used to try and identify genes causing eye disorders. The results of these tests will be kept strictly confidential. You will also be asked to undergo a routine eye examination and have some images taken of the back of your eye using several imaging techniques. The imaging techniques are similar to having a photograph taken of the back of your eyes. You may also have the length of your eye measured with ultrasound (a small probe will touch your eye after a local anaesthetic drop has been instilled). For the imaging we will need to dilate your pupils. This procedure is conducted routinely in eye clinics. The use of these drops causes some temporary blurring of vision especially for near and as they increase the size of the pupil, they may be associated with increase sensitivity to light. It is advisable that you bring along sunglasses to wear on your journey home. For most people, it takes around 8 hours for the pupil of the eye to return to its normal size following dilation although vision recovers sooner. It is advisable not to drive for 5-6 hours after the drops have been instilled. We will pay your travel expenses to and from London. The tests are quite simple and last approximately 90 minutes although the length of the examination varies from person to person.

In some cases we will ask you to return for additional tests. These tests will involve either the examination of your ability to see targets in your peripheral vision, or measurement of your vision at low light levels (these tests last approximately 2 hours)

What will happen to the blood sample?

The laboratory will extract the genetic material DNA from the cells in the blood sample so that this can be used to study the genes that we think may have an effect on the risk of developing childhood retinal dystrophy.

What will happen to the results of the research study?

All the information from the study will be published in medical journals and presented to relevant health professionals at meetings and conferences. We would also be pleased to provide information about the results of the study to anyone who has taken part. Individual patients will not be identified in any reports or publications arising from the study.

Will information from the study be kept confidential?

All information collected for the study will be kept strictly confidential. The research team will not pass on your personal details to anyone else. The samples will be coded and scientists working in the laboratory will be provided with relevant medical information relating to the samples but will not be given the names of the people from whom the samples were obtained.

Working with other research groups to speed things up

Finding the genes that are important in childhood retinal dystrophy is a major challenge and may take many years. To speed up the research, we may join forces with other research teams in this country or abroad, in which case we may want to provide them with some of the sample stored from yourself and others for them to work on. In order to make this possible, on the consent form you are asked to agree to donate your sample to the research team as a gift. This means that you give up all rights to the sample and cannot at a later date ask for the sample to be destroyed or returned to you. It also means that at the discretion of the research team your sample can be used by others for research on the causes of childhood retinal dystrophy.

What are the possible benefits of taking part?

It is unlikely that you will benefit personally from helping with this research project, but the results of the research should be of benefit to patients affected by childhood retinal dystrophy in the future.

Will you be told the results of the eye examination or genetic testing?

The purpose of the eye examination is to obtain information we need for the research study. This sort of technical information is unlikely to have any implications for yourself. It is possible but unlikely that in the course of examining your eyes we may discover a problem with your eyes that you were not aware of. Please let us know if you would prefer not to be told if this situation arises. Otherwise we will assume that you would like us to bring it your attention, and with your permission, pass on information to your general practitioner. If you are a car driver, one reason you may choose not to be told about unexpected findings might be the implications this could have for holding a driving licence.

The genetic testing that we will be carrying out will have the aim of identifying the changes in a specific gene which is causing your eye disorder. It may take months or even years before the specific change causing your eye disease is identified. We will inform you if we identify the change in your case. Please let us know if you do not wish to know the result. We will not inform your GP of the result unless you specifically ask us to.

What are the possible disadvantages of taking part?

Your eyes will be photographed, which requires having drops put in your eyes to dilate the pupils. This may cause brief discomfort and some temporary blurring of your near vision so you will not be able to drive a car for the rest of the day. Dilating the pupils is a routine procedure in hospital eye clinics which doesn't usually cause any problem, but you should be aware that a painful rise in the pressure in the eye (acute glaucoma) is a rare but treatable complication. You will be asked to provide a blood sample for the study. This will be done with care by qualified staff but may cause some discomfort and occasionally bruising.

Who is organising and funding the research?

The Special Trustees on Moorfields Eye Hospital using funding donated by the Eranda foundation

What if something goes wrong?

If you are harmed by taking part in this research project, there are no special compensation arrangements. If you are harmed due to someone's negligence, then you may have grounds for a legal action but you may have to pay for it. Regardless of this, if you wish to complain or have any concerns about any aspect of the way you have been approached or treated during the course of this study, the normal National Health Service complaints mechanisms would be available to you.

Contact for Further Information:

Professor AT Moore Moorfields Eye Hospital, City Road, London EC1V 2PD
Tel 0207 566 2260

Dr Arundhati Dev Borman, Research Fellow, Genetics Office, Professorial Unit,
Moorfields Eye Hospital NHS Trust, 162 City Road, London EC1V 2PD
Tel: 0207 566 2265 Email: a.dev-borman@ucl.ac.uk

Thank you for reading this information leaflet and for considering taking part in this study

7.1.2 Consent form – Adult

Title of Project: A clinical and molecular genetic investigation of childhood retinal dystrophies

Name of Researcher: Professor A T Moore

1. I confirm that I have read and understand the information sheet dated January 2004 for the above study and have had the opportunity to ask questions.

2. I understand that my participation is voluntary and that I am free to withdraw at any time, without giving any reason, without my medical care or legal rights being affected

3. I understand that sections of any of my medical notes may be looked at by the research team or individuals from regulatory authorities where it is relevant to my taking part in research. I give permission for these individuals to have access to my records.

4. I understand that the results of any new genes or novel alterations in these genes that are discovered to be responsible for inherited eye disorders will be published in scientific and medical journals. This information and any results obtained from the analysis of a blood sample will not be used by pharmaceutical companies in the future. In addition, I understand that I will not benefit financially if the results of this research lead to the development of new treatments, tests, or patents.

5. I give permission for clinical images and information gained from this study to be published in the scientific literature as long as all personal identifying information is removed.

6. I agree to take part in the above study.

Name of Patient

Date

Signature

Name of Person taking consent
(if different from researcher)

Date

Signature

Researcher

Date

Signature

7.1.3 Consent form – Child

Title of Project: A clinical and molecular genetic investigation of childhood retinal dystrophies

Name of Researcher: Professor A T Moore

1. I confirm that I have read and understand the information sheet dated January 2004 for the above study and have had the opportunity to ask questions.
2. I understand that the participation of my child is voluntary and that I may withdraw my child at any time, without giving any reason, without his/her care or legal rights being affected.
3. I understand that sections of any of my child's medical notes may be looked at by the research team or individuals from regulatory authorities where it is relevant to his/her taking part in research. I give permission for these individuals to have access to my child's records.
4. I understand that the results of any new genes or novel alterations in these genes that are discovered to be responsible for inherited eye disorders will be published in scientific and medical journals. This information and any results obtained from the analysis of a blood sample will not be used by pharmaceutical companies in the future. In addition, I understand that neither I, nor my child, will benefit financially if the results of this research lead to the development of new treatments, tests, or patents.
5. I give permission for clinical images and information gained from this study to be published in the scientific literature as long as all personal identifying information is removed.
6. I agree that my child may take part in the above study.

Name of Patient

Name of Parent/Guardian giving consent Date Signature

Relationship to child

Name of Person taking consent Date Signature
(if different from researcher)

Researcher Date Signature

[1 for patient; 1 for researcher; 1 to be kept with hospital notes]

7.1.4 Data Protection Consent Form

Data Protection Consent Form

1. I agree to my/my child's personal identifying details (name, address, telephone number) being kept on a secure electronic database.
2. I agree to information regarding my family pedigree (who is related to who) being kept in a secure electronic database
3. I agree to clinical and genetic information about my condition being kept on this database.
4. I understand that this information will be held on a database located at the Institute of Ophthalmology (& Moorfields Eye Hospital). The personal information gathered will only be accessed by the principal researcher and team. Any results published from this information will not contain any personal identifying data.

Name of Patient:

Date.....

Signature of patient:

Name of Parent (if child).....

Date.....

Signature of Parent.....

Relationship to child.....

Name of researcher.....

Date.....

Signature of researcher.....

1 copy in notes

1 copy to patient/parent

1 copy to researcher

7.2 Primer Sequences

7.2.1 *TULP1* Primers

Exon	Primer	T _m (°C)	PCR annealing temperature (°C)	Size of fragment (bp)
Exon 1F	TCGTGGGCTGTAGCACCTCCC	72.6	63	381
Exon 2R	CTACCCTGCGTGGGTTTACGC	69.4		
Exon 3F	TAATCTGCGGTTATTTCTGGCGG	69.3	63	257
Exon 3R	TCAAGCCCCTCCCTCCGCAGC	77.8		
Exon 4F	TGGGAGAAGTGTTGAAAGTGG	64.0	58	457
Exon 4R	TACCTGGCTCAAAGATAAGGCC	65.1		
Exon 5F	TGGTGCCCATGCACCACTTCC	74.6	60	348
Exon 5R	TGAGGCCTCAATCGCTGTGTC	69.9		
Exon 6F	TGTCAAGCTTTCAGCCTCCCTG	69.7	58	514
Exon 7R	TCTGGCAAACCTCCTTACCTAGC	63.3		
Exon 8F	TCCAAGTGAGACATGGGTGTTGG	70.2	61	289
Exon 8R	TAACCTCAAGTGGCTCCAAGCC	68.3		
Exon 9FA	TAAATCACAGAGCTCCCCAGAG			
Exon 11RA	TATGTACATCAAAGCGAGAGGC			
Exon 9F (old)	TGTCTCAGCACTGGGACCTGC	70.2	63	593
Exon 10R (old)	TCTACCAGGCACAGCAGGACAG	68.8		
Exon 12F (old 11F)	TGAATTGCTCAGTCCTAACTCACC	65.3	58	514
Exon 13R (old 12R)	TGGATGTGCTCAGGAGTTGG	69.6		
Exon 14F (old 13F)	TACCCTAATGGATGAAGATGTCC	62.7	58	424
Exon 14R (old 13R)	TCCCAGCTCTCGGGATAAAGGC	71.2		
Exon 15F (old 14F)	TGTTGAGTAACTGAGATGGTG	57.7	53	736
Exon 15R (old 14R)	TACCGCTCCGCTTGGCCAAGG	75.8		

Table 24 - Primers and PCR conditions for *TULP1*.

7.2.2 RGR Primers

Exon	Primer	T _m (°C)	PCR annealing temperature (°C)	Size of fragment (bp)
Exon 1F	ATAACCTGCATGTGCCTCCA	65.4	64	246
Exon 1R	GTGGCCTGGGTCCTCAGA	66.6		
Exon 2F	CCCCACACACACTGTTCTGA	64.9	60	329
Exon 2R	TGTAAGTAGTAAAAATGCCCTTGG	61.8		
Exon 3F	CAAGCTGTACTTGGCAGGTG	63.4	61	298
Exon 3R	TGGGAAACACGGAGCAGTAG	65.1		
Exon 4F	TCTTCGATCAGGAAGTCCA	63.8	61	299
Exon 4R	GGAGTTCAAAGCCAAGATTCC	63.7		
Exon 5F	CCACAACCGATCATCTAGGC	64.2	62	288
Exon 5R	ATTCTTTGTTCGGGACACCA	64.2		
Exon 6F	CTTGGCCACATAGGCTGT	65.0	61	248
Exon 6R	TGAGATGAGATGAGACAGAGA	62.9		
Exon 7.1R	CAGAGAGAGGATCAGTGGCTTT	63.7	62	398
Exon 7.1R	CTTGAGTGTAGGGGGCTGTG	64.6		
Exon 7.2F	TGGATAGATTGCCTAGTGGTG	61.5	60	444
Exon 7.2 R	TCAAAAAGAAACCTGCACTTG	61.7		

Table 25 - Primers and PCR conditions for *RGR*.

7.2.3 BEST1 Primers

Exon	Primer	PCR annealing temperature (°C)
Exon 2F	CACCTGCTGCAGCCCACTGCC	61
Exon 2R	CTTGTAGTGAAGTGGTACACTGGCC	
Exon 3F	GGACAGTCTCAGCCATCTCCTCG	59
Exon 3R	GCAGCTCCTCGTGATCCTCCCCTGG	
Exon 4F	CTAGGCCCGCTCGCAGCAGAAAGC	60
Exon 4R	CTTCCATTCTGCGCGCCCATCTC	
Exon 5/6F	CATCCCTTCTGCGTTCTC	59
Exon 5/6R	CTGGTCCTTCTAGCCTCAGTTTC	
Exon 7F	CTGGAGCATCCTGATTCAGGGTTC	59
Exon 7R	CTCTGGCCATGCCTCCAGC	
Exon 8/9F	GCTGGCTTTGAGGAGTTCTGCCTG	59
Exon 8/9R	GTGCTATTCTAAGTTCCTAGGCAG	
Exon 10F	GTAAGGGAGAAGTAAGGCCAGGTG	59
Exon 10R	GTAGGTCCAGTGTGCTCTGGCAG	
Exon 11F	GAAGGGACCTTCCATACTTATG	59
Exon 11R	CATTAAAGGCTGAAGTAGTCTGGG	

Table 26 - Primers and PCR conditions for *BEST1*.

7.3 Publications and Abstracts from this Study

1. Mackay DS, Ocaka L, **Dev Borman A**, Sergouniotis P, Russell-Eggitt I, Thompson DA, Moradi P, Henderson RH, Webster AR, Moore AT. **Analysis of the *SPATA7* gene in Patients with LCA & Childhood Onset Retinal Dystrophy.** Association for Research in Vision and Ophthalmology (ARVO) Meeting, USA. May 2010.
2. **Dev Borman A**, Davidson A, O’Sullivan J, Devery S, Wright G, Thompson DA, Robson AG, Holder GE, Black GCM, Webster AR, Manson F, Moore AT. **Paediatric Autosomal Recessive Bestrophinopathy.** Association for Research in Vision and Ophthalmology (ARVO) Meeting, USA. May 2010.
3. Mackay DS, Ocaka LA, **Dev Borman A**, Sergouniotis PI, Henderson RH, Moradi P, Robson AG, Thompson DA, Webster AR, Moore AT. **Screening of *SPATA7* in Patients with Leber Congenital Amaurosis and Severe Childhood-Onset Retinal Dystrophy Reveals Disease-Causing Mutations.** *IOVS* 2011;52:3032–3038.
4. **Borman AD**, Davidson AE, O’Sullivan J, Thompson DA, Robson AG, De Baere E, Black GC, Webster AR, Holder GE, Leroy BP, Manson FD, Moore AT. **Childhood onset autosomal recessive bestrophinopathy.** *Arch Ophthalmol* 2011;129(8):1088-93.

5. **Dev Borman A**, Ocaka L, Mackay DS, Ripamonti C, Robson AG, Holder GE, Black GCM, Webster AR, Fitzke F, Stockman A, Moore AT. **Childhood Onset Retinal Dystrophy Due to *LRAT* Mutations**. Association for Research in Vision and Ophthalmology (ARVO) Meeting, USA. May 2011.
6. Mackay DS, **Dev Borman A**, Moradi P, Henderson RH, Li Z, Wright GA, Waseem N, Gandra M, Thompson DA, Bhattacharya SS, Holder GE, Webster AR, Moore AT. ***RDH12* retinopathy: novel mutations and phenotypic description**. *Mol Vis* 2011;17:2706-2716.
7. **Dev Borman A**, Ocaka LA, Mackay DS, Ripamonti C, Henderson RH, Moradi P, Hall G, Black GC, Robson AG, Holder GE, Webster AR, Fitzke F, Stockman A, Moore AT. **Early onset retinal dystrophy due to mutations in *LRAT*: molecular analysis and detailed phenotypic study**. *IOVS* 2012;53(7):3927-3938.
8. **Dev Borman A**, Sergouniotis P, Ocaka L, Webster AR, Mackay DS, Moore AT. **A Survey of the Molecular Pathology and Genotype-Phenotype Correlation of Families With Autosomal Recessive Early Onset Severe Retinal Dystrophy**. Royal College of Ophthalmologists (RCOPhth) Congress, UK. May 2012.
9. Mackay DS, **Dev Borman A**, Sui R, van den Born LI, Berson EL, Ocaka LA, Davidson AE, Heckenlively JR, Branham K, Ren H, Lopez I, Maria M, Azam

M, Henkes A, Blokland E, LCA5 Study Group, Qamar R, Webster AR, Cremers FPM, Moore AT, Koenekoop RK. **Screening of a large cohort of Leber congenital amaurosis and retinitis pigmentosa patients identifies novel *LCA5* mutations and new genotype-phenotype correlations.** *Hum Mutat.* 2013 Nov;34(11):1537-46.

10. Dev Borman A, Pearce LR, Mackay DS, Nagel-Wolfrum K, Davidson AE, Henderson RH, Garg S, Waseem NH, Webster AR, Plagnol V, Wolfrum U, Farooqi IS, Moore AT. A homozygous mutation in the *TUB* gene associated with retinal dystrophy and obesity. *Hum Mutat.* 2014 Mar;35(3):289-93.